

Application Of Headed Bars in Concrete Members

**Approved by
Dissertation Committee:**

James O. Jirsa, Supervisor

John E. Breen

Michael E. Kreger

Jose M. Roesset

Stelios Kyriakides

Copyright

by

Tarek Refaat Bashandy

1996

To my Father and Mother

Application Of Headed Bars in Concrete Members

by

Tarek Refaat Bashandy, B.S.C.E., M.S.E.

Dissertation

Presented to the Faculty of the Graduate School of

The University of Texas at Austin

in Partial Fulfillment

of the Requirements

for the Degree of

Doctor of Philosophy

The University of Texas at Austin

December, 1996

Acknowledgments

The author would like to thank Dr. James O. Jirsa, the dissertation supervisor, for his continuous guidance and invaluable friendship. His suggestions in planning and conducting this research effort are greatly appreciated.

Sincere thanks are extended to Professors John Breen, Michael E. Kreger, Jose Roesset, and Stelios Kyriakides for serving on the supervising committee.

The assistance of the technical staff of the Phil M. Ferguson Structural Engineering Laboratory is acknowledged. Special thanks are expressed to Laurie Golding and Sharon Cunningham.

The author would like to express his gratitude to his fellow graduate students for their assistance and support. Special thanks to Richard DeVries for his valuable suggestions, and to Selim Marwat for his assistance in the experimental program.

Finally, I would like to thank my Parents who encouraged me to pursue my advanced studies. Without their support and encouragement throughout my life I could not fulfill my dreams. Without you, I wouldn't have done this, and without you, I wouldn't want to do this.

This study was conducted at the Phil M. Ferguson Structural Engineering Laboratory, and was sponsored by Heated Reinforcement Corporation.

Tarek R. Bashandy

October 23, 1996

Application Of Headed Bars in Concrete Members

Publication No. _____

Tarek Refaat Bashandy, PhD.
The University of Texas at Austin, 1996

Supervisor: James O. Jirsa

The introduction of high strength steel and concrete in reinforced concrete structures requires an efficient form of mechanical anchorage. Headed bars provide a practical alternative to hooked bars and eliminate congestion problems caused by standard hooks. Other attributes of headed bars are minimal slip, ease of placement, and more accurate dimensions of reinforcing cages.

The objective of this study was to determine the anchorage behavior of headed bars in joints. Three phases of experimental research were conducted to provide an understanding of the behavior of headed bars.

In the first phase of the study 25 pull-out tests were conducted to investigate the effects of cyclic loading, anchoring the head behind a crossing bar, and the possibility of using headed bars as transverse reinforcement. Cycling the load between 5 and 80% of the capacity did not affect the ultimate load. A

crossing bar improved the anchorage capacity significantly. Test results indicated that there is great potential for the use of headed bars instead of closed ties in large structural elements.

In the second phase of the study 32 large scale specimens simulating exterior joints in a structure were tested. The anchorage capacity of headed bars was independent of the bar diameter, head aspect ratio and orientation. The anchorage capacity was improved by increases in lead embedment, head area, concrete cover, and ties through the joint. In general, the anchorage performance of headed bars under monotonic loading was superior to that of hooked bars.

In the third phase of the study one exterior beam-column subassemblage was tested under cyclic loading. The behavior of the specimen was compared with a similar specimen constructed using hooked bars, which was reported in the literature. The headed bar specimen showed less deterioration in capacity than the hooked bar specimen even though the headed bars had a higher yield strength. There were no signs of bond deterioration for the headed bars throughout the test.

The results of this study provided an understanding of the behavior of headed bars in joints, and a comparison with hooked bars. Recommendations for code design provisions for anchorage of headed bars were provided.

Table of Contents

List of Tables	xii
List of Figures.....	xiii
Chapter 1: INTRODUCTION	1
1.1 General	1
1.2 Background.....	4
1.3 Objectives.....	5
1.4 Scope	6
1.4.1 Basic Studies on Headed Bars	6
1.4.2 Anchorage in Exterior Joints	7
1.4.3 Effects of Seismic Loading	7
Chapter 2: PREVIOUS RESEARCH	8
2.1 General	8
2.2 Anchor Bolt Studies.....	9
2.3 Headed Bar Studies	12
2.4 University of Toronto Tests.....	16
2.5 Clarkson University Joint Tests.....	17
2.6 Bridge Knee Joint.....	19
2.7 University of Texas Pull-out Tests	20
Chapter 3: BASIC STUDIES OF HEADED BARS	24
3.1 Introduction	24
3.2 Group 1: Pullout Tests.....	25
3.2.1 Design of Specimens	25
3.2.2 Variables.....	25
3.2.3 Materials	29
3.2.4 Instrumentation	31
3.2.5 Specimen Fabrication	32
3.2.6 Test Setup	34
3.2.7 Test Procedure.....	35
3.2.8 Test Results	35
3.2.9 Effects of Different Variables.....	38
3.3 Group 2: Transverse Reinforcement.....	53
3.3.1 Design of Specimens	53
3.3.2 Materials	55
3.3.3 Instrumentation	55
3.3.4 Specimen Fabrication	58
3.3.5 Test Results	61
3.3.6 Load-Slip Behavior.....	62
3.4 Summary.....	65

Chapter 4: ANCHORAGE IN EXTERIOR JOINTS - EXPERIMENTAL PROGRAM	66
4.1 Introduction	66
4.2 Background.....	67
4.3 Experimental Program	85
4.3.1 Design of Specimens	86
4.3.2 Variables.....	107
4.3.3 Materials	111
4.3.4 Specimen Fabrication	113
4.3.5 Instrumentation of the Test Specimens	115
4.3.6 Test Setup	118
4.3.7 Test Procedure.....	122
Chapter 5: ANCHORAGE IN EXTERIOR JOINTS - TEST RESULTS.....	124
5.1 Introduction	124
5.2 Specimens with Side Blow-Out Failures	125
5.2.1 Cracking Pattern	126
5.2.2 Load-Slip Behavior.....	134
5.2.3 Effects of Different Variables.....	140
5.3 Specimens Failing in Shear.....	170
5.3.1 Cracking Pattern	170
5.3.2 Load-Slip Behavior.....	173
5.3.3 Cracking Stress	179
5.3.4 Shear capacity.....	182
5.4 Head Strains.....	187
5.5 Summary.....	190
Chapter 6: Analysis of Test Results	192
6.1 Introduction	192
6.2 Comparison with Deep Embedment Tests.....	193
6.3 Comparison with Existing Design Methods.....	196
6.3.1 University of Texas Anchor Bolt Studies (Hasselwander)	197
6.3.2 University of Stuttgart Anchor Bolt Studies (Furche and Eligehausen).....	201
6.3.3 University of Texas Pullout Tests on Headed Bars (DeVries)	203
6.4 Statistical Analysis.....	205
6.4.1 Best Fit Equation	212
6.5 Physical Model	215
6.6 Comparison with Hooked Bar Tests.....	223
6.7 Design Implications	231
6.7.1 Comparison of Required Embedment for Hooked and Headed Bars	234
6.8 Failure Hypothesis for Specimens with Shear Failure	236
6.9 Summary.....	243

Chapter 7: EFFECTS OF CYCLIC LOADING.....	244
7.1 Background.....	244
7.2 Experimental Program.....	248
7.2.1 Specimen Design.....	251
7.2.2 Specimen fabrication.....	255
7.2.3 Instrumentation.....	256
7.2.4 Test Setup.....	259
7.2.5 Test Procedure.....	259
7.3 Test Results.....	263
7.4 Cracking Pattern.....	263
7.5 Load Deformation Relationships.....	271
7.5.1 Beam Load - Beam Drift.....	271
7.5.2 Joint Deformation.....	275
7.5.3 Head Slip.....	278
7.6 Measured Strains in Reinforcement.....	280
7.6.1 Beam Bar Stresses.....	280
7.6.2 Column Bars.....	284
7.7.3 Joint Ties.....	285
7.8 Summary.....	290
Chapter 8: SUMMARY AND CONCLUSIONS	291
8.1 Introduction.....	291
8.2 Basic Studies of Headed Bar Anchorage.....	292
8.3 Anchorage in Exterior Joints.....	293
8.4 Effects of Seismic Loading.....	296
8.5 Recommendations for Further Research.....	297
References.....	299
Vita.....	303

List of Tables

Table 3.1	Parameters for Pullout Tests (35 mm Bars).....	26
Table 3.2	Concrete mix proportions for pullout tests	31
Table 3.3	Results of Pullout tests	35
Table 3.4	Stirrup Tests - Properties and Test Results.....	57
Table 4.1	Parameters and results of Marques and Jirsa hooked bar tests [9].	71
Table 4.2	Parameters and results of Pinc and Jirsa hooked bar tests [11].	76
Table 4.3	Parameters and Results of Hamad and Jirsa Hooked Bar tests [12].	78
Table 4.4	Parameters and results of Burguieres and Jirsa Mechanical Anchorages tests [13].	81
Table 4.5	Parameters of Joint Test Specimens	87
Table 4.6	Head dimensions for joint specimens	88
Table 5.1	Test Results for Specimens with Side Blow-Out Failure.....	126
Table 5.2	Test results for group 1 and 2 specimens (shear failure)	171
Table 5.3	Shear stress at cracking	180
Table 5.4	Shear Stress at failure	184
Table 6.1	Comparison of Measured and predicted Capacities using Hasselwander's Equations.....	199
Table 6.2	Comparison of Measured and predicted Capacities using Furche and Eligehausen Equation	202
Table 6.3	Comparison of Measured and predicted Capacities using DeVries' Equation	204
Table 6.4	Comparison of Functions of Head Area	210
Table 6.5	Comparison of Measured and predicted Capacities using Analytical Models.....	214
Table 6.6	Comparison of Measured and predicted Capacities using Physical Model	221
Table 6.7	Comparison of Measured and predicted Capacities using the modified Physical Model.....	224
Table 6.8	Comparison between Headed and Hooked bar Specimens.....	225
Table 6.9	Comparison between Required Embedment for Hooked and Headed Bars	235
Table 6.10	Comparison of Measured and Predicted Shear Capacities	241
Table 6.11	Comparison between Specimens with Heads anchor behind Crossing Bars and Burguieres Tests.....	243
Table 7.1	Properties of Materials used by Smith [26]	251
Table 7.2	Properties of Materials used for the test specimen	255
Table 7.3	Comparison of Moment Degradation	274

List of Figures

Figure 1.1	Hooked Bar details specified by the ACI Building Code [1].....	2
Figure 1.2	Comparison between Anchorage Mechanisms of Headed and Hooked Bars	4
Figure 1.3	Headed Bar	5
Figure 2.1	Reinforcement Details for Beam Specimens [5].....	14
Figure 2.2	Reinforcement Details of Prism Tests [5].....	15
Figure 2.3	Specimens tested by Collins and Gupta [6]	16
Figure 2.4	Reinforcement Details of Knee Joint tested by McConnell and Wallace [7].....	18
Figure 2.5	Knee Joint specimen at end of Test - McConell and Wallace [7].....	18
Figure 2.6	Recommended Reinforcement Detail - McConnell and Wallace [7].....	19
Figure 2.7	Reinforcement of Joint and Cap - SEQAD [8]	20
Figure 2.8	Blow-out Areas for various configurations - DeVries [2].....	23
Figure 3.1	Head Anchorage behind Crossing Bars	28
Figure 3.2	Stress - Strain curves for 25M and 35M Bars	30
Figure 3.3	Concrete Strength for pullout tests.....	30
Figure 3.4	Setup used for measuring Head Slip	31
Figure 3.5	Specimen ready for casting.....	33
Figure 3.6	Test setup for Pullout Tests	34
Figure 3.7	Load-Slip behavior for Standard Tests	37
Figure 3.8	Cracking and failure patterns - Test P2.....	39
Figure 3.9	Effect of Cyclic Loading on the Anchorage Capacity - 15 Cycles.....	40
Figure 3.10	Effect of the Number of Cycles on the Anchorage Capacity - Corner Bars, 90x90 mm Heads.....	40
Figure 3.11	Effect of Load Cycling on the Load-Slip behavior of Edge Bars	42
Figure 3.12	Effect of Load Cycling on the Load-Slip Behavior of Corner Bars - 15 Cycles..	43
Figure 3.13	Effect of Load Cycling on the Load-Slip Behavior of Corner Bars - 10 Cycles..	43
Figure 3.14	Effect of Load Cycling on the Load-Slip Behavior of Corner Bars - 5 Cycles....	44
Figure 3.15	Effect of Crossing Bars on the Anchorage Capacity.....	46
Figure 3.16	Effect of 35 mm Crossing Bars on the Load-Slip behavior - 35x90 mm Heads ..	46
Figure 3.17	Effect of Crossing Bars on the Load-Slip behavior - 70x44 mm Heads	48
Figure 3.18	Effect of Crossing Bars on the Load-Slip behavior - 55x55 mm Heads	48
Figure 3.19	Failure Pattern after removing Spalled Concrete - P12.....	49
Figure 3.20	Effect of Head Dimensions on the failure pattern	51
Figure 3.21	Effect of Crossing Bars on Head Stresses - P10	52
Figure 3.22	Forces resulting from Anchorage Behind Crossing Bars	53
Figure 3.23	Setup for Stirrup Tests	54
Figure 3.24	Head interlock schemes for Stirrup tests.....	57
Figure 3.25	Head interlock schemes for Stirrup tests (continued).	58
Figure 3.26	Stress - Strain curves for the 20M Headed Bars	59
Figure 3.27	Head Slip measurement	60
Figure 3.28	Overall view before casting	60
Figure 3.29	Effect of Flash interlock on direction of Slip.....	62
Figure 3.30	Load-Slip behavior - Test S4	63
Figure 3.31	Load-Slip behavior - Test S9	63
Figure 3.32	Head Strains - Test S9	64

Figure 4.1	Exterior Joint used by Marques and Jirsa [9] for testing Hooked Bar Anchorages	68
Figure 4.2	Exterior Joint simulation by Marques and Jirsa [9]	69
Figure 4.3	Joint details of the J7 series of #7 Hooked Bar Specimens by Marques and Jirsa [9]	72
Figure 4.4	Joint details of the J11 series of #11 Hooked Bar Specimens by Marques and Jirsa [9]	73
Figure 4.5	Joint details of the #7 Hooked Bar Specimens by Pinc [11] and Hamad [12]	79
Figure 4.6	Joint details of the #11 Hooked bar Specimens by Pinc [11] and Hamad [12]	80
Figure 4.7	Mechanical anchorage type B, Burguires [13]	82
Figure 4.8	Mechanical anchorage type U, Burguires [13]	83
Figure 4.9	Reinforcement details - Specimens T1 through T3	89
Figure 4.10	Reinforcement details - Specimen T4	90
Figure 4.11	Reinforcement details - Specimen T5	91
Figure 4.12	Reinforcement details - Specimen T6	92
Figure 4.13	Reinforcement details - Specimen T7	93
Figure 4.14	Reinforcement details - Specimen T8	94
Figure 4.15	Reinforcement details - Specimen T9	95
Figure 4.16	Reinforcement details - Specimens T10 and T13	96
Figure 4.17	Reinforcement details - Specimen T11	97
Figure 4.18	Reinforcement details - Specimen T12	98
Figure 4.19	Reinforcement details - Specimen T14	99
Figure 4.20	Reinforcement details - Specimens T15, T18, and T19	100
Figure 4.21	Reinforcement details - Specimens T16	101
Figure 4.22	Reinforcement details - Specimen T17	102
Figure 4.23	Reinforcement details - Specimens T20, T23, T24, T28, T29, and T30	103
Figure 4.24	Reinforcement details - Specimens T21, T22, T27, 31, and T32	104
Figure 4.25	Reinforcement details - Specimens T25	105
Figure 4.26	Reinforcement details - Specimen T26	106
Figure 4.27	Stress-Strain curve for Series 6 Column Bars	112
Figure 4.28	Steel cages inside the forms	115
Figure 4.29	Specimens ready for concrete placement	116
Figure 4.30	Strain gage positions on headed bars	117
Figure 4.31	Schematic of the Test Setup, elevation view	119
Figure 4.32	Schematic of the Test Setup, top view	120
Figure 4.33	Test Setup for the Exterior Joints	121
Figure 5.1	Cracking prior to failure - Specimen T26	128
Figure 5.2	Appearance after failure - Specimen T26	129
Figure 5.3	Cracking and failure pattern - Specimen T21	130
Figure 5.4	Concrete Wedge and Pull-out Cone	131
Figure 5.5	Appearance of column bars after failure	133
Figure 5.6	Appearance of specimens with stirrups - Specimen T25	134
Figure 5.7	Applied Load vs Head Slip for Specimen T9	136
Figure 5.8	Head Load vs Applied Load for Specimen T9	136
Figure 5.9	Applied Load vs Head Slip for Specimen T21	139
Figure 5.10	Head Load vs Applied Load for Specimen T21	139
Figure 5.11	Effect of head area on the anchorage capacity - 35 mm bars, 76 mm cover	141
Figure 5.12	Effect of head area on the anchorage capacity - 25 mm bars, 76 mm cover	141

Figure 5.13	Effect of head area on the load-slip behavior - 35 mm bars, 76 mm cover.....	142
Figure 5.14	Effect of head area on the Applied Load - Head Load ratio 35 mm bars, 76 mm cover.....	143
Figure 5.15	Head Load vs. Slip for different head areas - 35 mm bars, 76 mm cover	144
Figure 5.16	Effect of head area on the load-slip behavior - 25 mm bars, 76 mm cover.....	145
Figure 5.17	Head Load vs. Slip for different head areas - 25 mm bars, 76 mm cover	146
Figure 5.18	Effect of head aspect ratio on the anchorage capacity - 35 mm bars, 76 mm cover	148
Figure 5.19	Effect of head aspect ratio on the load-slip behavior - 35 mm bars, 76 mm cover	149
Figure 5.20	Applied Load vs. Head Slip for Specimen T23	149
Figure 5.21	Applied Load vs. Head Slip for Specimen T24	150
Figure 5.22	Effect of Aspect Ratio on the wedge angle	151
Figure 5.23	Effect of bar diameter on the anchorage capacity, 76 mm cover	153
Figure 5.24	Effect of bar diameter on the load-slip behavior.....	154
Figure 5.25	Effect of Bar Diameter on the Applied Load - Head Load Ratio.....	155
Figure 5.26	Effect of Side Concrete Cover on the Anchorage Capacity	156
Figure 5.27	Effect of Side Concrete Cover on the load-slip behavior.....	158
Figure 5.28	Effect of Side Concrete Cover on the Applied Load - Head Load ratio, 25M Bars	159
Figure 5.29	Effect of embedment length on the anchorage capacity - 76 mm cover, 35M Bars	161
Figure 5.30	Effect of Development Length on the Load-Slip behavior 76 mm cover, 35M bars	161
Figure 5.31	Effect of Embedment Length on the Applied Load - Head Load ratio 76 mm cover, 35M Bars	162
Figure 5.32	Effect of Embedment Length on the Maximum Head Load	164
Figure 5.33	Effect of Development Length on the Load-Slip behavior - 38 mm cover, 25M Bars	166
Figure 5.34	Effect of Embedment Length on the Applied Load - Head Load ratio 38 mm cover, 25M Bars	166
Figure 5.35	Effect of Confining Reinforcement on the Anchorage Capacity 76 mm cover, 35M Bars	168
Figure 5.36	Effect of Confining Reinforcement on the Load-Slip behavior 76 mm cover, 35M Bars	168
Figure 5.37	Effect of Confining Reinforcement on the Applied Load - Head Load Ratio....	169
Figure 5.38	Cracking and failure patterns - Specimen T2.....	172
Figure 5.39	Failure pattern of specimen T15	174
Figure 5.40	Applied Load vs. Head Slip for Specimen T2	174
Figure 5.41	Head Load vs. Applied Load for Specimen T2	175
Figure 5.42	Effect of shear reinforcement on the Load-Slip behavior	176
Figure 5.43	Effect of Shear Reinforcement on the Applied Load - Head Load Ratio.....	177
Figure 5.44	Effect of the Anchorage Condition on the Load-Slip behavior.....	178
Figure 5.45	Effect of Anchorage Condition on the Applied Load - Head Load Ratio	178
Figure 5.46	Compressive Stress Distributions in Test Specimens and in Joints	184
Figure 5.47	Stresses in Shear Reinforcement - Specimen T6.....	185
Figure 5.48	Anchorage conditions of group 2 specimens	186
Figure 5.49	Head Strains on the top and bottom of the bar - Specimen T21	188

Figure 5.50	Head Strains in the inner and outer sides of the head - Specimen T28	188
Figure 5.51	Head Strains on the inner and outer sides of the head - Specimen T15	189
Figure 6.1	Comparison of Anchorage Capacities of Joint and Pull-Out Tests 25 mm Bars.....	193
Figure 6.2	Comparison of Anchorage Capacities of Joint and Pull-Out Tests 35 mm Bars.....	194
Figure 6.3	Load-Slip Behavior of Joint and Cube Tests	195
Figure 6.4	Anchorage Capacity versus Embedment Length.....	207
Figure 6.5	Comparison of Measured and Predicted Capacities using Total Head Area.....	216
Figure 6.6	Comparison of Measured and Predicted Capacities Using Net Bearing Area ...	217
Figure 6.7	Geometry of Blow-Out Failure	219
Figure 6.8	Comparison of Capacities of 35 mm Headed Bars with various Head Areas and Hooked Bar Specimens	227
Figure 6.9	Comparison of Capacities of 25 mm Headed Bars with various Head Areas and Hooked Bar Specimens	228
Figure 6.10	Comparison of Load-Slip behavior for Specimen T9 to similar Hooked bar Specimens.....	229
Figure 6.11	Comparison of Load-Slip behavior for Specimen T16 to Specimen 11-18	229
Figure 6.12	Comparison of Load-Slip behavior for Specimen T13 to Specimen J11-90-15-3-H	230
Figure 6.13	Comparison of Load-Slip behavior for Specimen T14 to Specimen J11-90-15-3-L.....	230
Figure 6.14	Effect of Shear Span on the Shear Strength	236
Figure 6.15	Comparison between the Joint Shear Capacity and Continuous Deep Beam Tests	239
Figure 6.16	Joint Shear resisted by Stirrups - Specimen T6	240
Figure 7.1	Concrete Dimensions and Reinforcement Details of Unit 4 [26].....	250
Figure 7.2	Concrete Dimensions and Reinforcement Details of the Headed Bar Specimen	252
Figure 7.3	Stress-Strain curves for Specimen Reinforcement	254
Figure 7.4	Concrete Strength Gain.....	255
Figure 7.5	Reinforcement Cage and Form before casting	257
Figure 7.6	Instrumentation for measuring rotations	258
Figure 7.7	Schematic of the Test Setup.....	260
Figure 7.8	Test setup.....	261
Figure 7.9	Load History used by Smith [26]	262
Figure 7.10	Load History applied	262
Figure 7.11	Cracking Pattern after Cycle 1	264
Figure 7.12	Cracking Pattern after Cycle 2.....	264
Figure 7.13	Cracking Pattern after Cycle 4.....	265
Figure 7.14	Cracking Pattern after Cycle 6.....	265
Figure 7.15	Cracking Pattern after Cycle 10.....	266
Figure 7.16	Cracking Pattern after Cycle 12.....	267
Figure 7.17	Cracking Pattern after Cycle 13.....	268
Figure 7.18	Appearance after removing the cover	269
Figure 7.19	Applied Load versus Beam Drift for the Headed bar Specimen	272
Figure 7.20	Applied Load versus Beam Ductility for Unit 4 (Tested by Smith [26])	273
Figure 7.21	Applied Load versus Beam Ductility for the Headed Bar Specimen	273
Figure 7.22	Applied load versus joint Rotation for the Headed Bar Specimen.....	276

Figure 7.23	Applied Load versus Joint Shear Distortion	277
Figure 7.24	Schematic diagram to measure Joint Distortion.....	278
Figure 7.25	Applied load versus Head Slip - Beam Bar under compression in Cycle1	279
Figure 7.26	Applied load versus Head Slip - Beam Bar under tension in Cycle1	279
Figure 7.27	Strains along Beam Bars during the first 3 increments of Cycle 1.....	281
Figure 7.28	Applied Load versus Bar Strain at the Head.....	283
Figure 7.29	Applied Load versus Strain 356 mm from head (Beam Bar).....	283
Figure 7.30	Strains along a column Bar during the first 3 increments of Cycle 1	285
Figure 7.31	Applied Load versus Column Bar Strain - 127 mm outside Joint.....	285
Figure 7.32	Applied Load versus Tie Strains - Tie at center of Joint.....	286
Figure 7.33	Applied Load versus Tie Strains - Tie at the top of the Joint.....	287
Figure 7.34	Plot of Joint Shear resisted by Concrete and Transverse Reinforcement Cycle 1	289
Figure 7.35	Plot of Joint Shear resisted by Concrete and Transverse Reinforcement Cycle 2.....	289
Figure 7.36	Plot of Joint Shear resisted by Concrete and Transverse Reinforcement Cycle 3.....	290

Chapter 1

INTRODUCTION

1.1 General

In reinforced concrete elements, compression forces are resisted by concrete and steel, while tensile forces are resisted by steel only. For this process to exist, there must be a force transfer, or bond, between the two materials. A smooth bar develops bond by adhesion between the concrete and the bar. This adhesion is quickly lost when the bar is loaded in tension. To solve this problem, deformed bars are used. In deformed bars the bond is transferred primarily by bearing on the deformations of the bar. When there is insufficient length to develop a deformed bar a standard hook is used to provide additional anchorage. Two types of standard hooks are specified by the ACI Building Code [1](Section 12.5): 90° and 180° hooks (Figure 1.1).

There are several problems associated with hooked bar anchorages. The hook occupies a large space which may lead to congestion of reinforcement and poor concrete quality. Furthermore, the required dimensions of standard hooks

frequently govern the size of the element in which the hook is anchored. Anchorage failure of a hooked bar involves crushing of concrete bearing against the inner radius of the hook. At failure, bond along the straight bar ahead of the hook will be lost and the anchorage may exhibit large slip. Slip of hooked bars is significantly larger than that of straight bars. The crushed concrete bearing against the hook forms a wedge which may cause side spalling especially if cover over the plane of the hook is small. The capacity of a hooked bar is dependent primarily on the bearing stress inside the hook which is, in turn, a function of the bar diameter. The capacity is also affected by side cover, concrete strength, and confining reinforcement.

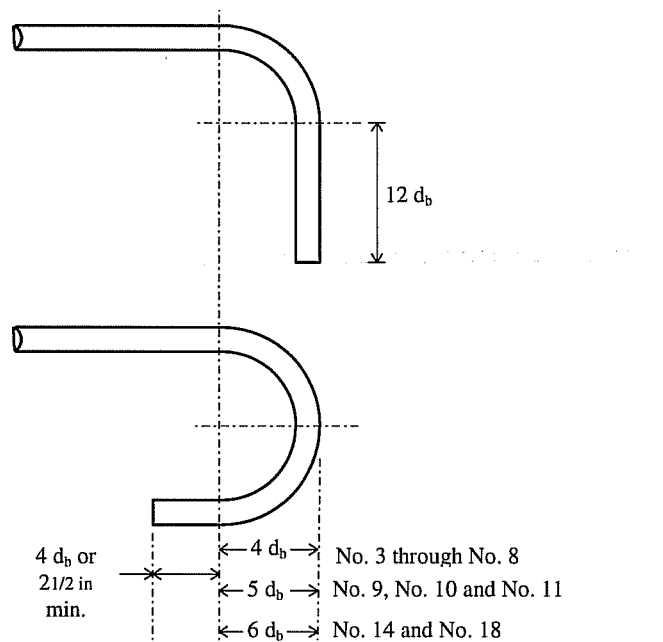


Figure 1.1 Hooked Bar details specified by the ACI Building Code [1]

In designing a hooked bar anchorage for a given element dimension it may be necessary to reduce the bar size and provide a larger number of small bars. However, such a solution aggravates congestion problems. Increasing use of high strength concrete in structures generally results in smaller cross sections leading to higher reinforcement densities. In order to use high strength concrete to its full potential, higher strength steel and larger reinforcing bars may be used.

Headed bars are ordinary deformed reinforcing bars with steel plates attached to their ends. The bar force is transferred to concrete by bearing in front of the head (Figure 1.2). The head can be varied, so that the anchorage capacity of a headed bar is independent of the bar size. Furthermore, the head occupies much less space than a hook, which means less congestion, ease of placement, more accurate dimensions for the reinforcing cage, and better concrete quality. The use of headed bars with corrosion protection (epoxy coating) may eliminate problems associated with epoxy-coated hooked bars that are bent after coating. The bending process may crack and delaminate the coating which has to be patched before concrete is placed. Headed bars used as transverse reinforcement are also expected to provide better confinement because of the head bearing effects. For these reasons, mechanical anchorages represent superior alternatives to hooked bars.

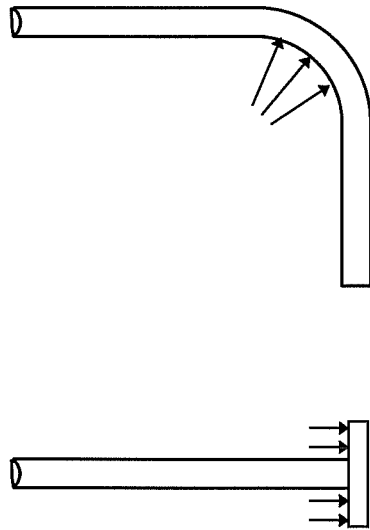


Figure 1.2 Comparison between Anchorage Mechanisms of Headed and Hooked Bars

1.2 Background

The use of headed bars was introduced in the construction of offshore platforms for petroleum and gas products in the North sea. During the last decade, headed bars were used in large quantities as longitudinal and shear reinforcement in such platforms. In these types of structures, with very high reinforcement densities, headed bars provided a practical and economical alternative to bundled hooked bars. Recently, headed bars were also used in strengthening and repairing footings of highway structures.

Headed bars are manufactured by attaching steel plates (or heads) to the reinforcing bars either by some form of welding or by threading the bar and the

head and screwing them together. However, the increasing use of headed bars is a result of the introduction of an economical and reliable welding process, called friction welding. In this process, the head is rotated with a high speed (about 1500 rpm) with the bar pressed against it. The heat resulting from friction welds the bar and the head together (Figure 1.3). Friction welding technique ensures that the full capacity of high strength reinforcement can be developed. Other advantages are economic production and consistent weld quality with minimal quality control provided that the steel in the bar and the plate has certain chemical properties.

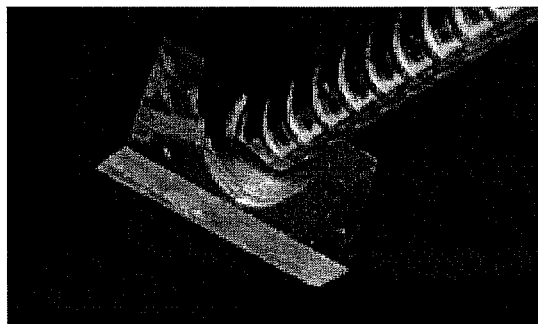


Figure 1.3 Headed Bar

1.3 Objectives

The goals of this study are to determine the anchorage behavior of headed bars in joints between structural elements. The overall behavior of joints

constructed using headed bars will be investigated also. The test data gathered from this study will be used to develop mathematical models for determining the behavior of headed bars in joints. Recommendations for code design provisions for anchorage of headed bars will be provided.

1.4 Scope

To provide an understanding of the anchorage behavior of headed bars this study was divided into three phases.

1.4.1 Basic Studies on Headed Bars

This phase consisted of pull-out tests on headed bars embedded in concrete cubes. Tests were designed to assess the influence of load cycling and anchorage conditions on the behavior of headed bars anchored near concrete surfaces (edge bars). The variables included head dimensions, number of load cycles, and anchoring the head behind a crossing bar.

Eleven exploratory tests were also conducted to investigate the possibility of using headed reinforcement as shear and confinement reinforcement. The performance of headed bars in orientations simulating confining reinforcement was studied by constructing simple specimens in which headed bars overlapping at a corner at right angles to each other were subjected to static loads. Variables

included head dimensions and orientation. Concrete cover over the bars was varied to simulate spalling of concrete.

1.4.2 Anchorage in Exterior Joints

The behavior of exterior joints constructed using headed bars instead of hooked bars was studied. Thirty-two large scale specimens simulating exterior joints in a structure were tested to assess the effects of different variables on the behavior of joints under monotonic loading. The variables included head area, head aspect ratio and orientation, size of anchored bars, embedment length, side concrete cover, and confining reinforcement.

1.4.3 Effects of Seismic Loading

The goal of this phase of the research program was to provide an insight to potential benefits of using headed bars in connections exposed to seismic loads. One exterior beam to column subassembly was constructed and tested to examine the effect of headed bars on behavior under cyclic loading. The behavior of this specimen was compared to a similar specimen constructed with standard 90-degree hooked bars, reported in the literature.

Chapter 2

PREVIOUS RESEARCH

2.1 General

Several studies on headed bars were reported in the last decade. Most of these studies were directed towards offshore applications. However, in the last few years designers recognized the potential of using headed bars in regular structural applications and initiated several studies involving structural subassemblages simulating elements in residential and highway structures.

Previous research on headed bars consists mainly of proof tests conducted to examine the performance of a specific application. The number of tests conducted in each study was limited, preventing a systematic evaluation of the effects of different variables. The first phase of this study, conducted by DeVries [2], was the only comprehensive study directed towards understanding the effects of different variables on the anchorage behavior of headed bars. However, several studies on anchor bolts placed near concrete edges provide

useful information. Therefore, in this chapter, relevant research on anchor bolts as well as headed bars will be reviewed.

2.2 Anchor Bolt Studies

In 1979 Hasselwander [3] reported 23 pullout tests on high strength anchor bolts embedded in specimens simulating typical drilled shaft footings. The end anchorages of the bolts consisted of a nut or a nut and a washer. Variables included bolt diameter, embedment length, clear cover, and bearing area. In addition, Hasselwander reported a series of 12 exploratory tests to investigate the effects of cyclic loading, application of axial load normal to the edges of the specimen, interaction between groups of bolts, and transverse reinforcement on the behavior.

The embedment depths used in this test program were relatively large (a minimum of 10 times the bolt diameter). As a result, the failure modes of the specimens did not include pull-out cone failure. The modes of failure fell into three categories: (1) failure of the bolt shaft, (2) cover spalling, and (3) wedge splitting of the cover. Although these three categories represent distinct failure modes, combinations of these modes were observed in several instances. The anchor bolts transferred the applied load to concrete through three mechanisms in sequence: (1) steel to concrete bond, (2) bearing against the anchorage device,

and (3) wedging action by the cone of crushed and compacted concrete in front of the anchorage device. The exact mechanism of transmission from one mechanism to the next was highly indeterminate. However, steel to concrete bond was always lost in the very early stages of loading. The load transferred through the each of the other two mechanisms was dependent on the concrete cover and embedment length. Test results indicated that the clear cover and the bearing area were the prime variables influencing the strength of anchor bolts. Hasselwander developed the following analytical model for single anchor bolts loaded in tension,

$$T = A_b \sqrt{f'_c} \left[96 + 142 \ln \left(\frac{1}{1 - \frac{C_w}{C'}} \right) \right] \quad 2.1$$

where T is the anchorage capacity of the anchor bolt in lb, A_b is the net bearing area in in.², C_w is the clear cover over the anchorage device in in., and C' is the clear cover over the bolt in in.

Exploratory tests indicated that cyclic loads at service level did not influence the slip or capacity of the bolts. Placing transverse reinforcement (hair pins) close to the anchorage device provided lateral restraint to cover spalling, and increased strength and ductility. Applying axial load normal to the edges of the specimen to a level causing concrete cracks on the side close to the anchor bolt

resulted in significant reduction in strength. The strengths of two bolts with small spacing were drastically reduced over that of isolated bolts due to the interaction of the spalled side cover for each bolt.

Furche and Eligehausen [4] conducted 35 tests on single headed studs placed near a free concrete edge. The variables included embedment depth, edge distance, and head diameter. Side spalling, or side blow-out failure, occurred in most of the tests. The diameter of the lateral blow-out area was 6 to 8 times the edge distance. Test results indicated that the critical edge distance at which the failure mode switches from pullout cone to side blow-out depended on the embedment depth and the bearing area. For practical values of load bearing areas, a ratio between the edge distance and embedment depth ranging between 0.2 and 0.4 represents a transition zone between the two failure modes. Once the failure was governed by side blow-out mode, changes in embedment depth did not affect the capacity. The side blow-out capacity increased with increase in bearing area and was almost directly proportional to the edge distance.

Furche and Eligehausen developed a model for the anchorage capacity using the assumption that the lateral blow-out failure is caused by the quasi hydrostatic pressure in the area of the head. This pressure produces a lateral force, Z , equal to αF , where F is the bolt force. The factor α was taken as

$$\alpha = 0.1 \sqrt{P_u / f'_c} \quad 2.2$$

with $P_u = F_u / A_b$

where f'_c is the concrete strength in MPa, F_u is the failure load in N, and A_b is the net bearing area in mm^2 . Using Equation 2.2 the anchorage capacity as governed by side blow-out failure is given by

$$F_u = 31 \cdot m \cdot A_b^{1/3} \cdot f_c'^{2/3} \quad 2.3$$

The influence of concrete strength in Equation 2.3 ($f_c'^{2/3}$) is larger than usually assumed in models describing the splitting strength of concrete ($\sqrt{f'_c}$). Therefore, a multiple regression analysis was performed assuming that F_u is proportional to $\sqrt{f'_c}$, and the following equation was obtained after rounding up exponents:

$$F_u = 16.8 \cdot m \cdot \sqrt{A_b} \cdot \sqrt{f'_c} \quad 2.4$$

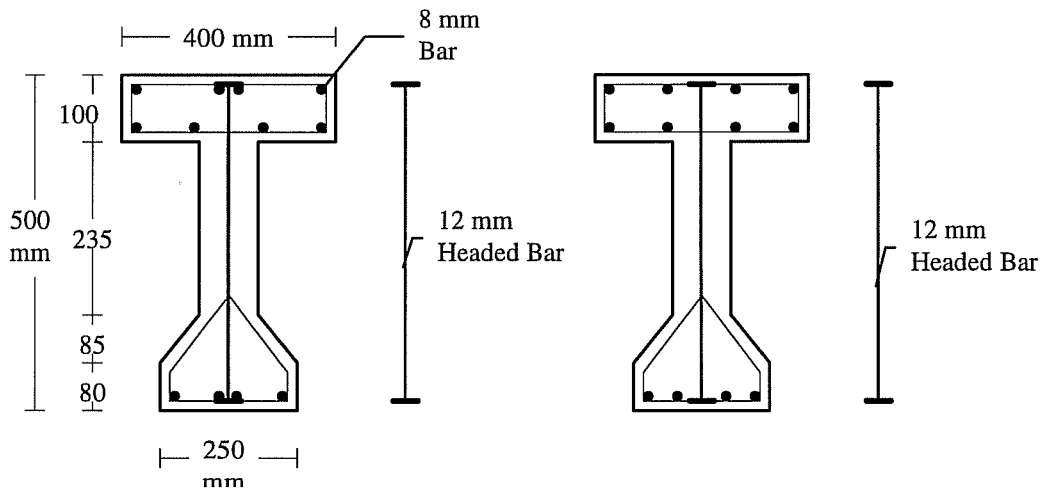
2.3 Headed Bar Studies

In 1993 Olav Olsen [5] published a report summarizing previous studies concerning the use of headed bars in reinforced concrete. These studies included pull-out tests, beam tests, and axial load tests.

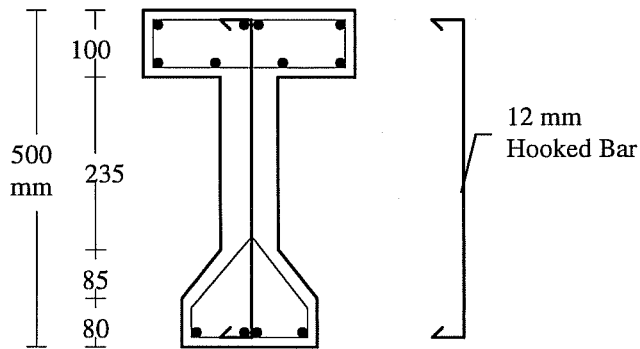
Eight pull-out tests of 20 mm (#6) bars embedded at the center of 300 mm (11.8 in.) concrete cubes were conducted to investigate the anchorage behavior of headed bars in normal and light weight aggregate concrete, and the effect of crossing bars in the anchorage zone of the head. The concrete strength in this study was relatively high (59 MPa or 8560 psi for normal density concrete, and 72 MPa or 1040 psi for light weight concrete). Head dimensions were 65×30×16 mm. All tests were terminated at yielding of the bar without any sign of anchorage failure. No damage in the anchorage zone was observed. However, some minor cracks were observed in the normal density concrete specimens when they were examined using a microscope. The load slip curves under cyclic loading revealed that the behavior for normal density and light weight aggregate concrete specimens was very similar. The slip in the light weight aggregate specimens was slightly lower than normal density concrete specimens and the difference is attributed to variation in concrete strength. As cracking in the anchorage area was almost absent, no difference was observed between specimens with and without crossing bars in the anchorage zone.

The report summarized shear tests of 3 reinforced concrete I-beams with identical cross sections (Figure 2.1). Shear reinforcement in one of the beams consisted of 90° bent stirrups. Double headed bars were used in the other two specimens. One of the headed bar specimens had longitudinal bars passing

through the anchorage zone of the head. The load-deflection curves for the three specimen were almost identical. As the shear reinforcement in all beams yielded before failure without significant slip, the influence of using headed bars for shear reinforcement and placing longitudinal bars in the anchorage zone was not assessed.



a) Headed Shear Reinforcement



b) Hooked Shear Reinforcement

Figure 2.1 Reinforcement Details for Beam Specimens [5]

Two prisms were tested under axial load to determine the effectiveness of headed bars in confining the concrete. The specimens dimensions were 406×406×1067 mm (Figure 2.2). The transverse reinforcement consisted of headed bars with a reinforcement ratio of 1.5% in both directions. Test results indicated that there was very little reduction in the axial capacity after spalling of the concrete cover. The confined core was capable of maintaining the capacity up to 3% axial strain. This exceptional behavior was attributed to the positive anchorage of the heads which reduced slip of the transverse reinforcement and limited cracks in concrete.

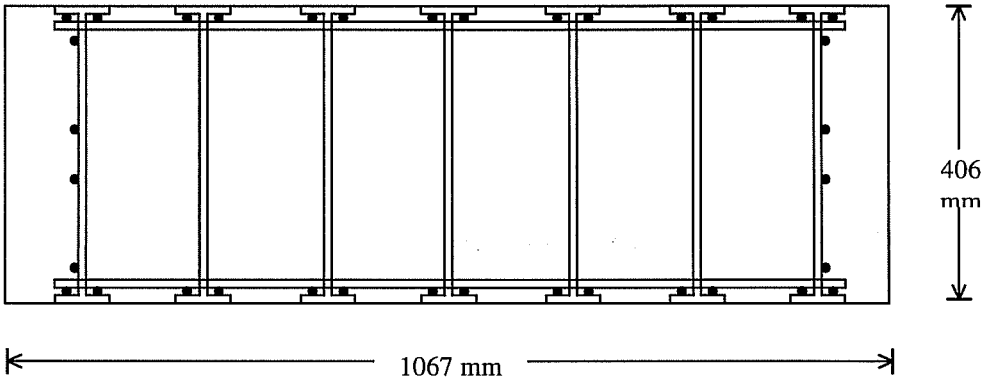


Figure 2.2 Reinforcement Details of Prism Tests [5]

2.4 University of Toronto Tests

Collins and Gupta [6] tested 14 beams to investigate the behavior of high performance reinforced concrete elements subjected to high compression (up to $0.9 f_c'$) and shear. The specimens were divided into 3 groups; 5 specimens without shear reinforcement, 6 specimens with headed transverse reinforcement used for shear reinforcement, and 3 specimens with 90° bent stirrups for shear reinforcement. Typical reinforcement details are shown in Figure 2.3.

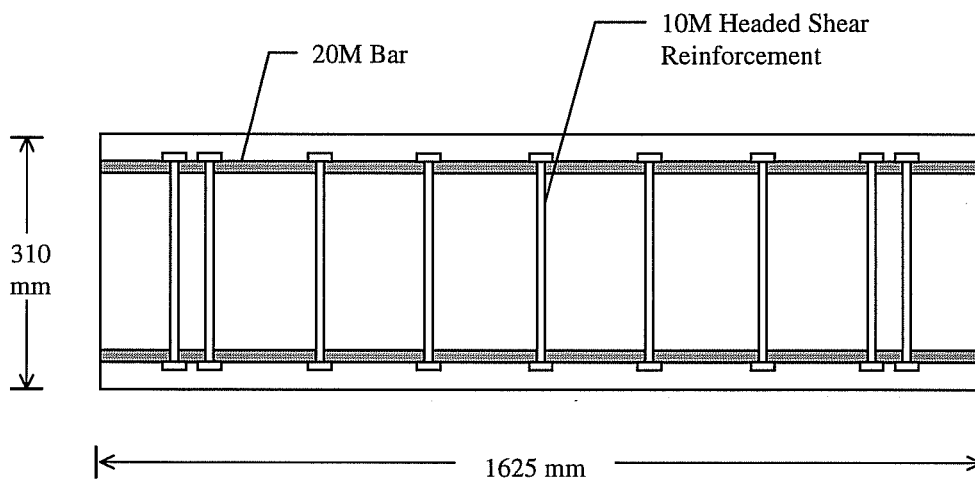


Figure 2.3 Specimens tested by Collins and Gupta [6]

In general, the use of transverse reinforcement caused a substantial increase in the strength of the specimens. Headed stirrups were more effective than 90° bent stirrups. Initially the behavior of the specimens was similar, but at

large strain levels the 90° hooks opened and the stirrups lost their effectiveness. Headed bars were also more effective in restraining longitudinal bars, preventing buckling.

2.5 Clarkson University Joint Tests

McConnell and Wallace [7] reported 18 beam-column knee joints tested under cyclic loading to develop recommendations for seismic design and to compare the performance of knee joints constructed using headed and hooked bars. Three joints were constructed using headed bars for longitudinal reinforcement. Reinforcement details of one of these specimens is shown in Figure 2.4.

The behavior of the headed bar specimens was as good as, or superior to, similar joints constructed using 90° standard hooks in the cases where vertical stirrups with areas at least equal to half the beam bar areas were placed close to the beam bar heads (Figure 2.4). In the specimen without these stirrups, concrete on the top side of the beam spalled and the top bars pulled out. This failure mode was prevented by the restraining effect of the vertical stirrups. The condition of the specimen after testing is shown in Figure 2.5. A concrete block on the top corner of the joint was pushed out due to the compressive forces resisted by the heads. McConnell and Wallace recommended the reinforcement detail shown in

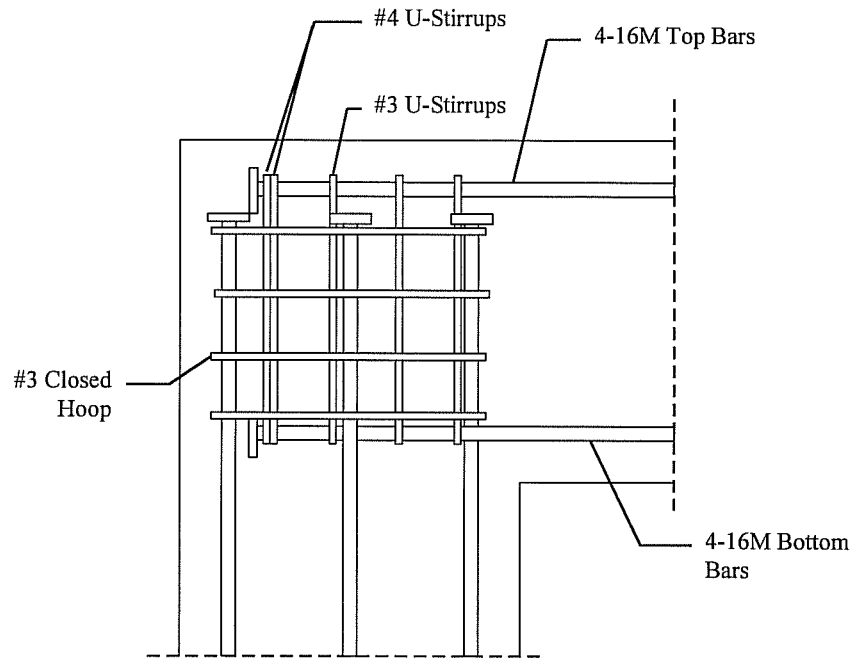


Figure 2.4 Reinforcement Details of Knee Joint tested by McConnell and Wallace [7]

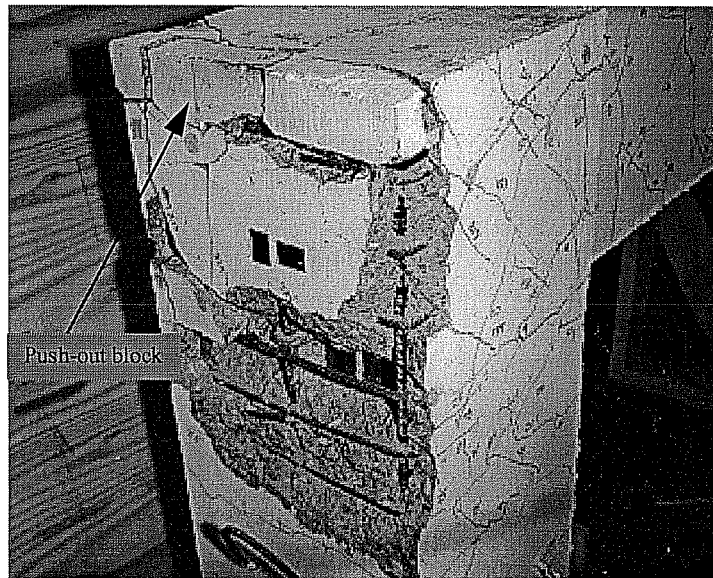


Figure 2.5 Knee Joint specimen at end of Test - McConell and Wallace [7]

Figure 2.6 to prevent this failure mode. Although the recommended detail was not tested, the improved capacity of the headed bar specimens (over hooked bar specimens) indicated that the reduced slips of headed bars leads to improvement of the overall behavior.

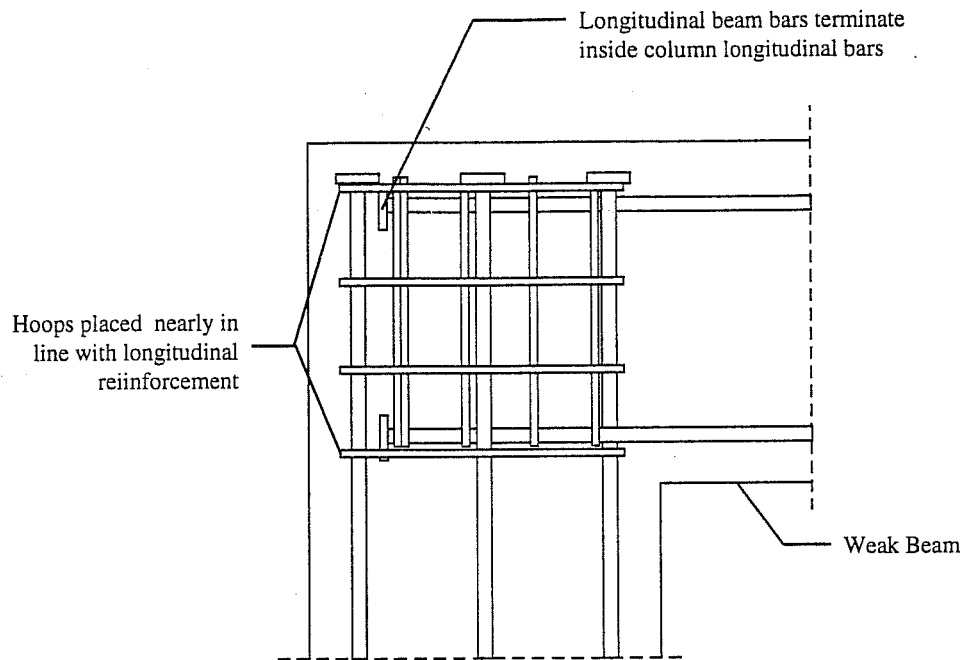


Figure 2.6 Recommended Reinforcement Detail - McConnell and Wallace [7]

2.6 Bridge Knee Joint

SEQAD Consulting Engineers [8] tested a bridge column/cap-beam knee joint using headed reinforcement wherever possible (Figure 2.7). All column and beam longitudinal rebar was headed. Cap-beam stirrups were made of U-shaped headed bars. Joint transverse reinforcement consisted of headed horizontal links.

The specimen was patterned after a previous test series on specimens constructed using hooked bars and closed ties or spirals, to allow comparison. The load-deflection behavior of the headed bar specimen was identical to that of a well-designed conventionally reinforced companion unit. Degradation was very gradual and the strength dropped 22% only after 5 inelastic cycles. The test indicated that heads provide excellent anchorage to all types of terminating reinforcement.

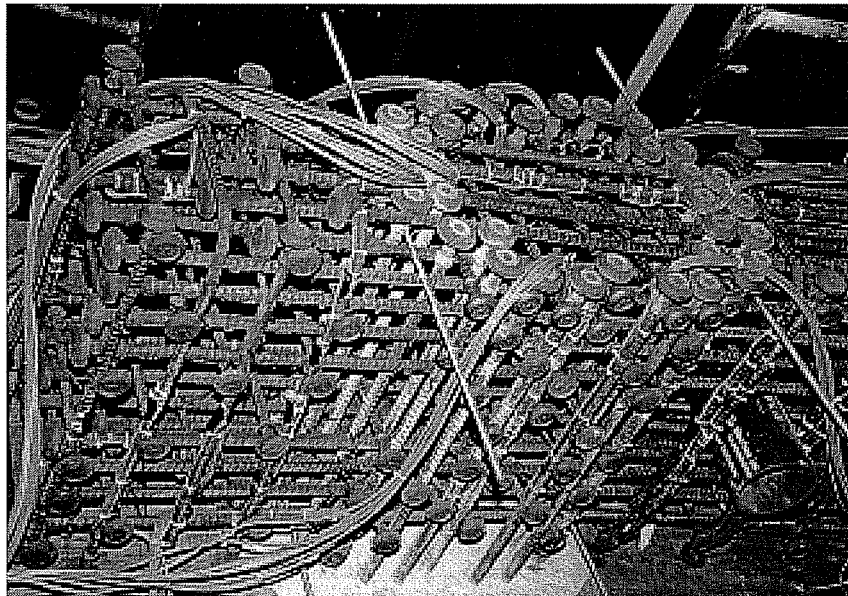


Figure 2.7 Reinforcement of Joint and Cap - SEQAD [8]

2.7 University of Texas Pull-out Tests

DeVries [2] conducted over 140 pull-out tests on headed bars embedded near the edges of concrete cubes in a study directed towards developing

comprehensive design recommendations to predict the anchorage capacity of headed reinforcement. Variables included embedment depth, concrete cover, concrete strength, transverse reinforcement, spacing of bars, and bar diameter. Other variables related to the anchorage head were orientation, area, shape, and thickness.

Two modes of failure were observed; pullout cone and side blow-out. While the pullout cone failure was comparable to that of anchor bolts under tension, side blow-out failure is more likely to occur under anchorage situations in real structural elements. The results of 21 tests with pullout cone failure indicated that the anchorage capacity increased significantly with the increase of embedment depth, edge distance, and concrete strength. On the other hand, the side blow-out capacity of headed bars was increased with the increase of edge distance, head bearing area, and concrete strength. Corner placement and close spacing of bars reduced the ultimate load significantly. Transverse reinforcement improved the ductility but did not increase the anchorage capacity.

DeVries developed a physical model for the side blow-out capacity using the assumption that tensile stresses over the blown-out area resist side spalling. The assumed failure surface consisted of a pyramid with a base dimension equal to 6 times the concrete cover. The model utilized the same assumptions used by Furche and Eligehausen, except that Equation 2.2 was calibrated to headed bar

test results and changed to $\alpha = 0.517 \sqrt{P_u / f'_c}$. The new model had the following form,

$$F_u = 0.0107 \cdot C^{1.33} \cdot A_n^{1/3} f'_c{}^{2/3} \quad 2.5$$

where F_u is the capacity in KN, C is the edge distance of the bar, A_n is the net bearing capacity in mm^2 , and f'_c is the concrete strength in MPa.

Test results were also used in a multiple regression analysis to develop a best fit equation. After rounding exponents and assuming that F_u is proportional to $\sqrt{f'_c}$, the equation had the following form,

$$F_u = 0.017 \cdot m \cdot \sqrt{A_b} \sqrt{f'_c} \quad 2.6$$

This equation is very close to Equation 2.4 developed by Furche and Eligehausen. Separate multipliers were developed to account for corner placement and close spacing of bars. Equation 2.6 is multiplied by the ratio of the available failure surface area and the typical failure surface area of the bar, given by A_{bo} / A_{bon} (as defined in Figure 2.8). In addition, the capacity of corner bars is further reduced to account for lack of resistance at a corner by a factor ψ , given by

$$\psi = 0.7 + 0.3 \frac{C_2}{3C_1} \leq 1 \quad 2.7$$

where C_2 is the larger edge distance. Implementing these factors led to better estimates of measured capacities of corner bars and groups of bars.

Although the proposed design equation does not indicate that the head thickness affect the anchorage capacity, DeVries proposed that the head should be thick enough to prevent yielding.

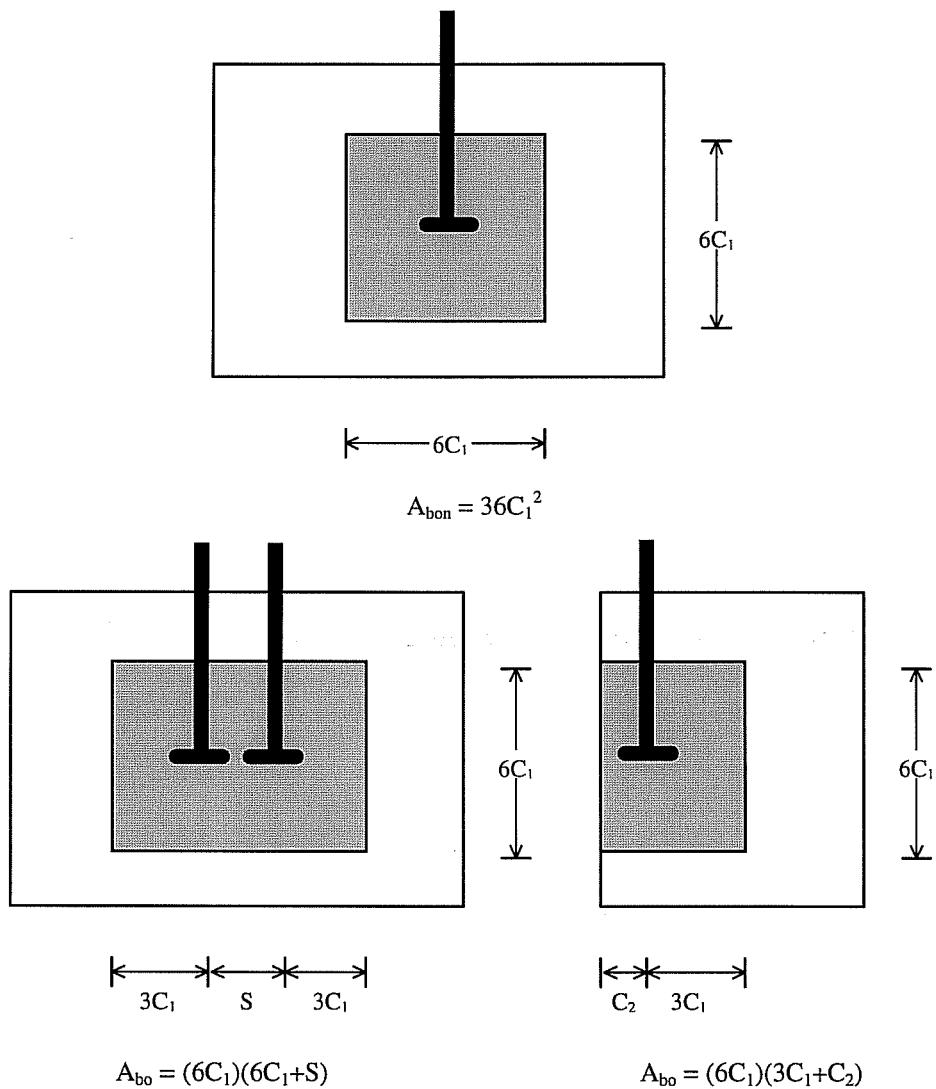


Figure 2.8 Blow-out Areas for various configurations - DeVries [2]

Chapter 3

BASIC STUDIES OF HEADED BARS

3.1 Introduction

In this phase of the test program, additional pullout tests were conducted to investigate the effects of load cycling and anchorage condition at the head on the capacity and behavior of headed bars. The planning of these tests was based on the results reported by DeVries [2], and the tests were divided into two groups.

The first group consisted of 14 pullout tests on bars embedded in concrete cubes (similar to those used by DeVries). The variables included head dimensions, number of load cycles, and anchoring the head behind crossing bars.

The second group consisted of 11 exploratory tests investigating the possibility of using headed bars as transverse reinforcement. The performance of headed bars in orientations simulating closed hoops was studied by constructing simple specimens in which headed bars overlapping at a corner at right angles to each other were subjected to static loads.

3.2 Group 1: Pullout Tests

3.2.1 Design of Specimens

The specimen design for group 1 was similar to that used by DeVries [2] for deep embedment tests in order to avoid concrete cone failure. Previous research [4] recommended embedment depth greater than 2.5 to 5 times the concrete cover in order to prevent a concrete cone failure. In this test series, the minimum ratio between embedment depth and concrete cover was 10. The large embedment depth was required to make sure that confinement effects of the reaction from load application did not affect the anchorage capacity.

Headed bars were embedded near the edges of 915 mm (36 in.) deep concrete cubes. All bars were sheathed with PVC tubes to eliminate transfer of force to concrete along the bar. The minimum spacing between the bars was 432 mm (17 in.) to prevent overlapping of the blown out area for adjacent tests. This group included a total of fourteen tests, out of which four tests were corner bars.

3.2.2 Variables

The properties of the fourteen pullout tests are summarized in Table 3.1. All of the headed bars were 35 mm (#11) to allow application of relatively high loads without yielding. Tests P1 through P4 were standard edge bar tests, similar to those conducted by DeVries. The heads of these specimens were not anchored

behind crossing bars, and monotonic load was applied up to failure. Standard 90x90 mm heads (as provided by the manufacturer) were used for corner bars. Because the increase in capacity due to anchoring the heads behind crossing bars could not be estimated, smaller heads were used for edge bar tests to reduce the capacity and avoid bar yielding. The head The following variables were studied in this phase of the test program:

Table 3.1 Parameters for Pullout Tests (35 mm Bars)

Test	Head (mm)	Head Area (mm ²)	Cover (mm)	Orientation	Load	Crossing Bar
P1	35x90x20	3150	57	edge	Mono	-
P2	70x44x20	3080	57	edge	Mono	-
P3	90x90x20	8100	38	corner	Mono	-
P4	55x55x25	3025	57	edge	Mono	-
P5	90x35x20	3150	57	edge	15 cycles	-
P6	70x44x20	3080	57	edge	15 cycles	-
P7	90x90x20	8100	38	corner	15 cycles	-
P8	90x90x20	8100	38	corner	10 cycles	-
P9	90x90x20	8100	38	corner	5cycles	-
P10	35x90x20	3150	57	edge	Mono	#11
P11	35x90x20	3150	57	edge	Mono	#8
P12	70x44x20	3080	57	edge	Mono	#11
P13	70x44x20	3080	57	edge	Mono	#8
P14	55x55x25	3025	57	edge	Mono	#8

1) Cyclic Loading

Tests P5 and P6 were used to determine the influence of cyclic loading on the anchorage capacity and load-slip behavior of edge bars. Both specimens were initially loaded up to 80% of the estimated anchorage capacity (taken as the anchorage capacities of standard tests P1 and P2, respectively). After the load was cycled 15 times between a range of 5% and 80% of the estimated capacity the specimens were loaded up to failure in the 16th cycle.

The influence of cyclic loading on corner bars was determined using a similar procedure in test P7 (compared to standard test P3). In addition, the load was cycled in tests P9 and P8 (corner bars) 5 and 10 times, respectively, to assess the effect of the number of cycles on the anchorage capacity and load-slip behavior.

2) Placing a Crossing Bar in the anchorage zone of the Head

The heads in tests P10 through P14 (edge bars) were anchored behind crossing bars. The effect of this anchorage condition was assessed by comparing the anchorage behavior of these tests to those of P1, P2, and P4.

Two sizes of crossing bars were used, 25 mm (#8) and 35 mm (#11) to simulate longitudinal bars in the structural element in which headed bars are anchored. The length of the crossing bars was 610 mm (24 in.), divided equally

on both sides of the headed bar. Although the concrete cover over the headed bars was 57 mm, the clear cover over the 25 mm crossing bars was about 23 mm (0.9 in.), because the flash (a by product of the welding process) prevented placing it in contact with the headed bar (Figure 3.1). As the cover over the headed bars was kept constant to allow comparison of capacities, the clear cover over the 35 mm (#11) crossing bars was even less (about 13 mm or 0.5 in.). Although the concrete cover over a crossing bar in most reinforced concrete applications is more than 38 mm (1.5 in.), increasing the side cover was avoided to prevent yielding of the headed bars before failure and to avoid introducing another variable.

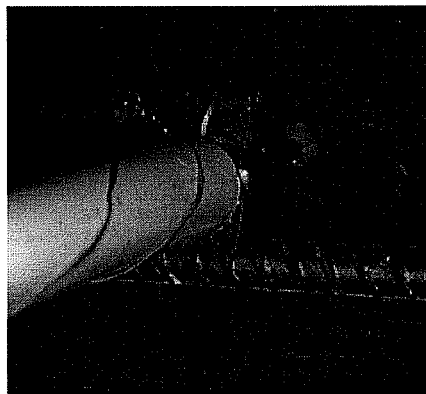


Figure 3.1 Head Anchorage behind Crossing Bars

3) Head Dimensions

Tests P10 through P14 were designed to determine the influence of head aspect ratio on the anchorage capacity for heads anchored behind crossing bars.

Although DeVries [2] concluded that there is no correlation between the head aspect ratio and the anchorage capacity, it was expected that the effectiveness of anchorage behind crossing bars will be significantly influenced. Tests P10 and P11 represent a favorable anchorage condition, in which the clear head dimension (beyond the flash) is about 19 mm (3/4 in.) on each side of the bar. On the other hand, test P14 represents the worst possible condition (for a head anchored behind a crossing bar), with a clear head dimension equal to 2 mm (0.08 in.). Tests P12 and P13 represent an intermediate condition.

3.2.3 Materials

In all the specimens tested, each bar size (35 mm or #11, and 25 mm or #8) was from the same heat and had a parallel deformation pattern. The stress strain diagrams for both sizes are shown in Figure 3.2. The diagrams are based on elongations measured over a 203 mm (8 in.) gage length.

The concrete cubes were constructed using a nominal 27.5 MPa (4000 psi) concrete, supplied from a local-ready mix plant. The mix properties are shown in Table 3.2. Ten gallons of water were added at the time of casting (in the laboratory) in order to maintain a 102 mm (4 in.) slump. The variation of concrete compressive strength with time is shown in Figure 3.3. The concrete

strength at the time of testing was 22 MPa (3200 psi). The strength was obtained from tests of standard 152×305 mm (6×12 in.).

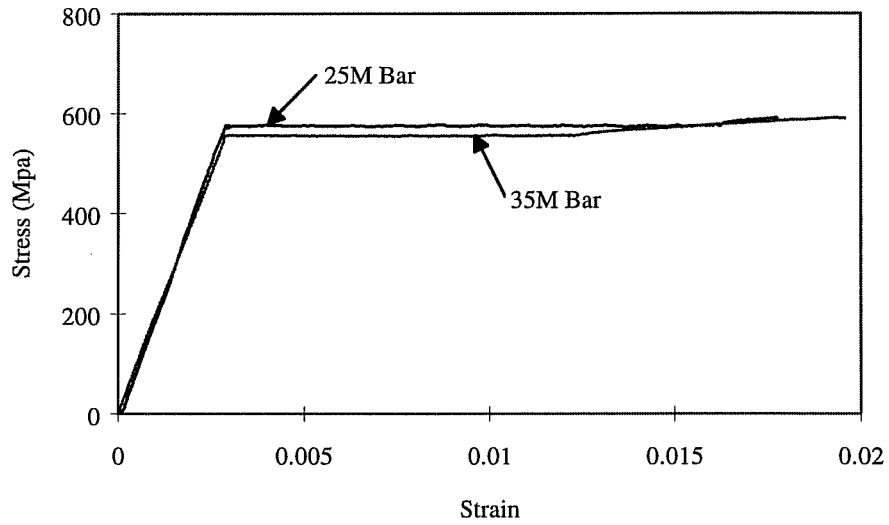


Figure 3.2 Stress - Strain curves for 25M and 35M Bars

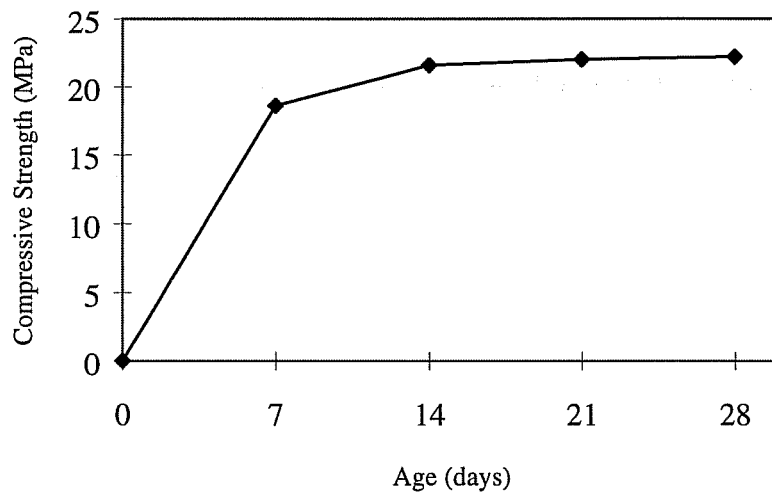


Figure 3.3 Concrete Strength for pullout tests

Table 3.2 Concrete mix proportions for pullout tests

UT4000A	
Nominal f'_c , psi (MPa)	4000 (27.6)
Max. size aggregate, in. (mm)	3/4 (19)
Cement, lb/cyd	400
Fly ash, lb/cyd	-
Water, lb/cyd	267
Course aggregate, lb/cyd	1862
Fine Aggregate, lb/cyd	1422

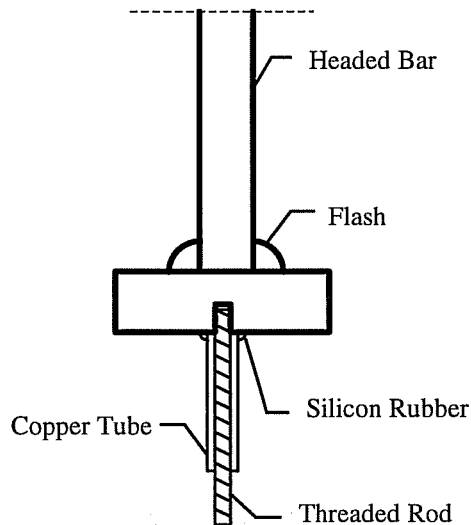


Figure 3.4 Setup used for measuring Head Slip

3.2.4 Instrumentation

Each test was instrumented to measure the applied load and head slip of the anchored bars. Strain gages were placed 23 mm (0.9 in.) from the edge of the head on both sides of the bar in P10.

The applied load was determined using a 900 kN (200 kip) capacity load cell. Slip of the anchored headed bars was measured through a threaded rod attached to the head. This was accomplished by drilling a hole in the center of the head, threading the hole and screwing a 6 mm (1/4 in.) threaded rod in it (Figure 3.4). A 13 mm (1/2 in.) copper tube was placed over the length of the threaded rod exposed to concrete to allow the free movement of the rod and to prevent bond. The copper tube was sealed at the bar using silicon rubber to prevent concrete from entering the tube. The threaded rods extended from the heads of the anchored bars to the bottom of the specimens (through the bottom of the form). A 50 mm (2 in.) linear potentiometer was attached to each threaded rod to measure its movement relative to the bottom surface of the cube, which was taken as the reference point. All instrumentation was connected to a data acquisition system and readings at each load increment were taken. In addition, an electronic voltmeter with a peak-hold capability was connected to the load cell to capture the maximum load in case the specimen failed during loading.

3.2.5 Specimen Fabrication

Three forms were constructed for casting four 914 mm (36 in.) deep concrete blocks, used for the pullout tests. The plan dimensions of the cubes were either 914×914 mm (36×36 in.) or 1220×1220 mm (48×48 in.). Forms were built

using 19 mm (3/4 in.) plywood stiffened with 51×108 mm (2×4 in.) lumber, in separate sections then bolted together to allow for the easy removal and reuse. Wooden braces were used to control cover over the bar and to keep the bars in vertical position during casting. Figure 3.5 shows the form and steel in place prior to casting. Concrete was placed directly from a ready-mix truck. After consolidating the concrete, the exposed concrete surface was screeded and trowelled to provide a smooth surface for bearing the reaction from load application.

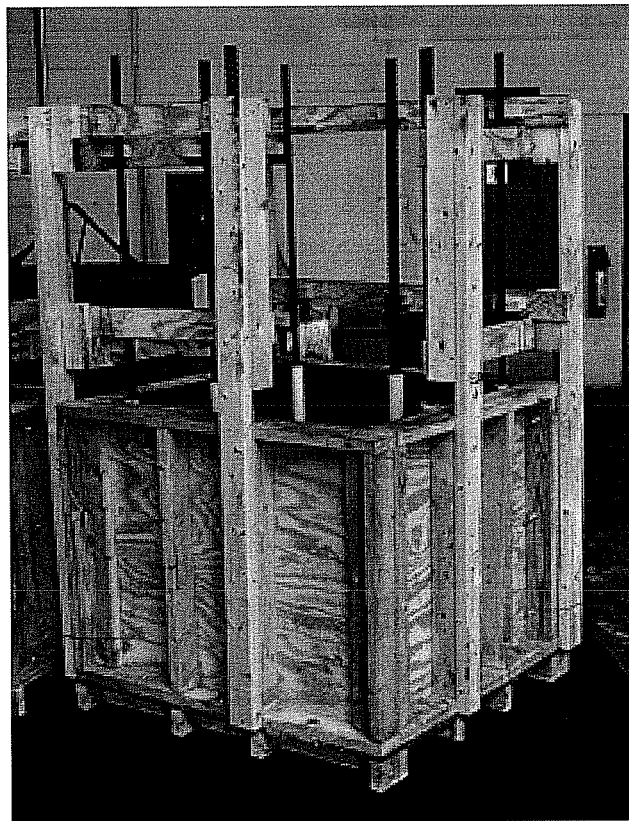


Figure 3.5 Specimen ready for casting

3.2.6 Test Setup

The setup used for testing is shown in Figure 3.6. Hydrostone was placed between the concrete surface and a 25 mm (1 in.) bearing plate to provide a horizontal bearing surface, and uniform pressure on the concrete. The tensile load was applied using a 900 KN (200 kip) capacity center-hole hydraulic ram. The ram and the load cell were centered over the bar, with the ram bearing on the steel plate. The ram load was transferred to the test bar by means of a wedge grip assembly. The assembly was mounted over the load cell with the wedges gripping the bar.

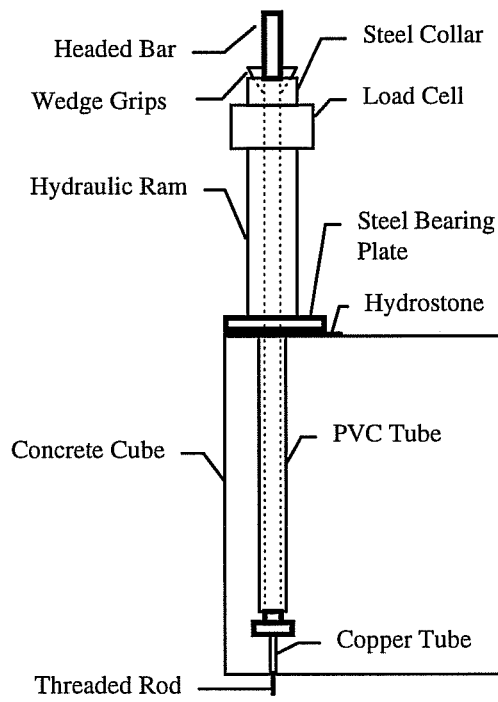


Figure 3.6 Test setup for Pullout Tests

3.2.7 Test Procedure

After all instrumentation and loading equipment were in place, testing began by applying tension to the anchored bars in 22 KN (5 kip) increments up to failure, in the case of monotonic loading. Each load stage was sustained for two minutes during which the specimen was examined and cracks were marked before applying the following increment. In specimens P5 to P9 this sequence of loading was used up to 80% of the estimated capacity. The same load increment was used in the first, second, fifth, tenth, and fifteenth cycles. In other cycles, readings were taken at the high load (80%) and the low load (5%) only. In the last load cycle, a 22 KN (5 kip) load increment was used, and the bar was loaded up to failure.

3.2.8 Test Results

The ultimate loads of the eighteen pullout tests are summarized in Table 3.3. The corresponding head slips are also listed. The behavior of the standard tests (P1 to P4) will be described in detail in this section. The behavior of other tests will be compared in the following section to evaluate the influence of the different variables on the anchorage capacity and the load-slip behavior.

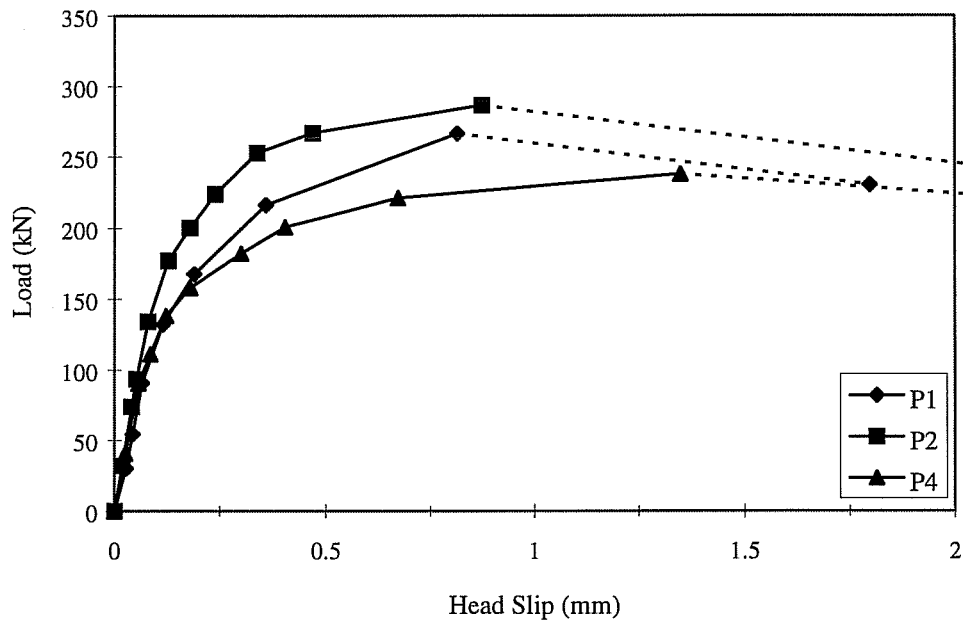
The load-slip responses of tests P1, P2, P3 and P4 are shown in Figure 3.7. Head slip increased with a constant stiffness until the load was about 160 KN

Table 3.3 Results of Pullout tests

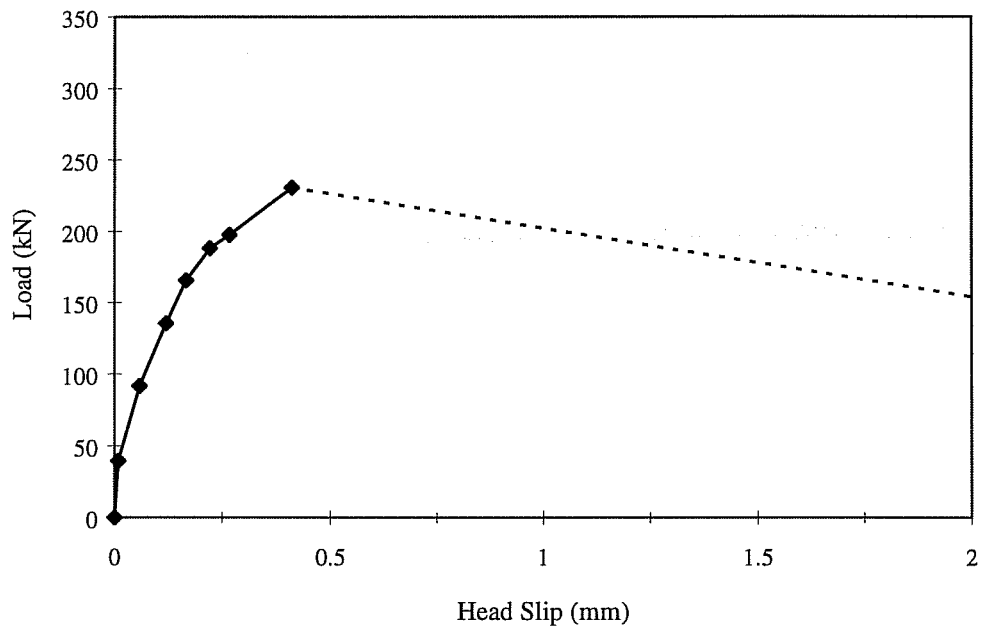
Test	Orientation	Load type	Crossing Bar	Slip (mm)	P _{max} (KN)
P1	edge	Mono		0.81	289
P2	edge	Mono		0.87	302
P3	corner	Mono		0.41	230
P4	edge	Mono		1.35	238
P5	edge	15 cycles		1.06	292
P6	edge	15 cycles		1.17	276
P7	corner	15 cycles		0.4	222
P8	corner	10 cycles		0.27	231
P9	corner	5cycles		0.38	228
P10*	edge	Mono	#11	-	369
P11	edge	Mono	#8	1.28	357
P12	edge	Mono	#11	1.6	324
P13	edge	Mono	#8	1.98	335
P14	edge	Mono	#8	1.66	263

* Slip measurements were not reliable for this test

(36 kip). Beyond this point, the stiffness decreased up to the peak load. At maximum load, the head slip for tests P1, P2, and P4 (edge bars) was 0.8, 0.9, and 1.4 mm (0.032, 0.034, and 0.05 in.), respectively. The head slip for P3 (corner bar) was 0.4 mm (0.016 in.) at maximum load. It should be noted that the head area for the corner bar was about 2.6 times larger than that of edge bars. At failure, the load dropped to a fraction of the maximum and the head slip increased significantly.



a) Edge Bars



b) Corner Bar (P3)

Figure 3.7 Load-Slip behavior for Standard Tests

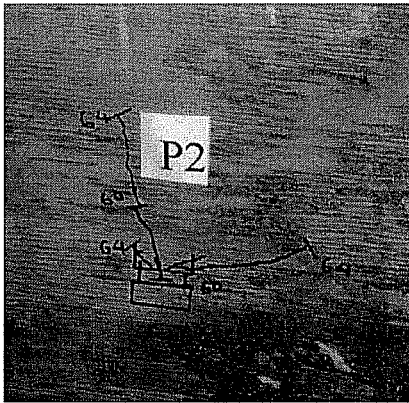
Cracking was observed around the head when the specimen was close to failure (at about 95% of the capacity). At failure the side cover spalled suddenly (with a popping sound in some cases). Figure 3.8 shows the cracking patterns just before failure and after failure for test P2. The spalled cover was easily removed, and a wedge (similar to that described in previous studies) was noted on the bearing side of the head. Although the three edge tests (P1, P2, and P4) had the similar side cover and almost the same head area, the areas of the spalled concrete as well as the ultimate loads were not identical.

3.2.9 Effects of Different Variables

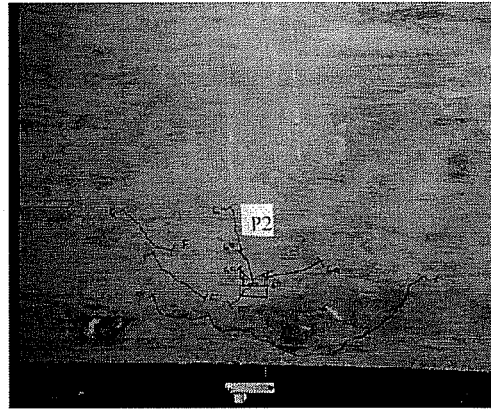
1) Cyclic Loading

The effect of cycling the load 15 times between 5% and 80% of the anchorage capacity is shown in Figure 3.9. The maximum strength reduction due to load cycling was 9% (test P6). The influence of the number of cycles on the anchorage capacity is shown in Figure 3.10. Increasing the number of cycles from 5 to 10 did not cause any reduction in capacity. Cycling the load 15 times caused a 4% decrease in capacity. The differences in capacities described above (shown in Figures 3.9 and 3.10) are within the experimental scatter recognized in the previous phase of the experimental program [2]. However, it should be noted that while two tests out of the five conducted with cyclic loading showed recognizable

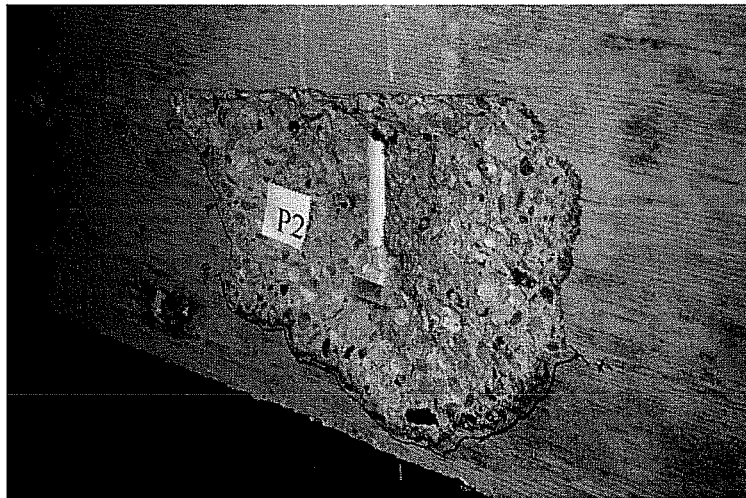
reduction in capacities (9 and 4%), none of the other three tests showed significant increase in capacity (when compared to standard tests), indicating that load cycling might have caused a slight drop in capacity.



a) Cracking Pattern just before failure



b) Failure Pattern



c) After removing Spalled Concrete

Figure 3.8 Cracking and failure patterns - Test P2

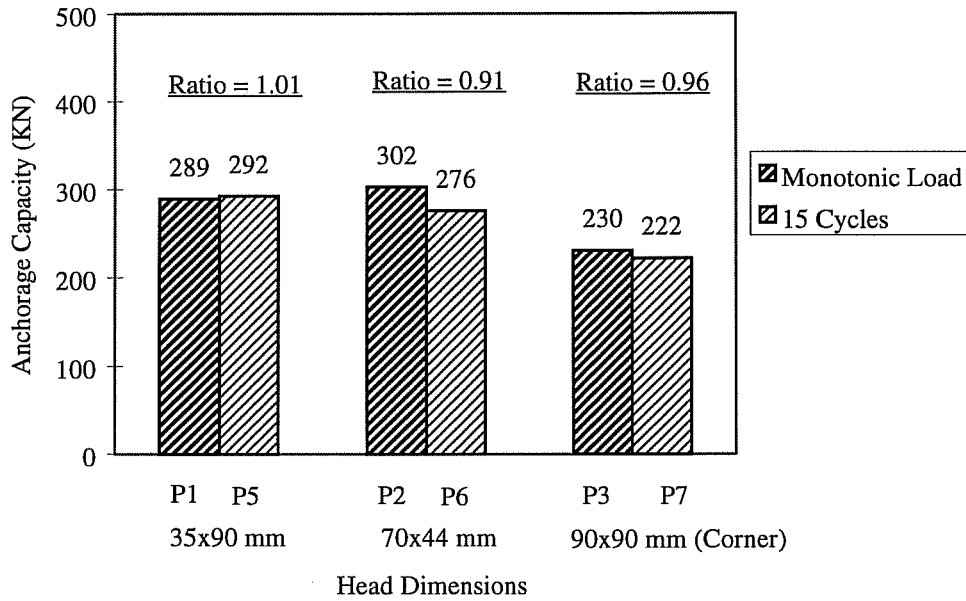


Figure 3.9 Effect of Cyclic Loading on the Anchorage Capacity - 15 Cycles

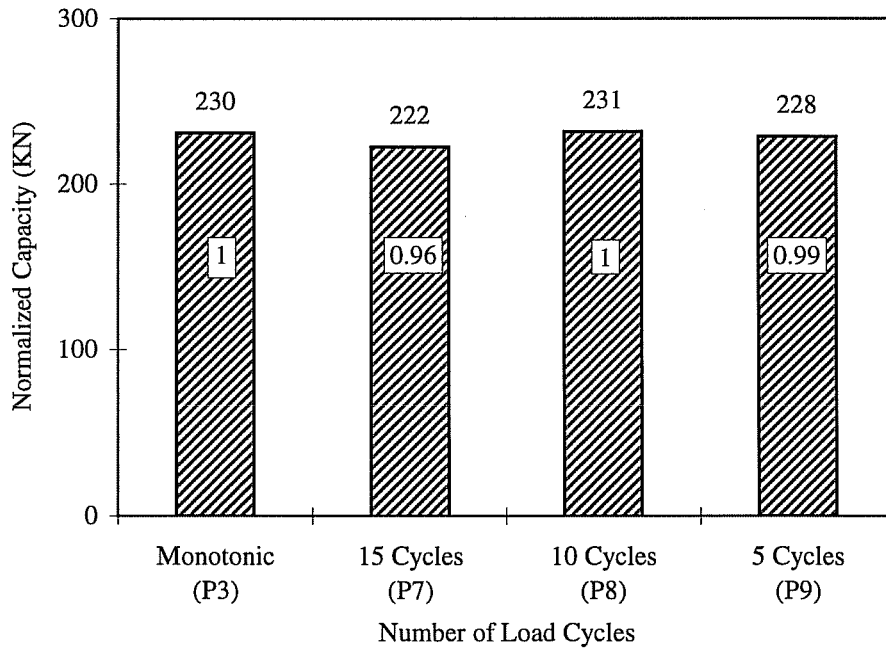
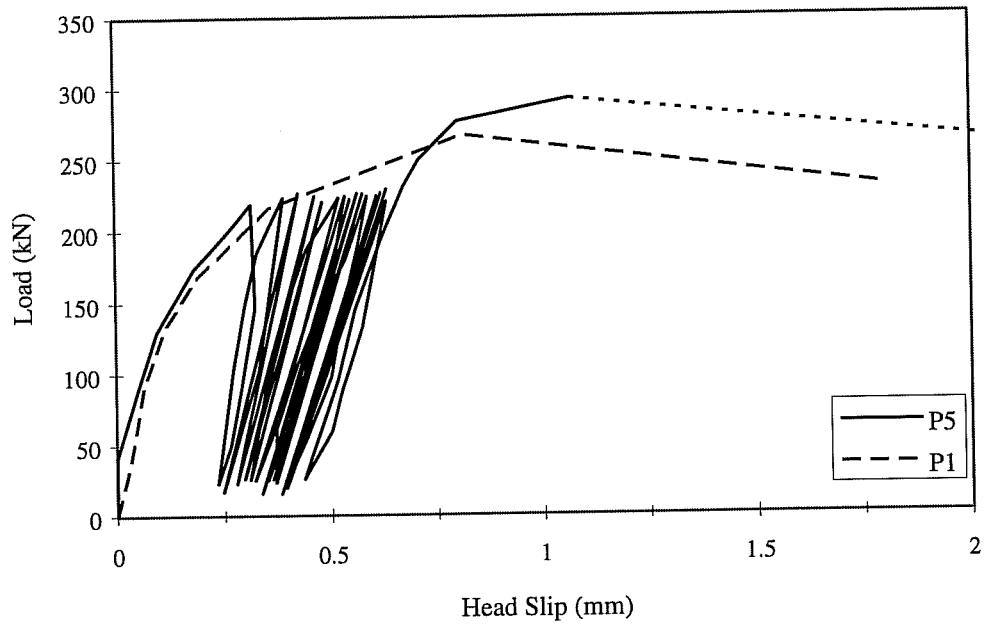


Figure 3.10 Effect of the Number of Cycles on the Anchorage Capacity - Corner Bars, 90x90 mm Heads

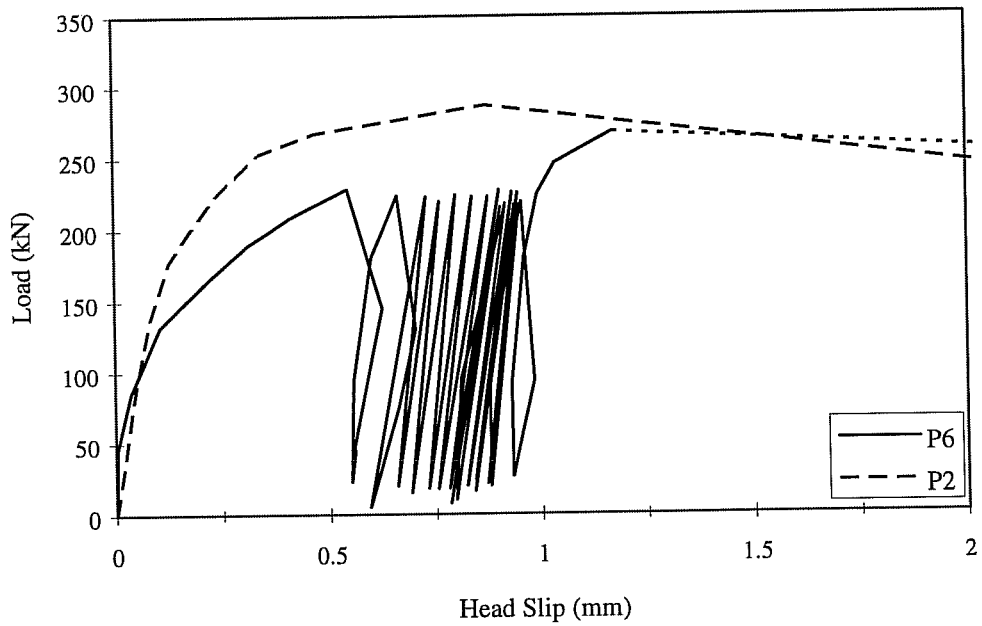
in Figures 3.9 and 3.10) are within the experimental scatter recognized in the previous phase of the experimental program [2]. However, it should be noted that while two tests out of the five conducted with cyclic loading showed recognizable reduction in capacities (9 and 4%), none of the other three tests showed significant increase in capacity (when compared to standard tests), indicating that load cycling might have caused a slight drop in capacity.

The effect of load cycling on the slip behavior of edge bars is shown in Figure 3.11. Although the capacity of P5 (15 cycles) was slightly larger than that of P1 (monotonic loading), the slip at the maximum load was higher by 0.27 mm (0.01 in.) or 31%. A similar increase in head slip at the maximum load was noted in comparing tests P2 and P6 (0.3 mm or 34%). In test P5, the head slip increased from 0.32 mm (0.013 in.) at the end of the first cycle to 0.67 mm (0.026 in.) at the same load level in the 16th and last cycle (an increase of 0.36 mm or 112%). In the case of P6, the increase in slip was 0.45 mm (0.018 in.) or 82%. The increase in slip during load cycling was larger than the overall increase in slip at failure in both cases. The initial loading cycle for test P6 (Figure 3.11) had significantly lower stiffness than that of P2, which implies that the large drop in capacity is more of a result of experimental scatter, rather than load cycling.

The effect of load cycling on corner bars is shown in Figures 3.12 to 3.14. Unlike edge bars, slip increase was minimal after the first two cycles. In the three



a) 90x35 mm Head



b) 70x44 Head

Figure 3.11 Effect of Load Cycling on the Load-Slip behavior of Edge Bars

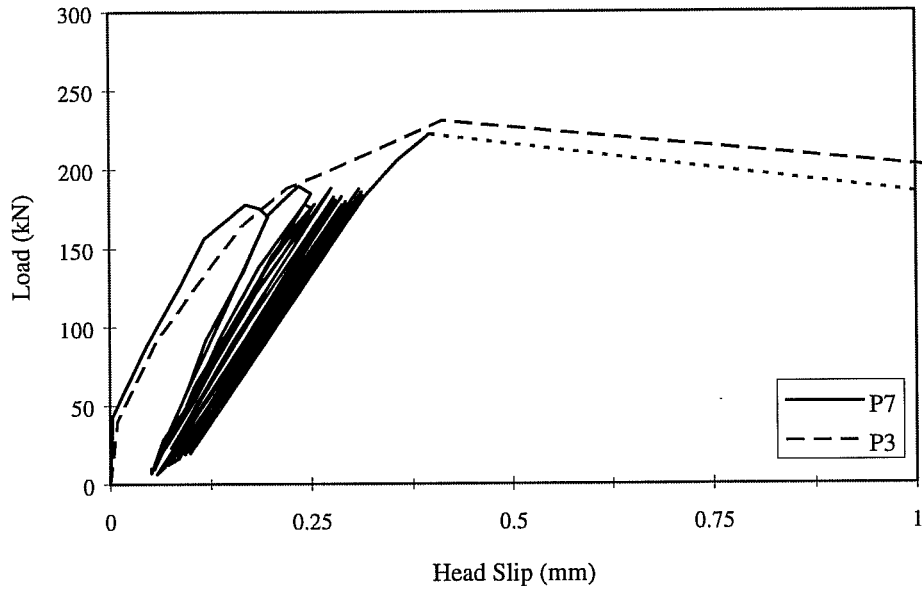


Figure 3.12 Effect of Load Cycling on the Load-Slip Behavior of Corner Bars - 15 Cycles

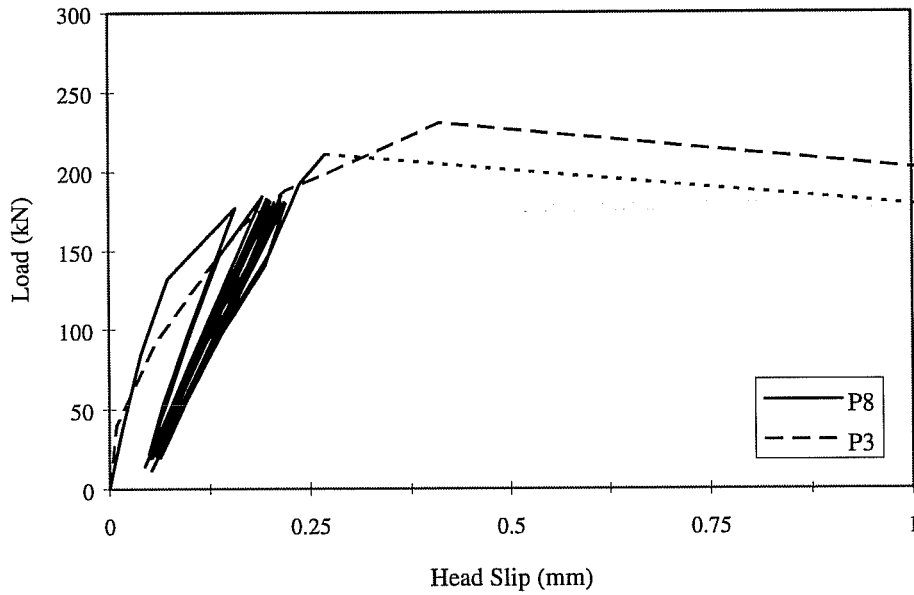


Figure 3.13 Effect of Load Cycling on the Load-Slip Behavior of Corner Bars - 10 Cycles

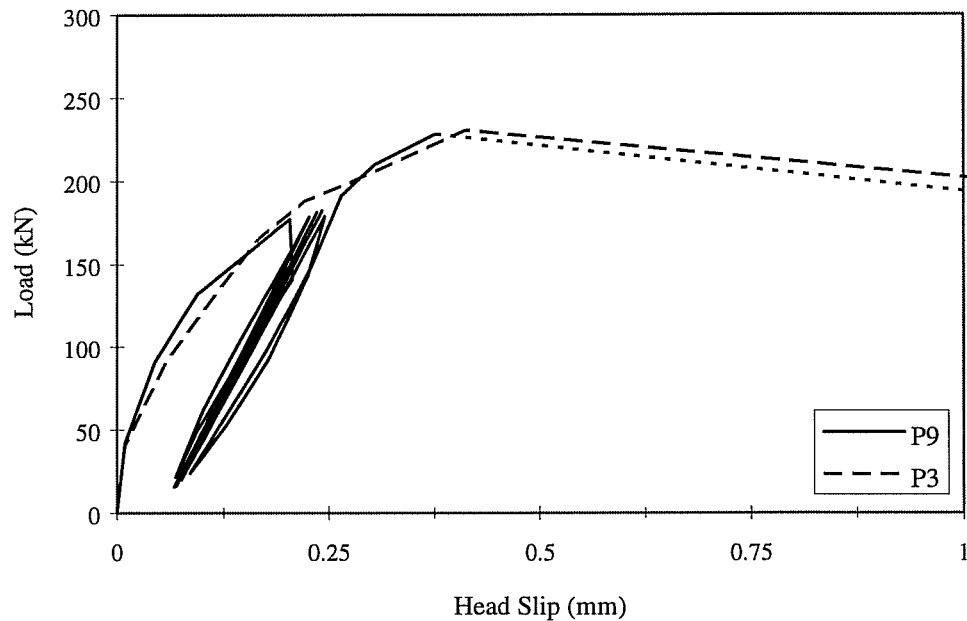


Figure 3.14 Effect of Load Cycling on the Load-Slip Behavior of Corner Bars - 5 Cycles

tests with cyclic loading, the head slip at the maximum load did not exceed that of P3 (monotonic loading). The load-slip curve for P3 was almost an envelope for other tests.

Based on the discussions presented above, it can be concluded that cyclic loading (up to 15 cycles) does not significantly influence the anchorage capacity of headed bars. While 15 load cycles resulted in a 30 to 35% increase in head slip at ultimate load for edge bars, head slip did not increase in the case of corner bars.

The difference in the slip behavior between edge and corner bars can be attributed to the ductility of both types of orientation. In the case of edge bars, 80% of the ultimate load represented a load beyond the elastic behavior, where head slip was increasing rapidly and stiffness had dropped significantly. Cycling the load at this level caused large head slips. On the other hand, the behavior of corner bars was more brittle. At 80% of the ultimate load, the behavior was nearly elastic, and the drop in stiffness was much less than that of edge bars. Cycling the load at this level caused less permanent deformation, and thus less increase in head slip.

2) Placing a Crossing Bar in the anchorage zone of the Head

The effect of anchoring the head behind a crossing bar on the anchorage capacity is shown in Figure 3.15. A 25 mm (#8) crossing bar increased the capacity of P11 by 23% (compared with P1). The capacities of P13 and P14 (compared to that of P2 and P4) were increased 11% only. A 35 mm (#11) crossing bar increased the capacity by 28% and 7%.

The load-slip behavior of tests P1 and P11 are compared in Figure 3.16. The head slip measurements for test P10 were not reliable and are not included. Initially, the curves for both tests were identical. Although stiffness started to decrease in both tests at the same level (135 KN or 30 kip), P11 (anchored behind

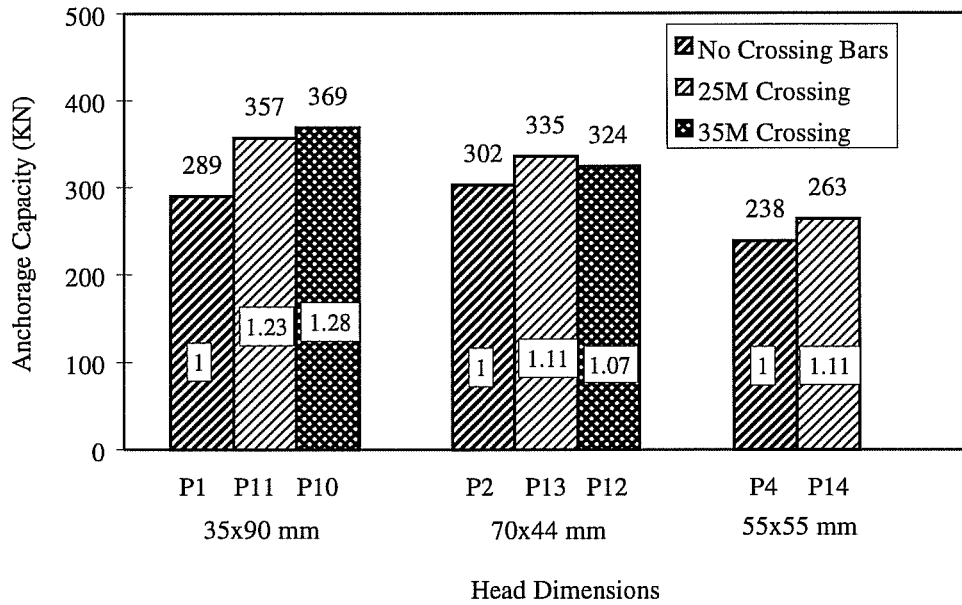


Figure 3.15 Effect of Crossing Bars on the Anchorage Capacity

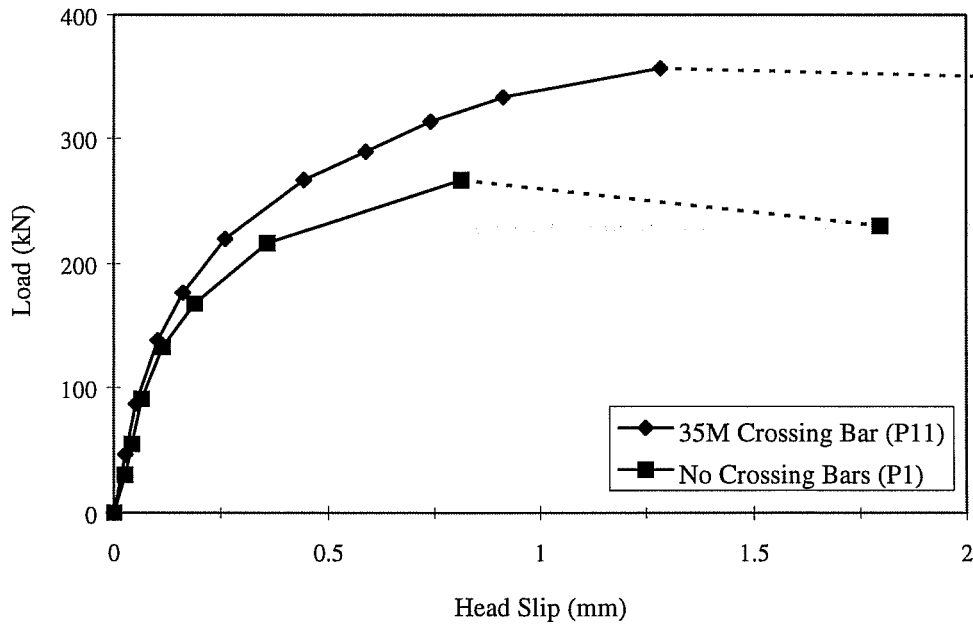


Figure 3.16 Effect of 35 mm Crossing Bars on the Load-Slip behavior - 35x90 mm Heads

a 25 mm bar) maintained slightly higher stiffness and was capable of resisting increasing loads up to 1.3 mm (0.05 in.) head slip (60% higher than that of P1). After failure, the load drop in P11 (2.5%) was much less than that of P1 (14%).

Similar observations were noted by comparing the load-slip behavior of tests P12 and P13 to P2 (Figure 3.17), and test P4 to P14 (Figure 3.18). The initial stiffnesses of P2, P12 and P13 were relatively close (up to 135 KN or 30 kip). Although the initial loss of stiffness in P2 was less than other tests, the curve started to flatten quickly at an applied load of 224 KN (50 kip). The rate of loss of stiffness in P12 and P13 (anchored behind 35 mm and 25 mm bars, respectively) was less than that of P2. The two tests were capable of resisting loads up to head slips of 1.6 and 2 mm (0.06 and 0.08 in.) (84 and 129% higher than that of P2).

In all tests with the heads anchored behind crossing bars, no cracks were noticed up to failure. The spalled concrete area was significantly larger than that of the proof tests. In one test (P12), the width of the spalled concrete was almost the same as the length of the crossing bar, which fell off when the spalled concrete was removed (Figure 3.19). No relationship between the size of the crossing bars and the spalled area could be established based on the limited number of tests conducted for each bar size.

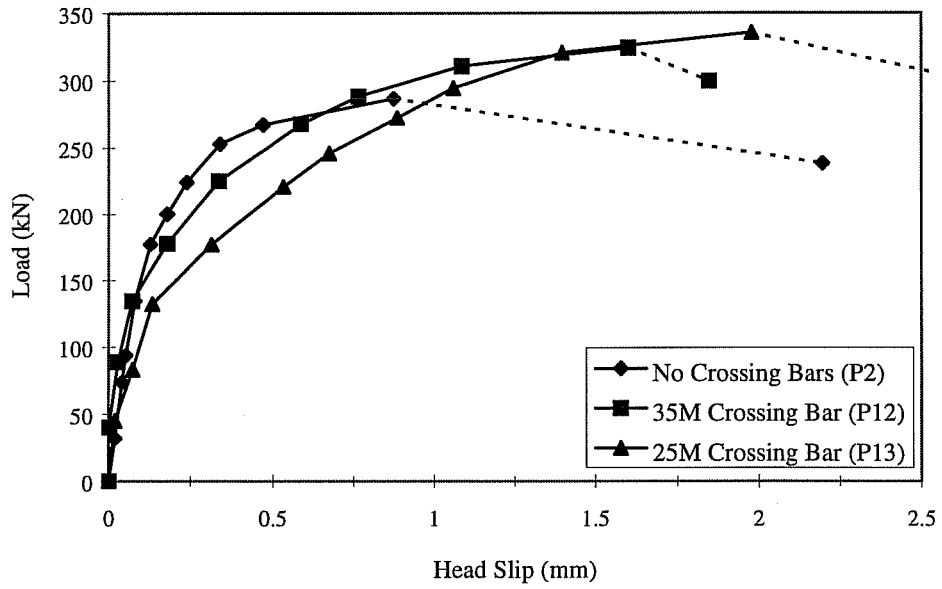


Figure 3.17 Effect of Crossing Bars on the Load-Slip behavior - 70x44 mm Heads

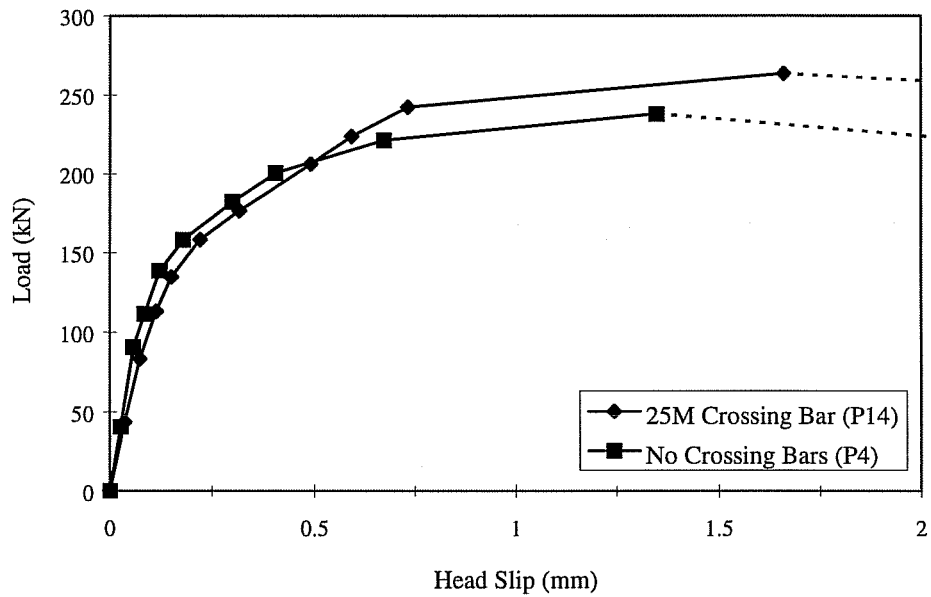


Figure 3.18 Effect of Crossing Bars on the Load-Slip behavior - 55x55 mm Heads

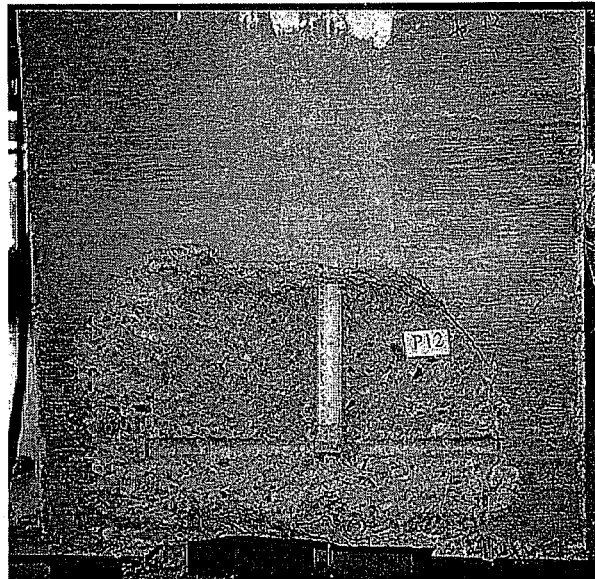


Figure 3.19 Failure Pattern after removing Spalled Concrete - P12

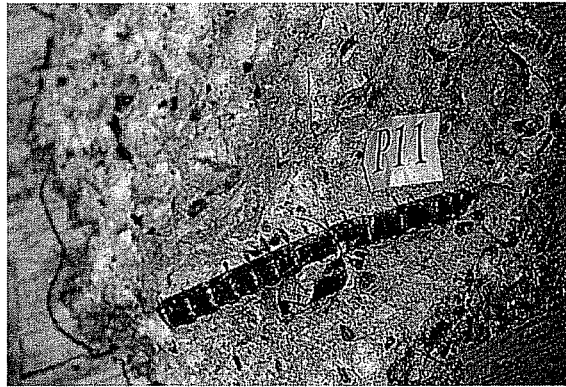
3) Head Dimensions

The increase in capacity due to anchoring the head behind a 25 mm (#8) crossing bar in test P11 (with 90×35 mm head) was significantly larger than that in the other tests (23% versus 11%). Furthermore, the reduction of the clear head dimension from 9 mm (0.35 in.) in P13 to 2 mm (0.08 in.) in P14 did not cause any difference in the increase of capacity.

Another significant observation is that using a 35 mm (#11) (instead of 25 mm or #8) crossing bar caused further increase in capacity in the case of P10 (from 23 to 28%), but resulted in less increase in capacity in the case of P12 (from 11 to 7%).

The above observations can be explained by the failure patterns shown in Figure 3.20. A crossing bar increases the anchorage capacity through two mechanisms:

- a) It provides a lateral restraint against side blow-out failure. Failure occurs only after the crossing bar is pushed outwards (due to the wedging action). As this bar has considerable stiffness, the concrete area to be blown out is larger, thus provides more concrete mass resisting failure (compare Figure 3.8-c to 3.19). This mechanism is effective after the concrete wedge starts to form (when the load-slip curve has already lost most of its stiffness), and is expected to cause less drop in load after failure and a slight increase in capacity.
- b) If the head is bearing against a crossing bar, then some of the bearing stress is transferred to concrete through the top surface of the bar, increasing the overall bearing area, and thus delaying the formation of the wedge. The difference in stresses on both sides of the head (Figure 3.21) indicates higher bearing on the side of the crossing bar. Figure 3.20-a shows the wedge forming over the top of the crossing bar. The effective bearing area is a function of the crossing bar stiffness. A 35 mm (#11) crossing bar is stiffer than a 25 mm (#8) bar and is expected to cause a greater increase in strength. This mechanism is more effective in increasing the anchorage capacity than increasing the residual strength after failure.



a) 90 x 35 mm Head



b) 70 x 44 mm Head

Figure 3.20 Effect of Head Dimensions on the failure pattern

In tests P10 and P11 both mechanisms were effective. The difference in the increase in capacities resulted from the increase in the stiffness of the crossing bar. On the other hand, the first mechanism only was effective in tests P12, P13 and P14, in which the clear head dimension was less than half the crossing bar diameter. This caused an outward force component resulting from the head

bearing against and the crossing bar (Figure 3.22). This force component is expected to increase with the increase of the bar diameter, and caused the drop in capacity with a 35 mm (#11) bar instead of a 25 mm (#8) crossing bar.

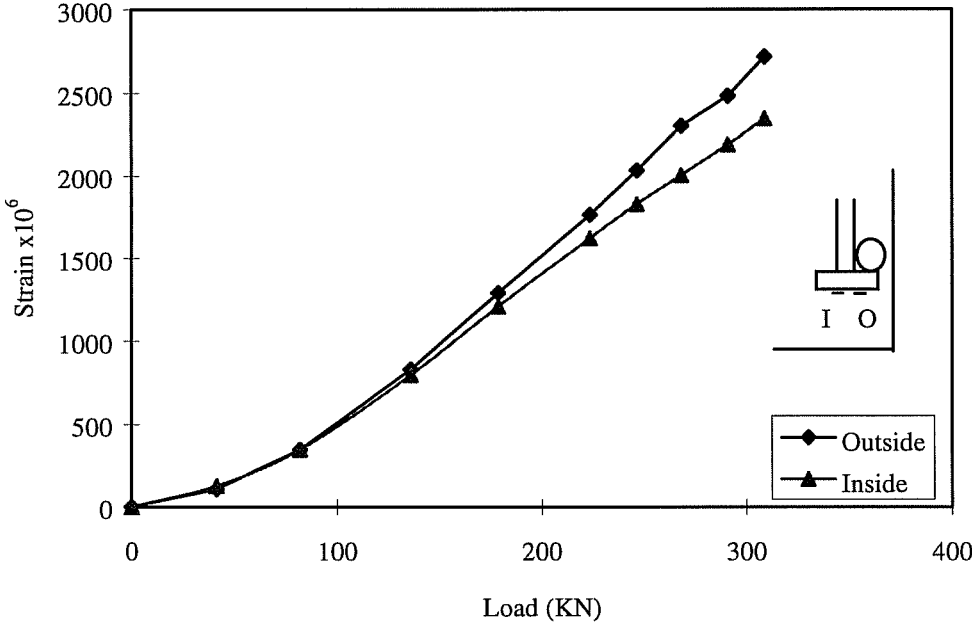


Figure 3.21 Effect of Crossing Bars on Head Stresses - P10

Based on the behavior of P10 and P11, it is conservative to assume that the increase in anchorage capacity due to anchoring the heads behind a crossing bar (25 mm or greater) is at least 25%. This increase in capacity should only be considered if the heads are positively anchored to the crossing bars, where a positive anchorage means that the clear head dimension is at least equal to half the

crossing bar diameter. Although tests without a positive anchorage showed an increase in capacity, it is safe to neglect other anchorage situations (where the clear head dimension is less than half the crossing bar diameter). It should be noted that these results are based on crossing bars 610 mm (24 in.) long, without any lateral constraints (e.g. ties). Longer crossing bars which are restrained by other reinforcement might produce further increase in the anchorage capacity.

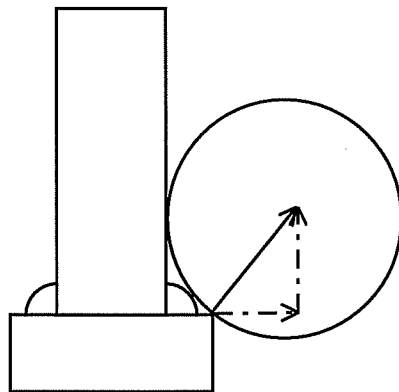


Figure 3.22 Forces resulting from Anchorage Behind Crossing Bars

3.3 Group 2: Transverse Reinforcement

3.3.1 Design of Specimens

Confining reinforcement is effective after the spalling of concrete cover due to compressive forces. In order to investigate the behavior of fairly large

diameter headed bars (20 mm or #6) as confining reinforcement, large scale specimens would be required. These specimens would require very large compressive forces in order to cause concrete spalling. As this was only an exploratory phase of the test program, investigating the possibility of using headed bars as confining reinforcement, it was decided to construct specimens in which the load could be applied directly to the headed bars.

The setup used for testing group 2 specimens is shown in Figure 3.23. Tensile force was applied to both bars simultaneously in 22 KN (5 kip)

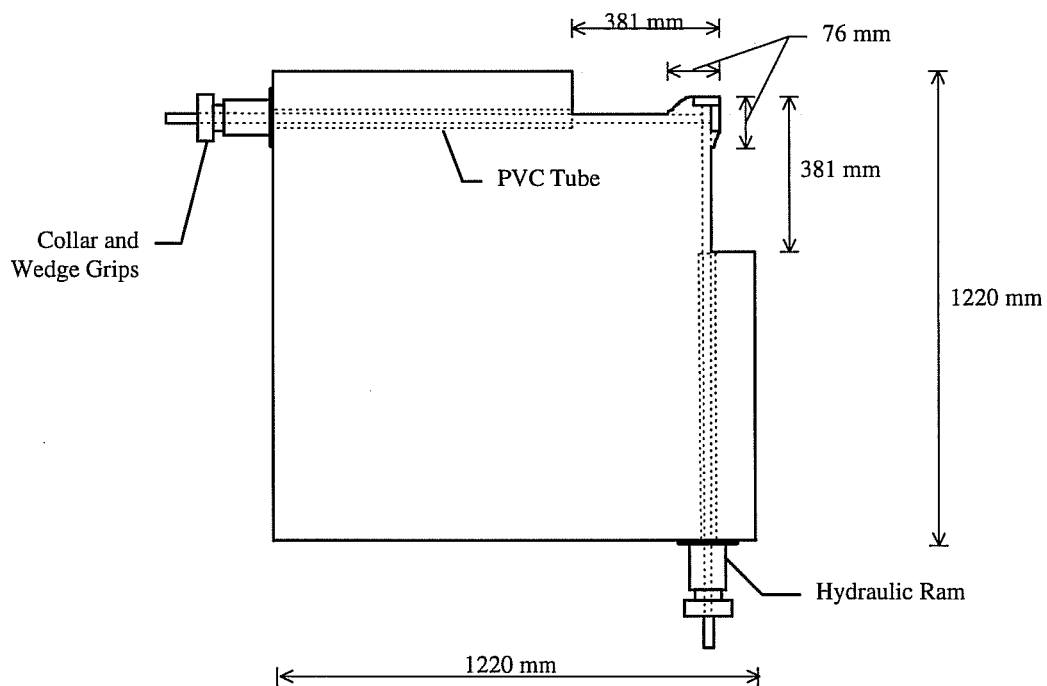


Figure 3.23 Setup for Stirrup Tests

increments up to yield. The yield load was sustained until the head slip stabilized (usually about 5 minutes). The headed bars used were 20 mm (#6) diameter. Three head dimensions were tested, one square head (50×50×12 mm) and two rectangular heads (70×35×16 and 100×55×25 mm). The properties of the 11 tests are summarized in Table 3.4. Photographs of the tests are shown in Figures 3.24 and 3.25. The variables include head interlock setup and the use of crossing longitudinal bars in addition to head dimensions. The concrete cover in Tests S1 to S3 was 38 mm (1.5 in.). There was no cover in the rest of the tests.

3.3.2 Materials

The headed bars had a nominal yield strength of 540 MPa (78.3 ksi). A typical stress strain curve is shown in Figure 3.26. The concrete mix used was the same as that described in Section 3.2.4. No additional water was required at the time of casting as the slump was 102 mm (4 in). The strength at the time of testing was 27.2 MPa (3950 psi).

3.3.3 Instrumentation

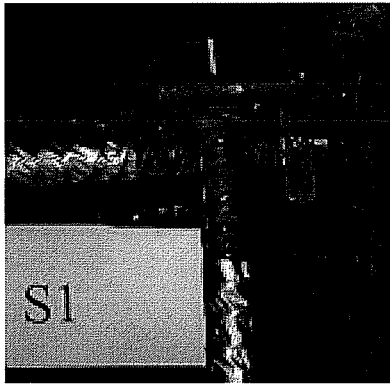
Each test was instrumented to measure the applied load and head slip of the anchored bars. Head strains were measured on one of the heads in each test. Strain gages were placed 22 mm (0.86 in.) from the edge of the head in the case of

rectangular heads. In square heads, strain gages were placed 12 mm (0.47 in.) from the edge.

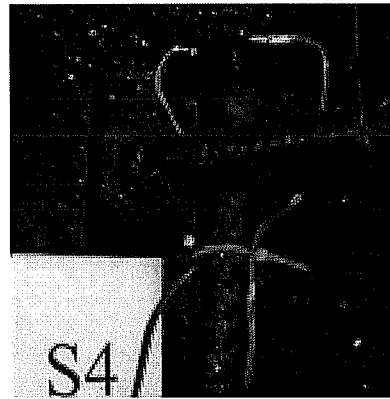
Table 3.4 Stirrup Tests - Properties and Test Results

Test	Head Dimensions (mm)	Cover (mm)	Crossing Bar	Max Deflection (mm)	Other Head Deflection (mm)
S1	50x50x12	38	-	0.008	0.004
S2	70x35x16	38	-	0.003	0.002
S3	100x55x25	38	-	0.001	-0.001
S4	70x35x16	-	-	0.17	0.17
S5	70x35x17	-	-	0.14	-0.001
S6	70x35x18	-	-	0.13	0.08
S7	70x35x19	-	-	0.23	0.18
S8	50x50x12	-	-	0.007	0.002
S9	70x35x21	-	35M	0.01	0.003
S10	50x50x12	-	35M	0.16	0.14
S11	50x50x13	-	-	0.04	0

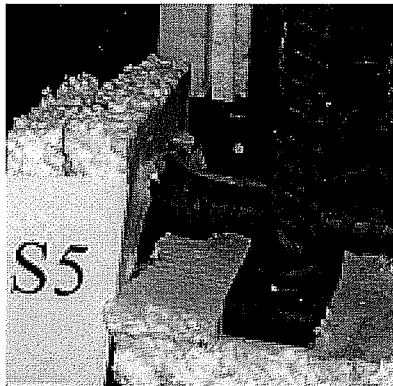
The applied load was determined using a 70 MPa (10,000 psi) capacity pressure transducer which measured the oil pressure in the rams. The oil pressure was multiplied by the ram area in order to determine the applied load. In the three tests with concrete cover (S1, S2, and S3), slip of the anchored headed bars was measured through a threaded rod attached to the head, in a manner similar to that described in Section 3.2.5. In the rest of the tests, linear transducers were placed in contact with the heads to measure slip directly (Figure 3.27).



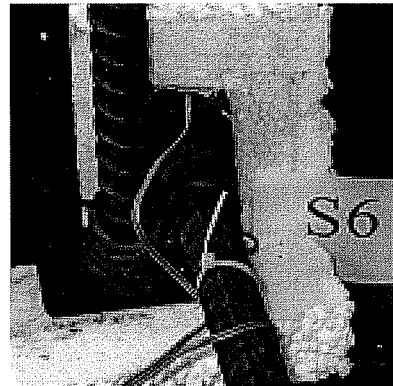
a) S1, S2, and S3



b) S4

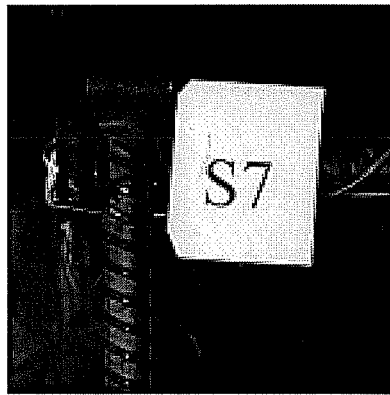


c) S5

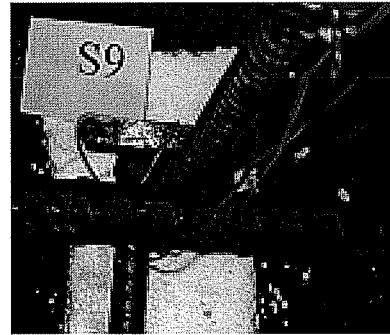


d) S6

Figure 3.24 Head interlock schemes for Stirrup tests



a) S7 and S8



c) S9 and S10



c) S11

Figure 3.25 Head interlock schemes for Stirrup tests (continued).

3.3.4 Specimen Fabrication

A 1220×1220×914 mm (48×48×36 in.) concrete cube was cast in one of the forms previously used for pullout tests. Styrofoam sheets were placed between the bars and the forms to simulate cover spalling, for a distance equal to

381 mm (15 in.) from the heads. Figure 3.28 shows specimen after the Styrofoam sheets were placed. These sheets were easily removed after stripping the forms. Unfortunately, most of the strain gages were damaged during this process. PVC tubes were used to prevent anchorage along the rest of the bar. In the case of specimens with concrete cover, duct tape was used to prevent bond along 305 mm (12 in.) out of this 381 mm (15 in.) distance (Figure 3.24-a).

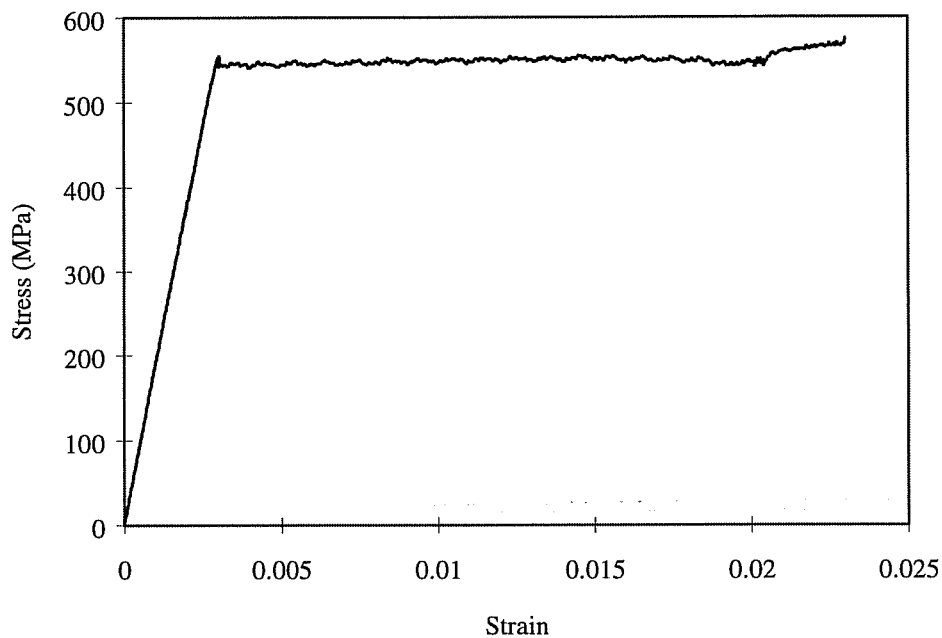


Figure 3.26 Stress - Strain curves for the 20M Headed Bars

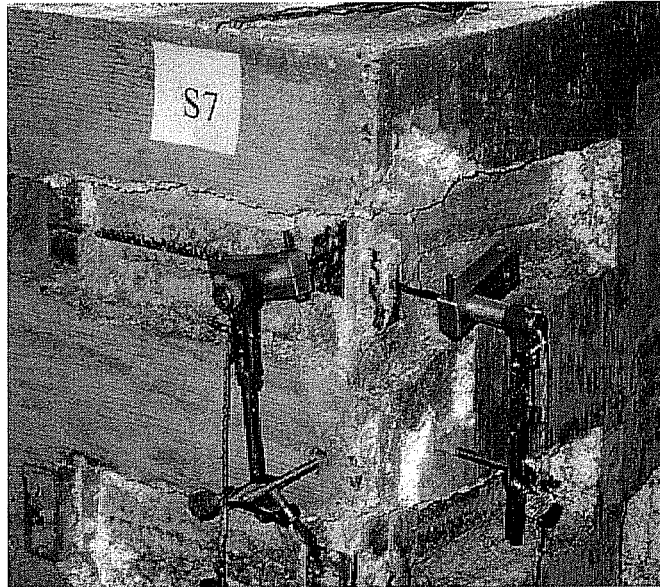


Figure 3.27 Head Slip measurement

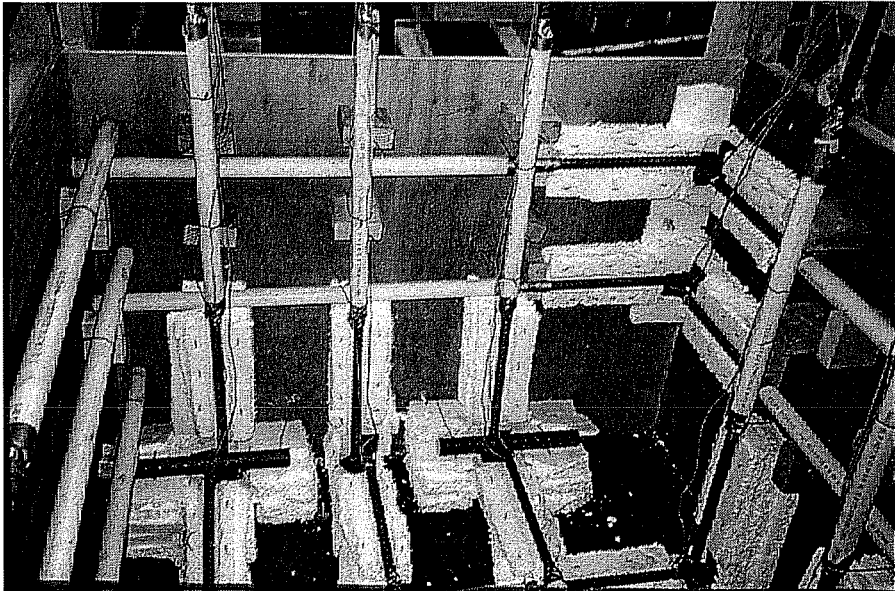


Figure 3.28 Overall view before casting

3.3.5 Test Results

The bars were capable of developing the yield load without anchorage failure in all tests. The heads of overlapping bars provided adequate confinement and prevented blow-out failures, even in tests without concrete cover over the bar. However, the head slips varied significantly in these tests, and in some cases was lower in tests designed to resemble erratic construction (S4, S5, and S11). Table 3.4 shows the maximum slip measured for each of the tests. The maximum slip of the other bar is also presented. Some of these values are negative, indicating that the head moved in the opposite direction of the load. This is attributed to the interlock between the flash on the headed bars. In order for one of the heads to move in the direction of the load, the other head has to move in the opposite direction (Figure 3.29).

There was no significant slip (more than one hundredth of a millimeter) measured in the three tests with concrete cover (S1, S2, and S3). Although tests without concrete cover had higher slips, there was no correlation between the anchorage condition and the maximum slip. Tests S9 and S10, in which the headed bars were anchored behind a 35 mm (#11) crossing bar, did not show consistent reduction in slips.

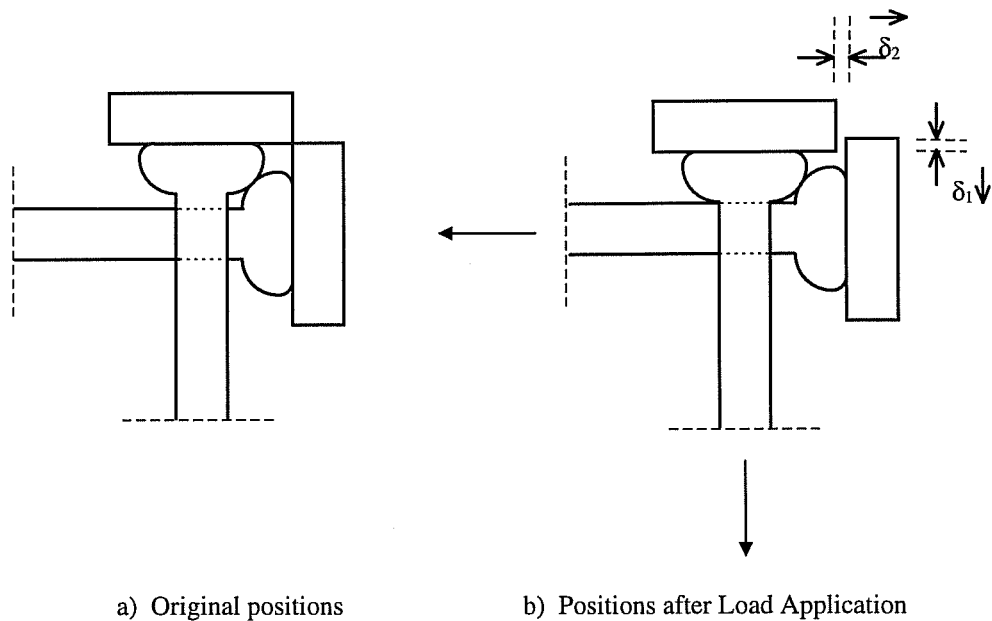


Figure 3.29 Effect of Flash interlock on direction of Slip

3.3.6 Load-Slip Behavior

The load-slip diagrams of tests S4 and S9 represent the behavior of the rest of the tests, and are discussed in the this section.

The load-slip diagram of test S4 (a test with relatively high head slips) is shown in Figure 3.30. While the head slip of one of the bars started increasing with the increase of the applied load, the other head moved backwards. The head slip of both bars started increasing significantly while the yield load was sustained.

The load-slip diagram for test S9 (a test with low head slips) is shown in Figure 3.31. The head slips for both bars were very close to zero throughout all of

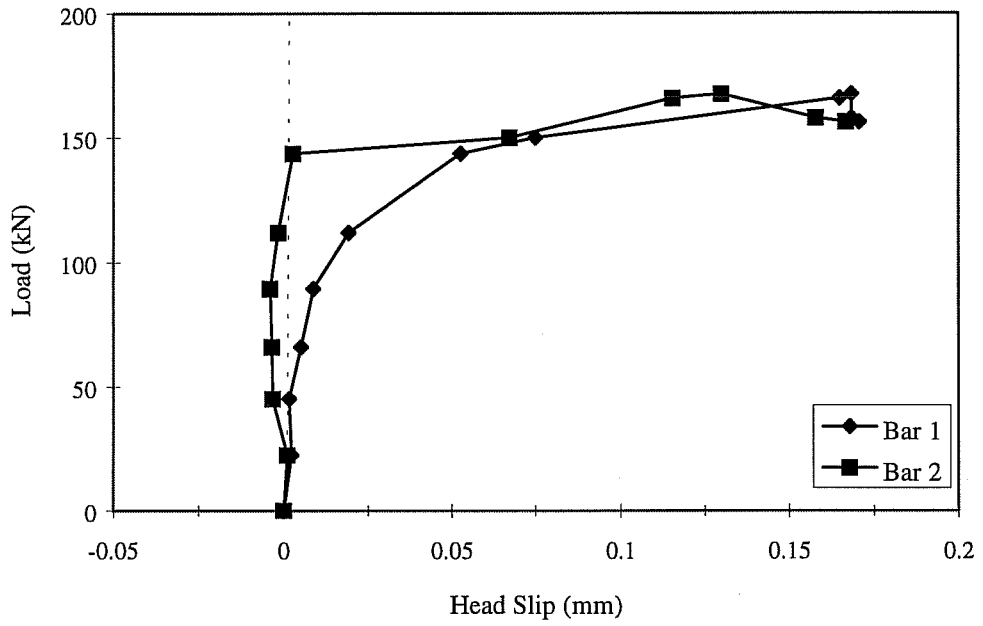


Figure 3.30 Load-Slip behavior - Test S4

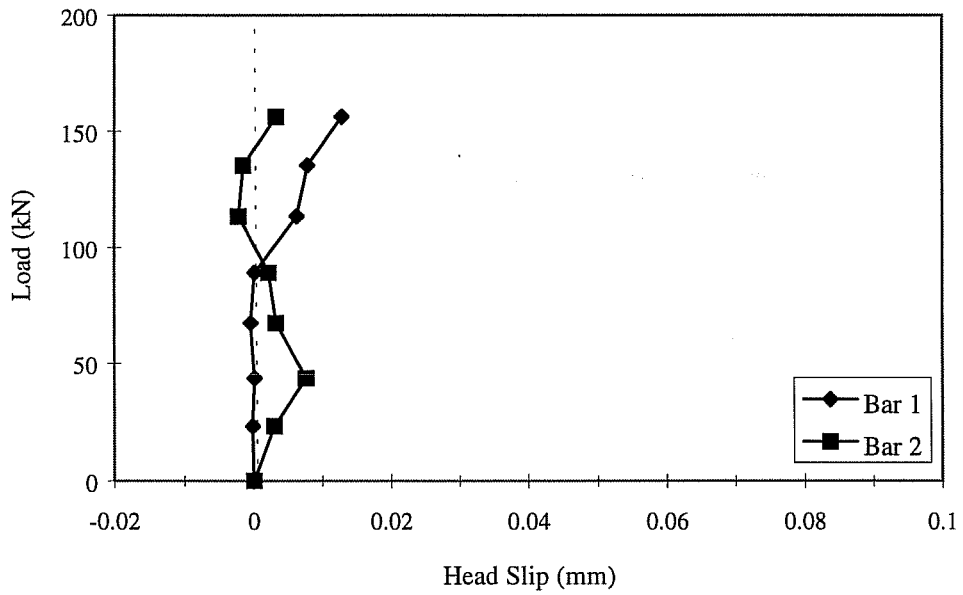


Figure 3.31 Load-Slip behavior - Test S9

the test. One of the heads showed a slight increase in slip as the applied load approached the yield load of the bar. The slip of the other head was fluctuating around zero.

The measured head stresses on both sides of the bar for test S9 are shown in Figure 3.32. The stresses on both sides increased steadily as the load exceeded 40 KN (9 kip). The side of the head anchored behind the other bar was under higher stress throughout most of the test (22% higher at the bar yield load).

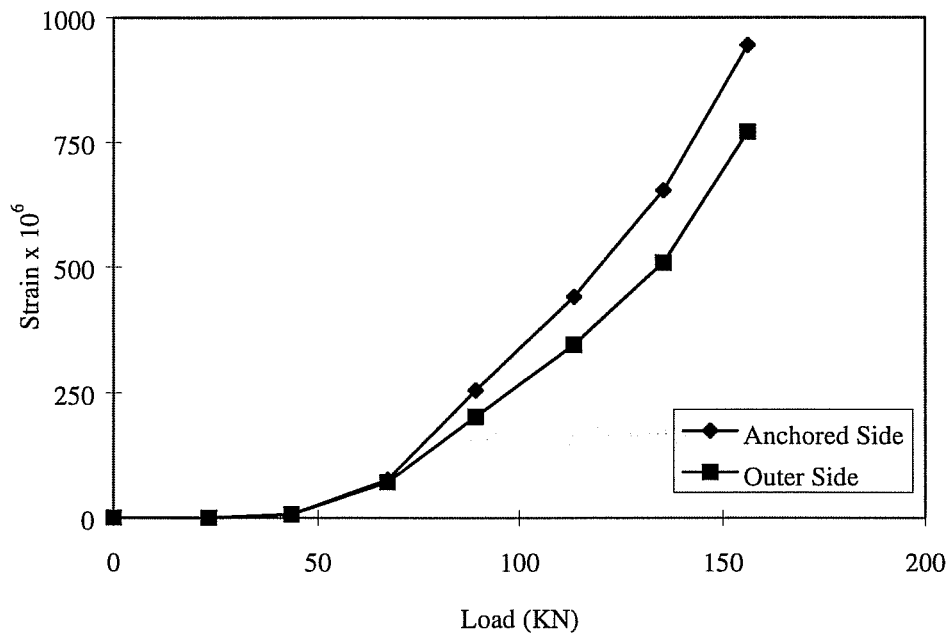


Figure 3.32 Head Strains - Test S9

The conclusions that could be drawn from this limited number of tests are that interlocking heads are capable of providing sufficient anchorage to develop

the yield force of the bar, even with slight construction errors. The difference in head stresses on both sides of the bar was similar to that observed in heads anchored behind crossing bars. The head slips measured in different tests were not consistent with the interlock scheme. A larger number of tests will be required to develop a statistical database describing the effect of head orientations on slip.

3.4 Summary

Based on the results reported by DeVries [2] additional tests were conducted to evaluate the effects of load cycling and anchoring the heads behind crossing bars on the anchorage capacity and the slip behavior. Cycling the load (up to 15 cycles) did not cause significant drop in the anchorage capacity. However, the head slip increased at failure by 30 to 35% for edge bars. The increase in anchorage capacity due to positive anchorage of the heads behind crossing bars was in the order of 25%.

The results obtained from a limited number of tests on interlocking headed bars showed that the use of these bars as confining reinforcement is promising. All of the anchorage situations were capable of developing the yield force of the bars.

Chapter 4

ANCHORAGE IN EXTERIOR JOINTS - EXPERIMENTAL PROGRAM

4.1 Introduction

During the late sixties and seventies several studies were conducted to examine the anchorage capacities of hooked reinforcing bars. These studies were divided into two phases. The first phase consisted of tests of bent bars anchored in concrete blocks. The simple specimen allowed testing a large number of specimens to determine the influence of geometric configuration on bent bar behavior. In the second phase, specimens modeling dimensions and boundary conditions of reinforced concrete beam-column joints were tested, leading to the development of design provisions for hooked bars.

In this chapter, some of the second phase studies on hooked bars are described. The headed bar test series is also described. Specimen design, materials used, specimen fabrication, and the test setup are presented.

4.2 Background

Marques and Jirsa [9] tested 19 specimens simulating typical isolated exterior beam columns in a structure to evaluate the anchorage capacity of hooked beam reinforcement subjected to various degrees of confinement at the joint. The types of confinement included vertical column reinforcement, lateral reinforcement through the joint, side concrete cover, and column axial load. Marques used full scale models of beam column joints in order to permit the use of fairly large diameter bars. Hooked bars used conformed with the ACI standards [1] for hook geometry. A diagram of the specimen that Marques selected to simulate a typical exterior beam column joint is shown in Figure 4.1. The column cross section was either 381×305 mm (15×12 in.) or 305×305 mm (12×12 in.). The beam cross section was 305 mm (12 in) wide and 508 mm (20 in.) deep. The height of the column in all tests was 1270 mm (50 in.). The dimensions of the beam and the column were chosen so that the specimen would be a realistic simulation of the beam column joint, eliminating scale effects. To facilitate fabrication, the beams were not cast with the columns. To simulate moment action the anchored bars that extended from the face of the column were connected to threaded rods which were loaded in tension with hydraulic rams. The compression zone of the beam was duplicated with a steel plate bearing against the face of the column over an area which approximated that of the

compression zone of the assumed beam (Figure 4.2). Although the compressive strains in the simulated compression zone might vary from that of a real beam column joint, the anchorage capacity should not be affected.

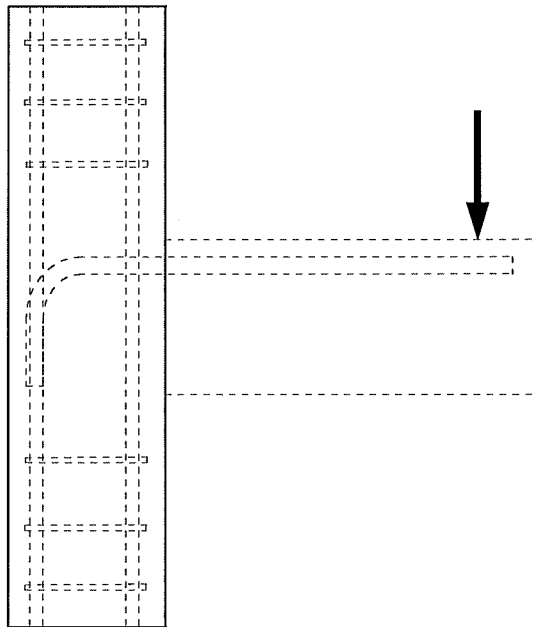


Figure 4.1 Exterior Joint used by Marques and Jirsa [9] for testing Hooked Bar Anchorages

In all of the 381×305 mm (15×12 in.) columns the column reinforcement consisted of six 25 mm (#8) longitudinal bars, and 10 mm (#3) closed ties at 127 mm (5 in.) outside the joint. The clear cover over the ties was 38 mm (1.5 in.). The tests were conducted with either two 22 mm (#7) or 35 mm (#11) bars anchored to the columns. All tests were conducted using either 90-degree or 180-

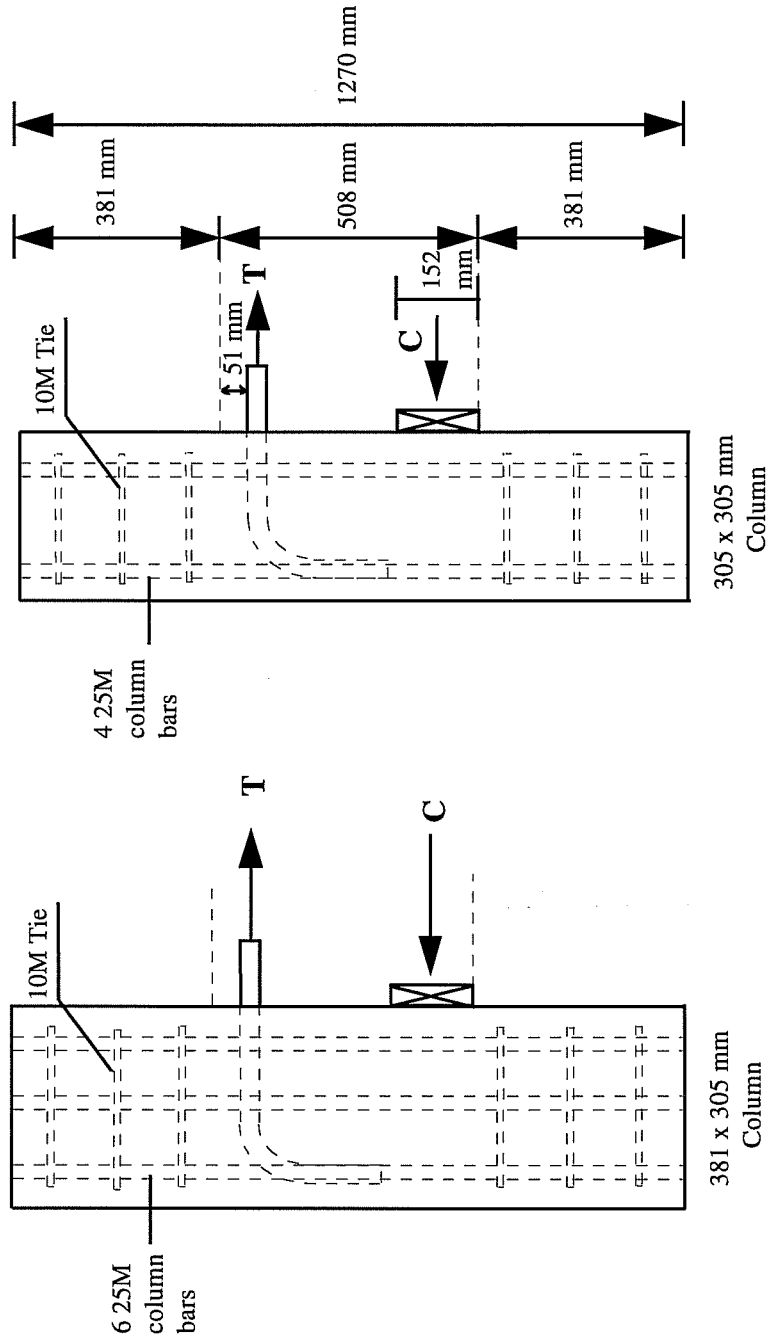


Figure 4.2 Exterior Joint simulation by Marques and Jirsa [9]

degree hooks conforming to ACI 318-71 specifications [10]. For these hooks the inside diameter of the bend was 6 bar diameters for the 22 mm (#7) bars, and 8 bar diameters for the 35 mm (#11) bars. For the 90° hook the extension beyond the bend was 12 bar diameters, and for the 180° hook the tail portion was 4 bar diameters. The lead embedment before the hook portion of the anchored bar was varied by changing the size of the column. The properties of the 19 specimens are summarized in Table 4.1. Dimensions and reinforcement details are shown in Figures 4.3 and 4.4.

To determine the effect of column bars, tests were run with column bars placed outside and inside the beam bars. In both cases the concrete cover over the beam bars was 73 mm (27/8 in.). The influence of the column ties in the joint was isolated by retaining the same column steel, placing the column bars inside the beam bars, and carrying ties through the joint. In this case the confinement was 73 mm (27/8 in.) plus 10 mm (#3) ties at either 127 mm (5 in.) or 64 mm (21/2 in.) spacing through the joint. The effect of concrete cover was determined by conducting one test with concrete cover reduced from 73 mm (27/8 in.) to 38 mm (1.5 in) and placing column bars inside the beam bars so that only concrete cover confined the anchored beam bars.

Table 4.1 Parameters and results of Marques and Jirsa hooked bar tests [9].

Specimen Notation*	Column Size (mm)	Axial load (KN)	Hook Angle (deg)	f'_c (MPa)	Lead Embedment (mm)	Confinement**	Max Load (KN)
J7-90-15-1-H	381×305	2424	90	31.7	241	1	245
J7-90-15-1-M	381×305	1197	90	34.8	241	1	267
J7-90-15-1-L	381×305	645	90	33.1	241	1	258
J7-90-12-1-H	305×305	1868	90	28.6	165	1	165
J7-180-15-1-H	381×305	2424	180	27.6	241	1	231
J7-180-12-1-H	305×305	1890	180	30	165	1	165
J7-90-15-2-H	381×305	2424	90	32.8	241	2	262
J7-90-15-2-M	381×305	1219	90	32.8	241	2	254
J7-90-15-3-H	381×305	2469	90	32.1	241	3	276
J7-90-15-3a-H	381×305	2380	90	25.9	241	3a	262
J7-90-15-4-H	381×305	2438	90	31	241	4	196
J11-90-15-1-H	381×305	2402	90	33.8	152	1	334
J11-90-15-1-L	381×305	685	90	32.8	152	1	360
J11-90-12-1-H	305×305	1944	90	31.7	76	1	294
J11-180-15-1-H	381×305	2402	180	30.3	152	1	311
J11-90-15-2-H	381×305	2402	90	34.5	152	2	338
J11-90-15-2-L	381×305	556	90	31	152	2	369
J11-90-15-3-L	381×305	667	90	33.4	152	3	431
J11-90-15-3a-L	381×305	778	90	33.5	152	3a	480

* J7-90-15-1-H means #7 (22 mm) bars, 90-degree hook, 15×12 in. (381×305 mm) column, confinement type 1, and high level of column axial load.

** Lateral confinement codes:

- 1 = Column bars + 73 mm cover
- 2 = Only 73 mm cover
- 3 = 73 mm cover + 10 mm (#3) ties at 127 mm
- 3a = 73 mm cover + 10 mm (#3) ties at 64 mm
- 4 = Only 38 mm cover

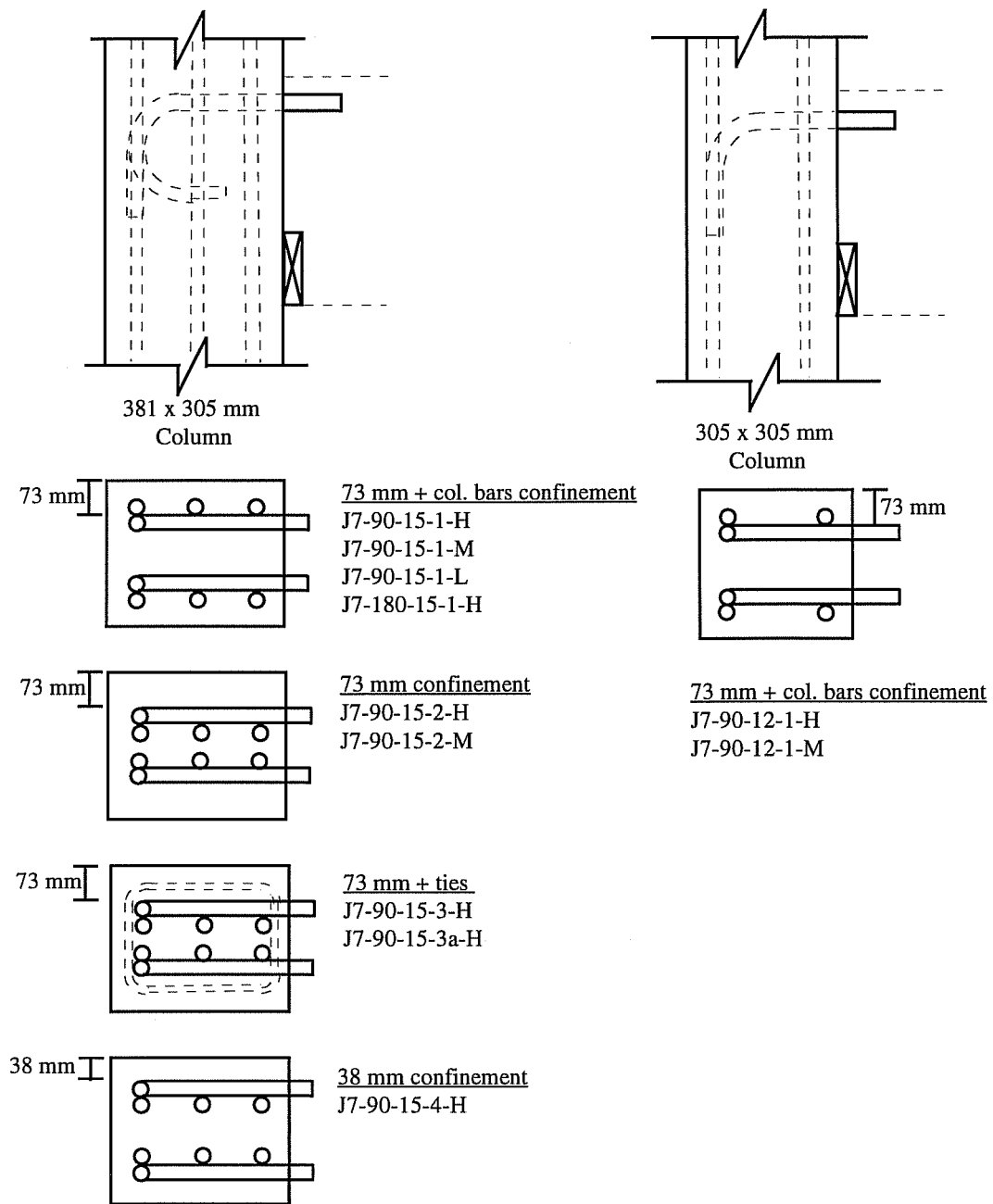


Figure 4.3 Joint details of the J7 series of #7 Hooked Bar Specimens by Marques and Jirsa [9]

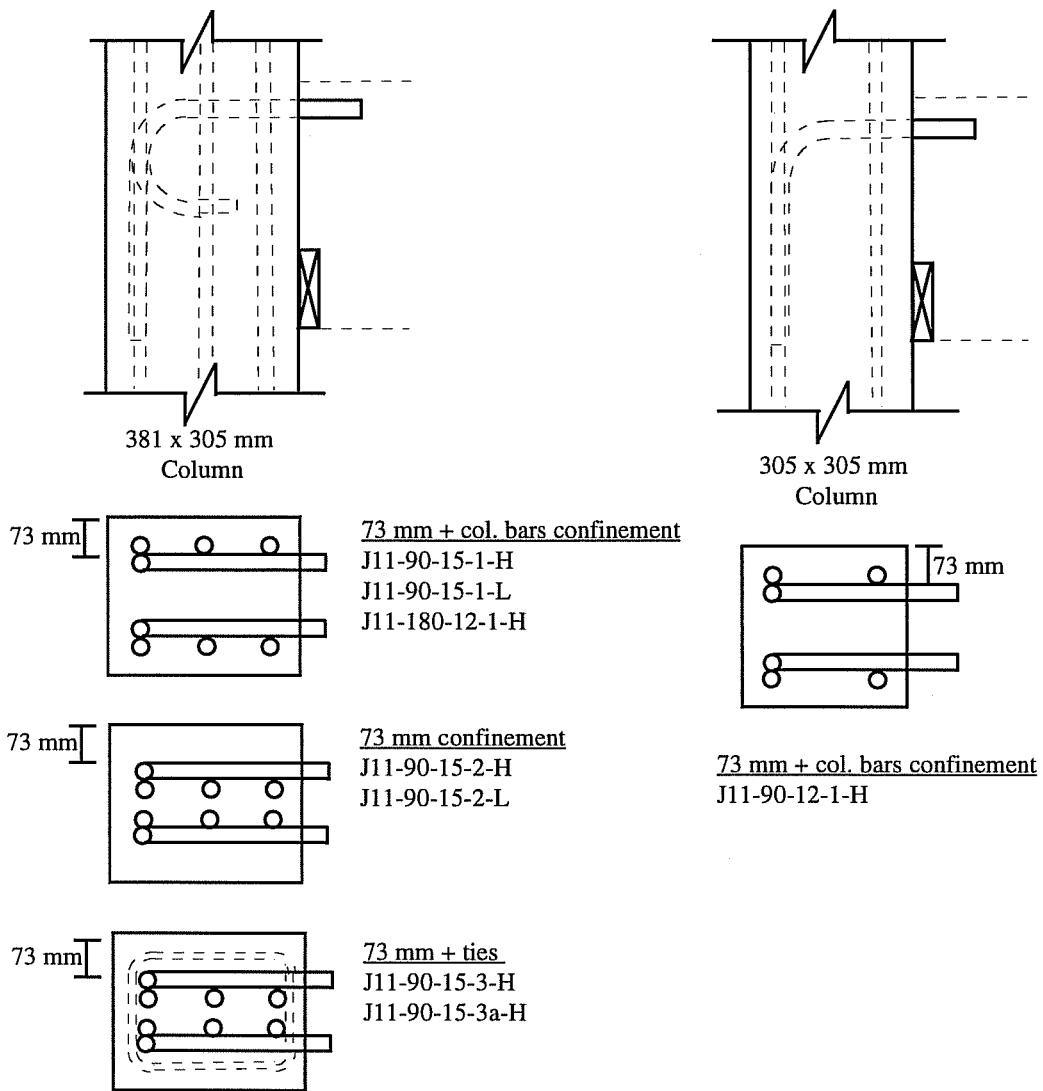


Figure 4.4 Joint details of the J11 series of #11 Hooked Bar Specimens by Marques and Jirsa [9]

To determine the influence of column loads tests were run holding all specimens dimensions and details constant and varying the level of axial load.

Nominal axial loads of 600, 1200, and 2400 KN (135, 270, and 540 kips, respectively) were imposed on the 381×305 mm (15×12 in.) columns. To retain the same stress levels the 2400 KN (540 kips) was reduced to 1870 KN (420 kips) in the 305×305 mm (12×12 in.) columns. The actual values of axial load measured during testing are listed in Table 4.1. In each test, the column axial load was applied and maintained constant throughout the loading sequence to represent the dead load on a structure. The anchored bars were loaded in tension until one pulled out of the column. In general, failure was fairly sudden and resulted in the entire side face of the column spalling away to the level of the hooked bar anchorage, and the load dropping immediately. After the side cover was removed, a concrete wedge was always noted on the inside of the hook. The lateral forces inducing side spalling were attributed to this wedge.

Based on slip and strain measurements, Marques and Jirsa made the following conclusions:

- 1) The effect of the column axial load appears to be negligible.
- 2) There is a very little difference between the capacity of 90- and 180-degree hooks. However, the slip at a given stress is slightly higher for 180-degree hooks.
- 3) The embedment length between the beginning of the hook and the critical section at the face of the column is the prime factor in determining the

capacity of hooked bar anchorages. Furthermore, slip was greater at all stress levels for specimens with shorter lead embedment.

- 4) Side concrete cover did not influence stress-slip characteristics of hooked bars. Reduction of concrete cover from 73 mm (27/8 in.) to 38 mm (1 1/2 in.) drastically reduced the stress and the deformation capacity at failure.
- 5) Placement of the column bars inside or outside the anchored beam bars did not influence stress or slip characteristics of the anchored bars.
- 6) Ties through the joint with small spacing (relative to the diameter of the bend of the anchored beam bar) reduced slip and increased anchorage capacity.

Based on these test results, Marques proposed design equations to estimate the anchorage capacity of hooked bars. The tensile stress developed in a bar by a standard hook in a joint was given by:

$$f_h = 700(1 - 0.3d_b) \Psi \sqrt{f'_c} \quad 4.1$$

Where f_h is the stress developed by the hook in psi, d_b is the bar diameter in inches, and f'_c is the concrete compressive strength in psi. The stress given by this equation is limited to the bar yield stress. The coefficient Ψ is taken as unity, but could be increased to 1.4 for 35 mm (#11 bars) or smaller if the lead straight embedment is not less than four bar diameters or 101 mm (4 in.) and the side

concrete cover is not less than 64 mm (2.5 in.) and the cover on the tail extension is not less than 51 mm (2 in.). The value of Ψ may be taken as 1.8 if the joint is confined by closed ties at a spacing of three bar diameters or less. If additional development length is required the straight lead embedment length (in inches) between the critical section and the hook shall be computed by

$$l = \left[0.04 A_b (f_y - f_h) / \sqrt{f'_c} \right] + l' \quad 4.2$$

where A_b is the area of the bar in square inches, f_y is the bar yield stress in psi, and l' is equal to four bar diameters or 101 mm (4 in.), whichever is greater.

In 1977 Pinc and Jirsa [11] conducted an experimental investigation patterned after the study by Marques. The same specimen configuration and testing procedure was used. The main variable in this study was the lead embedment length. The embedment length was varied by varying the size of the column. The columns' cross section varied from 305×305 mm (12×12 in.) to 610×305 mm (24×12 in.) with increments of 76 mm (3 in.). The anchored bars used were 29 mm (#9) and 35 mm (#11) bars with 90-degree hooks. The properties of the 8 tests conducted in this study are given in Table 4.2.

Table 4.2 Parameters and results of Pinc and Jirsa hooked bar tests [11].

Specimen Notation*	Column Size (mm)	Column Axial load (KN)	Hook Angle (deg)	f'_c (MPa)	Lead Embedment (mm)	Side cover (mm)	Max Load (KN)
9-12	305×305	480	90	32.4	111	73	209
9-15	381×305	627	90	26.2	187	73	191**
9-18	457×305	805	90	32.4	264	73	329
9-21	533×305	898	90	24.8	340	73	262**
11-15	381×305	516	90	37.2	152	73	347
11-18	457×305	770	90	32.4	229	73	402
11-21	533×305	836	90	35.9	305	73	506
11-24	610×305	1023	90	29	381	73	534

* 9-12 means: #9 (29 mm) bars and 12×12 in. (305×305 mm) column.

** The concrete quality in this test was questionable.

Pinc emphasized that the lead embedment length is the major variable affecting the stress and slip characteristics of a hooked bar. Test results showed that longer lead embedment lengths result in higher stress at failure in all cases. Pinc also confirmed that slip is greater at all stress levels with shorter lead embedment. Using test data from his study and previous studies, Pinc suggested that design procedures can be adjusted to reflect realistically the strength of hooked bar anchorages by considering the contribution of the hook and the straight lead embedment as a unit.

In a recent study, Hamad and Jirsa [12] conducted a similar experimental investigation to study the anchorage behavior of epoxy coated bars in exterior

joints. In this study, 12 out of the 24 specimens tested were manufactured using regular (uncoated) reinforcing bars. A summary of these 12 specimens is given in Table 4.3. Figures 4.5 and 4.6 show Hamad and Pinc specimens' reinforcement details.

Table 4.3 Parameters and Results of Hamad and Jirsa Hooked Bar tests [12].

Specimen Notation*	Column Size (mm)	Column Axial load (KN)	Hook Angle (deg)	f'_c (MPa)	Lead Embed. (mm)	Confinement	Max Load (KN)
7-90-U(1)	305×305	-	90	37.2	152	-	163
11-90-U(1)	381×305	-	90	37.2	305	-	334
7-90-U-T4	305×305	-	90	25.5	152	10M @102 mm	174
11-90-U-T6	381×305	-	90	25.5	305	10M @152 mm	319
7-180-U-T4	305×305	-	180	26.9	152	10M @102 mm	154
11-180-U-T6	381×305	-	180	26.9	305	10M @152 mm	++
7-90-U	305×305	-	90	17.7	152	-	116
11-90-U	381×305	-	90	17.7	305	-	214
7-90-U-SC**	305×305	-	90	29.1	152	-	133
11-90-U-T4	381×305	-	90	29.1	305	10M @102 mm	370
11-90-U-HS ⁺	305×305	-	90	49.6	152	-	328
11-180-U-HS ⁺	381×305	-	180	49.6	305	-	262

* 7 90-U-T4 means #7 (22 mm) uncoated bars, with 10 mm (#3) ties spaced at 4 inches (102 mm) through the joint.

** The nominal side concrete cover over the hooked bars was 48 mm (1 7/8 in.) with the column bars placed inside the beam bars. In all other test specimens the nominal side cover was 73 mm (2 7/8 in.) with the beam bars placed inside the column bars.

+ High strength concrete.

++ The specimen could not be tested.

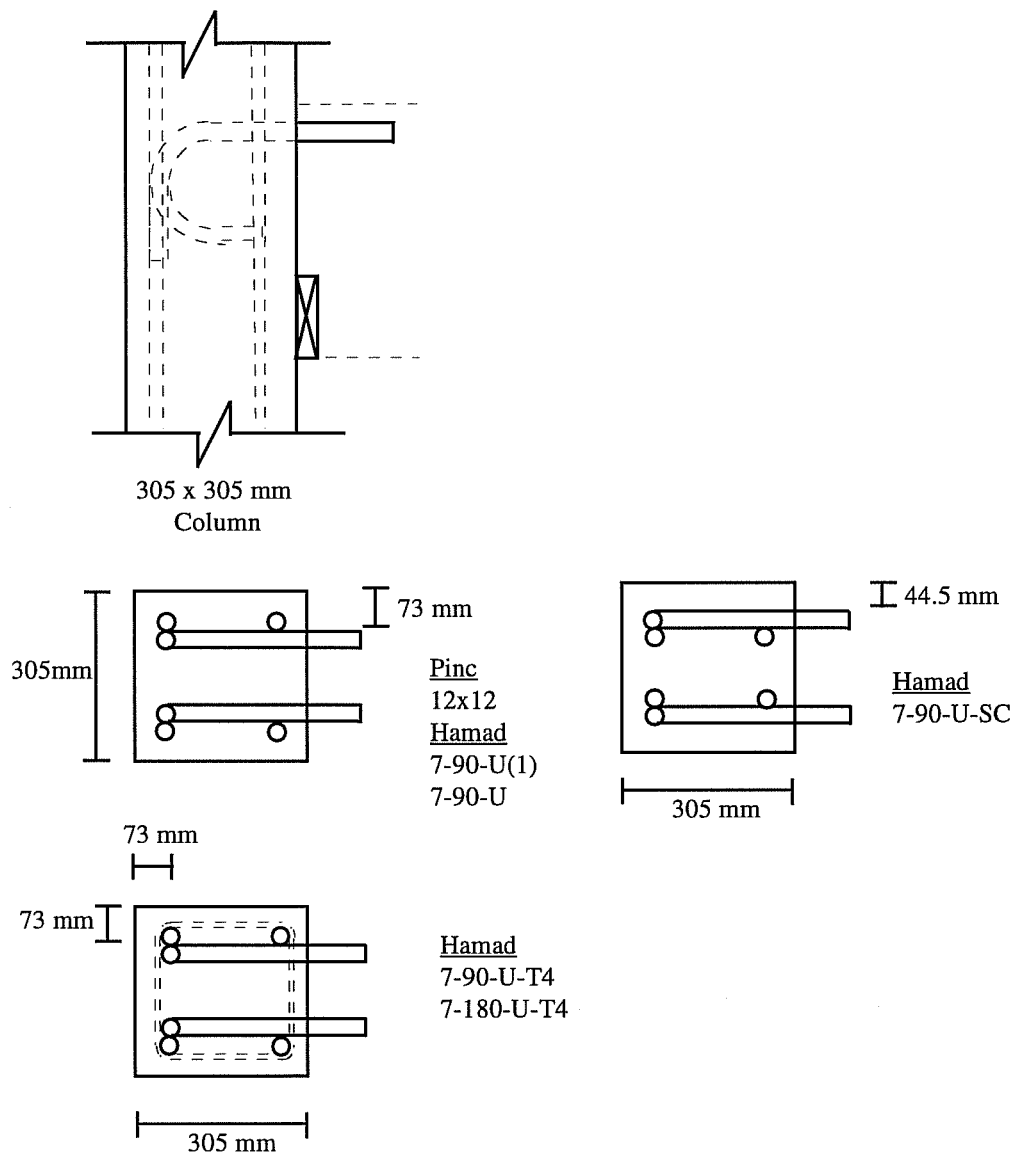


Figure 4.5 Joint details of the #7 Hooked Bar Specimens by Pinc [11] and Hamad [12]

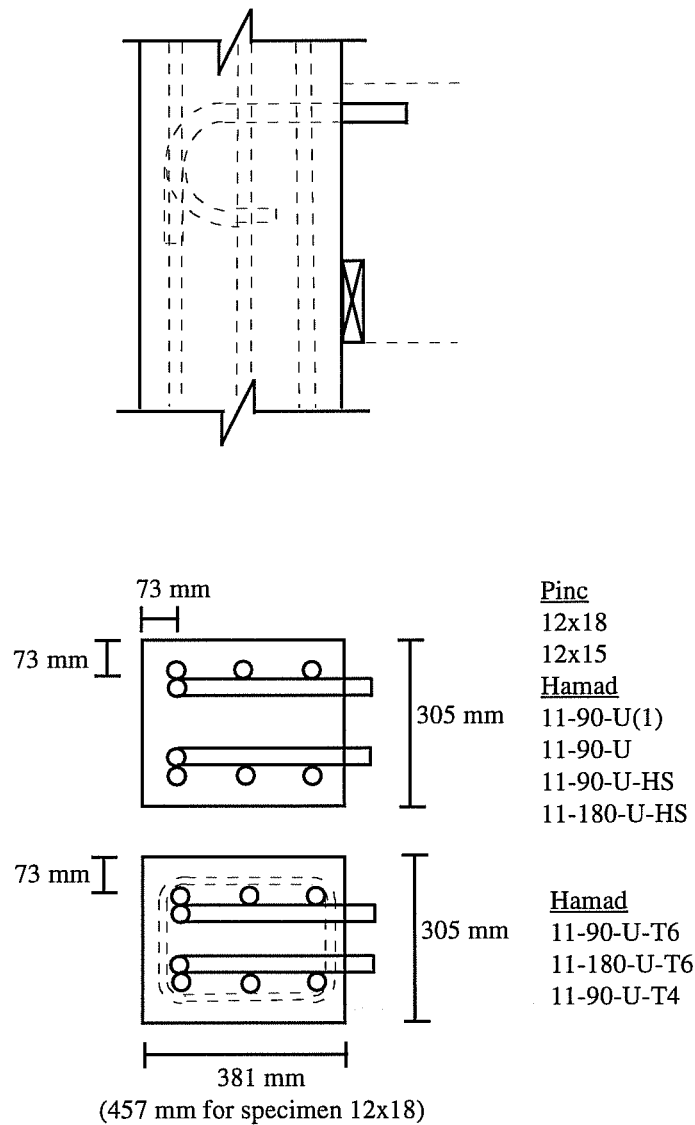


Figure 4.6 Joint details of the #11 Hooked bar Specimens by Pinc [11] and Hamad [12]

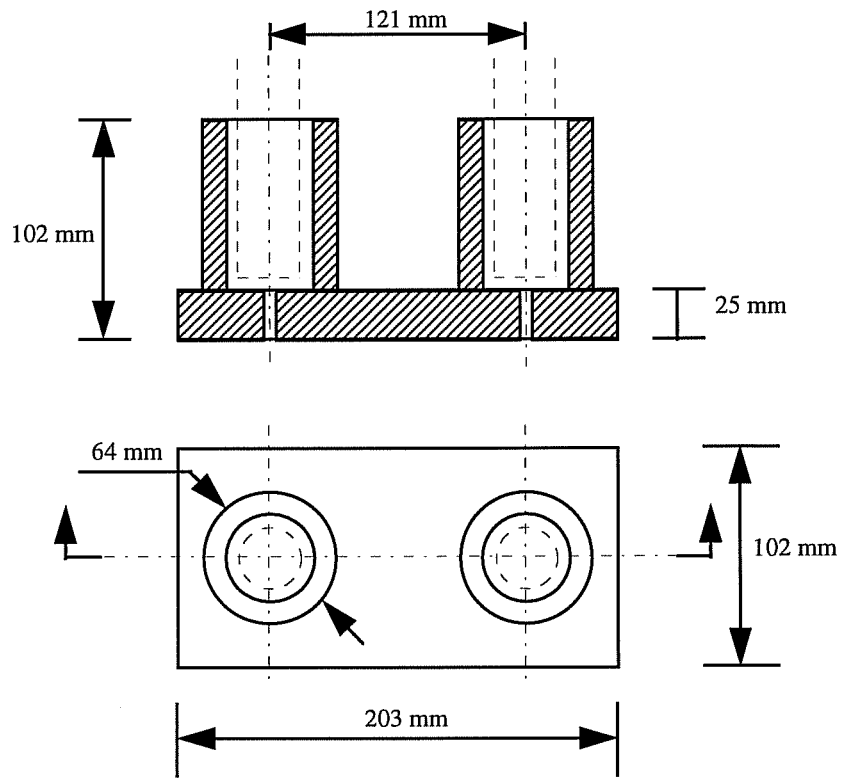
The performance of mechanical anchorages in beam column joints was examined in an earlier study by Burguieres [13]. The mechanical anchorage

consisted of a single plate attached to the beam reinforcing bars. Two types of anchorage devices were used (Figures 4.7 and 4.8). Six specimens were tested to determine basic behavioral characteristics and trends. The specimens simulated exterior beam-column joints and were patterned after the study by Marques. The main variables in this study were the type of anchorage device and the amount of lateral reinforcement. An axial load of approximately 75 percent of the ultimate axial capacity was applied to all specimens. The properties of the 6 specimens tested in this study are summarized in Table 4.4.

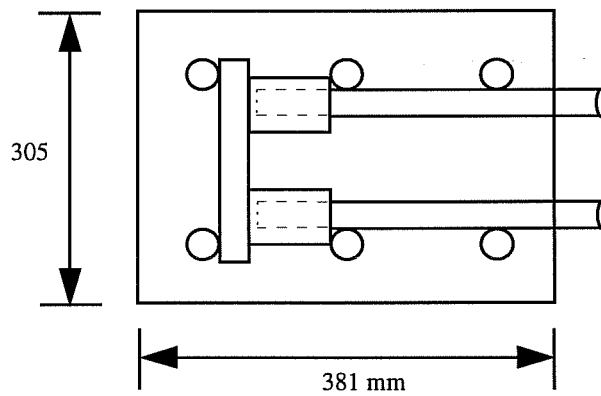
Table 4.4 Parameters and results of Burguieres and Jirsa Mechanical Anchorages tests [13].

Specimen Notation*	Column Size (mm)	Column Axial load (KN)	Anchor age type	f'_c (MPa)	Side cover (mm)	Max Load (KN)
CJ-1-0-B	381×305	480	B	20.3	73	291
CJ-2-5-B	381×305	627	B	31.6	73	Yield
CJ-3-2.5-B	381×305	805	B	29.4	73	Yield
CJ-4-0-U	381×305	898	U	22.5	73	291
CJ-5-5-U	381×305	516	U	34.4	73	Yield
CJ-6-2.5-U	381×305	770	U	29.7	73	458

* CJ-2-5-B means: Joint 2, 10 mm (#3) ties at 5 in. (127 mm), and anchorage type B.

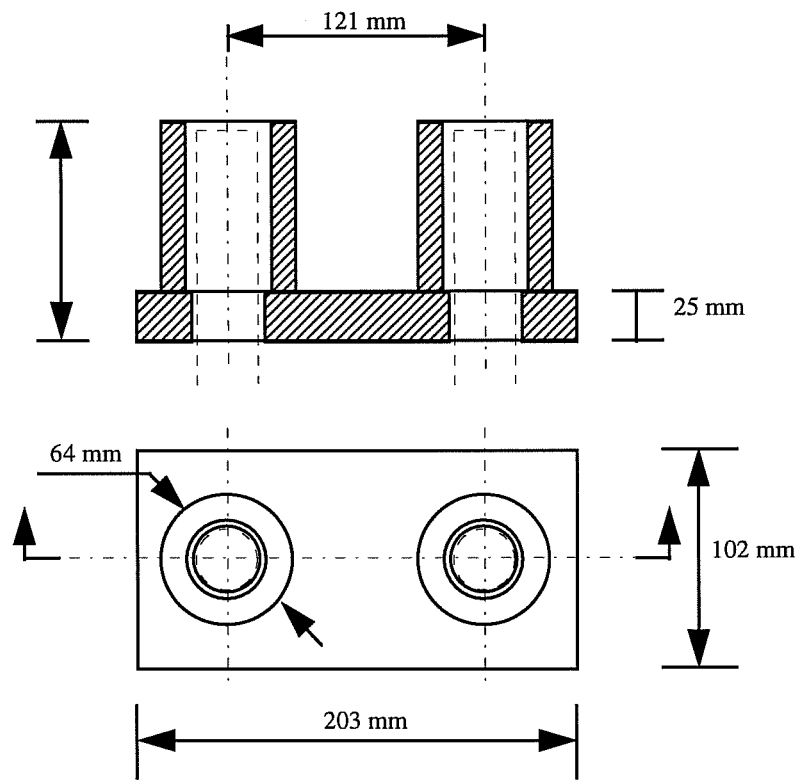


a) Anchorage device detail

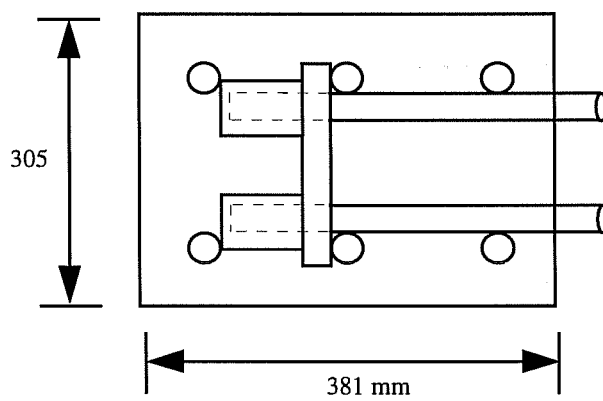


b) Location - Plan view

Figure 4.7 Mechanical anchorage type B, Burguires [13]



a) Anchorage device detail



b) Location - Plan view

Figure 4.8 Mechanical anchorage type U, Burguires [13]

Although it was difficult to arrive at a comprehensive explanation of the observed behavior and strength of the anchorages tested based on the limited test program in that study (note that only 3 specimens failed), a failure hypothesis was developed. The nature of the anchorage devices used eliminated the governing mode of failure for hooked bars. Hooked bar anchorage studies indicated that the ultimate anchorage capacity was for the most part governed by splitting and spalling of the side concrete cover induced by wedging action in the bearing area inside the hook. In both types of anchorage devices used by Burguières the bearing area was much larger than that of a hooked bar. Furthermore the steel plate in the devices used restrained the outward splitting of the bars. The failure pattern observed was vertical cracking near the anchor plate extending and widening with the increase of load. At failure, bar slip increased significantly, and the applied load dropped suddenly. This type of failure was compared to that of a deep beam, in which the bearing plate resembles the applied load, and the beam compressive zone resembles a close support. The axial load effectively made the column a prestressed element. No consistent verification of that hypothesis could be achieved based on the limited test program. Equations for the shear capacity of deep beams reported in the literature provided a wide range of capacities, and none of them were consistent with the results from this study. In addition to this, the influence of lateral reinforcement on the capacity was not

clearly established, because of the variance of concrete strength, and the yielding of the beam bars in three of the four specimens with lateral reinforcement. The anchorage capacity of the only failing specimen with lateral reinforcement was not greatly affected. However the anchorage stiffness was improved by lateral reinforcement after cracking.

4.3 Experimental Program

To study the main parameters affecting the anchorage capacity in exterior beam column joints a study comprising 32 large scale specimens was conducted. The specimen used in this study are similar to those used by Marques, Pinc, and Hamad for hooked bars, and by Burguieres in his study on mechanical anchorages in beam column joints.

As in previous studies, an attempt was made to closely simulate realistic beam-column joint conditions. The main criteria the test program was based on are:

- 1) The specimens should be large scale models of beam-column joints in order to eliminate scale effects, and to permit the application of relatively large forces on the anchored bars.
- 2) The specimens should be small enough to be easily handled and inexpensive to fabricate.

- 3) The specimens and the testing setup should approximate the loads and the stresses which would be expected in the joint region, especially where the beam bars are anchored.
- 4) The specimen dimensions and the size of anchored beam bars should be close to those used in the previous hooked bar studies to allow direct comparison.

4.3.1 Design of Specimens

In Tables 4.5 and 4.6, the properties of the 32 specimens tested in this study are summarized. The specimens were manufactured in seven series, with the first three series consisting of four specimens each, and the last four series consisting of five specimens each. The specimens were numbered in the order of manufacturing. In the first series (T1 to T4) the column height was 1270 mm (50 in.), similar to that used in hooked bar studies. In the following specimens the column height was increased to 1473 mm (58 in.) in order to increase joint shear. The width of all specimens was 305 mm (12 in.). The width of the beam was equal to that of the column. This allowed a spacing of about 89 mm (3.5 in.) between two 35 mm (#11) beam bars anchored inside the column bars. While the column depth was one of the variables, the height of the assumed beam was kept constant at 508 mm (20 in.). Geometrical and reinforcement details of all seven series are shown in Figures 4.9 to 4.26.

Table 4.5 Parameters of Joint Test Specimens

Specimen Notation	Column Size (mm)	Bar Size	Side Cover (mm)	Confinement	f'_c (MPa)
T1	381×305	35	76	-	26.7
T2	381×305	35	76	-	29.4
T3	381×305	35	76	-	29.4
T4	305×305	25	76	-	26.7
T5	381×305	35	76	-	22.5
T6	381×305	35	76	10M @ 102 mm	22.5
T7	381×305	35	76	10M @ 64 mm	23.2
T8	305×305	25	76	10M @ 102 mm	29.6
T9	381×305	35	76	-	34.5
T10	381×305	35	38	-	34.5
T11	381×305	35	76	10M @ 102 mm	35
T12	305×305	25	38	-	35
T13	381×305	25	38	-	38.3
T14	381×305	35	76	10M @ 102 mm	37.2
T15	381×305	35	76	-	40
T16	457×305	35	76	-	39.6
T17	305×305	35	76	-	36.1
T18	381×305	35	76	-	36.2
T19	381×305	35	76	-	36.2
T20	305×305	35	76	-	35.2
T21	305×305	25	76	-	35.2
T22	305×305	25	76	-	35.2
T23	381×305	35	76	-	33.2
T24	381×305	35	76	-	32.3
T25	381×305	35	76	10M @ 51 mm	32.3
T26	533×305	35	76	-	31.4
T27	305×305	35	76	-	31.4
T28	381×305	35	76	-	33.3
T29	381×305	35	76	-	33.3
T30	381×305	25	76	-	22.1
T31	305×305	35	76	-	33.3
T32	305×305	25	76	-	33.3

Table 4.6 Head dimensions for joint specimens

Specimen Notation	Head Dimensions (mm)	Head Orientation	Strain gage position (a, mm)*	Head Area (mm ²)	$\frac{\text{HeadArea}}{\text{BarArea}}$
T1	100×55×25	Vertical	32	5500	5.5
T2	55×100×25	Horizontal	32	5500	5.5
T3	90×90×20	-	27	8100	8.1
T4	80×40×18	Vertical	27	3200	6.4
T5	100×55×25	Vertical	-	5500	5.5
T6	100×55×25	Vertical	-	5500	5.5
T7	100×55×25	Vertical	-	5500	5.5
T8	80×40×18	Vertical	-	3200	6.4
T9	55×55×25	-	-	3025	3
T10	55×54×25	-	-	2970	3
T11	100×55×25	Vertical	28	5500	5.5
T12	80×40×18	Vertical	23	3200	6.4
T13	80×40×18	Vertical	21	3200	6.4
T14	55×55×25	-	-	3025	3
T15	90×90×20	-	23	3025	3
T16	55×55×25	-	-	3025	3
T17	55×55×25	-	-	3025	3
T18	35×90×20	Horizontal	23	3150	3.2
T19	55×54×25	-	-	2970	3
T20	65×65×20	-	-	4225	4.2
T21	80×40×18	Vertical	24	3200	6.4
T22	58×28×18	Vertical	13	1624	3.2
T23	90×33×20	Vertical	23	2970	3
T24	33×90×20	Horizontal	23	2970	3
T25	55×55×25	-	-	3025	3
T26	55×54×25	-	-	2970	3
T27	55×55×25	-	-	3025	3
T28	90×90×20	-	23	8100	8.1
T29	100×55×25	Vertical	-	5500	5.5
T30	80×40×18	Vertical	-	3200	6.4
T31	62×62×20	-	-	3844	7.7
T32	100×38×25	Vertical	-	3800	7.6

* See figure 4.32

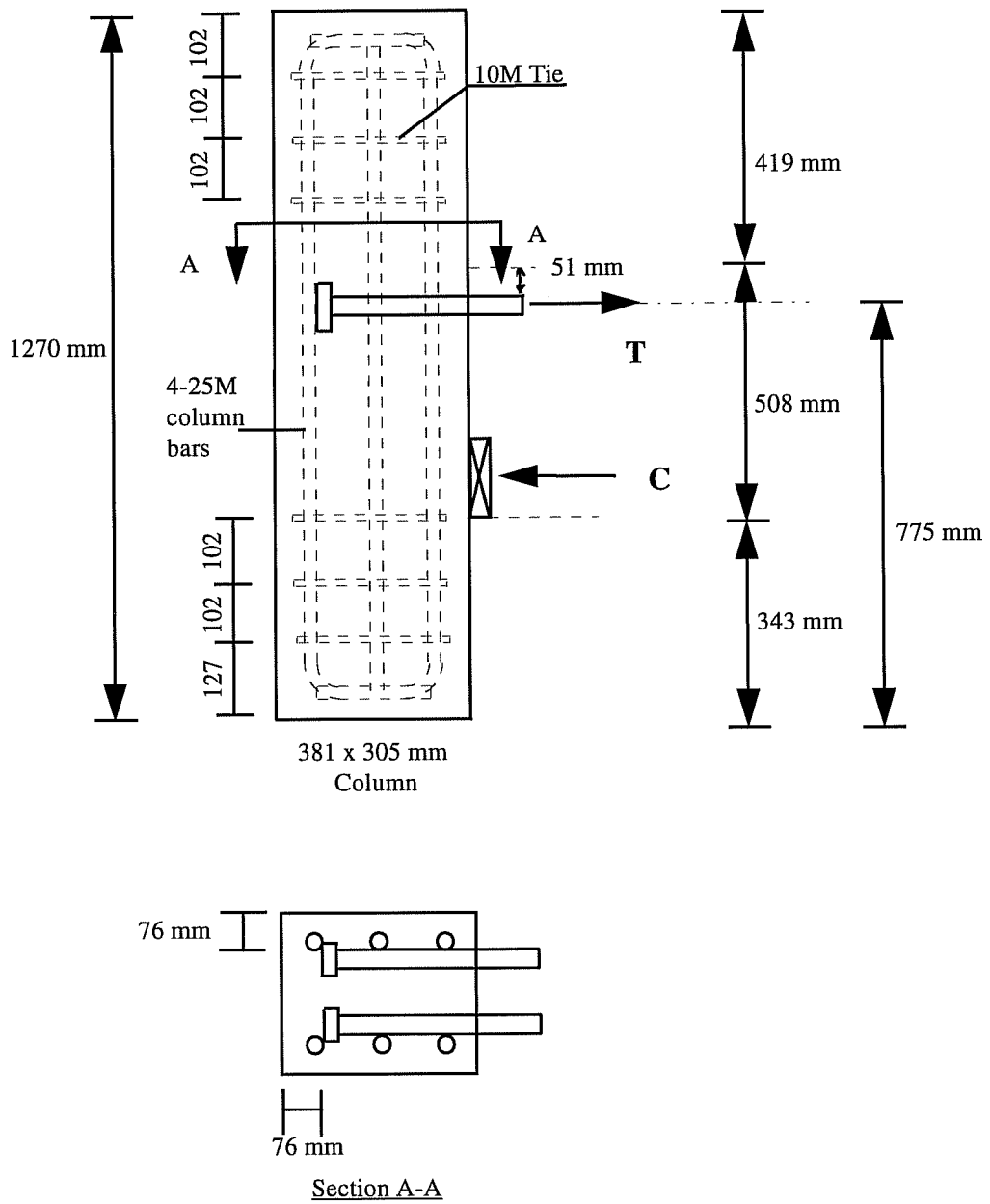
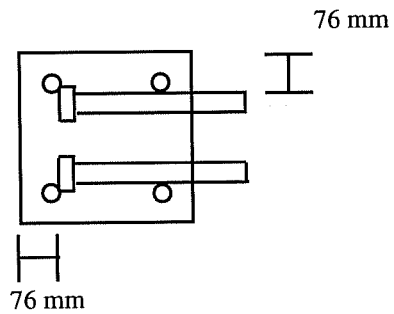
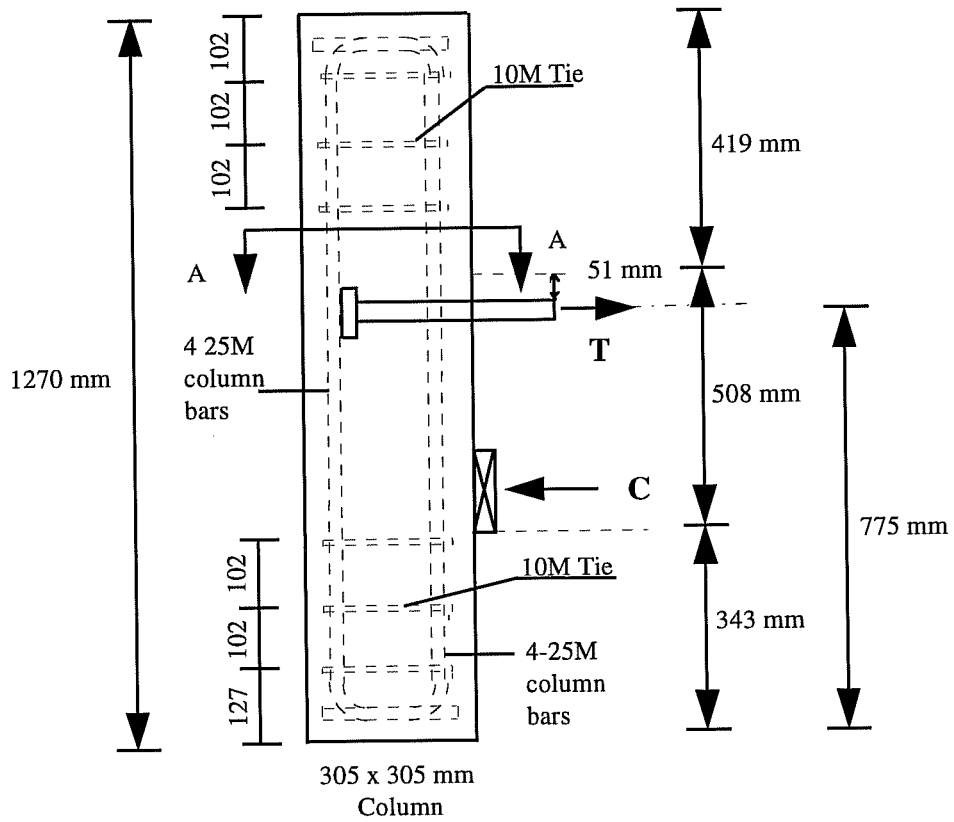
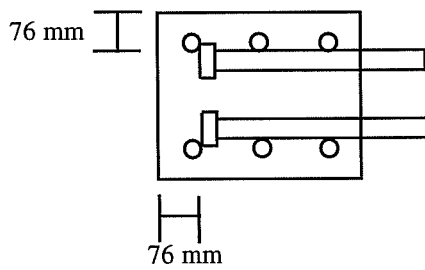
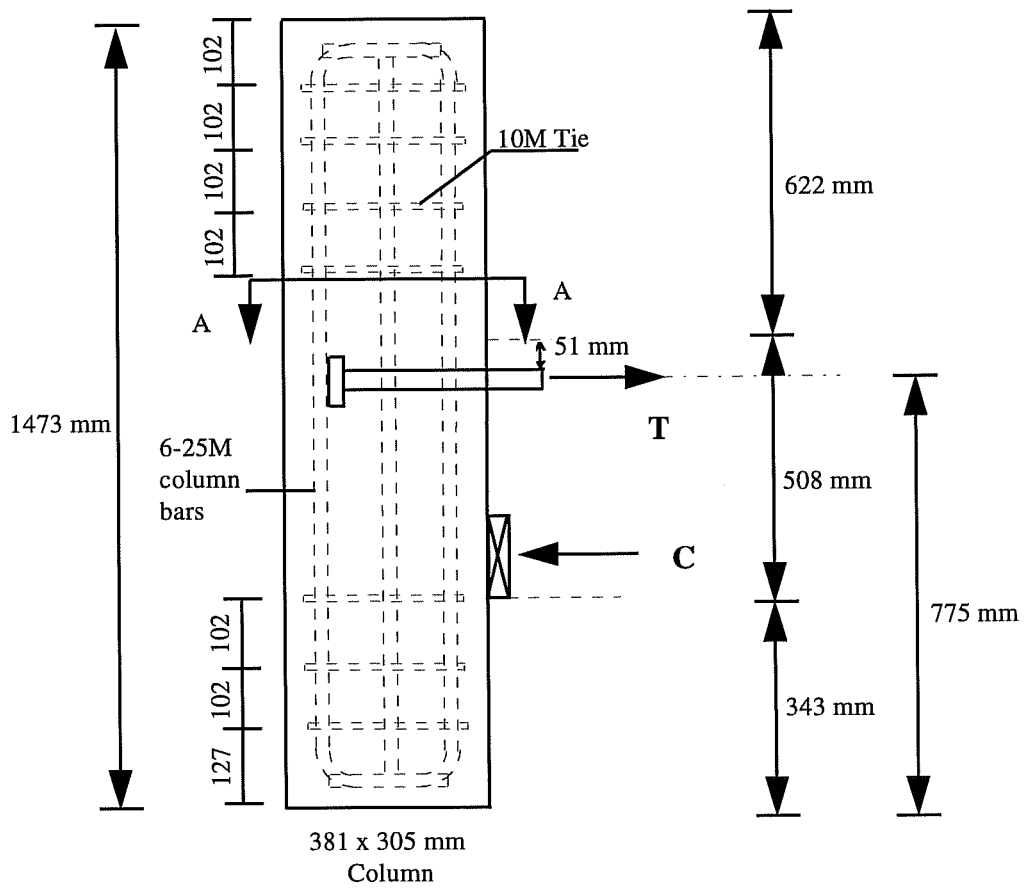


Figure 4.9 Reinforcement details - Specimens T1 through T3



Section A-A

Figure 4.10 Reinforcement details - Specimen T4



Section A-A

Figure 4.11 Reinforcement details - Specimen T5

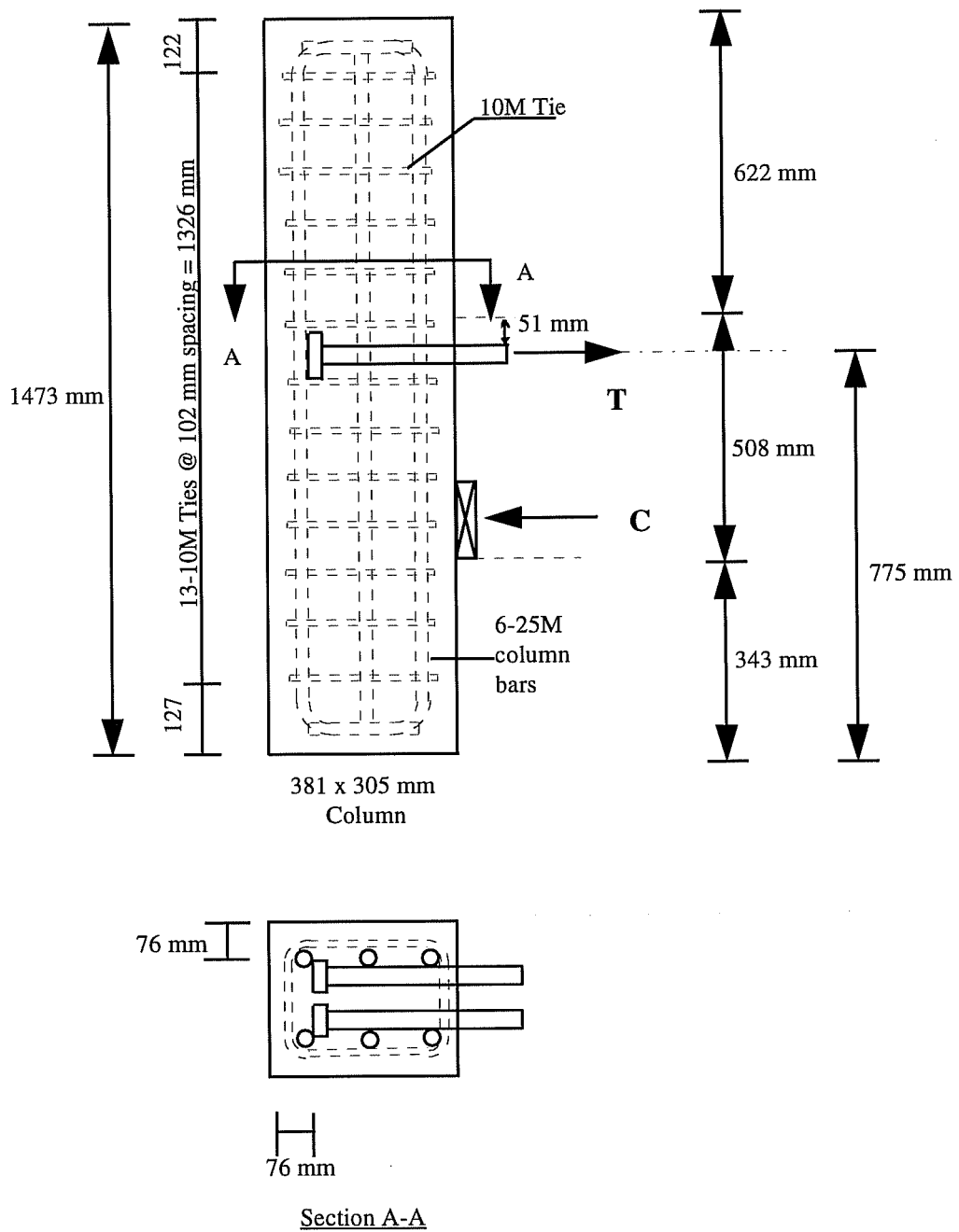
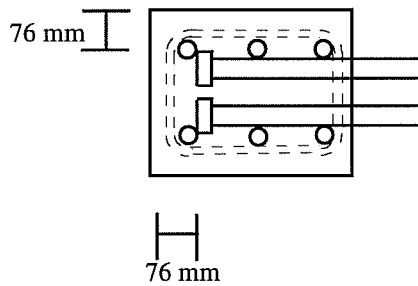
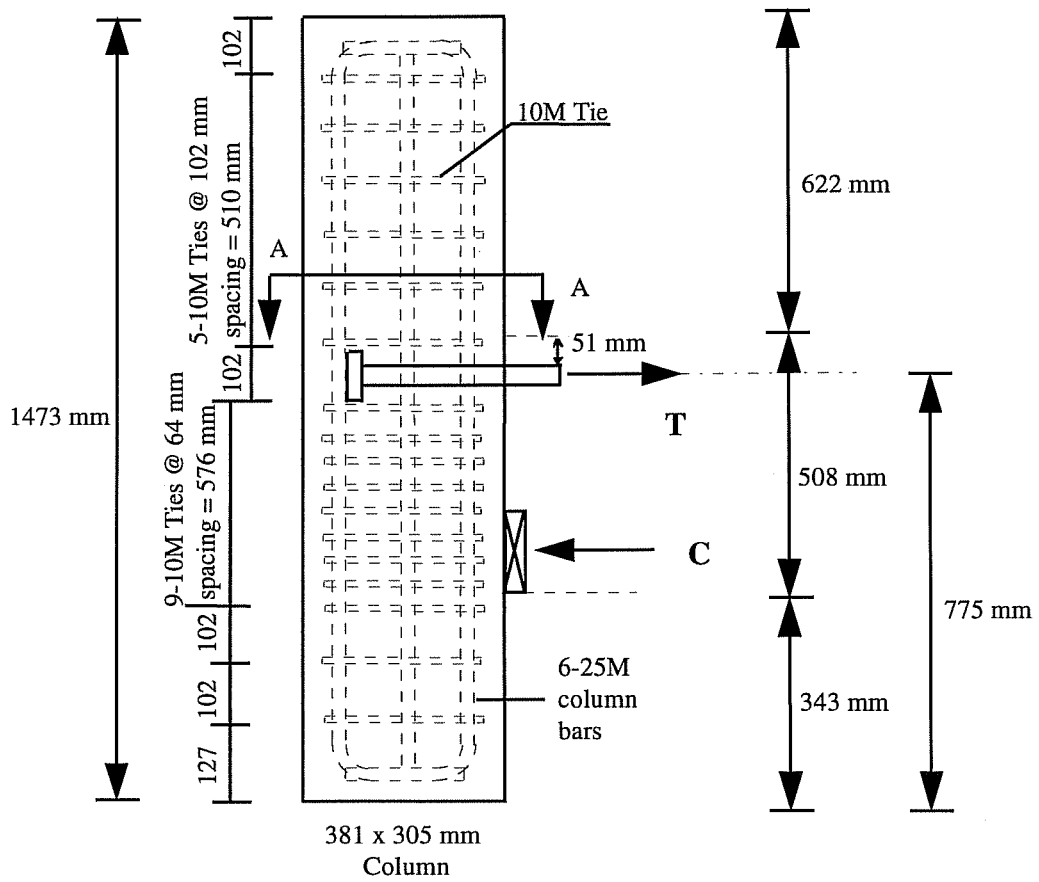


Figure 4.12 Reinforcement details - Specimen T6



Section A-A

Figure 4.13 Reinforcement details - Specimen T7

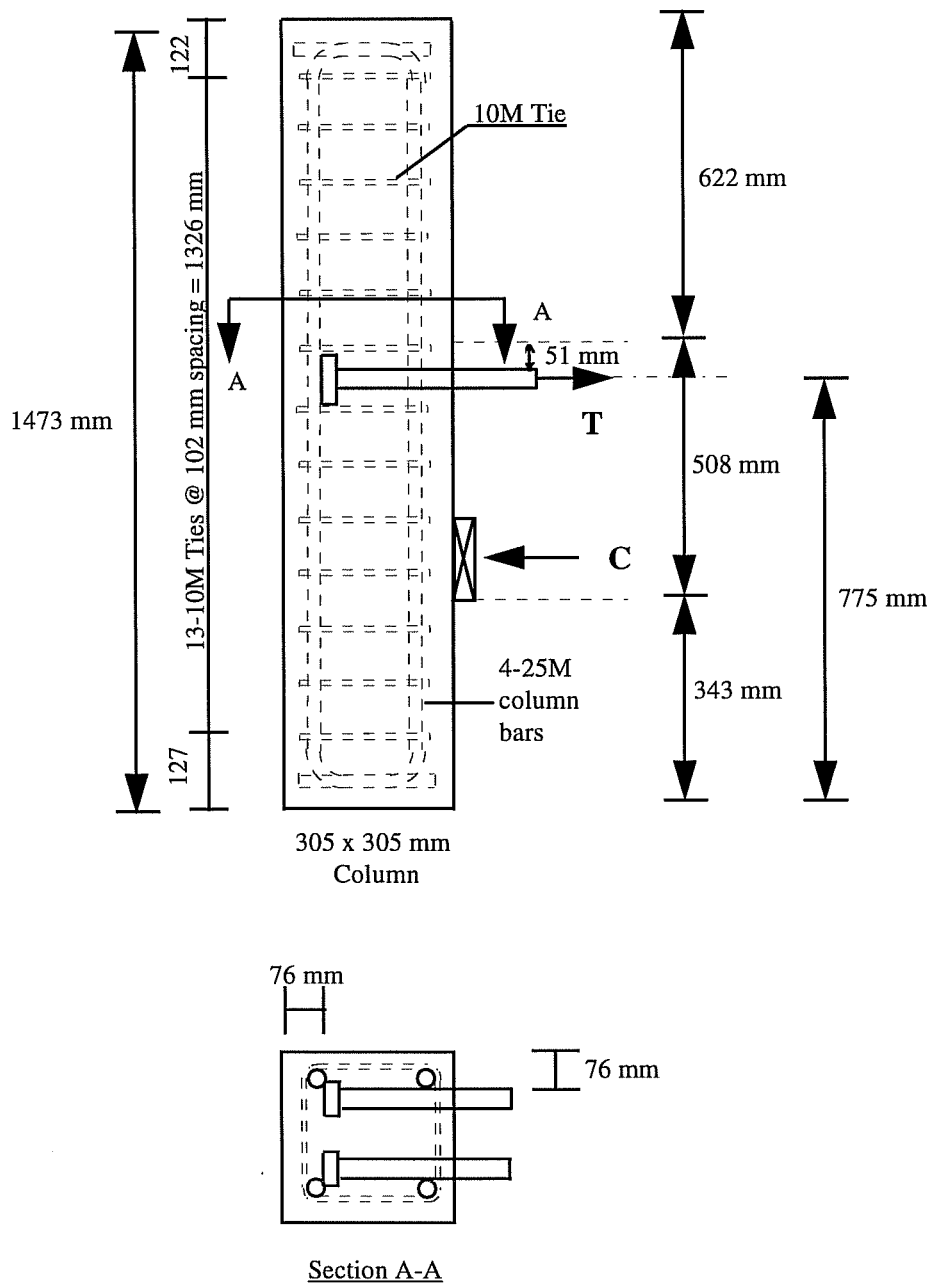
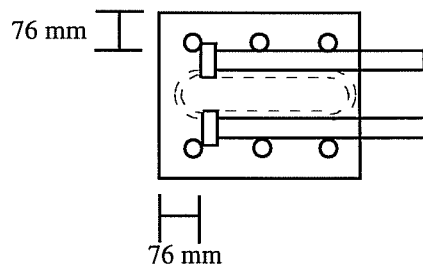
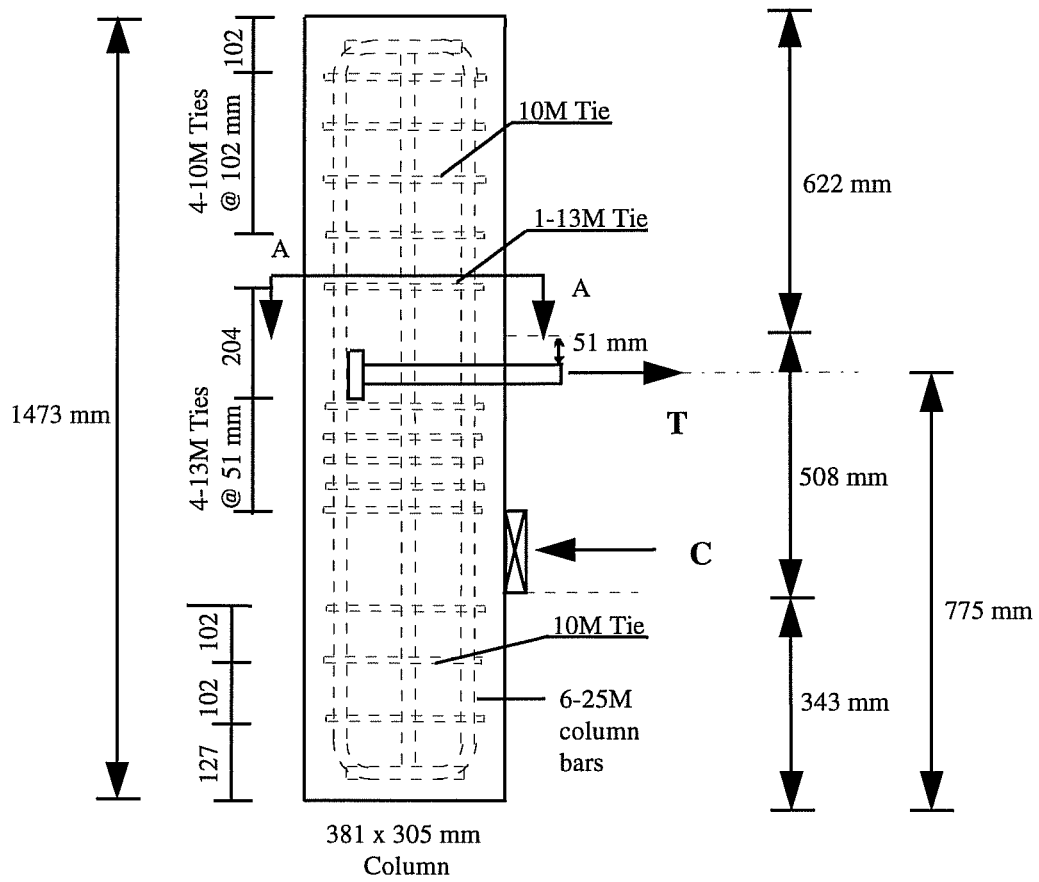


Figure 4.14 Reinforcement details - Specimen T8



Section A-A

Figure 4.15 Reinforcement details - Specimen T9

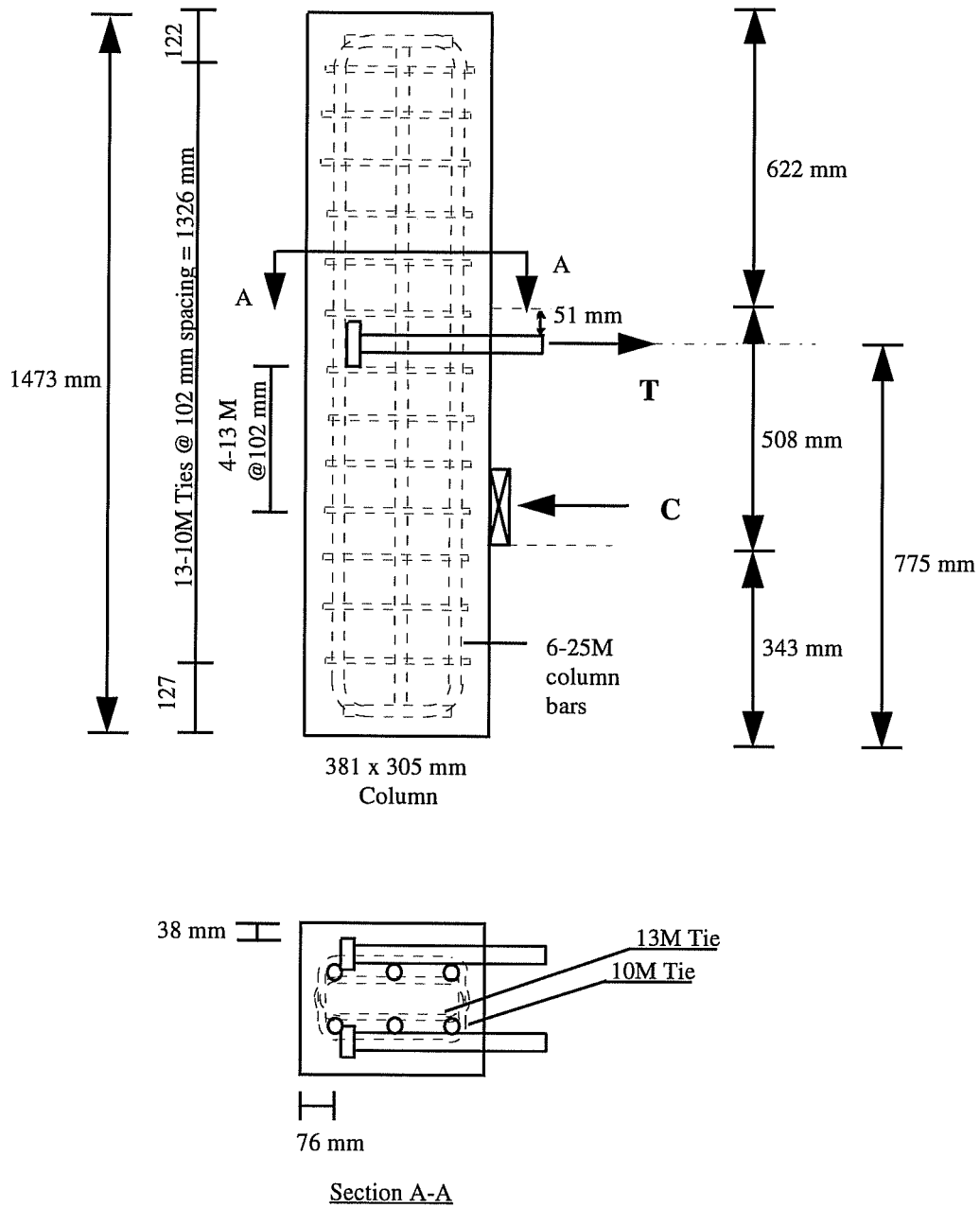


Figure 4.16 Reinforcement details - Specimens T10 and T13

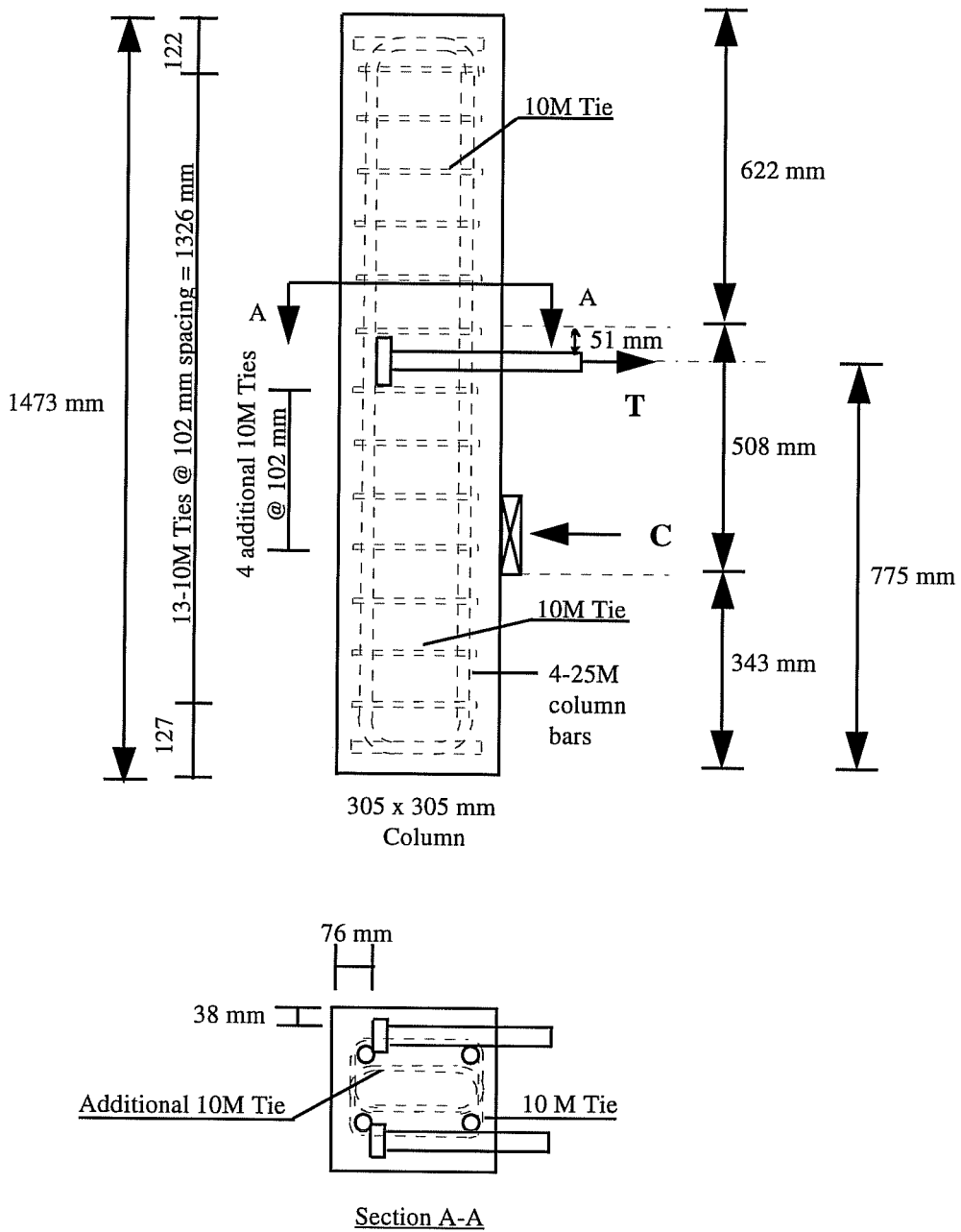


Figure 4.18 Reinforcement details - Specimen T12

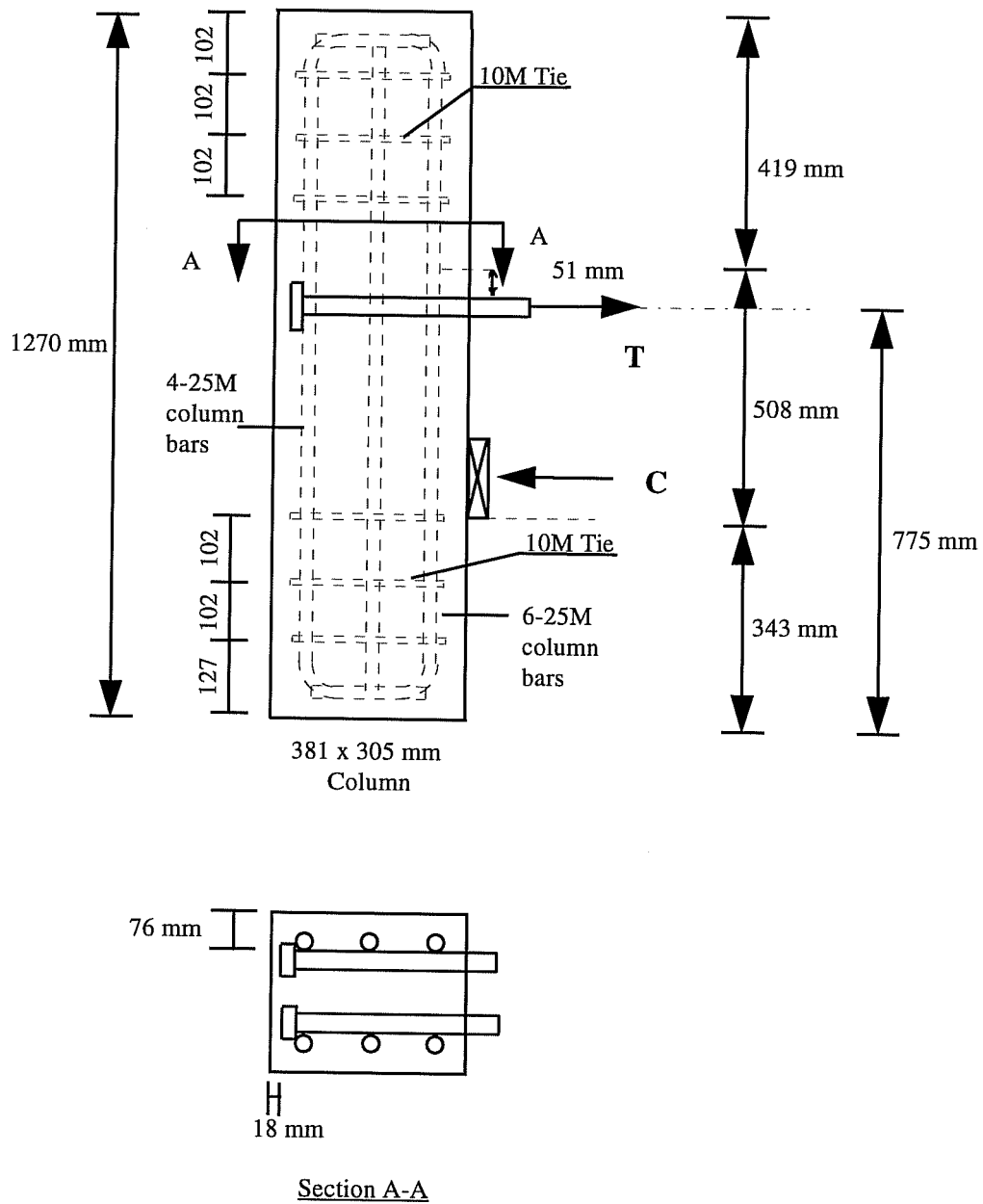
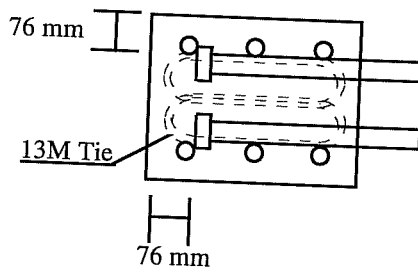
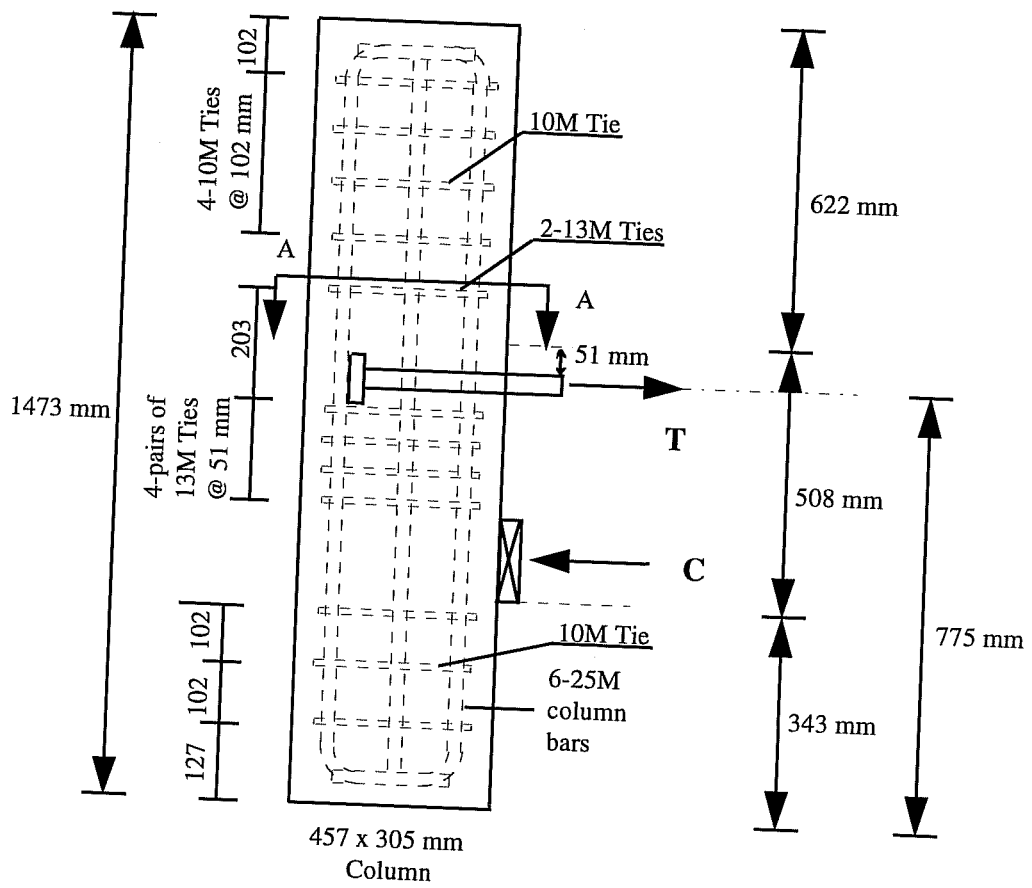


Figure 4.20 Reinforcement details - Specimens T15, T18, and T19



Section A-A

Figure 4.21 Reinforcement details - Specimens T16

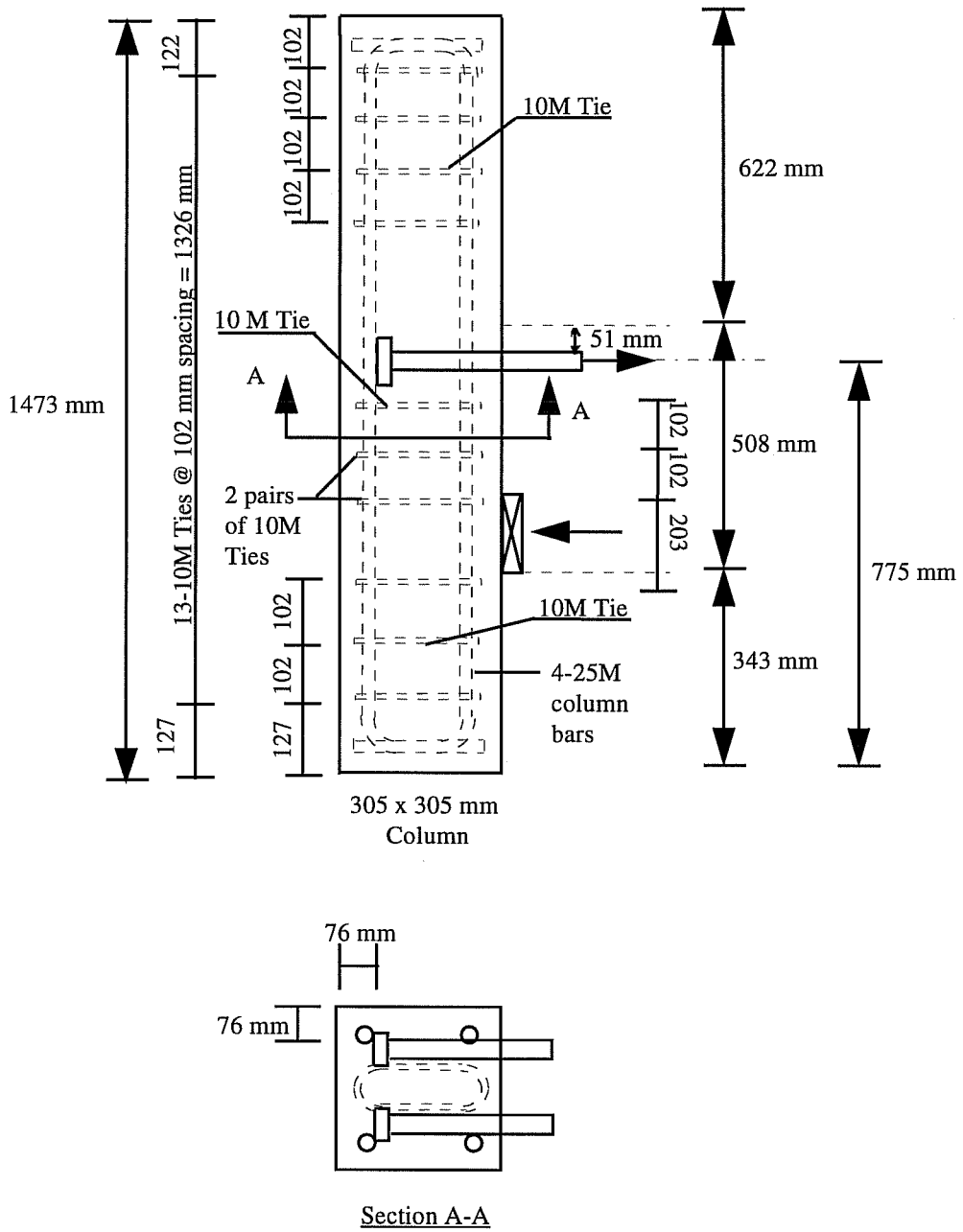
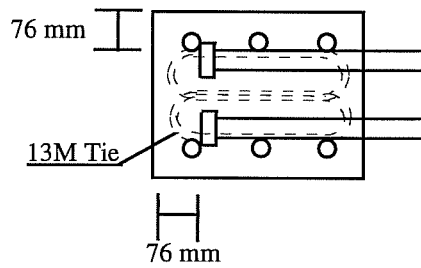
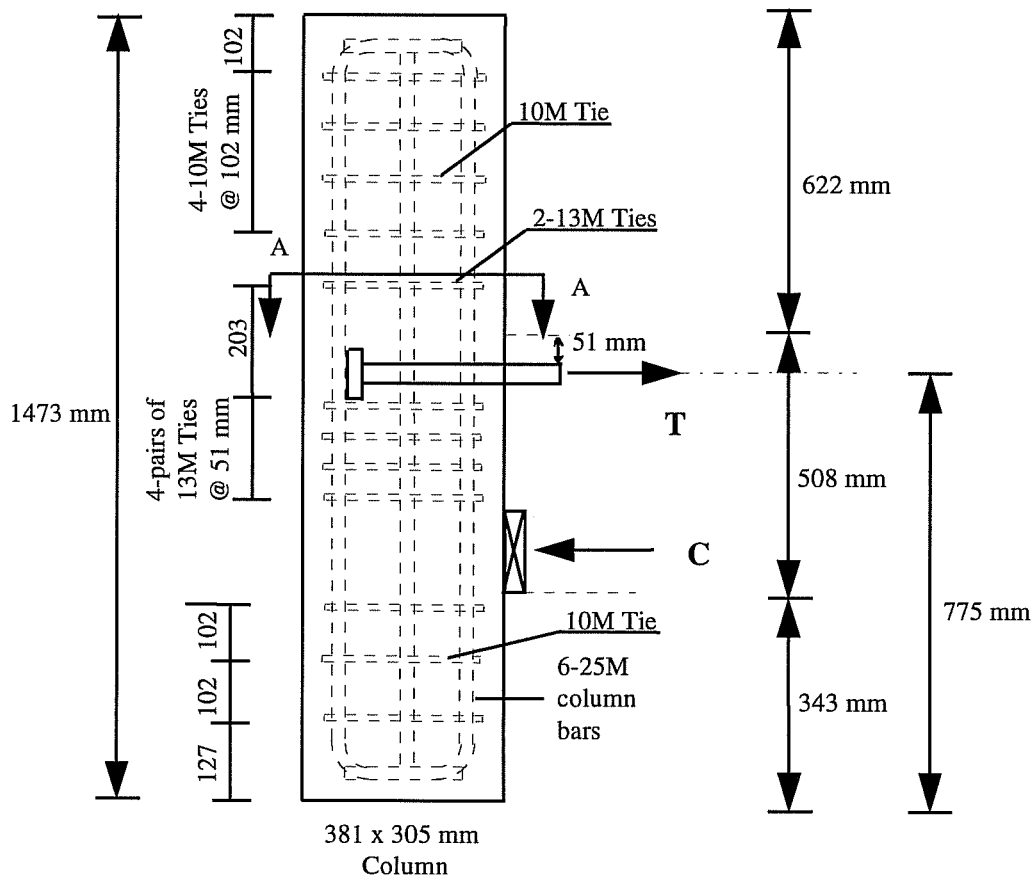


Figure 4.22 Reinforcement details - Specimen T17



Section A-A

Figure 4.23 Reinforcement details - Specimens T20, T23, T24, T28, T29, and T30

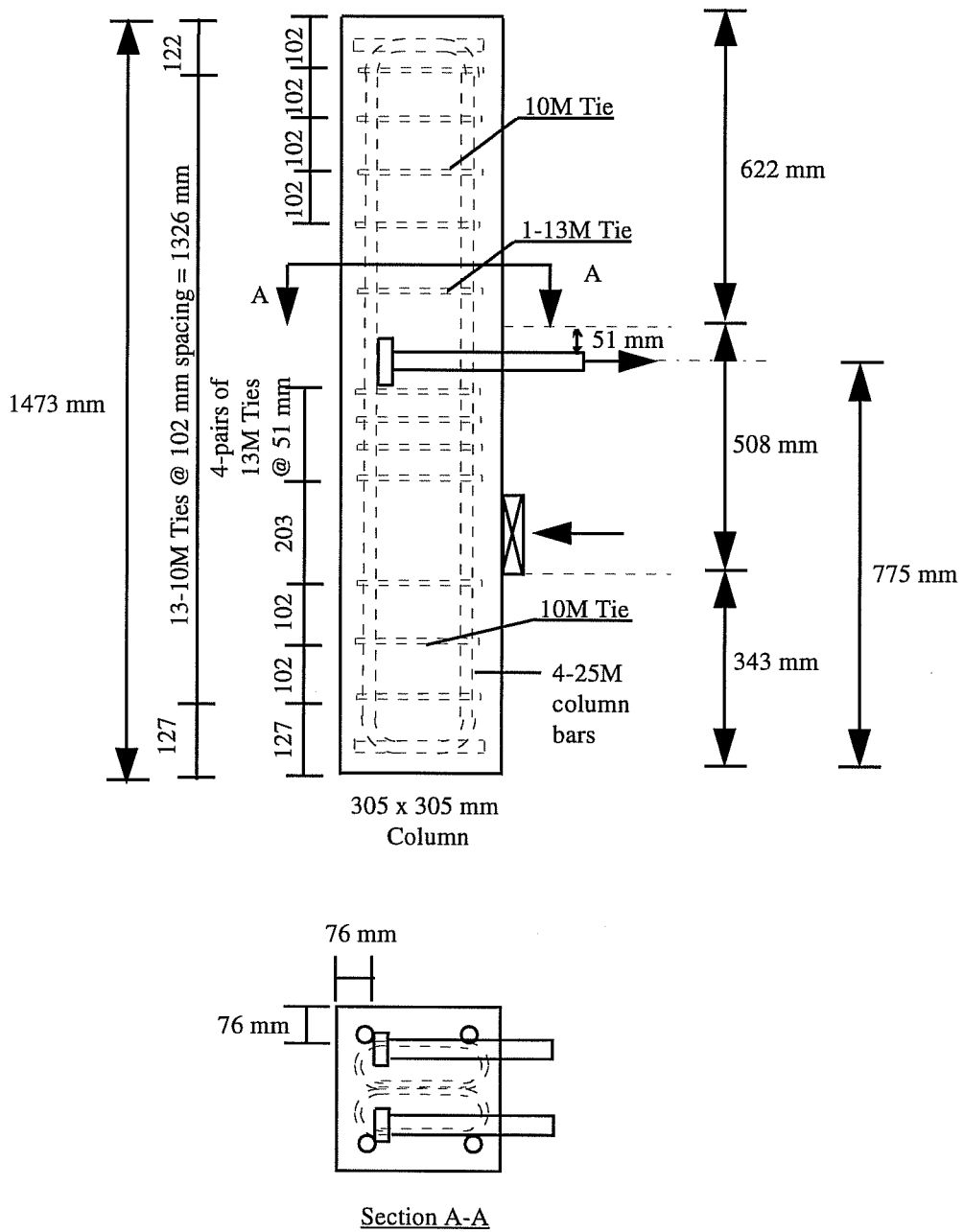


Figure 4.24 Reinforcement details - Specimens T21, T22, T27, 31, and T32

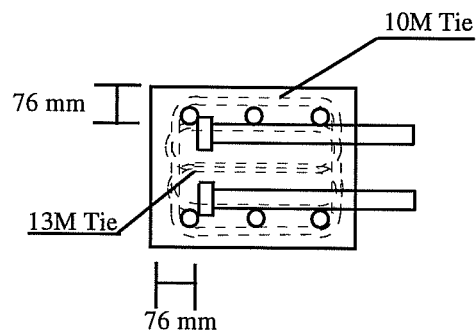
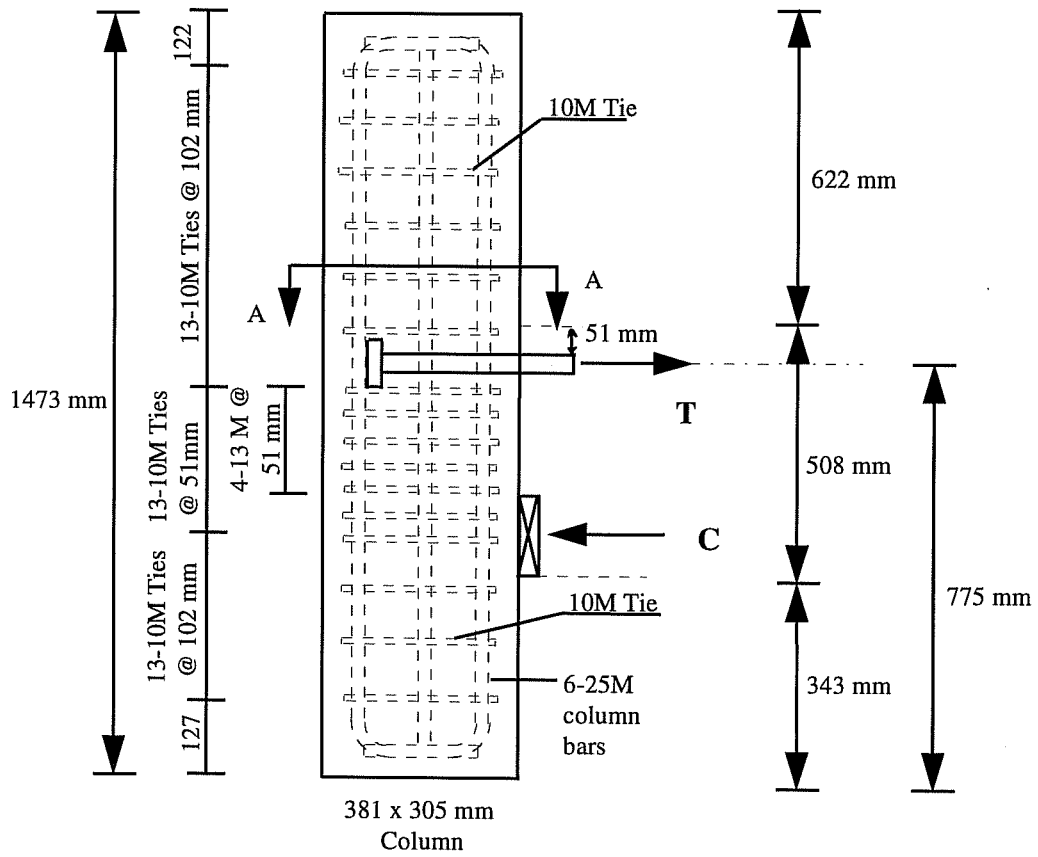
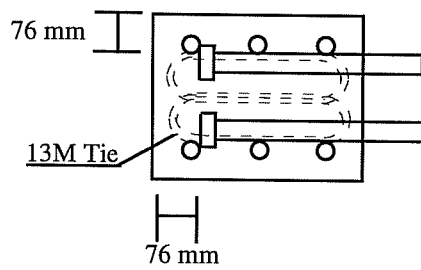
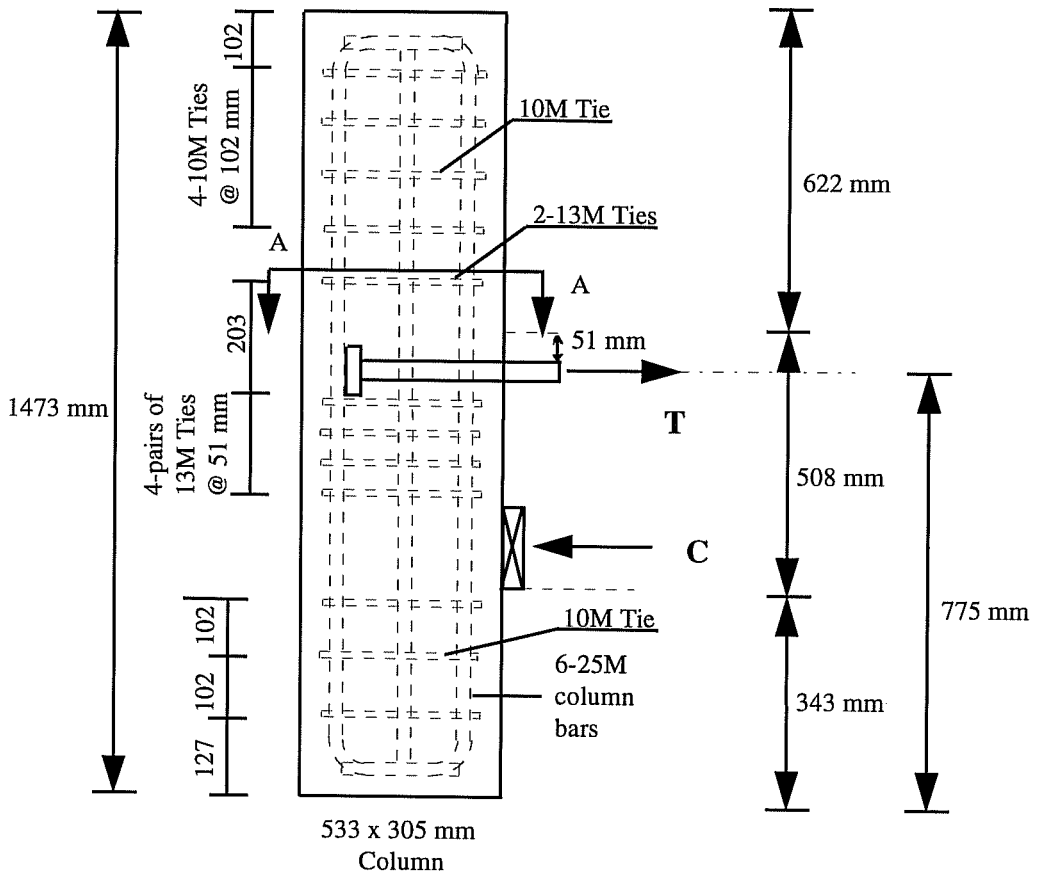


Figure 4.25 Reinforcement details - Specimens T25



Section A-A

Figure 4.26 Reinforcement details - Specimen T26

The 305×305 mm (12×12 in.) columns were reinforced with four 25 mm (#8) longitudinal bars. The longitudinal reinforcement in all other columns consisted of six 25 mm (#8) bars. Longitudinal column bars, except for those at the column center, had 90-degree hooks at both ends to prevent anchorage failure. All columns had 10 mm (#3) ties spaced at 102 mm (4 in.) outside the joint. The clear cover over the column ties was 38 mm (1.5 in.) providing a 76 mm (3 in.) cover over the anchored bars, except for the specimens in which the column bars were located inside the beam bars in order to provide an assessment of the effect of concrete side cover. In such case the concrete cover over the column ties was increased to provide a 38 mm (1.5 in.) over the anchored beam bars (Figures 4.16 and 4.18).

4.3.2 Variables

1) Anchored beam bars:

The tests were conducted with either two 25 mm (#8) or 35 mm (#11) bars anchored to the columns to allow comparison with hooked bar tests previously conducted using 22 mm (#7), 29 mm (#9), and 35 mm (#11) bars. For a 305×305 mm (12×12 in.) column and 381×305 mm (15×12 in.) column the 25 mm (#8) bar is a fairly practical anchorage situation. Increasing the beam

reinforcement to 35 mm (#11) bars gave an indication of the anchorage capacities of a fairly small joint, and allowed for higher tensile loads for larger columns. Using two bar sizes, with a relatively large difference in bar diameter, was essential to assess the effect of bar diameter on the anchorage behavior and capacity of headed bars.

2) Head Dimensions

To determine the influence of head area on headed bar anchorages, tests were conducted in which the head area was the only variable, ranging from 1624 mm² to 9100 mm² (2.5 in² to 14.1 in²). Tests T9, T20, and T28 had 35 mm (#11) bars anchored in the columns, with head area ratio of 1:1.4:2.7. Tests T21 and T22 had 25 mm (#8) bars anchored in the columns with head area ratio of 1:0.5. The effect of head aspect ratio and orientation was assessed in a similar manner. Tests T9, T23, and T24 had 35 mm (#11) bars anchored in the columns with similar head area and aspect ratios of 1, 2.7, and 0.37 respectively.

3) Embedment Length

The embedment length of a headed bar was defined as the length from the column face to the end of the bar, including the head. Although the effective embedment length does not include the head thickness, using the whole length provides ease of calculations for designers. Furthermore, this approximation

should not have any significant effect because the head thickness is usually much smaller than the lead embedment. By varying the size of the column, the embedment length was varied. For the 35 mm (#11) bars embedment lengths 229 mm (9 in.), 305 mm (12 in.), 381 mm (15 in.), and 457 mm (18 in.) were provided using columns with dimensions varying from 305×305 mm (12×12 in.) to 533×305 mm (21×12 in.) with increments of 76 mm (3 in.). A lead embedment length of 279 mm (11 in.) was also provided by anchoring the head behind the 381×305 mm (15×12 in.) column longitudinal bars in tests T15, T18, and T19. For the 35 mm (#8) bars, embedments of 229 mm (9 in.) and 305 mm (12 in.) were tested using 305×305 mm (12×12 in.) and 381×305 mm (15×12 in.) columns. Longer embedments were not tested to prevent yielding of the bars before failure.

4) Confinement and Shear Reinforcement

The effects of two types of confinement were considered, concrete cover and confining reinforcement. The influence of concrete side cover on the anchorage behavior was determined by comparing tests T9, T21, and T30 to tests T10, T12, and T13, respectively. In the first group of tests the anchored bars were confined with 76 mm (3 in.) of concrete cover in a addition to the column longitudinal bars. The latter group consisted of similar specimens in which the

beam bars were confined with 38 mm (1.5 in.) of concrete cover only. According to tests by Marques and Jirsa [9] the position of the column longitudinal bars (inside or outside the anchored beam bars) did not affect the stress-slip characteristics or the anchorage capacity.

The influence of column ties was determined by comparing tests T9 (without confining reinforcement through the joint) to tests T14 and T25 in which 10 mm (#3) ties confining the concrete outside the anchored bars were spaced at 102 mm (4 in.) and 51 mm (2 in.) respectively through the joint.

Tests T1 through T8 failed in a pattern similar to that observed by Burguieres. As it was desirable to have side-spalling failure type in order to examine the effect of the different variables on the anchorage capacity, the specimens design had to be changed. Instead of changing the column width (which would require changing the test setup and making new forms), 13 mm (#4) stirrups were used to increase the shear strength of the columns in the joint region. The new stirrups were not placed outside the anchored beam bars in order to prevent any confining effect. The only effect of these stirrups was to increase the joint shear capacity. The amount of shear reinforcement was altered based on the behavior of the specimens and stresses in the shear reinforcement.

The 32 specimens tested in this study were not axially loaded. Although some limited tests by Untrauer and Henry [14] indicated that normal pressure reduces the tendency for splitting the cover over the anchored bars and thus might have a beneficial effect on the anchorage strength of the bars in the joint, the study by Marques indicated that the effect of axial load is negligible on the stress-slip behavior and the anchorage capacity. It is believed that the relatively small size of the specimens tested by Untrauer affected his results.

4.3.3 Materials

a) Headed Bars

In all the specimens tested, each bar size (35 mm or #11, and 25 mm or #8) was from the same heat and had a parallel deformation pattern. The stress strain diagrams for both sizes are shown in Figure 3.2. These curves are based on nominal bar areas and elongations measured over a 203 mm (8 in.) gage length.

b) Other Reinforcement

For each series, each size of column reinforcing bars came from the same heat. The strength properties of the ties are summarized in Table 4.7. A typical stress-strain diagram for a column longitudinal bar (from series 6) is shown in Figure 4.27. While headed bars were supplied by the sponsor, the column bars and ties were supplied by a local vendor.

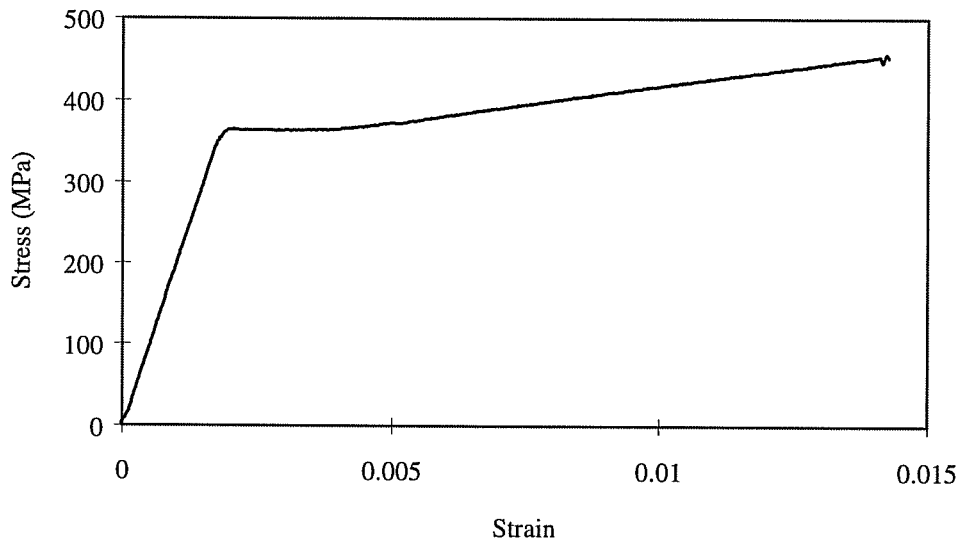


Figure 4.27 Stress-Strain curve for Series 6 Column Bars

c) Concrete

It was intended that the concrete strength in this study range from 27.5 MPa (4000 psi) to 34.5 MPa (5000 psi), to allow comparison with previous hooked bar studies. Two concrete mixes were ordered from a local ready-mix company and were proportioned to yield the required strength. The first mix had a maximum aggregate size of 19 mm (3/4 in.) and a 102 mm (4 in.) slump. This mix was used in series 1 and 2. In the remaining series, shear reinforcement in the joint caused congestion and it was felt that the maximum size aggregate should be decreased to 10 mm (3/8 in.) for the rest of the specimens. The rest of the mix ingredients were changed accordingly in order to sustain the target

strength and slump. Mix proportions for both mixes are shown in Table 4.8. The amount of water added at the time of casting in the laboratory in order to obtain a 102 mm (4 in.) slump is also presented. The measured concrete strength at the time of testing is shown in Table 4.5. The concrete strength was obtained from tests of standard 152×305 mm (6×12 in.) cylinders. The values presented in Table 4.5 are the average compressive strength of three cylinders broken on the same day the specimen was tested.

4.3.4 Specimen Fabrication

Four units of formwork were initially built so that four specimens could be cast from the same batch of concrete. One form was made for the 305×305 mm (12×12 in.) columns, and three were made for the 381×305 mm (15×12 in.) columns. In order to allow varying the embedment length of the beam bars a fifth adjustable form was built after testing the third series. The new form allowed the construction of specimen with a cross section up to 610×305 mm (24×12 in.). All the forms were built using 19 mm (3/4 in.) plywood stiffened with 51×108 mm (2×4 in.) lumber. The forms were built in sections then bolted together to allow for the easy removal and reuse of the formwork.

Column reinforcing bars and stirrups were cut and bent to the required dimensions by the vendor. Instrumentation of all bars was completed before assembling the reinforcement cages. The forms were prepared so that the columns would be cast in a horizontal position, with the column front face towards the top. The column reinforcement cages were placed inside the forms and steel chairs and wooden spacers were used to maintain the required side cover (Figure 4.28). After the beam headed bars were placed and aligned in a vertical position with a water level, the cage was tied. Wooden braces were used to keep the beam bars in a vertical position during casting (Figure 4.29). For each batch, slump was measured before casting. Additional water was added to increase the slump to the required level (102 mm or 4 in.) in all of the seven series. Concrete was placed in the forms directly from the ready-mix truck. Electrical vibrators were used to consolidate the fresh concrete during pouring. Eighteen standard 152×305 mm (6×12 in.) concrete cylinders were cast with each series. The exposed concrete surface (the face of the column) was screeded and trowelled to form a smooth surface.

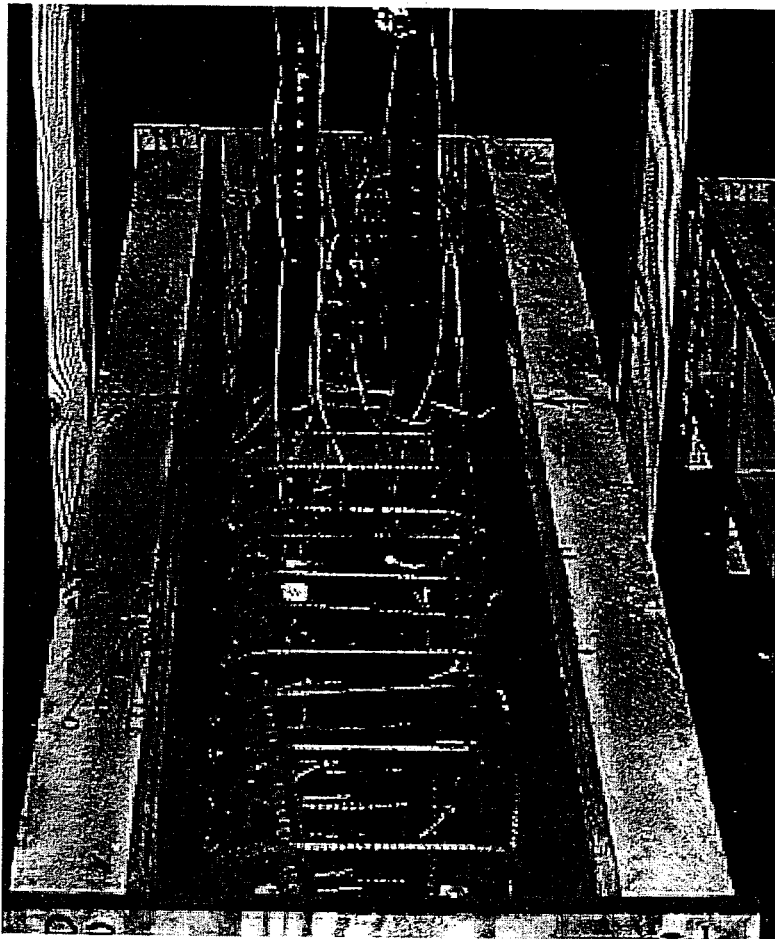


Figure 4.28 Steel cages inside the forms

4.3.5 Instrumentation of the Test Specimens

Each test was instrumented to measure the applied load, slip of the anchored headed bars, and stresses in the headed bars and selected shear reinforcement.

The applied load was determined using a 70 MPa (10,000 psi) capacity pressure transducer which measured the oil pressure in the rams. The oil pressure

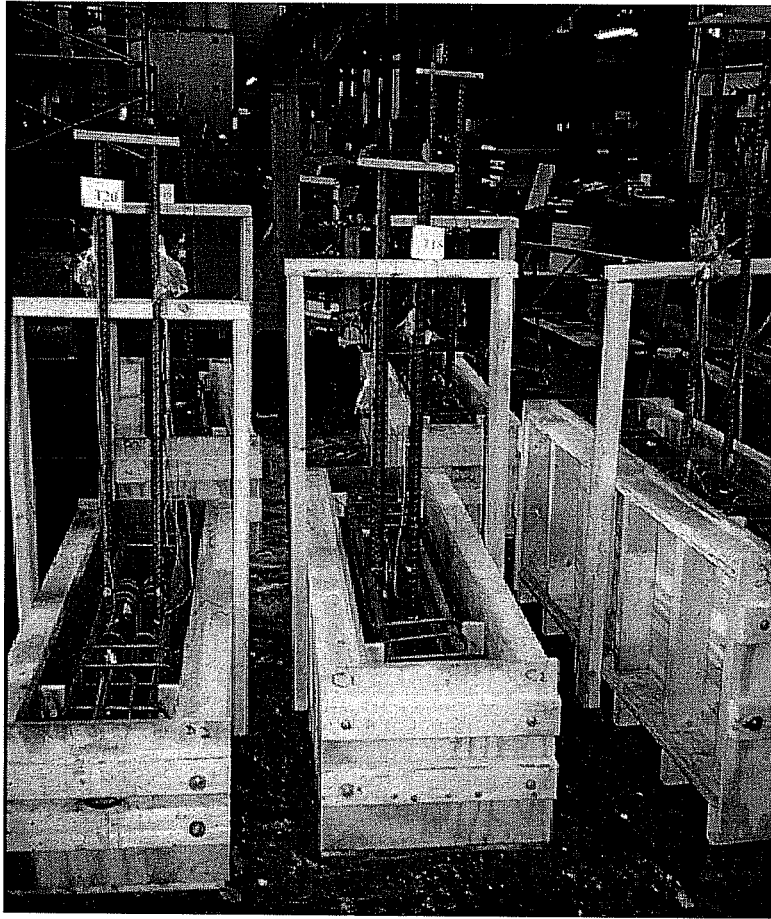
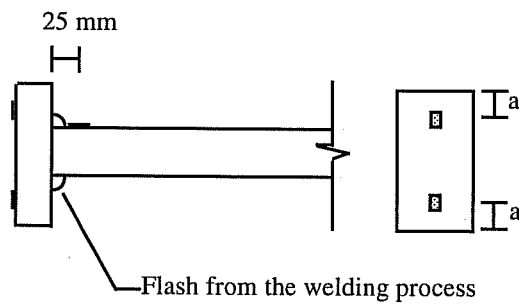


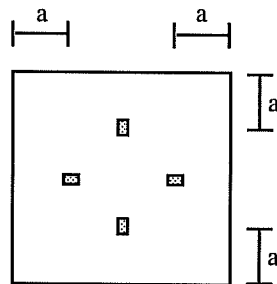
Figure 4.29 Specimens ready for concrete placement

was multiplied by the ram area in order to determine the applied load. Slip of the anchored headed bars was measured through a threaded bar attached to the head and a 50 mm (2 in.) linear potentiometer using the same procedure described in Section 3.2.5. Five mm (0.2 in.) electrical resistance strain gages were glued to the anchored bars 25 mm (1 in.) from the head. These strain gages were used to determine the anchorage force provided by the head. 2 mm (0.08 in.) strain gages

were used to measure the strains at the bar heads and in the joint shear and confining reinforcement in some specimens. Strain gages were placed on opposite sides of the head in order to compensate for any bending of the bar. Figure 4.30 shows the position of strain gages on headed bars. All instrumentation was connected to a data acquisition system and readings at each load increment were taken. In addition, an electronic voltmeter with a peak-hold capability was connected to the pressure transducer to capture the maximum load in case the specimen failed during loading.



a) Strain gage positions



b) Strain gage positions on specimen T28 head

Figure 4.30 Strain gage positions on headed bars

4.3.6 Test Setup

The loading of the specimen was intended to approximate the forces on an exterior joint in a typical frame. As discussed earlier, the beam was not cast with the specimens, and bending moment was applied at the face of the specimen by a couple consisting of a tensile force on the headed bars and a compressive force at 362 mm (14 1/4 in.) below the center line of the bars. This set of forces simulated those produced by a beam column connection similar to the one shown in Figure 4.1.

The forces described above were applied using a vertical reaction column consisting of two C12×30 channels stiffened by 25 mm (1 in.) thick plates. The channels were welded to a 25 mm (1 in.) thick base plate and bolted to the laboratory's floor using four 25 mm (1 in.) threaded rods. An overall view of the test setup is shown in Figures 4.31 to 4.33. The anchored beam reinforcing bars passed between the two channels and two 60-ton center hole hydraulic rams, of the single-action spring-return type, were placed over the bars. Both rams had a 156 mm (6 in.) stroke and 9260 mm² (13.75 in.²) effective area. The rams applied tension to the bars by reacting against the steel reaction columns. In order to simulate the compressive zone of the assumed beam a 51 mm (2 in.) thick plate was welded to the reaction column simulating a 156 mm (6 in.) deep compression zone. A layer of hydrostone was placed between the steel plate and the specimen

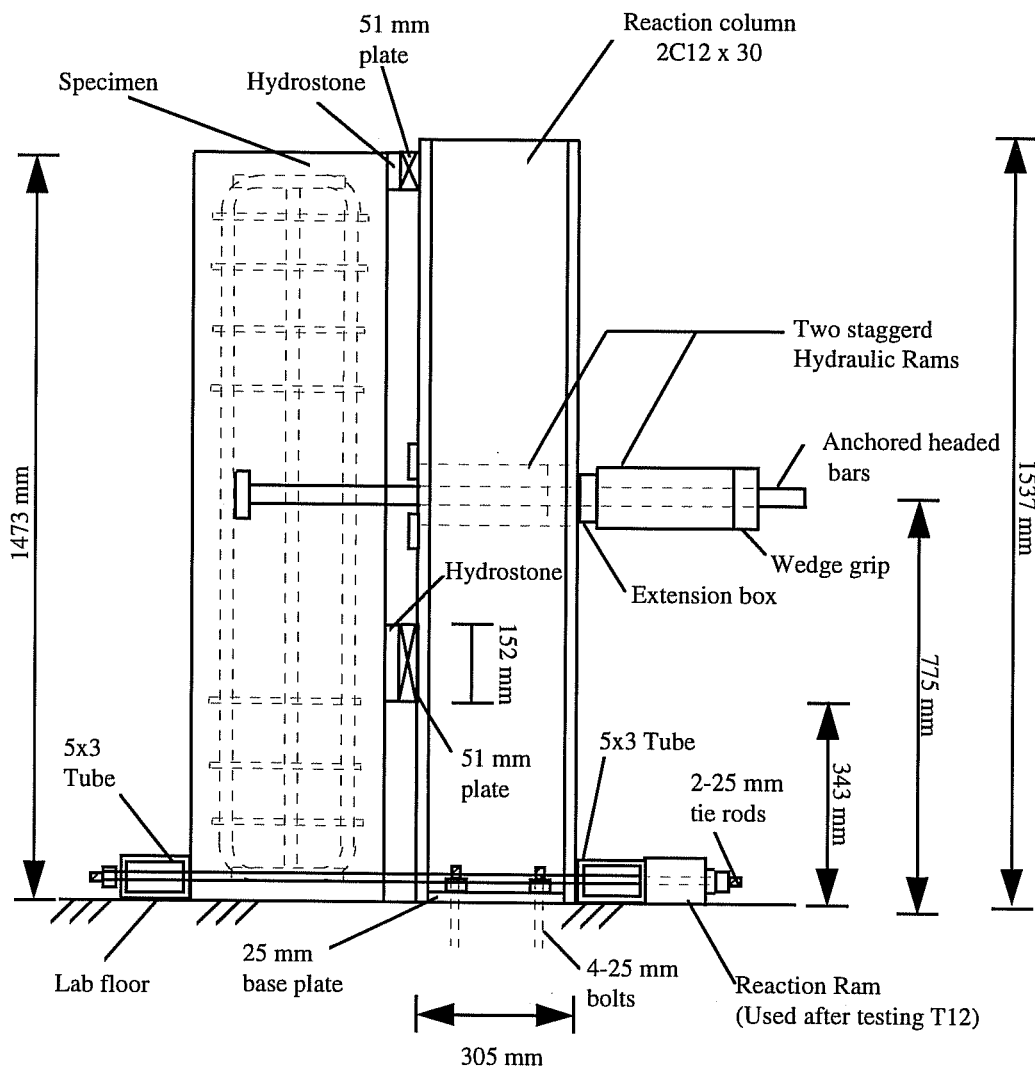


Figure 4.31 Schematic of the Test Setup, elevation view

to provide a uniform bearing surface and to ensure full contact. Because of the limited space between the two anchored bars, the hydraulic rams were staggered using a structural tube extension. To balance the moment imposed by the

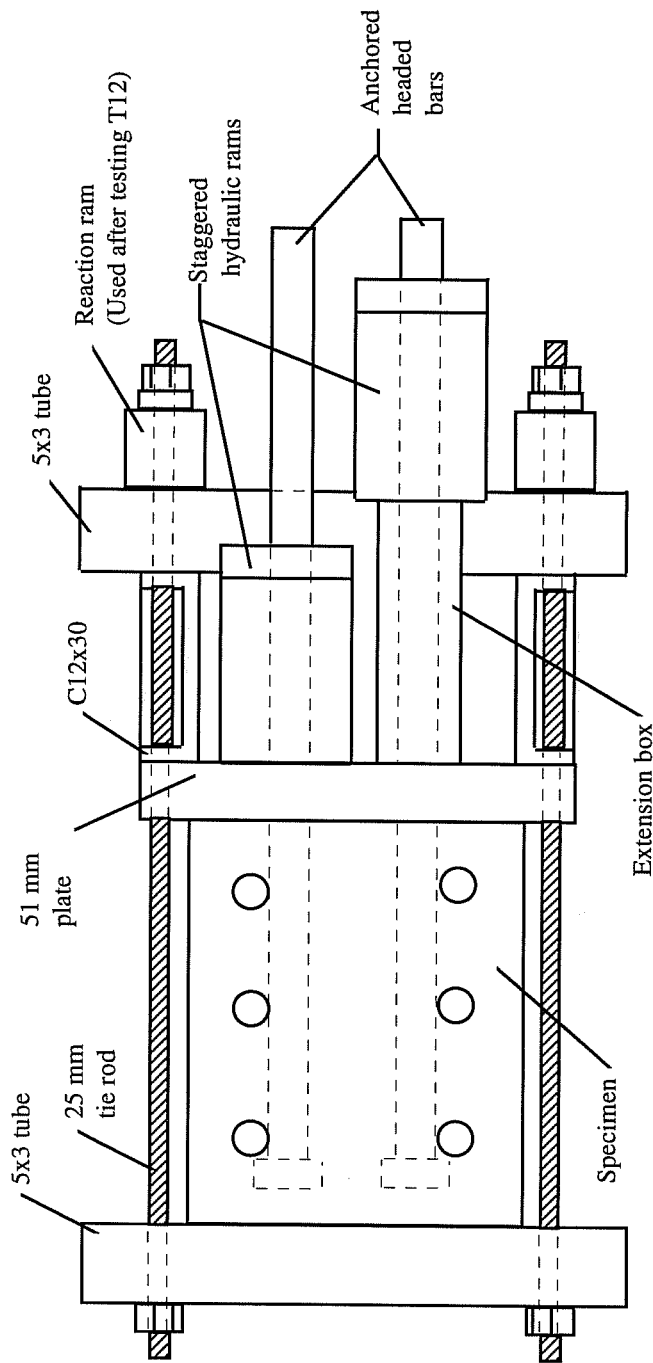


Figure 4.32 Schematic of the Test Setup, top view

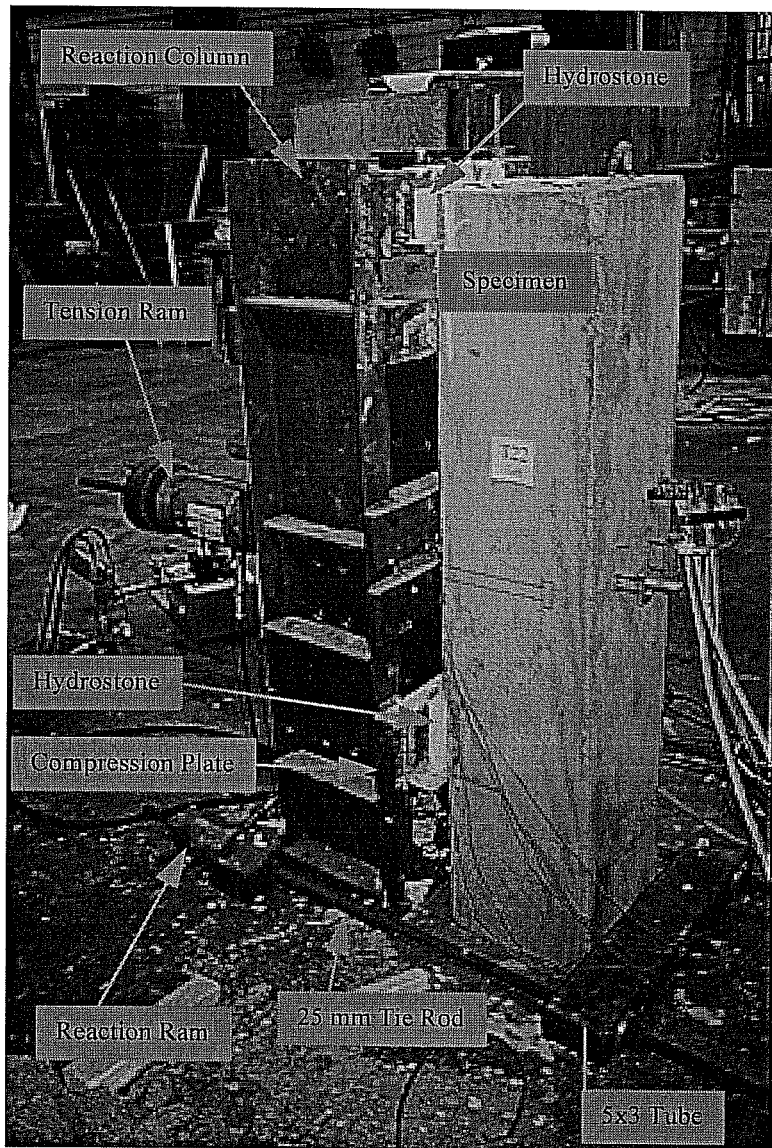


Figure 4.33 Test Setup for the Exterior Joints

simulated beam two horizontal reactions were provided, one at the top of the column, and the other at the bottom. The top reaction was provided by a 51 mm

(2 in.) thick plate welded to the top of the steel column. The bottom reaction was provided through two 25 mm (1 in.) threaded rods at the bottom of the steel column. The threaded rods were connected to a 2×5 structural tube bearing on the back of the specimens. After specimen T12 was tested, it was felt that the column shear - joint shear ratio was high compared to that of a real structure. Therefore, in the all of the following specimens (in addition to T2 and T3 which were not tested yet) two 20-ton center hole hydraulic rams were used to apply tension to the threaded rods. The two rams had an effective area of 3065 mm² (4.75 in.²). These reaction rams were connected to the same pump as the other rams to keep the oil pressure equal in all rams, and to make sure joint shear increased at the same rate as the force on the anchored bars load.

4.3.7 Test Procedure

After the specimen was placed in the loading frame, hydrostone was placed between the specimen and both the compressive zone and the top reaction plates. Hydrostone was allowed for an hour to harden before testing begun. After all instrumentation and loading equipment were in place, tension was applied to the anchored bars, generally in 22 KN (5 kip) increments. The increments were dropped to 11 KN (2.5 kip) at critical stages (when the first joint crack was expected or when the specimen was close to failure). The load was monitored

using the oil pressure transducer. Each load stage was sustained for two minutes during which the specimen was examined and the cracks were marked before applying the following increment.

Chapter 5

ANCHORAGE IN EXTERIOR JOINTS

TEST RESULTS

5.1 Introduction

In this chapter, results of the thirty-two beam column joint tests are summarized and discussed. Emphasis has been placed on reporting experimental results which have bearing on understanding the behavior of headed reinforcement in beam-column joints and leading to the development of mathematical models for behavior of joint reinforcement. The behavior of test specimens is described in terms of cracking patterns, bar tensile load and head slip relationships, and the strains along the headed bars and the shear reinforcement.

The test specimens were divided into two major groups depending on the failure mode. Eighteen specimens failed by spalling of concrete side cover, in a mode referred to as “side blow-out failure.” This failure mode is a function of embedment length, head dimensions, confining reinforcement, and concrete side cover. The second failure mode was shear related. Fourteen specimens fall in

this group in which the failure mode is a function of the embedment depth and shear reinforcement.

5.2 Specimens with Side Blow-Out Failures

The ultimate loads of eighteen tests with side blow-out failure are summarized in Table 5.1. The corresponding head slips are also listed. The ultimate load for each specimens normalized to 34.5 MPa (5000 psi) concrete strength by multiplying the ultimate load for each specimen by the ratio of the square root of the concrete compressive strength $\sqrt{f'_c/34.5}$. Although the variation in concrete strength for all specimens (except for T30) was relatively low, the normalized value allowed direct comparison between tests eliminating the influence of concrete strength on anchorage capacity. The normalization procedure was not used in other diagrams in order to prevent affecting the stiffness of the anchored bars (available test data indicated that variations in concrete strength do not have the same effect on different variables). It should also be noted that while the ultimate capacity was obtained from the voltmeter reading (see section 4.3.5), the rest of the data was obtained through the data acquisition system recorded up to the increment preceding failure. An additional data point was recorded after failure, but the peak was usually not captured by the

data acquisition system. As a result there may be slight differences between the ultimate capacities presented in Table 5.1 and load-slip diagrams.

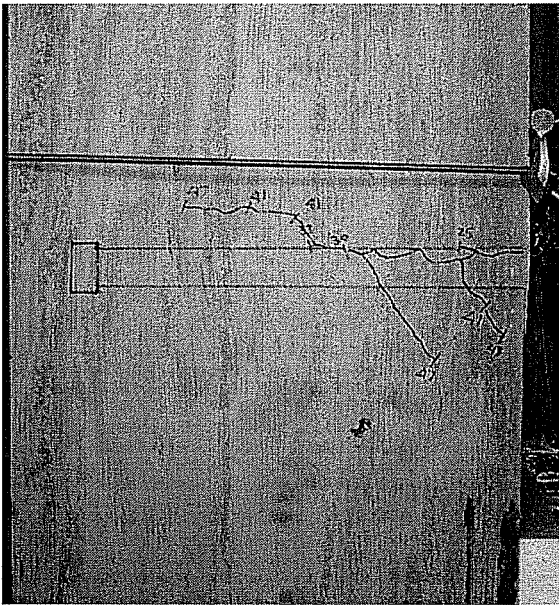
Table 5.1 Test Results for Specimens with Side Blow-Out Failure

Test	f_c (MPa)	Head Slip (mm)	P_{max} (KN)	P_{max} Normalized (KN)
T9	34.5	2.47	340	340
T10	34.5	0.72	271	271
T12	35.2	0.5	178	176
T13	38.3	0.51	273	259
T14	37.2	1.45	416	400
T16	39.6	1.71	426	397
T20	35.2	1.16	349	345
T21	35.2	1.33	218	216
T22	35.2	0.72	183	182
T23	33.2	1.45	306	311
T24	32.3	1.6	357	369
T25	32.3	1.94	426	440
T26	31.4	1.02	495	519
T27	31.4	1.52	198	207
T28	33.3	2.68	432	439
T29	33.3	1.94	385	392
T30	22.1	1.57	279	349
T32	33.3	1.32	216	220

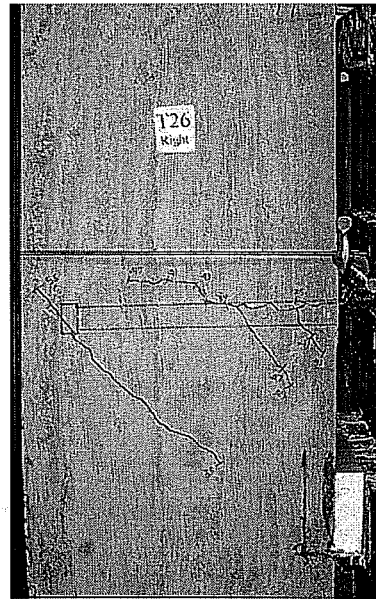
5.2.1 Cracking Pattern

On the sides of the specimens, cracks first initiated at the face of the column along the lead portion of the embedded bar (Figure 5.1-a). Looking at the

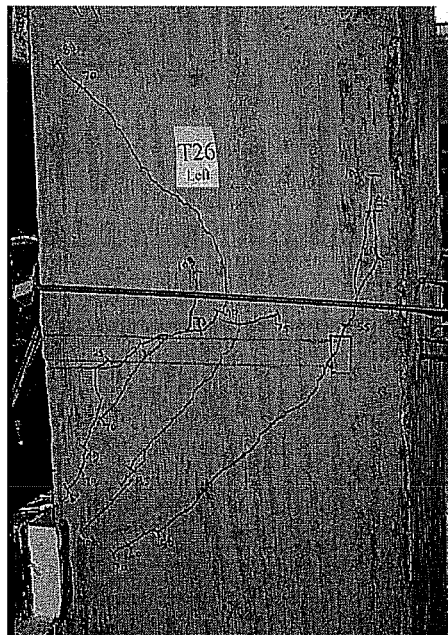
face of the column, cracks were detected propagating radially from the anchored bars in a manner similar to that of splitting cracks associated with straight deformed bars. Diagonal cracks initiating from the head bar plate and propagating towards the assumed compressive beam zone appeared in the joint region as loads increased (Figure 5.1-b). Further increase of load resulted in the propagation of these cracks in the column above the joint region (Figures 5.1-c and 5.3-a). A flexural crack could be detected at the bottom of the joint on the back of the column with increased of load. As the applied load reached ultimate, the specimens were severely cracked on both sides. In some cases, a horizontal crack, spanning between the two bars and extending to the column sides, could be detected on the back of the column. In most cases failure was sudden, and the load dropped to a fraction of the maximum level. In the majority of the tests (all tests except for T20, T24, and T28, which will be discussed later in further detail) only one of the bars failed. At failure, a concrete cone with a depth approximately equal to the concrete cover over the column bars was pulled out with the lead end of the anchored bar (Figure 5.4). Failure of a bar was accompanied by a large increase in the slip of that bar causing a drop in oil pressure and a drop in the applied load thus preventing failure of the other bar. After failure, slip increased significantly without increase in the applied load and side cover spalled (Figure 5.2). The cracking pattern on both sides of the specimens were almost identical,



a) Cracking along embedment length

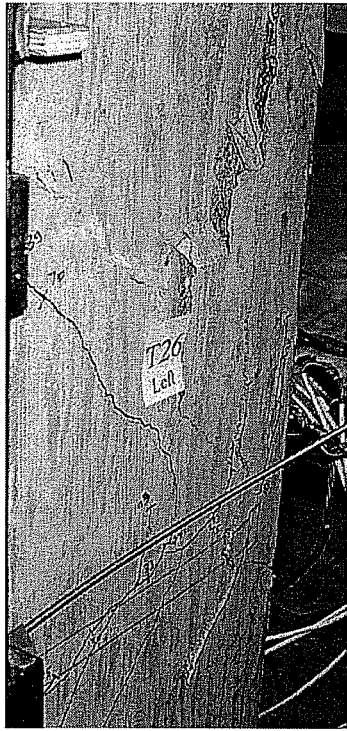


b) Diagonal shear crack



c) Cracking pattern before failure

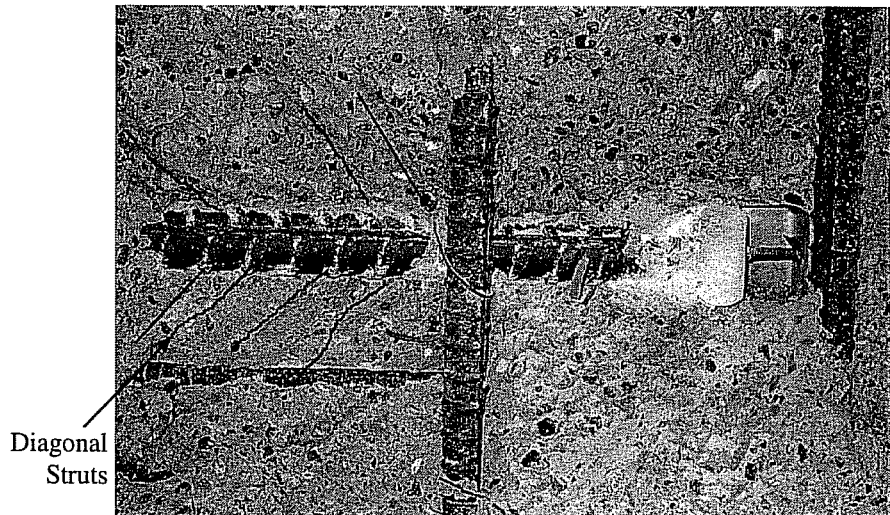
Figure 5.1 Cracking prior to failure - Specimen T26



a) Side spalling at failure

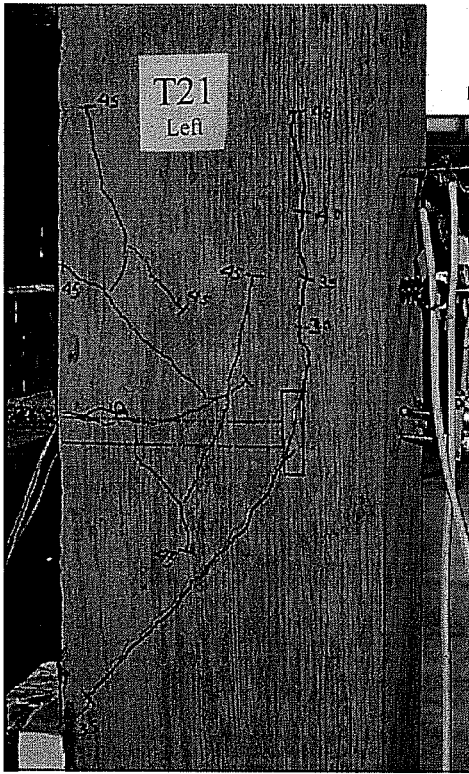


b) After spalled concrete fell off

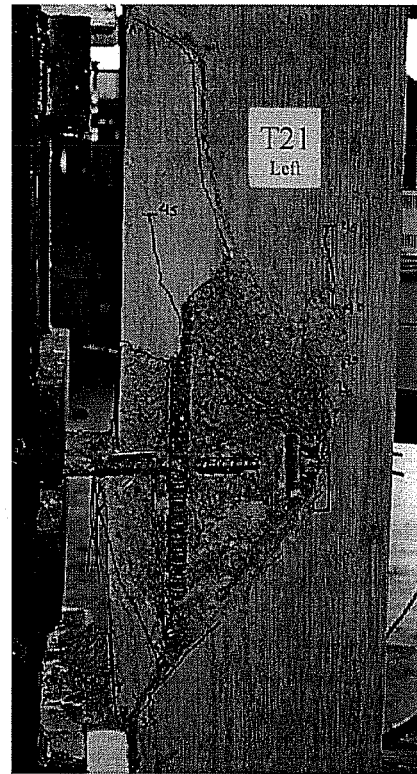


c) Appearance of head after failure

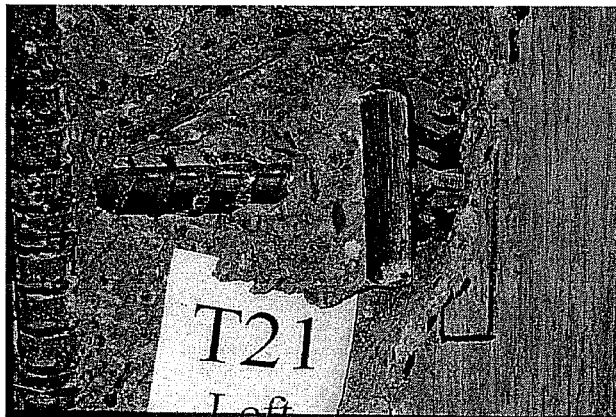
Figure 5.2 Appearance after failure - Specimen T26



a) Cracking prior to failure

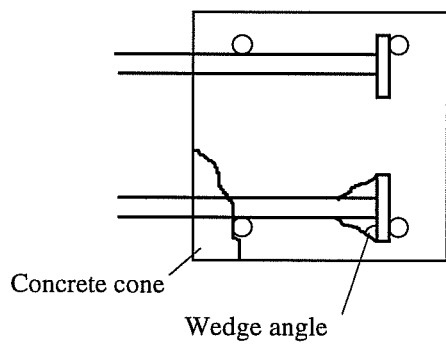


b) Appearance after failure

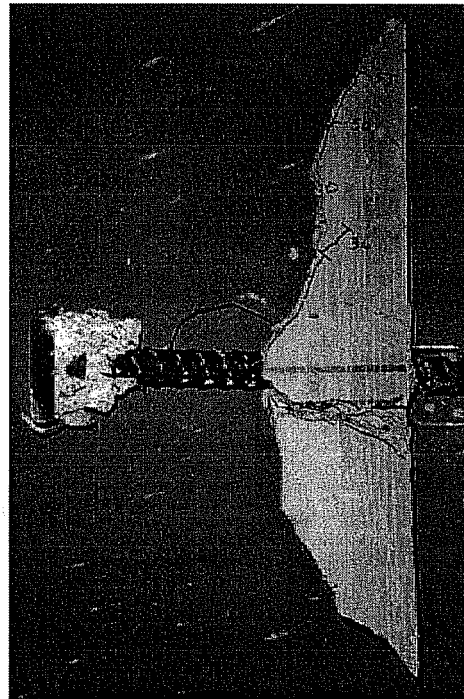


c) Concrete Wedge

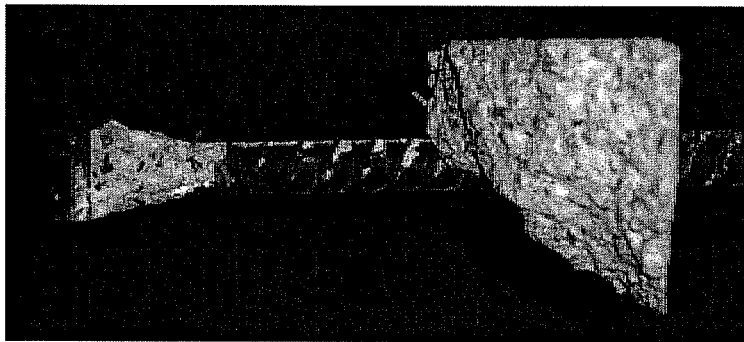
Figure 5.3 Cracking and failure pattern - Specimen T21



a) Schematic of the failure pattern



b) Side view



c) Top view

Figure 5.4 Concrete Wedge and Pull-out Cone

showing that the failure of the other bar was imminent. Furthermore, the head slip of both bars was always very close up to failure.

In several cases, the side cover spalled completely at failure. In the rest of the specimens, except for those with confining reinforcement over the anchorage bars, the spalled side cover was easily removed for examining the cracking in concrete and bearing (crushing) at the head and along the embedment length of the bar. In the case of deeper columns (T16 and T26), a larger area of concrete spalled (Figure 5.2-b). For the 305×305 mm (12×12 in.) and the 381×305 mm (15×12 in.) columns the spalling area usually had the shape of a triangle with its base at the face of the column, and the vertex close to the anchor head (Figure 5.3-b). In the case of specimens with confining reinforcement in the joint area the stirrups held the spalled concrete in place. A pry and a hammer were required to remove it.

After removing the loose concrete, crushed concrete could be seen on the bearing sides of the deformations along the embedment length of the bar. In some cases, diagonal struts protruding from the bar deformations could be detected from the concrete failure pattern (Figure 5.2-c). A $75^\circ \pm$ concrete wedge on the bearing side of the head could be easily detected (Figure 5.4). The wedge caused an outward force which lead to spalling of the side cover, and bent the anchored bars outwards. As a result, these bars pushed the center column bars outwards as

well (Figure 5.5). Increasing slip of the anchored bars after failure increased the outward bending of the column bars. In the case of specimens with confining reinforcement near the head, the stirrups restrained the concrete (Figure 5.6). However, stirrups close to the head were bent outwards as a result of the wedging action.



Figure 5.5 Appearance of column bars after failure

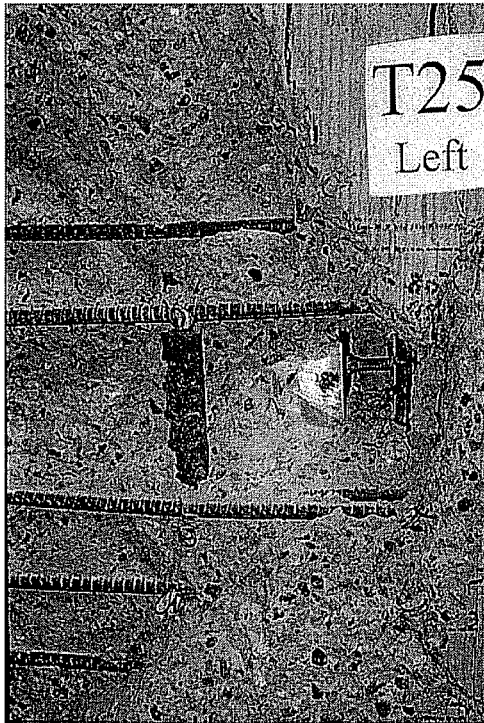


Figure 5.6 Appearance of specimens with stirrups - Specimen T25

5.2.2 Load-Slip Behavior

The crack propagation and pattern can be related to the load slip behavior, and the stresses along the anchored bars. To limit the discussion, the data from tests T9 and T21 only will be discussed in detail. The geometry of the test specimens were chosen so that a systematic evaluation of test variables affecting the anchorage capacity could be carried out. Specimens T9 and T21 represent typical specimens with 35 mm (#11) and the 25 mm (#8) headed bars. In most cases, the effect of different variables on anchorage behavior was

assessed by comparing the behavior of different specimens to these two specimens. Both T9 and T21 had 76 mm (3 in.) of side concrete cover and no confining reinforcement. Head areas were relatively close (3025 mm^2 or 4.7 in.^2 and 3200 mm^2 or 5 in.^2 , respectively). However, T9 is a $381 \times 305 \text{ mm}$ ($15 \times 12 \text{ in.}$) column with a $55 \times 55 \text{ mm}$ head, and T21 is a $305 \times 305 \text{ mm}$ ($12 \times 12 \text{ in.}$) column with an $80 \times 40 \text{ mm}$ head. The beam bars were placed inside the column bars in both specimens.

Data from other tests will be presented in the following section to evaluate the influence of different parameters considered in this study on anchorage capacity and load-slip behavior of headed bars.

The load-slip diagram for test T9 is shown in Figure 5.7, and the head anchorage load versus applied load diagram is shown in Figure 5.8. The head load was calculated using strain data from gages placed 25 mm (1 in.) from the head. The difference between the head anchorage load and the applied load is considered to be the force transferred to the concrete by the straight lead embedment.

As shown in Figure 5.7, there was no head slip up to about 133 kN (30 kip). At this load, cracks at the level of the anchored bars were detected along both sides of the column. The cracks initiated at the face of the column and reached halfway to the anchor head and indicated that the anchorage provided by

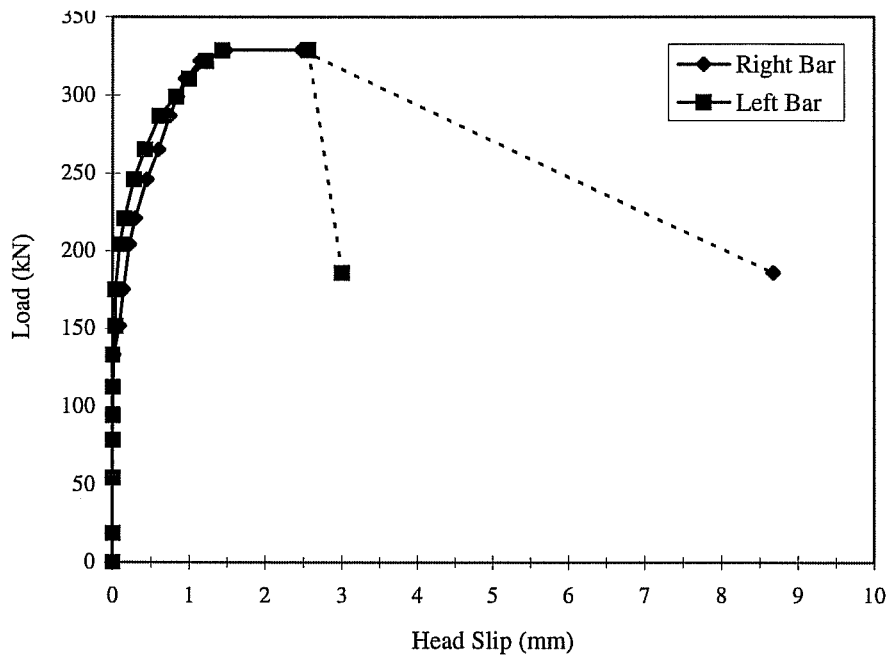


Figure 5.7 Applied Load vs Head Slip for Specimen T9

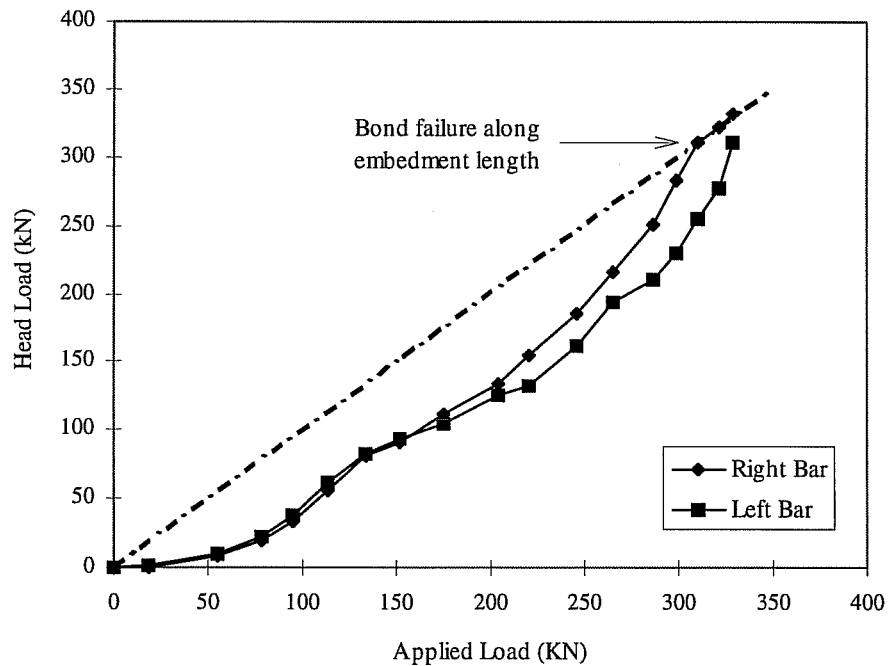


Figure 5.8 Head Load vs Applied Load for Specimen T9

the lead embedment reached its capacity. When applied load increased to 151 KN (34 kip), head slips of 0.08 and 0.04 mm were measured for the right and left bars, respectively. While the load was being sustained, a diagonal crack initiating from the bar head propagated toward the compressive zone. The diagonal crack extended to the compressive zone during the following load increment, and head slips increased to 0.14 and 0.08 mm. At this stage of the test, the increase in head load was then increase in applied load. When the applied load reached 300 KN (67.5 kip), the force transferred to concrete along the bar started to drop, and head force increased more rapidly. A diagonal shear crack appeared on top of the bar at 267 KN (60 kip) load. The maximum applied load (338 KN or 76 kip) dropped to 301 KN (67.5 kip), after two minutes without further pull of the anchored bars. The right bar failed in anchorage during the application of the next load increment. The slip of the right bar suddenly increased significantly, and the applied load dropped to 185 KN (41.5 kip). As the load dropped left bar slip increased slightly. Although the 305 mm (12 in.) lead embedment length transferred an anchorage force between 60 and 80 KN (13.5 and 18 kip) throughout most of the loading range, this force dropped quickly near failure. As shown in Figure 5.8, all of the bar stress was transferred to concrete through the anchorage head for the right bar at failure.

The load-slip diagram for test T21 is shown in Figure 5.9, and the head anchorage load versus applied load diagram is shown in Figure 5.10. The first anchorage crack appeared on the side of the column at a 67 KN (15 kip) load. The crack initiated at the face of the column and reached halfway to the anchor head. A diagonal joint crack was first detected on the side of the column after the next load increment. The crack along the embedment length of the anchored bar also extended in the direction of the head. This was accompanied by a drop in the force developed along the 229 mm (9 in.) lead embedment, from a maximum of 48 KN (10.8 kip) to 38 KN (8.5 kip). Further increase in load caused significant decrease in stiffness and severe cracking on both sides of the column. The force developed along the lead development length was also dropping slowly. Failure occurred in the right bar anchorage at a 218 KN (49 kip) load and a head slip of 1.3 mm (0.05 in.) for both bars. At failure the load dropped to 53.6 KN (12 kip), and the bar slip increased significantly. Although side spalling was detected on the left side of the column only, the left bar slip also increased to 5.1 mm (0.2 in.). The increase in slip is an indication that the left bar was very near failure. As shown in Figure 5.10, all of the right bar force was transferred to concrete through the anchorage head at failure. Figure 5.3-a shows the cracking pattern at failure, and Figure 5.3-b shows the specimen after the side cover spalled due to increasing

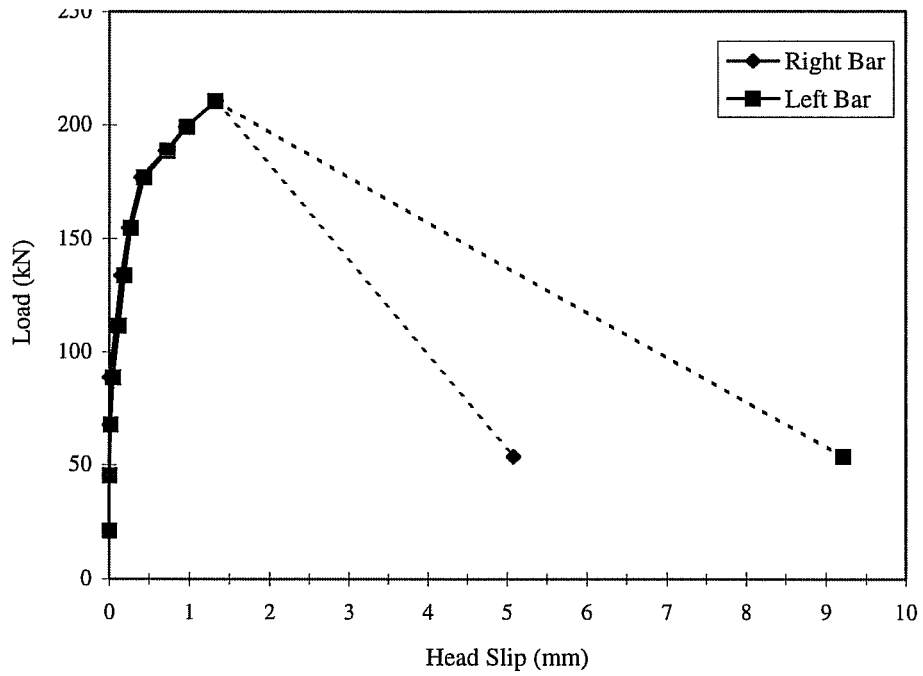


Figure 5.9 Applied Load vs Head Slip for Specimen T21

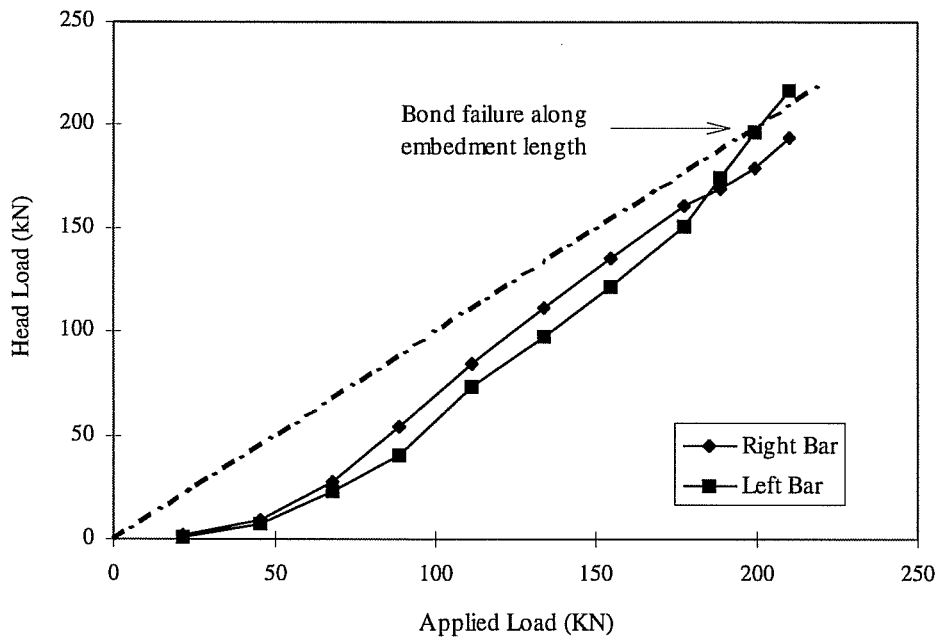


Figure 5.10 Head Load vs Applied Load for Specimen T21

slip after failure. Figure 5.3-c shows a close-up of the concrete wedge which formed in front of the head and initiated the side cover spalling.

5.2.3 Effects of Different Variables

In this section, the results of the eighteen specimens with side-blow-out failure are presented and analyzed in terms of the effect of each variable on the ultimate anchorage capacity, the load-slip behavior, and the applied load - head load ratio throughout the load history. The load slip curve for the failing bar in each specimen will be used to compare different tests. In all of the specimens, the strain gages were damaged at failure. As a result, strain gage data are available up to the load step before failure, and is similar for both anchored bars. The strains from the failing bar will be used to compare the applied load versus head load curves for different tests.

a) Effect of Head Area:

Figure 5.11 shows the normalized ultimate capacities of three 381×305 mm (15×12 in.) specimens with 35 mm (#11) anchored bars (T9, T20, and T28). The only difference between these specimens is the head area. Figure 5.12 shows a similar comparison between two 305×305 mm (12×12 in.) column specimens with 25 mm (#8) anchored bars and different head areas (T21 and T22). It is obvious that the anchorage capacity increases with the head area. However this

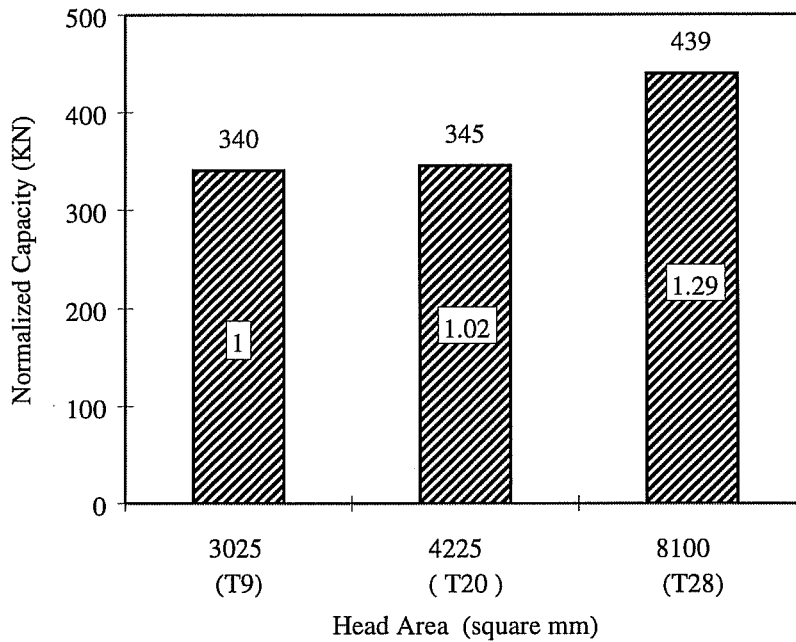


Figure 5.11 Effect of head area on the anchorage capacity - 35 mm bars, 76 mm cover

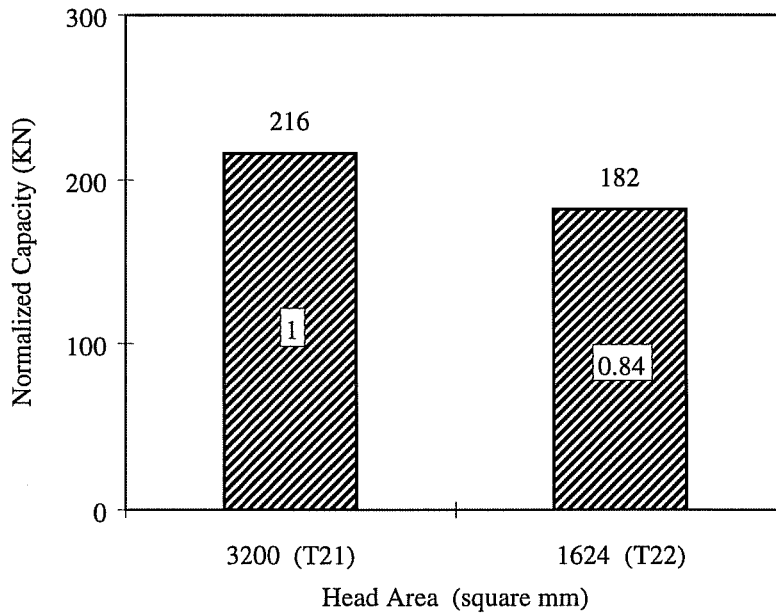


Figure 5.12 Effect of head area on the anchorage capacity - 25 mm bars, 76 mm cover

increase is not linear. The relation between head area and the anchorage capacity will be discussed in the following chapter in further detail.

The head slips for tests T9, T20, and T28 were very low up to about 133 KN (30 kips) (see Figure 5.13). At low loads the behavior of the anchored bars was dependent on the lead embedment length, which was similar for the three tests. When the diagonal shear crack started propagating in the joint, head slip started to increase. At a tensile load of 265 KN (60 kip) (about 80% of the ultimate anchorage capacity for T9), the head slip for specimens T20 and T28 was about 1/3 less than that of T9. The load-slip diagrams for the three tests have the same pattern, but T28, the specimen with the largest head area, was stiffer at loads

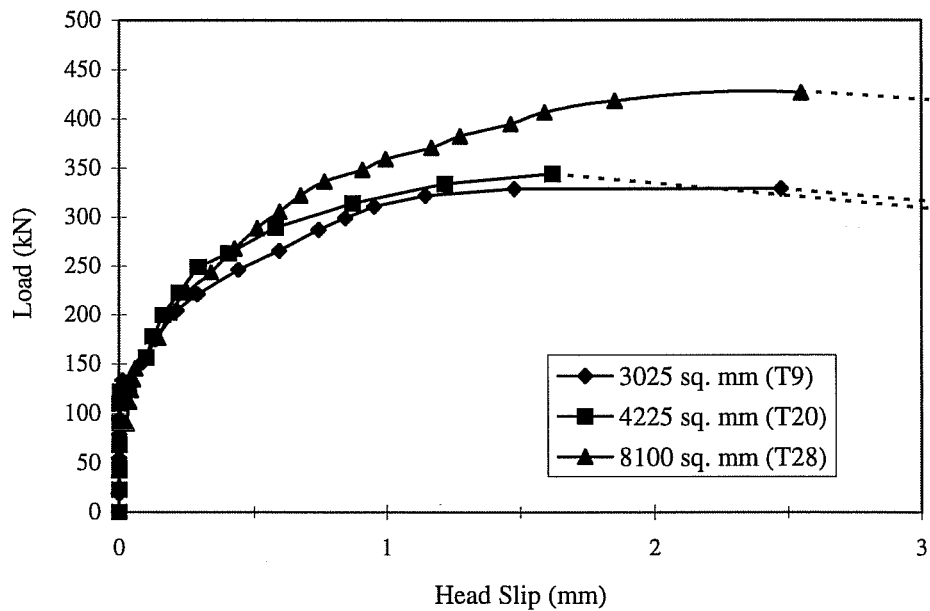


Figure 5.13 Effect of head area on the load-slip behavior - 35 mm bars, 76 mm cover

approaching ultimate. Figure 5.14 shows the head force versus applied load diagrams for the three tests. The head force curves are similar for the three tests up to about 330 KN (74 kip). at which point, all of the applied load was transferred to the concrete through the heads. The difference between the three specimens became more significant beyond this point. While T9 and T20 failed after a small increase in load, T28 resisted significantly higher load at higher head slip. The head loads (obtained from the strain gage data) are plotted against the head slip Figure 5.15 and show the effect of increased head area.

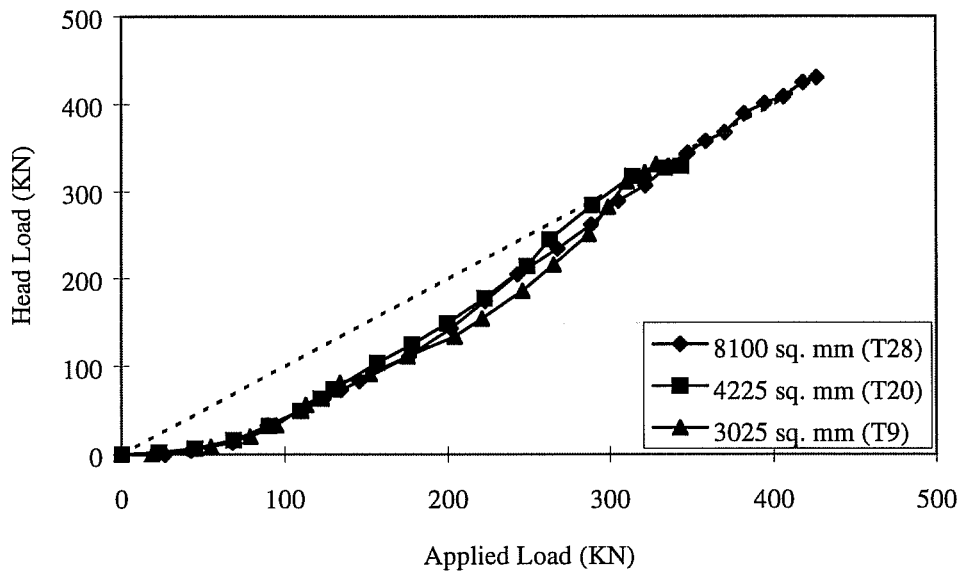


Figure 5.14 Effect of head area on the Applied Load - Head Load ratio - 35 mm bars, 76 mm cover

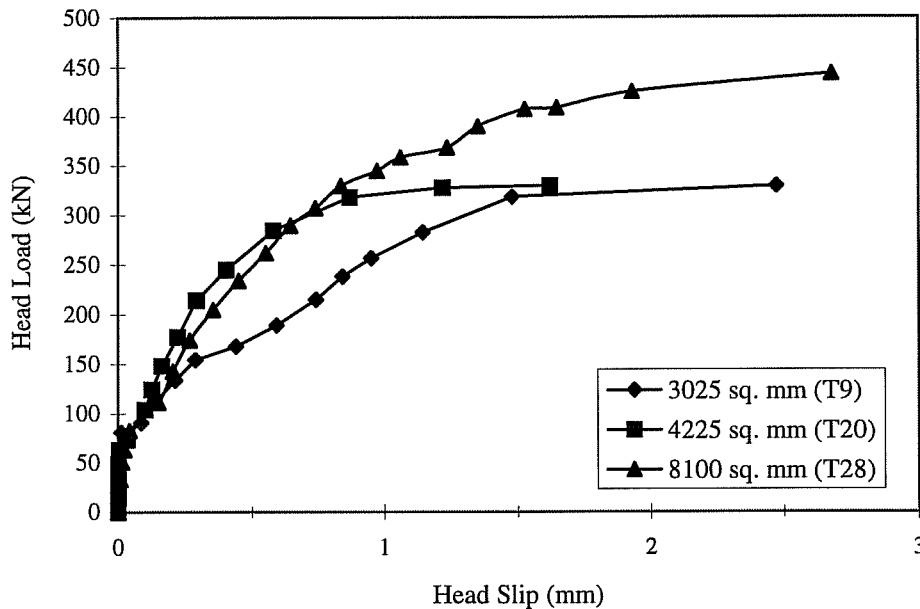


Figure 5.15 Head Load vs. Slip for different head areas - 35 mm bars, 76 mm cover

Similar observations can be made from Figure 5.16 for tests T21 and T22. The slip started increasing at about 90 kN (20 kip), indicating deterioration of bond along the development length. It should be noted that diagonal shear crack did not develop until the following load step. Head slip increases as the load transferred to concrete through the head increases shear crack is initiated. The head slip for both tests was very close up to about 155 kN (35 kip) which is about 3/4 of the capacity of the anchorage. As in the case of the 35 mm (#11) bars, the bar with a large head was able to resist higher loads and sustained larger head slips. The increase in head force for the two specimens was similar up to a

load equal to 174 kN (39 kip) where specimen T22 failed, with 91% of the applied load being transferred to concrete through the anchorage head. Specimen T21 did not fail until the applied load reached 218 kN (49 kip) and was resisted entirely by the anchorage head. Figure 5.17 shows the head load - head slip diagrams for both tests.

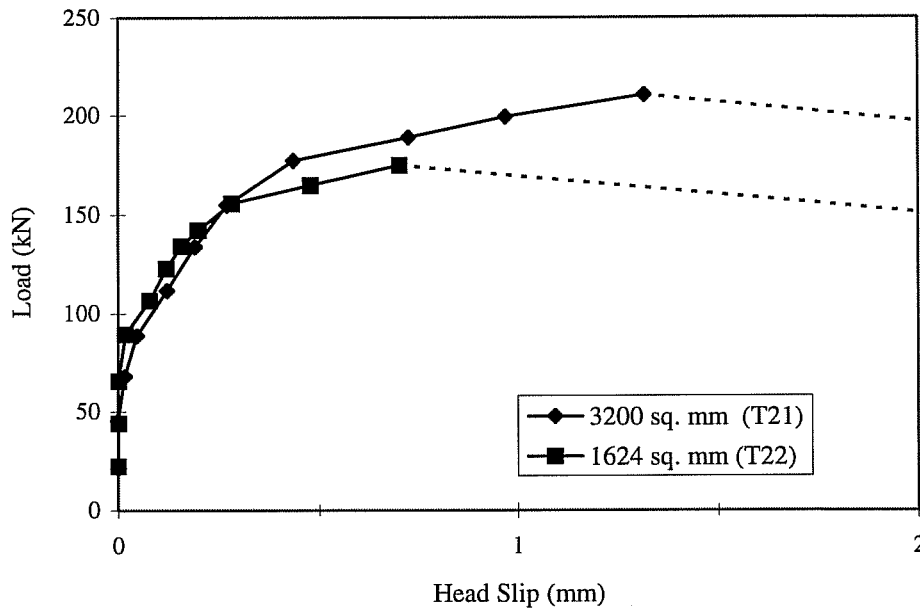


Figure 5.16 Effect of head area on the load-slip behavior - 25 mm bars, 76 mm cover

The effect of head area on the anchorage capacity can be summarized as follows. For a given cover and embedment length, the capacity increased with increasing head area. If the head force at failure is accompanied by large slip, the anchorage along the lead embedment was destroyed and the applied load was

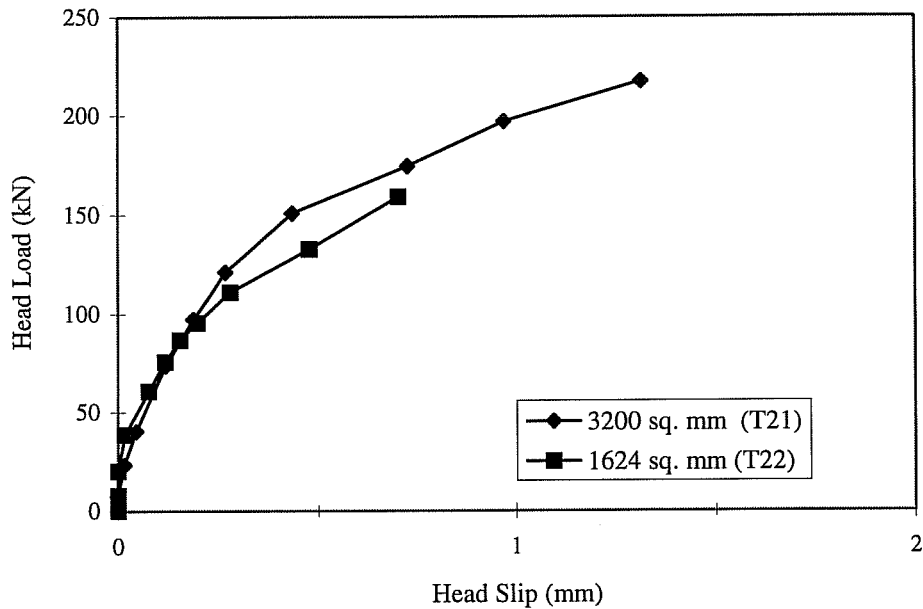


Figure 5.17 Head Load vs. Slip for different head areas - 25 mm bars, 76 mm cover

carried by the head at failure. Otherwise, the ultimate load was carried partially by anchorage along the lead embedment (or what is remaining of it), and the remainder by the head. In several cases the anchorage along the development length deteriorated quickly just before failure due to large slip along the lead embedment length as a result of increasing head slips and elastic elongation of the anchored bar. As anchorage along the bar decreased, the head load increased at a faster rate than the applied load and caused further increase in head slip. The high slip before failure was also attributed to concrete crushing in front of the head and the formation of a wedge. The effect of anchorage along the lead embedment on

the ultimate capacity will be further discussed on the section describing the effect of development length on the anchorage capacity.

b) Effect of Head Aspect Ratio and Orientation

The normalized anchorage capacities of tests T23, T9, and T24 are compared in Figure 5.18. The anchored bars in the three specimens had 90×33 mm, 55×55 mm, and 33×90 mm heads, respectively. The three heads have approximately the same area, but aspect ratios of 2.7, 1, and 0.37. The head aspect ratio is defined as the ratio between the vertical dimension (parallel to the free concrete surface) and the horizontal dimension (perpendicular to the free concrete surface). Headed bars in specimens T23 and T24 had the same rectangular head, but the head in T23 was in a vertical position, while that of T24 was in a horizontal position (aspect ratio is determined by the orientation relative to the free concrete surface). The cover over the bars was 76 mm (3 in.) in the three specimens. The difference between the anchorage capacities was $\pm 8\%$. As tests T23 and T24 represent extreme cases (note that the head width is less than the bar diameter) designed to capture the maximum effect on capacity due to variations in aspect ratio, such variation in capacity is not expected in practical situations. Considering scatter of data from similar experimental programs [2,9,11,12], the difference in capacity due to aspect ratio is not significant for

most practical head dimensions. This is especially true since identical specimens from previous hooked bar investigations had a larger difference in anchorage capacities as will be discussed later.

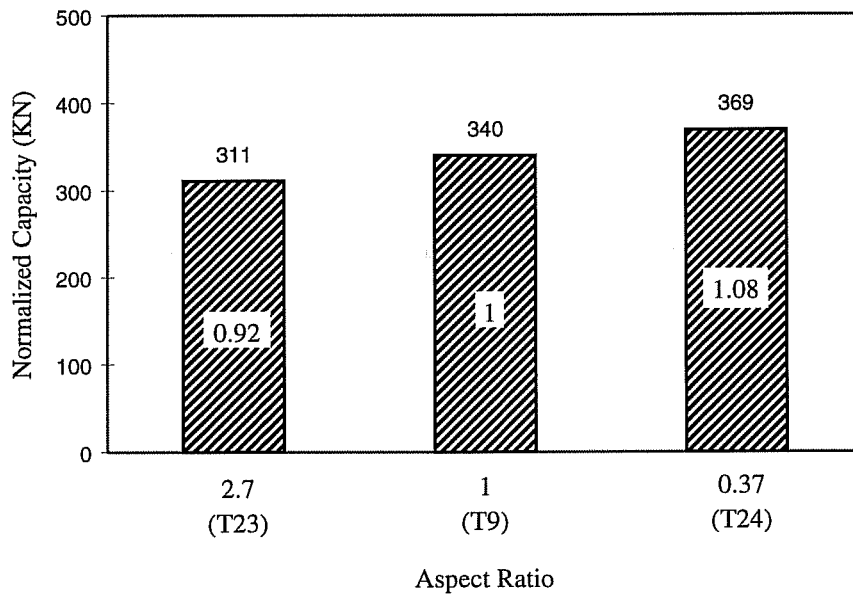


Figure 5.18 Effect of head aspect ratio on the anchorage capacity - 35 mm bars, 76 mm cover

Figure 5.19 show the load-slip diagrams for tests T9, T23, and T24. The three curves have very similar patterns. Figures 5.7, 5.20, and 5.21 show the applied load - head slip for both bars anchored in the three specimens. In the cases of T9 and T23 the load drop and slip increase were significantly higher than T24 at failure. It should also be noted that in the case of T24, both bars had the

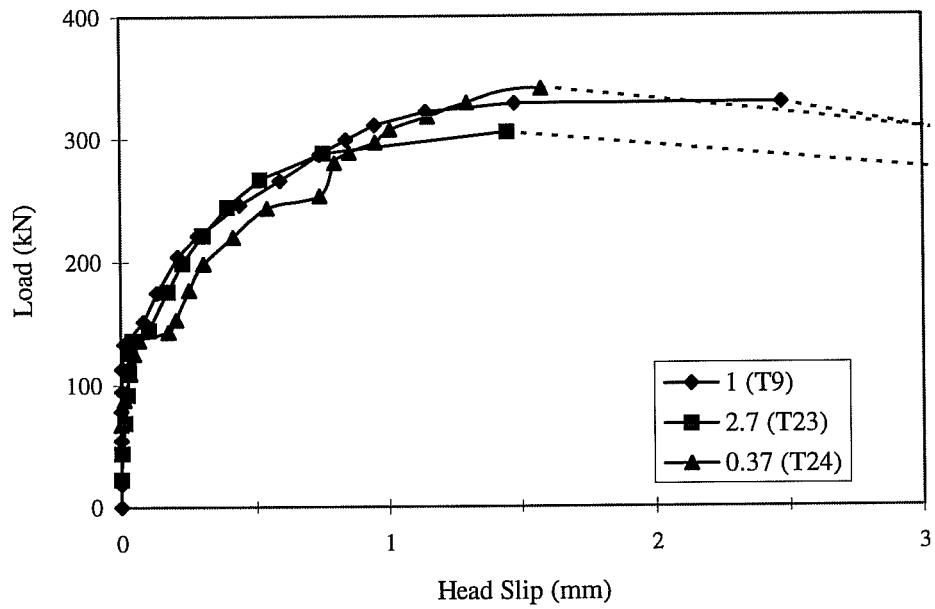


Figure 5.19 Effect of head aspect ratio on the load-slip behavior - 35 mm bars, 76 mm cover

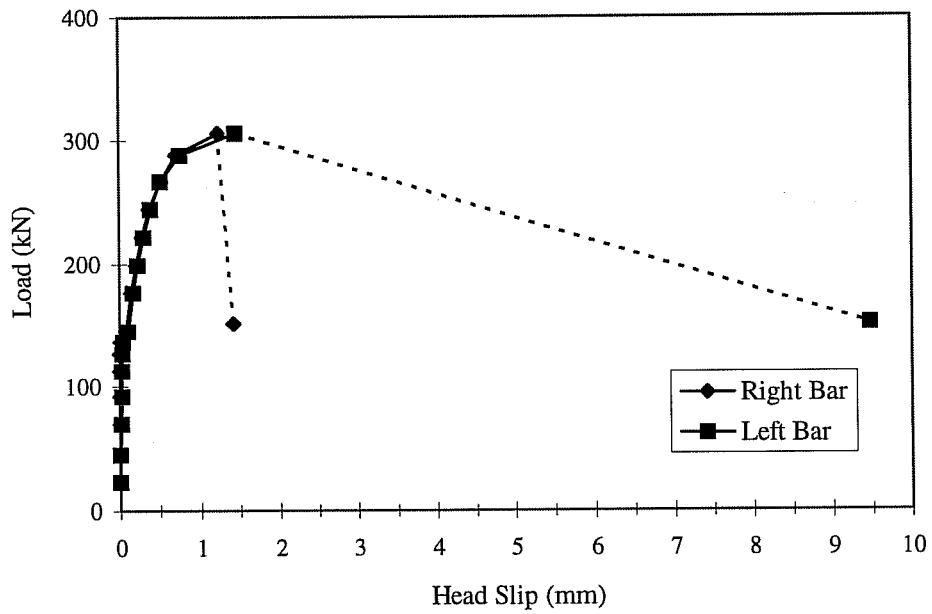


Figure 5.20 Applied Load vs. Head Slip for Specimen T23

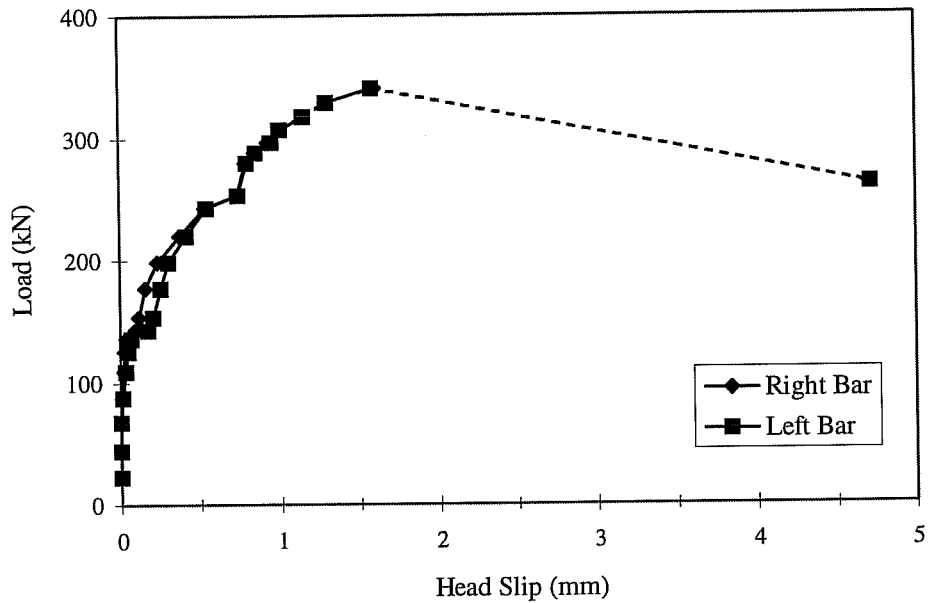


Figure 5.21 Applied Load vs. Head Slip for Specimen T24

same head slip after failure indicating that both bars failed but as higher slips were imposed the left side of the column spalled.

The wedges that formed on the bearing side of the heads in specimens T23 and T24 are shown in Figure 5.22. The wedge formed on the anchor head of specimen T9 is similar to the one shown in Figure 5.4. It can be noted that the wedge angle for T9 and T23 are about 75-degrees (similar to that shown in Figure 5.4) while that of T24 is 55 to 60-degrees. The difference in the behavior of T24 was attributed to the smaller wedge angle. A small wedge angle means that the



a) T23



b) T24

Figure 5.22 Effect of Aspect Ratio on the wedge angle

anchored bar had to go through larger outward movement (laterally) in order to increase the slip after forming the wedge. This implies that lateral resistance to blow-out will be more effective. Since load did not drop suddenly after the formation of the wedge on one head, the other anchored head also formed a wedge (probably in the same load increment). The smaller wedge angle also resulted in a slightly higher load capacity for T24 compared with T23. Similar behavior was observed for the other specimens (T20 and T28) in which the horizontal dimension of the head (perpendicular to the free concrete surface) was significantly larger than the bar (and the flash) diameter. Previous research [2] indicated that wedge shape and angle are dependent on both head area and dimensions.

In spite of the differences in post-failure behavior, it can be concluded that the head aspect ratio and orientation do not have a significant effect on the anchorage capacity of headed bars.

c) Effect of Bar Diameter

Although no groups of specimens in which the only variable is the bar diameter were tested, its effect on the anchorage behavior can be assessed if the effect of aspect ratio is neglected. It was observed that aspect ratio did not have significant influence on the anchorage capacity or the slip behavior of headed bars up to failure. Similar conclusions were also drawn by DeVries [2]. Taking this into account, the effect of bar diameter on the anchorage behavior can be studied by comparing three pairs of tests; T9, T10, and T27 had 35 mm (#11) anchored bars with 55×55 mm (2.2×2.2 in.) heads while T30, T13, and T21 had 25 mm (#8) anchored bars with 80×40 mm (3.1×1.6 in.) heads. It should be noted that the difference in head areas between the two groups (5%) was considered negligible.

The anchorage capacities (normalized with respect to concrete strength) of the three pairs of specimens are compared in Figure 5.23. The difference in anchorage capacities was less than 5% in all cases. Specimen T30 had lower

concrete strength (22 MPa or 3200 psi) than that of T9 (34.5 MPa or 5000 psi) in order to prevent bar yielding before an anchorage failure. The slip behavior of T9

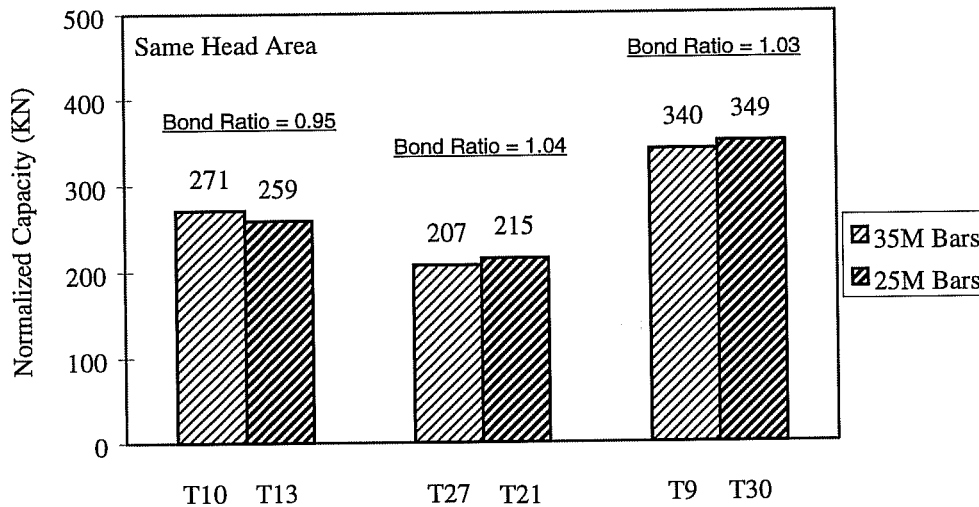
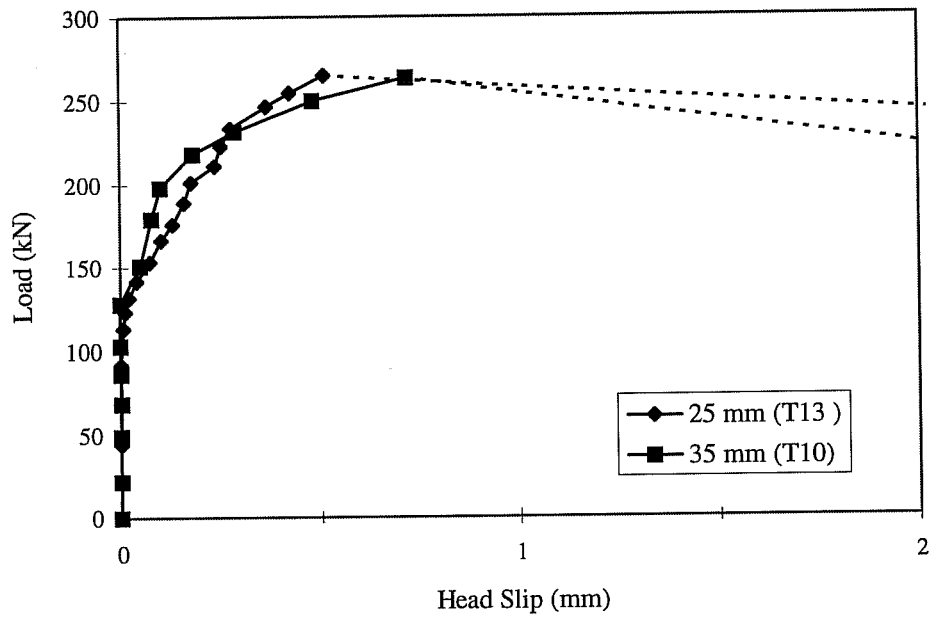
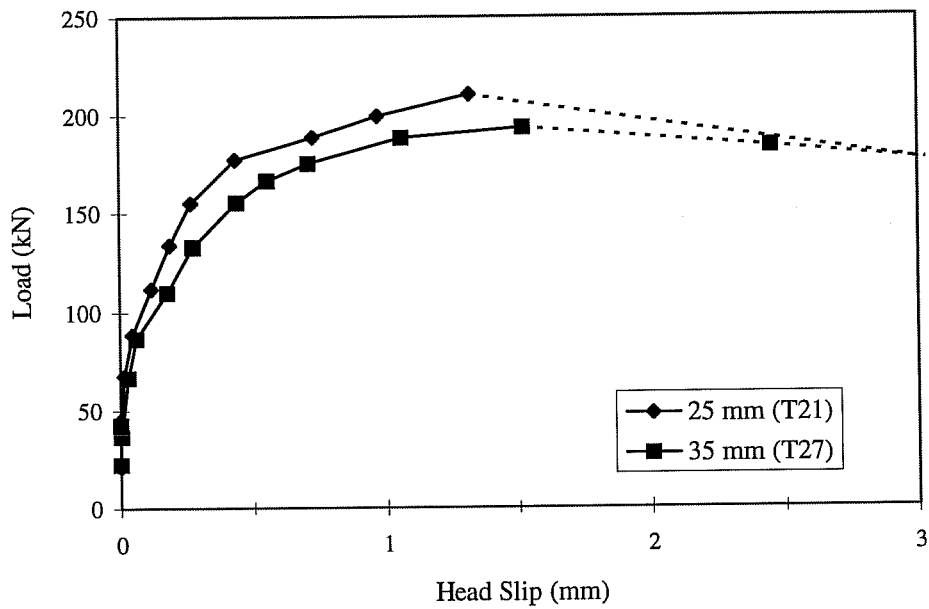


Figure 5.23 Effect of bar diameter on the anchorage capacity, 76 mm cover

and T30 could not be compared but Figure 5.24 shows a comparison between the applied load - head slip diagrams for the other two pairs of specimens. Both diagrams show that the bar diameter had a negligible effect on the load slip behavior. It was expected that the specimens with 25 mm (#8) bars will show head slip earlier than those with 35 mm (#11) bars (for the same bar force), because the bars provide less surface area for anchorage along the lead embedment length. However, head slip was first detected at almost the same load level for each pair. It seems that the lead anchorage was governed by the splitting cracks radiating from the bars rather than the bar surface area provided along the



a) Specimens with 38 mm cover



b) Specimens with 76 mm cover

Figure 5.24 Effect of bar diameter on the load-slip behavior

lead embedment. This can also be concluded by comparing the head force - applied load relationships of specimens T27 and T21 (Figure 5.25). The diagram shows that in T27 (the specimen with 35 mm bars), the head provided a higher anchorage force than that of T21 throughout the load history . However, it should be noted that the concrete strength of T21 was 11% higher than that of T27. Unfortunately, a similar comparison between T10 and T13 could not be done because the strain gages in T10 were not functional.

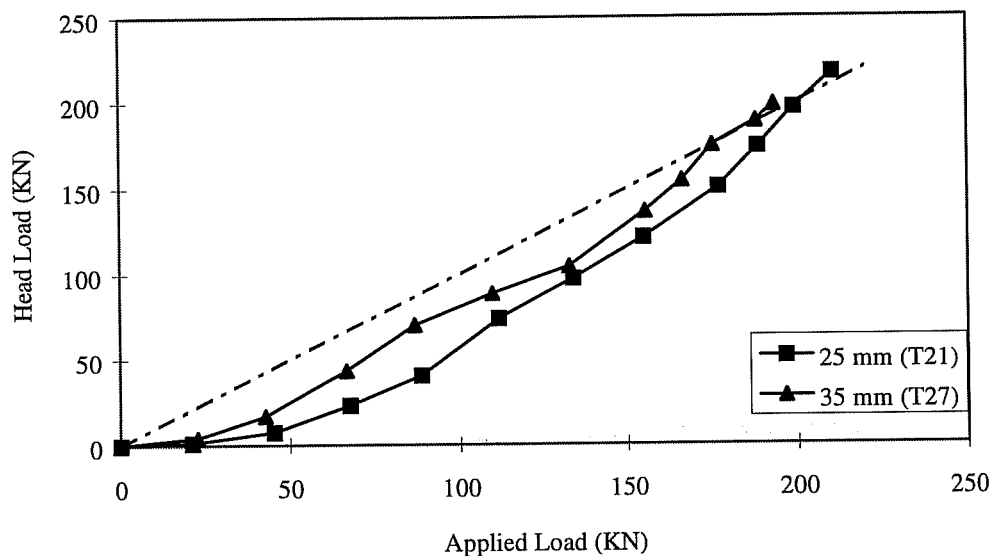


Figure 5.25 Effect of Bar Diameter on the Applied Load - Head Load Ratio

d) Effect of Concrete Cover

In pullout tests, side concrete cover provided confinement to headed bars, improving the bearing capacity at the head and resisting side spalling after the

wedge forms. In order to study its effect in exterior joints specimens with 76 mm (3 in.) and 38 mm (1 1/2 in.) side cover above the level of the anchored bars were compared.

The effect of decreasing the side cover on the anchorage capacity is shown in Figure 5.26. For the first and third pairs of tests, in which the lead embedment was 305 mm (12 in.), the anchorage capacity dropped 20 and 26% respectively. In the second pair, with 229 mm (9 in.) lead embedment, the anchorage capacity dropped 18%. It should be noted that specimen T30 had

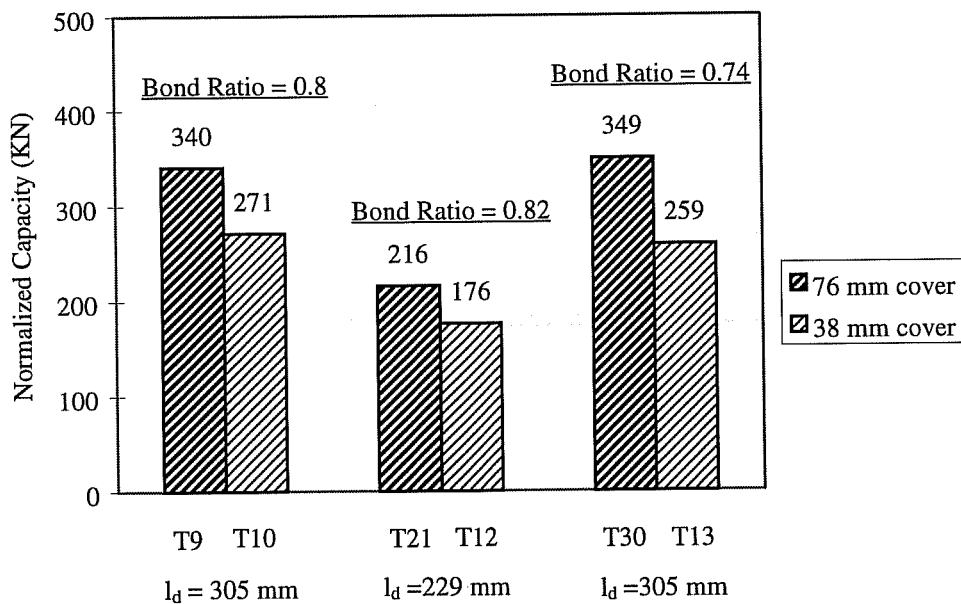
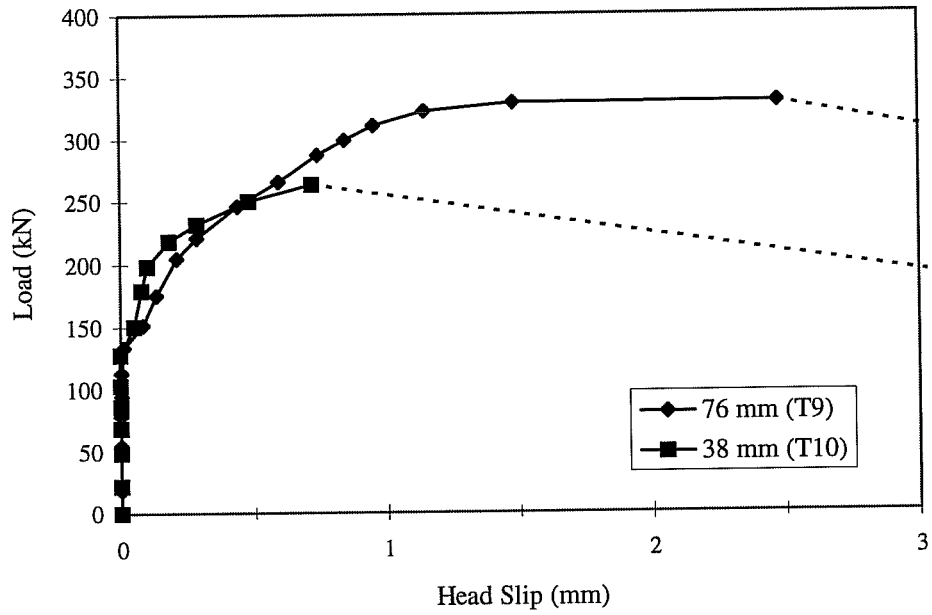


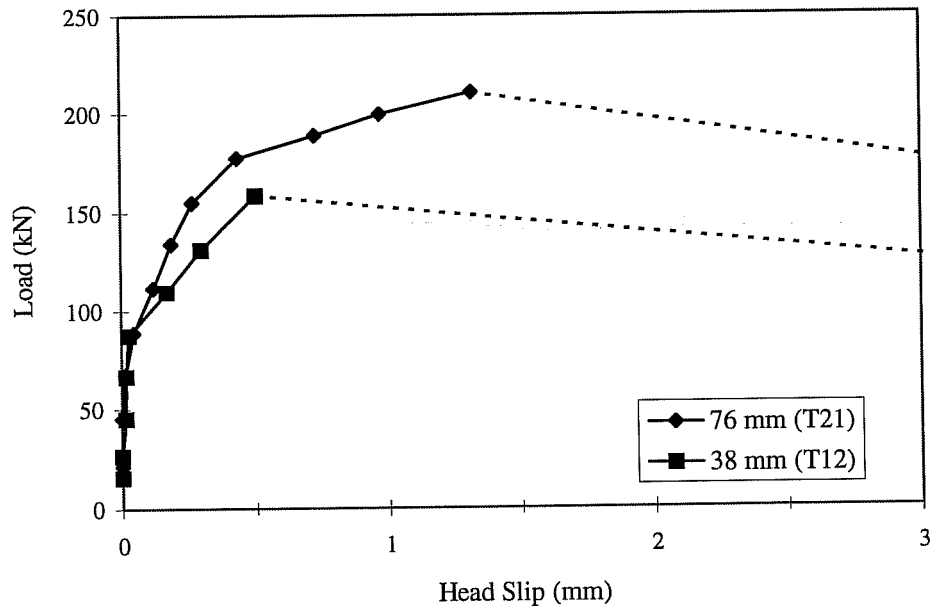
Figure 5.26 Effect of Side Concrete Cover on the Anchorage Capacity

significantly lower concrete strength, which might have caused some inaccuracies in the normalization process and prevented direct comparison of the load-slip diagram with the companion test. The applied load - head slip curves for the other two pairs of specimens are compared in Figure 5.27. In the case of T9 and T10, the curves were very similar up to the point where T10 reached its anchorage capacity, at a head slip of 0.7 mm (0.03 in.). Specimen T10, with 76 mm (3 in.) cover, was capable of resisting more load through larger slips, and reached head slip of 2.5 mm (0.1 in.).

Similar behavior can be observed in Figure 5.27-b, where T21 and T12 are compared. The curves for both specimens were identical up to about 90 KN (20 kip), showing very low head slip. Beyond this point, the slip of T12 was larger than that of T21. The head load for T12 exceeded that of T21 at this load level (Figure 5.28). At this point, the head was transferring all of the anchorage force in T12, while 15% of the applied load was still resisted by the lead development length for T21. Although its stiffness decreased significantly, T21 was capable of resisting an increase in load beyond this point, and didn't fail until a head slip of 1.3 mm (0.05 in.) was reached. As in the case of T12, the anchorage along the lead development length was lost at failure, and all of the applied load was resisted by the head.



a) Specimens with 305 mm lead embedment - 35M Bars



b) Specimens with 229 mm lead embedment - 25M Bars

Figure 5.27 Effect of Side Concrete Cover on the load-slip behavior

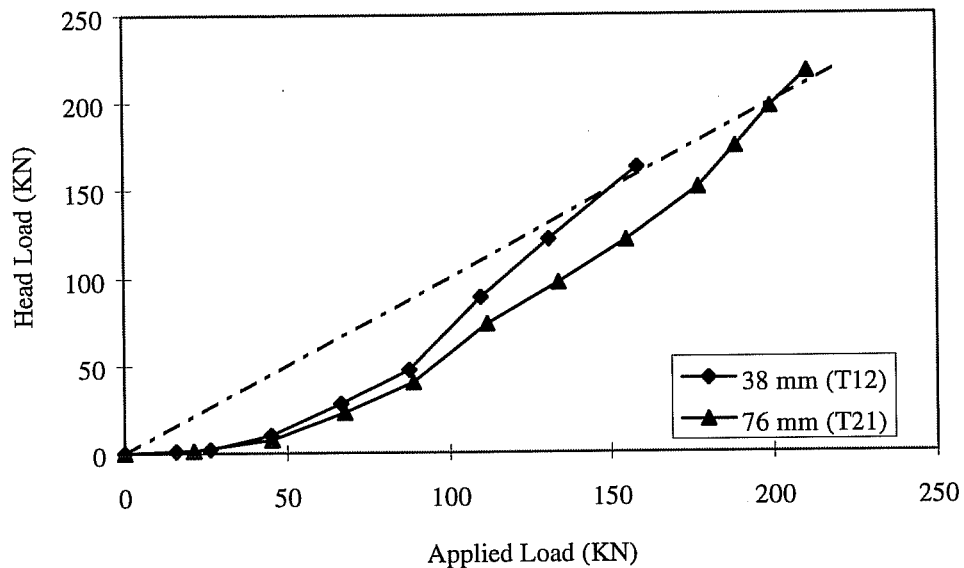


Figure 5.28 Effect of Side Concrete Cover on the Applied Load - Head Load ratio, 25M Bars

The main influence of side cover is providing confinement, thus delaying the wedge formation or forward movement of the wedge. Increased cover provides a larger mass of concrete to restrain side blow-out. In the specimens studied, any improvement in anchorage along the lead embedment due to an increase in the side cover did not improve anchorage capacity, because this force transfer along the bar was lost before failure in all specimens. However, in the case of T21, this force was lost at a higher load (compared to T12), thus decreasing slip. The effect of side cover on the anchorage along the lead embedment is expected to be more significant when longer embedments are provided, preventing the complete loss of force transfer along the length of the bar

at failure. However, when the bar yields, as would be expected in normal design procedures, bond degradation along a considerable part of the lead development length might cause a drop in the force transfer along the length of the bar.

E) Effect of Lead Embedment

Lead embedment is the major variable affecting the stress and slip characteristics of hooked bars. A similar influence was expected on headed bars. Previous research on headed bars and anchor bolts has not addressed this aspect of anchorage behavior.

The normalized anchorage capacities of T27, T9, T16, and T26 are compared in Figure 5.29. The specimens had 35 mm (#11) bars anchored with lead embedments varying from 229 mm (9 in.) to 457 mm (18 in.) with increments of 76 mm (3 in.). The ratio of the anchorage capacities of each specimen to that of T9 is also shown in the figure. The anchorage capacity seems to increase consistently with the increase of the lead embedment length. However, T27, the specimen with 229 mm (9 in.) lead embedment, had significantly lower anchorage capacity. The capacity was 39% lower than that of T9, while the lead embedment was only 25% less.

The load slip behavior of the four specimens is compared in Figure 5.30. Specimen T27 showed rapidly increasing slip at very low loads compared with the

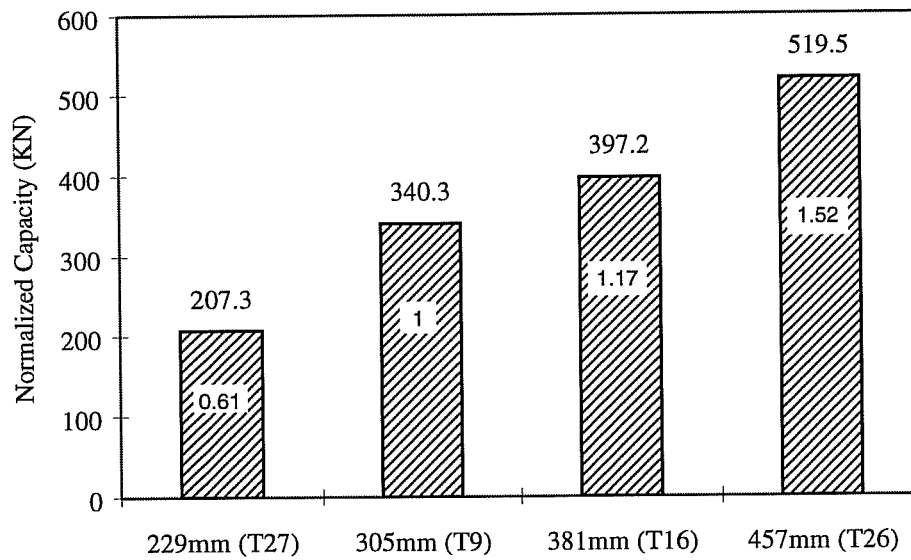


Figure 5.29 Effect of embedment length on the anchorage capacity - 76 mm cover, 35M Bars

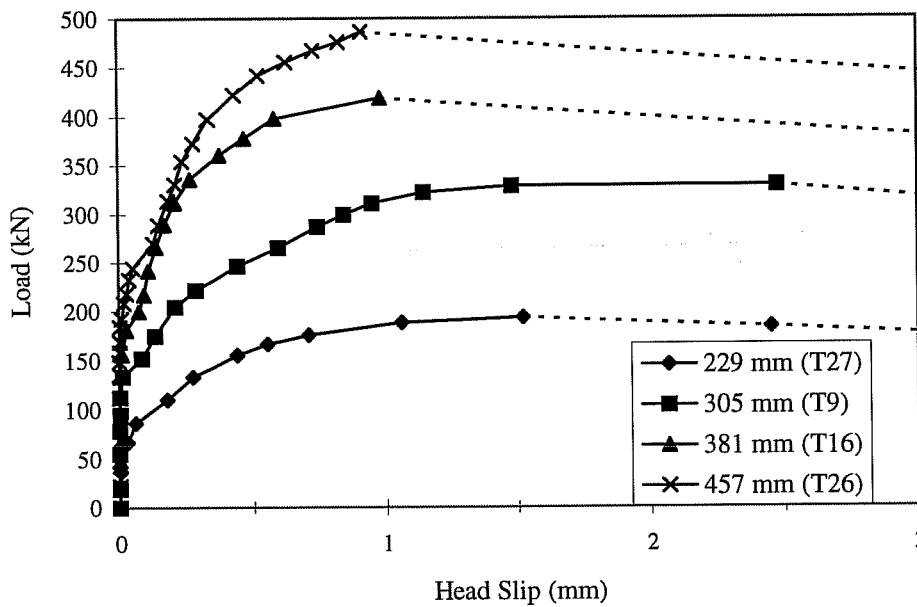


Figure 5.30 Effect of Development Length on the Load-Slip behavior - 76 mm cover, 35M bars

other three specimen. T26 maintained a high stiffness even after slip was first detected (at a load 56% higher than that of T9).

The behavior of the four specimens can be better understood by comparing the head forces. In the case of T27, the force transferred to concrete along the lead embedment was relatively low (Figure 5.31). Maximum force

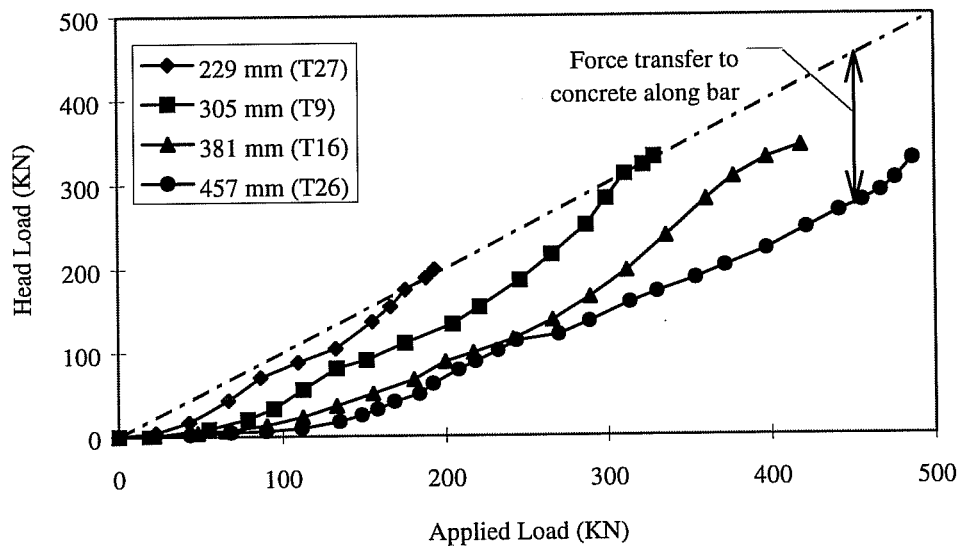


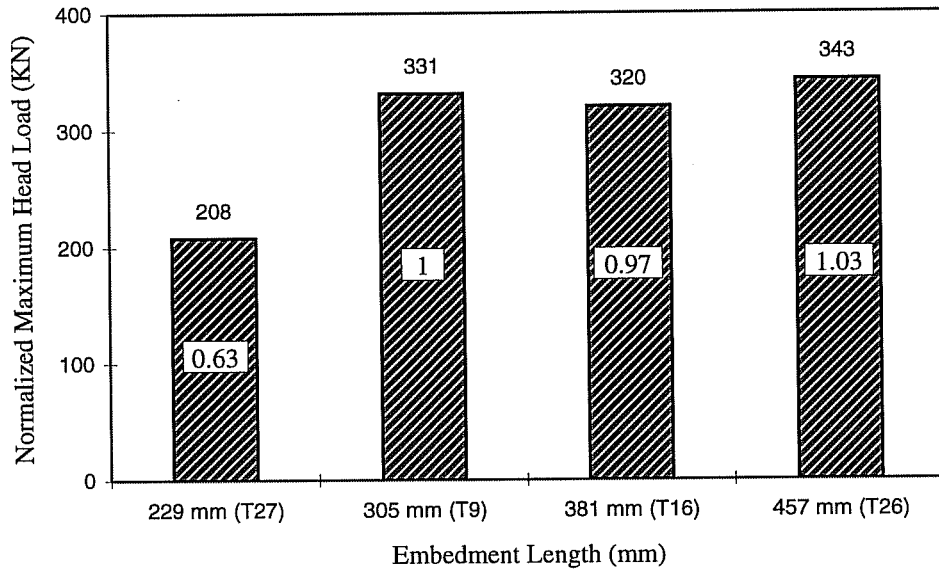
Figure 5.31 Effect of Embedment Length on the Applied Load - Head Load ratio - 76 mm cover, 35M Bars

transfer was only 28 KN (6.3 kip), or 15% of the anchorage capacity and was completely lost before failure. This behavior is somewhat comparable to that of T9. Although the force transferred along the lead embedment for T9 was higher, reaching 70 KN (15.7 kip), or 21% of the ultimate capacity, it was also completely lost before failure. In the case of T16, the load transferred along the

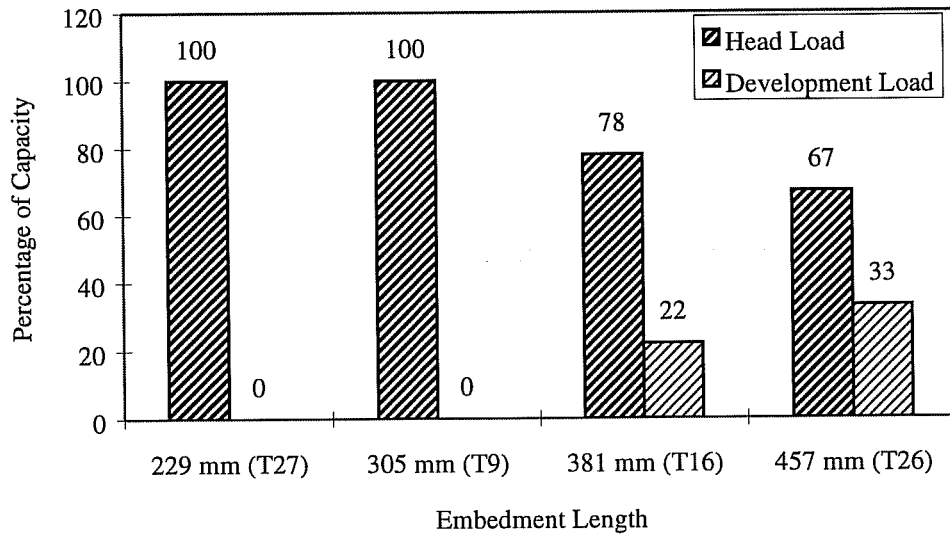
lead embedment length started to drop before failure (from a maximum of 114 KN, or 25.6 kip, to 76 KN, or 16.9 kip). However, at failure, this force was 22% of the anchorage capacity. In T26, the force transferred through the lead embedment kept increasing until the last load increment, where a slight drop could be noticed. The development length carried 33% of the applied load at failure.

The maximum measured head loads for the four specimens are compared in Figure 5.32. One can easily notice that the maximum head loads for T9, T16, and T26 are very close (note that these values are normalized for the difference in concrete strength). On the other hand, the maximum measured head load for T27 is significantly lower.

As mentioned above, the side concrete cover provided resistance to side blow-out failure. In the case of T9 the embedment length was adequate to develop the full head capacity (for the given head area and concrete cover). Increasing the embedment length in T16 and T26 did not increase the head load at failure. The increase in the overall anchorage capacity in these two specimens is attributed to the contribution of the anchorage along the development length. On the other hand, the lead embedment length for T27 did not provide adequate mass of concrete to develop the full head capacity, causing a significant drop in the anchorage capacity.



a) Effect on Head Load



b) Contributions of Head Load to Capacity

Figure 5.32 Effect of Embedment Length on the Maximum Head Load

The significant drop in anchorage capacity due to insufficient embedment length was confirmed by comparing specimens T30 and T13 to T21 and T12, respectively. In these cases, decreasing the lead embedment from 305 mm (12 in.) to 229 mm (9 in.) cause a drop of 38 and 32% in the anchorage capacities. However, it should be noted that in the latter pair of tests (T13 and T12), the side concrete cover over the anchored bars was 38 mm (1 1/2 in.). On the other hand, specimens T30 and T21 had 76 mm cover over, similar to that of the tests described above. Unfortunately, the anchorage behavior of this pair of specimens could not be compared due to the large difference in concrete strength. The load slip curves for specimens T12 and T13 are shown in Figure 5.33. Figure 5.34 shows that the force transfer along the development length was completely lost at failure for T12. The force transferred along the lead development length in T13 kept increasing up to failure, where it represented 36% of the anchorage capacity (Figure 5.34).

The maximum measured head loads for T12 and T13 were very close (4% difference) although the lead embedments are similar to those of T27 and T9 (76 mm cover, and 37% difference in head load at failure). Previous research [2,4] has shown that the blown out area is proportional to the concrete cover. In

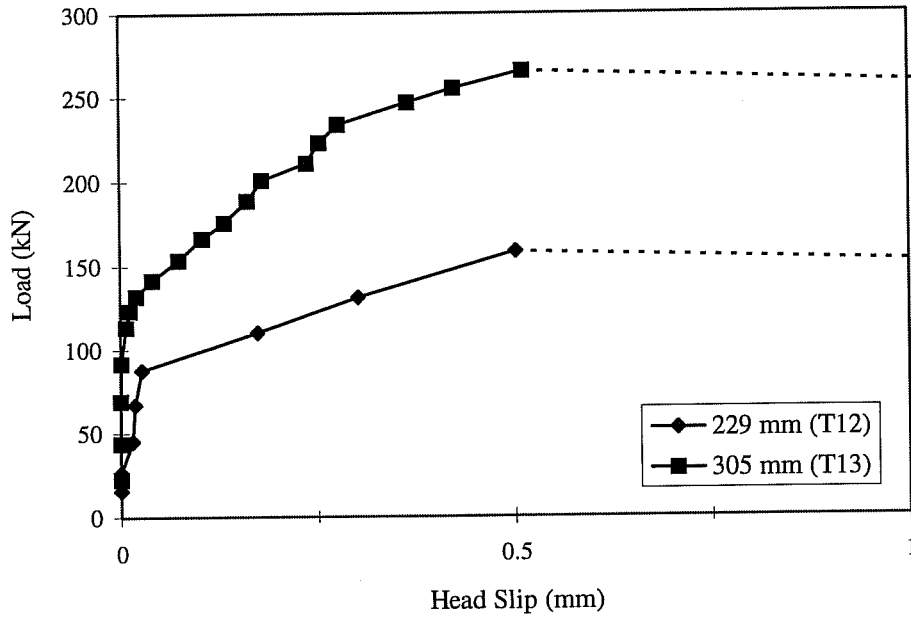


Figure 5.33 Effect of Development Length on the Load-Slip behavior - 38 mm cover, 25M Bars

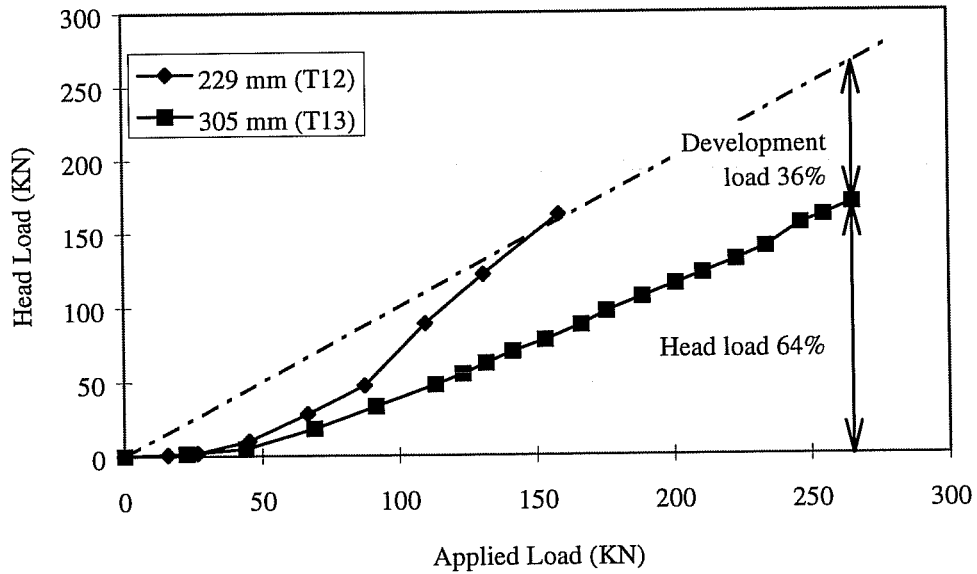


Figure 5.34 Effect of Embedment Length on the Applied Load - Head Load ratio - 38 mm cover, 25M Bars

the case of T12, a lead embedment length of 229 mm (9 in.) provided adequate area to develop the full head capacity for a concrete cover of 38 mm. The increase in the overall anchorage capacity of T13 was due to the anchorage along the lead development length.

f) Effect of Confining Reinforcement

The normalized anchorage capacities of specimens T9, T14, and T25 are compared in Figure 5.35. The first specimen did not have any confining reinforcement. T14 and T25 had 10 mm (#3) ties through the joint at 102 mm (4 in.) and 51 mm (2 in.), respectively. It should be noted that for T25, the tie spacing outside the joint (i.e. above the anchored bar) was increased to 102 mm (4 in.). The anchorage capacities of T14 and T25 were higher than that of T9 by 17 and 29%, respectively.

The applied load - head slip curves for the three specimens are shown in Figure 5.36. Although head slip started increasing around the same load (160 KN or 36 kip) for the three specimens, deformations in T9 increased rapidly beyond this point while T14 and T25 maintained their stiffnesses. At failure, head slip for T9 was significantly larger than the specimens with confining reinforcement. In the case of T9, the load dropped after failure to 54% of the maximum. The load drop was 9 and 12% from the maximum for T14 and T25, respectively. In all

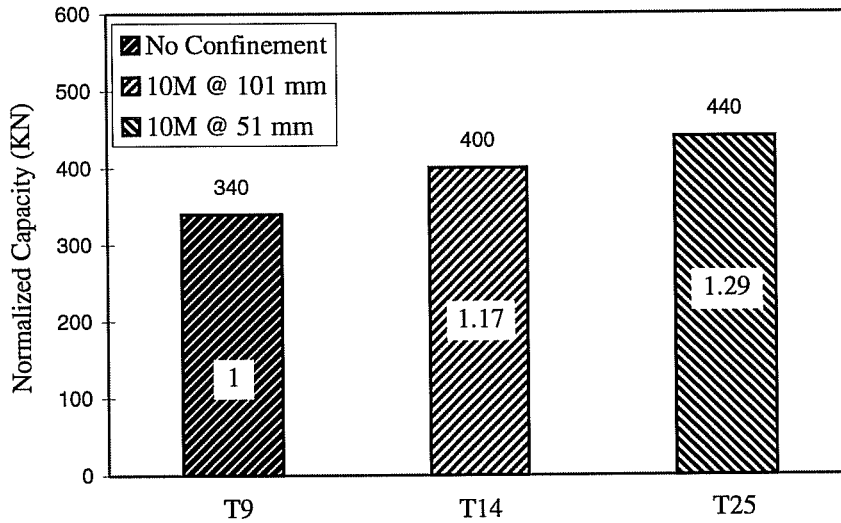


Figure 5.35 Effect of Confining Reinforcement on the Anchorage Capacity - 76 mm cover, 35M Bars

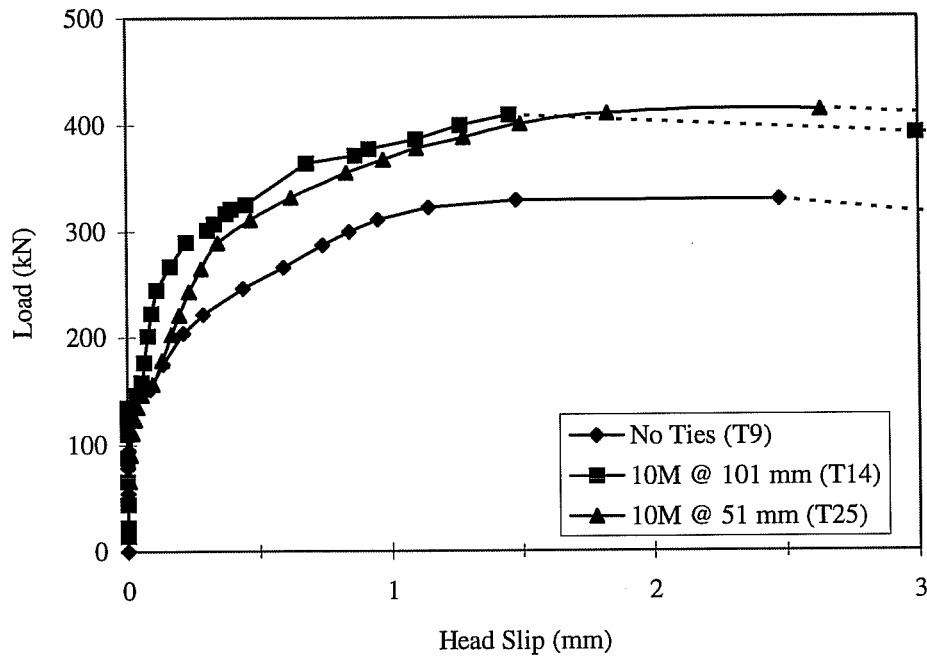


Figure 5.36 Effect of Confining Reinforcement on the Load-Slip behavior - 76 mm cover, 35M Bars

three specimens the head was responsible for transferring all of the applied load to concrete at failure (Figure 5.37). The rate of loss of anchorage along the lead embedment length was similar for the three specimens for most of the load history.

Confining reinforcement improved the anchorage behavior through two mechanisms. Concrete under the head had improved bearing capacity, leading to a reduction in head slip, and increasing the load at which the wedge starts to form. In addition to this, stirrups restrained the side cover, preventing spalling and movement of the wedge which reduced slip at failure and allowed load to be maintained at a higher level.

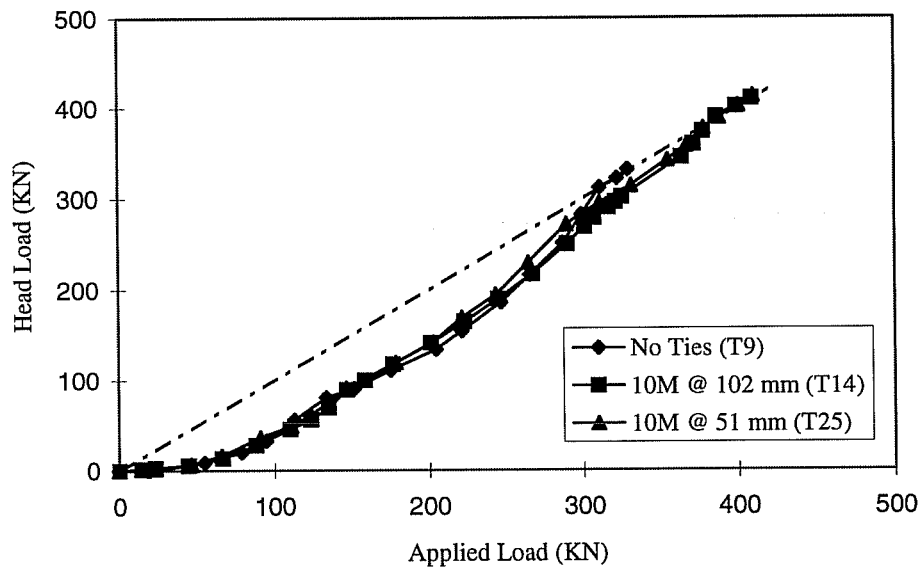


Figure 5.37 Effect of Confining Reinforcement on the Applied Load - Head Load Ratio

5.3 Specimens Failing in Shear

The fourteen specimens which failed in shear were divided into two groups. The first group consists of the specimens in which the heads were not anchored behind the column longitudinal bars. The second group consists of specimens T15, T18, and T19, in which the heads were anchored behind the column longitudinal bars. Table 5.2 shows the maximum loads (per anchored bar) for the specimens in the both groups. The load at the first diagonal shear crack is also presented.

5.3.1 Cracking Pattern

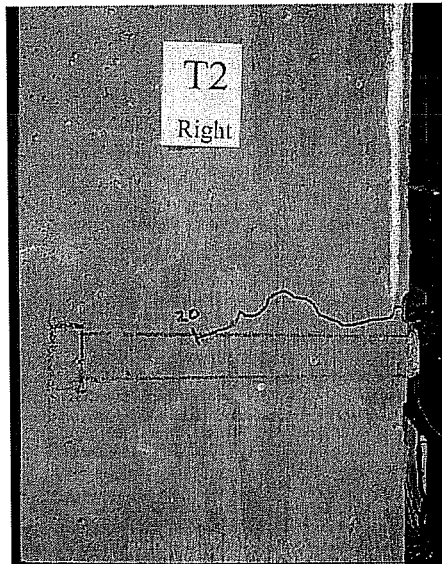
The cracking pattern was initially similar to that of the specimens with side blow-out failure (Section 5.2.1). The first crack appeared on the side of the column along the lead portion of the embedded bar (Figure 5.38-a). As mentioned earlier, this was a splitting crack radially propagating from the anchored bars to the surface and extending along the bar. With increasing the load, diagonal cracks initiating from the anchor head and propagating towards the top of the assumed compressive zone were detected (Figure 5.38-b). The width of this crack increased with the increase of the applied load. Failure occurred along the plane of this crack. In several cases, failure was not detected until attempting to increase the load in the following increment. At failure, several diagonal

cracks could be detected in the joint region (Figure 5.38-c). For these tests, the plane of the initial shear crack (connecting the anchor head to the top of the compression zone) was always the failure plane.

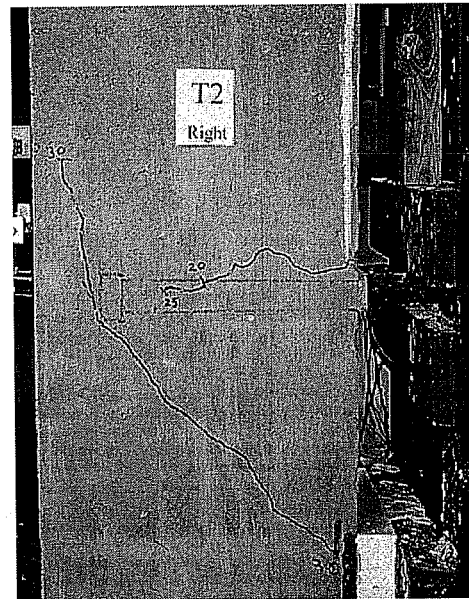
Table 5.2 Test results for group 1 and 2 specimens (shear failure)

Test	f'_c (MPa)	Joint Ties	P_{crack}^* (KN)	P_{max} (KN)
Heads anchored in front of column bars				
T1	26.7	-	138	227
T2	29.4	-	133	222
T3	29.4	-	133	232
T4	26.7	-	85	94
T5	22.5	-	114	167
T6	22.5	4-10M	122	294
T7	23.2	7-10M	134	316
T8	29.6	4-10M	100	183
T11	35.0	3-13M+4-10M	178	420
T17	36.1	5-10M	111	155
T31	33.3	-	100	173
Heads anchored in behind column bars				
T15	40	-	178	422
T18	36.2	-	189	361
T19	36.2	-	209	296

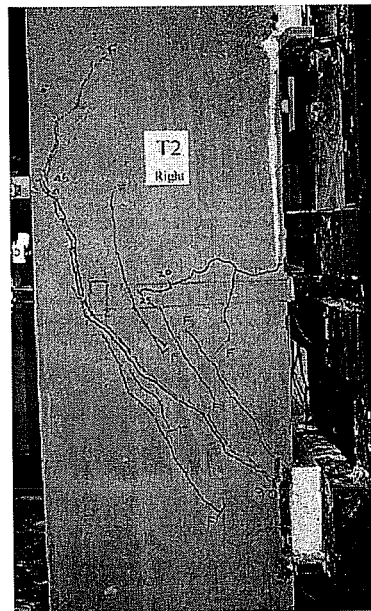
* First shear crack



a) Initial anchorage crack



b) First shear crack



c) Appearance at failure

Figure 5.38 Cracking and failure patterns - Specimen T2

Similar cracking patterns were detected in specimens with shear and confining reinforcement, but at higher loads. In some cases, the initial shear cracks were detected at a slightly higher load than those of specimens without shear reinforcement. In addition to this, there was more uniform crack distribution in the joint region. This improved behavior is attributed to the role of reinforcement in controlling cracks.

The specimens in which the heads were anchored to the column longitudinal bars showed superior behavior, similar to that of the specimens with heavy shear and confining reinforcement. Diagonal cracks were detected at about 30% higher load than in the case of specimens without shear reinforcement. These specimens also failed at a significantly higher load. Failure was sudden and occurred with a pronounced thud. Crushed concrete could be detected in the joint area along the diagonal between the anchorage head and the compression zone (Figure 5.39).

5.3.2 Load-Slip Behavior

The load slip behavior of specimen T2 is shown in Figure 5.40. The first head slip was measured at 133 KN (30 kip).applied load, the same load at which the first diagonal crack (in the joint) was detected. Beyond this point, head slip

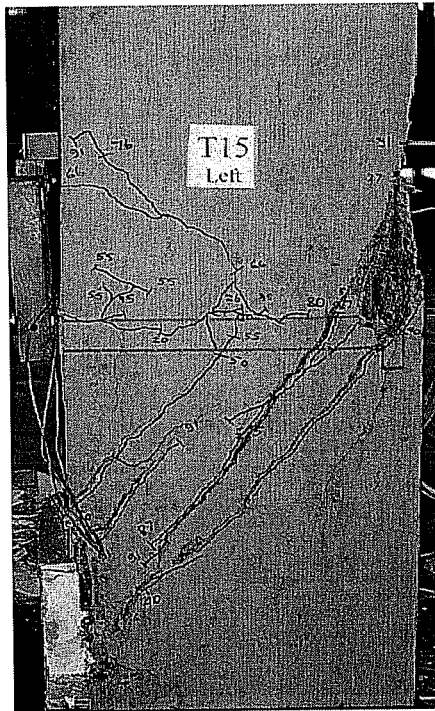


Figure 5.39 Failure pattern of specimen T15

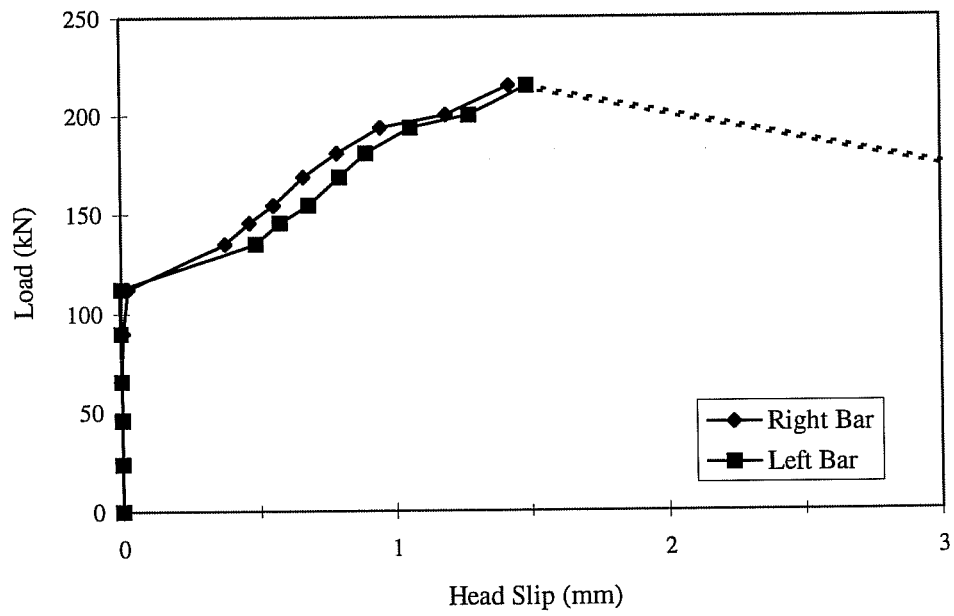


Figure 5.40 Applied Load vs. Head Slip for Specimen T2

continued increasing almost linearly. The specimen failed at an applied load equal to 222 KN (50 kip) per bar, and a head slip of 1.5 mm (0.06 in.). At failure, the applied load dropped to 144 KN (32 kip), and the head slip increased to 4.2 mm (0.17 in.). As in all of the specimens with shear failure, the load-slip curves for both bars were identical throughout the load history. The load transferred to concrete along the lead embedment length reached (34 KN) 7.6 kip at an applied load equal to 46 KN (10.3 kip) and was almost constant up to failure (Figure 5.41).

The applied load - head slip curves for T2 (without shear reinforcement) and T11 (with shear reinforcement) are compared in Figure 5.42. The two curves

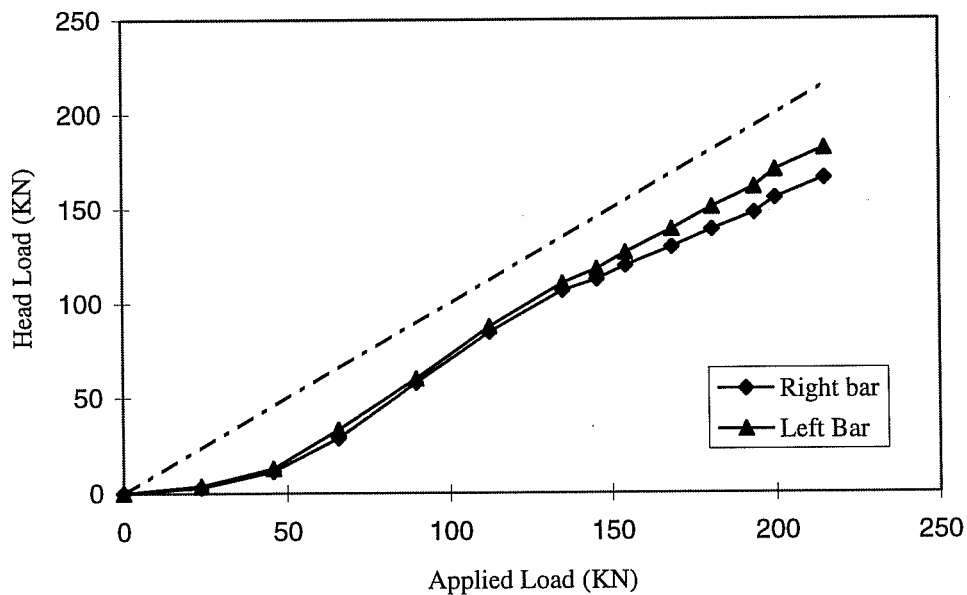


Figure 5.41 Head Load vs. Applied Load for Specimen T2

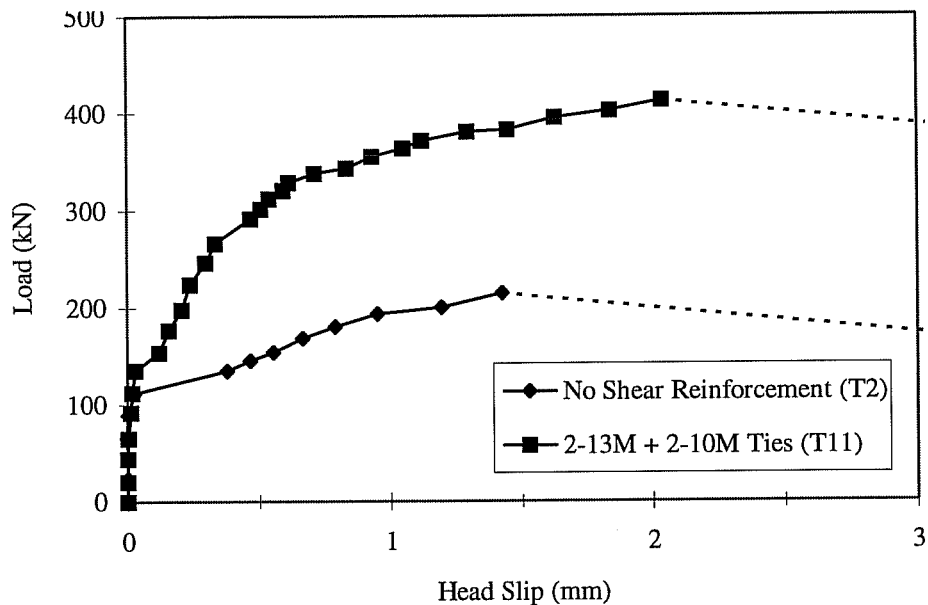


Figure 5.42 Effect of shear reinforcement on the Load-Slip behavior

are identical initially. Head slip started to increase at a slightly higher load in the case of T11. This was attributed to the difference in concrete strength. T11 was significantly stiffer beyond this point. The stirrup forces prevented further crack opening and improved aggregate interlock along the shear crack, thus decreasing the slip. At 80% of the ultimate capacity the stiffness of T11 was almost the same as T2 (at the same percentage of capacity). Figure 5.43 shows the head load for the two specimens. The curves for both specimens are similar up to failure of T2. For T11, all of the applied load was transferred to concrete through the anchorage head at failure, but in both specimens the head transferred a very large fraction of the load throughout the test.

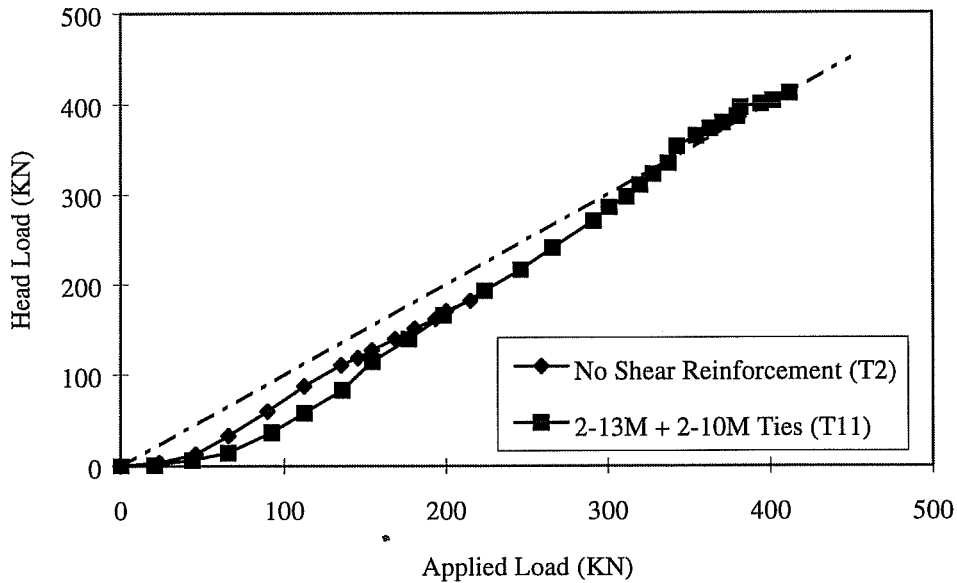


Figure 5.43 Effect of Shear Reinforcement on the Applied Load - Head Load Ratio

Figure 5.44 shows the load-slip behavior of the three specimens in which the head was anchored behind the column longitudinal bars. The curve for specimen T2 is also included for comparison. The head slip was very low up to an applied load of about 180 KN (40 kip). Beyond this point, slip started to increase rapidly. It should be noted that the diagonal cracks were first detected in all three specimens around this load. Figure 5.45 shows the head load for the four specimens presented in Figure 5.44. Anchorage along the development length was responsible for transferring a larger portion of the load in the second group of specimens (with heads anchored behind the column longitudinal bars). This

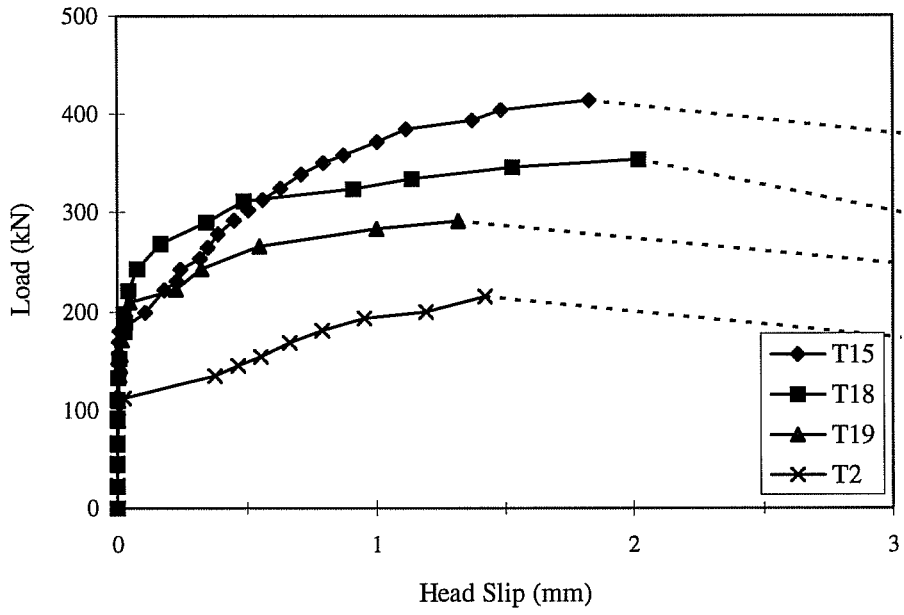


Figure 5.44 Effect of the Anchorage Condition on the Load-Slip behavior

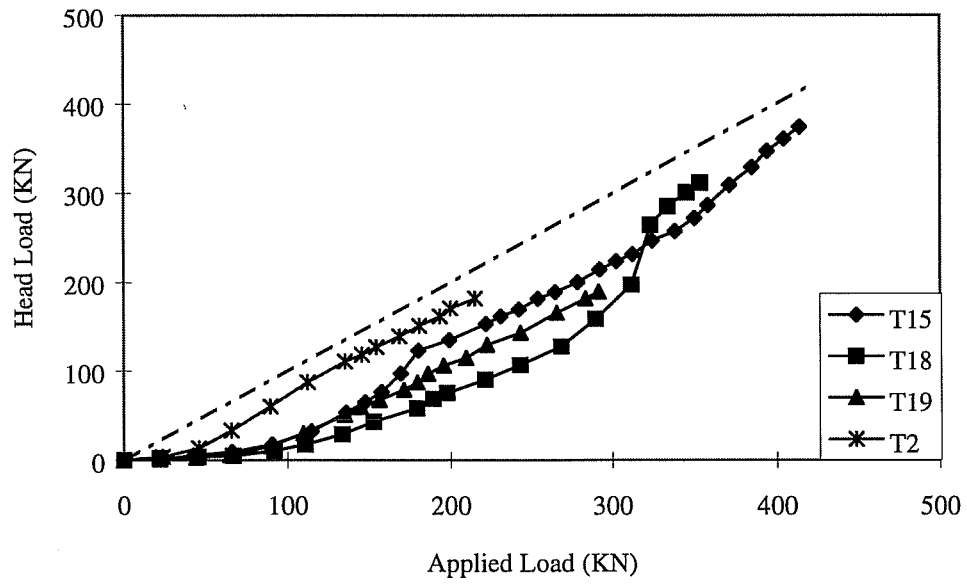


Figure 5.45 Effect of Anchorage Condition on the Applied Load - Head Load Ratio

improved anchorage along the lead embedment (compared to that of T2) is attributed to three factors; longer embedment length (by 16.7%), higher concrete strength, and the minimal head slip (resulting from the restraining effect of the column bars) during most of the load history.

5.3.3 Cracking Stress

In Table 5.3, the joint shear at the time the first diagonal crack was detected, is given for all thirty-two specimens. The joint shear was calculated taking into consideration height, slenderness, and whether the bottom reaction was adjusted or not (using the reaction rams). It should be noted that this load might be slightly larger than the actual cracking load, as the crack could have initiated during applying the load increment. To minimize the error, in most specimens, the load steps were dropped from 22 KN (5 kip) to 11 KN (2.5 kip) when the first diagonal crack was expected. Table 5.3 also presents the cracking joint shear stress expressed as a function γ_{cr} of the square root of f'_c . The coefficient was calculated using the following equation:

$$v_{cr} = \frac{V_{jcr}}{b \times d}, \quad \gamma_{cr} = \frac{v_{cr}}{\sqrt{f'_c}} \quad 5.1$$

Where v_{cr} is the joint shear stress at cracking in N/mm^2 , V_{jcr} is the joint shear when the crack is first detected in N, b and d are the column width and depth in mm. Although the effective depth might be considered as the distance to

Table 5.3 Shear stress at cracking

Specimen	Column Size (mm)	f'_c (MPa)	Cracking Joint shear (KN)	γ_{cr}
T1	381×305	26.7	185	0.37
T2	381×305	29.4	189	0.36
T3	381×305	29.4	189	0.36
T4	305×305	26.7	117	0.31
T5	381×305	22.5	153	0.33
T6	381×305	22.5	164	0.36
T7	381×305	23.2	180	0.39
T8	305×305	29.6	139	0.35
T9	381×305	34.5	203	0.36
T10	381×305	34.5	173	0.30
T11	381×305	35.0	239	0.42
T12	305×305	35.2	154	0.35
T13	381×305	38.3	220	0.37
T14	381×305	37.2	227	0.38
T15*	381×305	40.0	275	0.45
T16	457×305	39.6	309	0.41
T17	305×305	36.1	172	0.39
T18*	381×305	36.2	292	0.50
T19*	381×305	36.2	323	0.55
T20	305×305	35.2	199	0.35
T21	305×305	35.2	206	0.47
T22	305×305	35.2	165	0.38
T23	381×305	33.2	223	0.40
T24	381×305	32.3	213	0.39
T25	381×305	32.3	227	0.41
T26	533×305	31.4	378	0.47
T27	305×305	31.4	168	0.41
T28	305×305	33.3	220	0.39
T29	381×305	33.3	225	0.40
T30	381×305	22.1	213	0.47
T31	381×305	33.3	155	0.36
T32	305×305	33.3	155	0.36
			Average	0.38
			σ	0.04

* Specimens excluded from average calculations

the center of the anchorage plate, it is taken as the distance from the face of the column to the center of the longitudinal reinforcement at the back of the column, as the latter is the common definition of the depth of a structural element in most design practices. The maximum difference between the two definitions of depth is 25 mm (1 in.) and is not expected to cause any distortion to the data.

If the specimens of group 2 (heads anchored behind column bars) are excluded, the average value of value of γ_{cr} for the remaining 29 specimens is 0.384 (4.6 in customary units), with a maximum of 0.47, a minimum of 0.31 (5.7 and 3.7 in customary units), and a standard deviation equal to 0.04 (0.5 in customary units).

In order to determine the effect of the ratio between the column depth and the beam depth on the first cracking load, the 29 specimens were divided according to the column depth. The average value of γ_{cr} was almost the same for specimens with 381×305 mm (15×12 in.) and 305×305 mm (12×12 in.) columns (0.378 and 0.376, respectively), indicating that the column depth (in this range) does not have a significant effect on the cracking load. Note that the former group specimens has 6 longitudinal bars, while the latter has 4 longitudinal bars. The value of γ_{cr} for specimens T16 and T26, with 457×305 mm (18×12 in.) and 533×305 mm (21×12 in.) columns, were 0.41 and 0.47 (4.9 and 5.7 in customary

units), respectively. Although these values are relatively high, they are within the range of experimental scatter for shallower specimens. As only one specimen of each size was tested, it can not be determined if the increase in shear capacity is consistent with the increase in column size. On the other hand, γ_{cr} had an average value of 0.5 (6.4 for customary units) and was consistently higher for specimens T15, T18 and T19, in which the headed bars were anchored behind the column longitudinal bars.

5.3.4 Shear capacity

In Table 5.4, the joint shear at failure for the specimens that failed in shear is given. The area of reinforcement crossing the diagonal shear crack is also presented. This shear crack connected the center of the anchorage head to the top of the compression zone due to the variation of the compressive stress distribution from that in an actual beam column joint (Figure 5.46). As a result, the stirrups at the bottom of the joint did not affect the shear capacity. Specimen T31 was excluded as its failure pattern was different from all other specimens due to the movement of shear reinforcement during concrete pouring. The failure plane for this specimen did not pass through any shear reinforcement. In Table 5.4, the ultimate joint shear stress expressed as a function of the square root of f'_c is presented. The coefficient was calculated using the following equation:

$$v = \frac{V_u}{b \times d}, \quad \gamma = \frac{v}{\sqrt{f'_c}} \quad 5.2$$

Where v is the joint shear stress at failure in N/mm^2 , γ is the coefficient presented in Table 5.4, V_u is the joint shear at failure in N .

Although none of the first five specimens had shear reinforcement, specimens T1, T2, T3, and T5 (381×305 mm or 15×12 in. columns) had significant residual strength beyond cracking. On the other hand, T4 (305×305 mm or 12×12 in. column) failed after a slight increase in load after cracking. The higher shear capacity of deeper columns indicates that the behavior was controlled by deep beam effects.

Shear reinforcement improved the behavior of the specimens consistently. Specimen T11 had the highest γ value of the specimens failing in shear (0.98 or 11.9 in customary units). Furthermore, specimen T25 (did not fail in shear) had a γ value of 1.2 (14.4) at failure, indicating that the shear capacity can be increased significantly using ties. Figure 5.47 shows the stress in a tie 51 mm (2 in.) below the anchored bar for specimen. The stirrup stress started to increase at a steady rate after cracking and the specimen failed when the stirrup reached yield.

Table 5.4 Shear Stress at failure

Specimen	Column Size (mm)	f'_c (MPa)	Effective Reinforcement (mm^2)	Joint shear (KN)	γ
T1	381×305	26.7	-	304	0.61
T2	381×305	29.4	-	315	0.6
T3	381×305	29.4	-	330	0.63
T4	305×305	26.7	-	131	0.34
T5	381×305	22.5	-	224	0.49
T6	381×305	22.5	284	394	0.86
T7	381×305	23.2	426	424	0.91
T8	305×305	29.6	284	255	0.64
T11	381×305	35.0	800	563	0.98
T15	381×305	40.0	-	652	1.07
T17	305×305	36.1	284	239	0.54
T18	381×305	36.2	-	557	0.96
T19	381×305	36.2	-	457	0.78

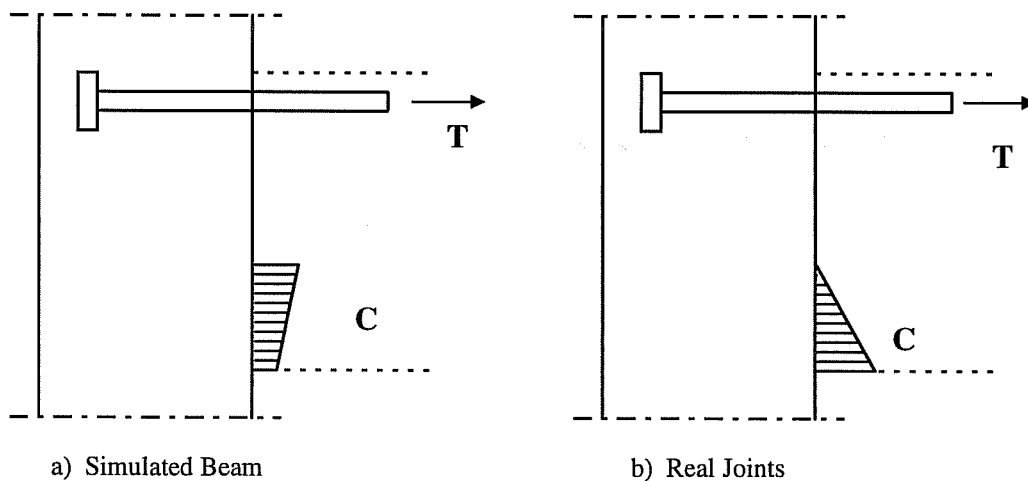


Figure 5.46 Compressive Stress Distributions in Test Specimens and in Joints

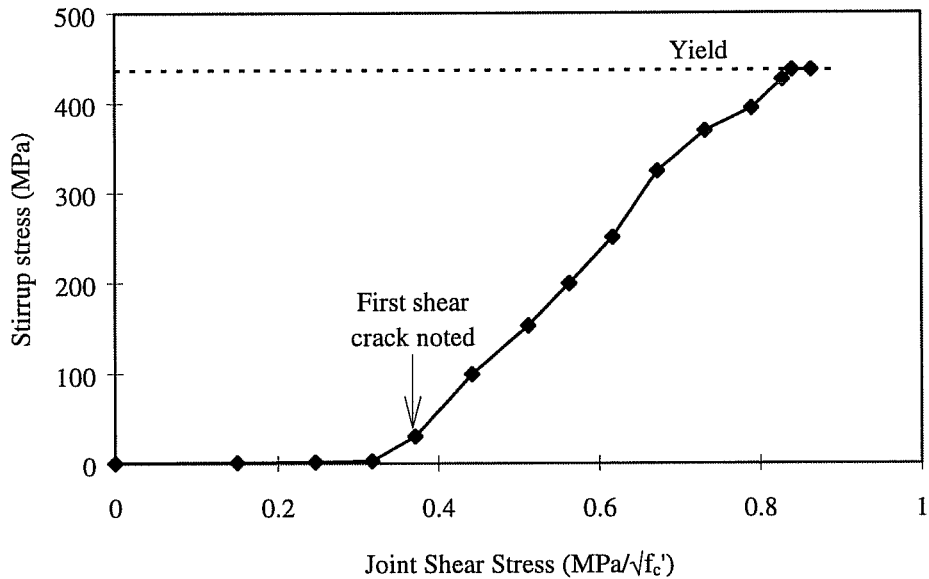


Figure 5.47 Stresses in Shear Reinforcement - Specimen T6

Specimens with the heads anchored behind column bars had significantly higher shear strength. In spite of the lack of shear reinforcement, the value of γ for T15, T18, and T19 was 1.1, 0.95, and 0.8 (12.8, 11.5, and 9.5 in customary units), respectively. The shear capacity for these specimens is significantly higher than similar specimens in group 1 (T1-T3 and T5).

The lower capacity of T19 (compared to T15 and T18) is attributed to the slip between the head and the column longitudinal bars. While the heads of T15 and T18 were wide enough to be positively anchored behind the column longitudinal bars, the head of T19 was narrow and there was little bearing against

the column bars (Figure 5.48). As a result, the column longitudinal bars were bent outward rather than forward at failure, decreasing the beneficial effect of anchoring the heads behind the longitudinal bars, as discussed previously in Chapter 3.



a) Anchored heads - Specimen T18



b) Anchored heads - Specimen T19



c) Specimen T19 after failure

Figure 5.48 Anchorage conditions of group 2 specimens

5.4 Head Strains

Strain gages placed on the anchor heads on opposite sides of the bar (Figure 4.30) were used to describe the flexural stress distribution in the head. Figure 5.49 shows the increase in head strains above and below the anchored bar with the increase in head load for specimen T21 (with 80×40×18 mm heads). The increase in strain was linear with increasing of head load for the major part of the curve. However, the curve flattens significantly near failure, indicating a change in the bearing stress distribution. Although 77% of the bar force was transferred through the joint to the compression zone (below the bar), the strains on both sides of the head were very close up to the flat part of the curve indicating a similar bearing stress distribution above and below the bar.

Figure 5.50 shows a comparison between the head strains on the outer and inner sides of the head (on the side of the cover and the side of the joint core) for specimen T28. The head load - head strain diagram indicates a slightly increasing rate of strain at higher loads. Again, the strains on both sides of the head are very close indicating similar bearing stress distribution up to failure. Although the strain gages were damaged at failure, it is expected that the bearing stress on the inner side became higher beyond this point.

Figure 5.51 shows the head strains for specimen T15, in which the head was anchored behind the longitudinal column bars. At failure the head strains on

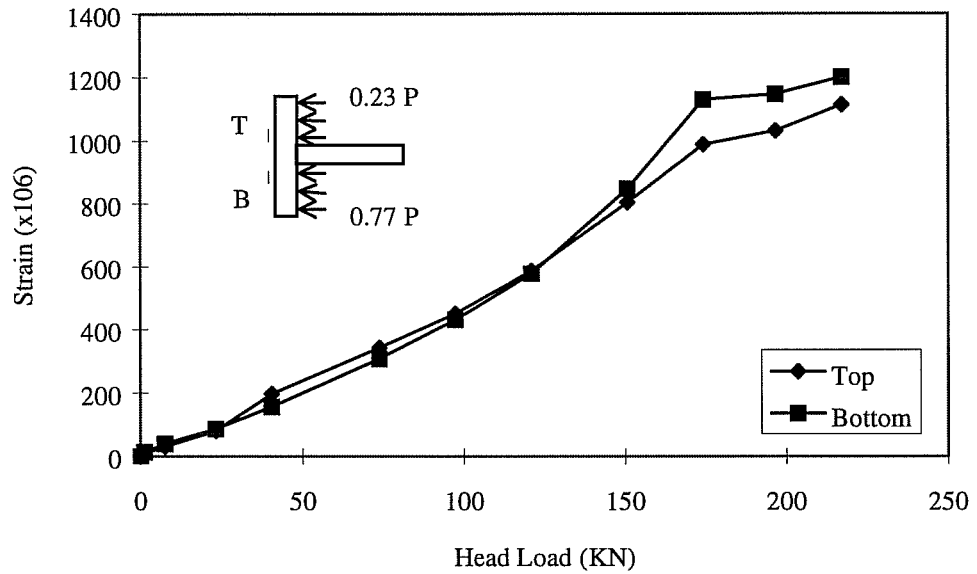


Figure 5.49 Head Strains on the top and bottom of the bar - Specimen T21

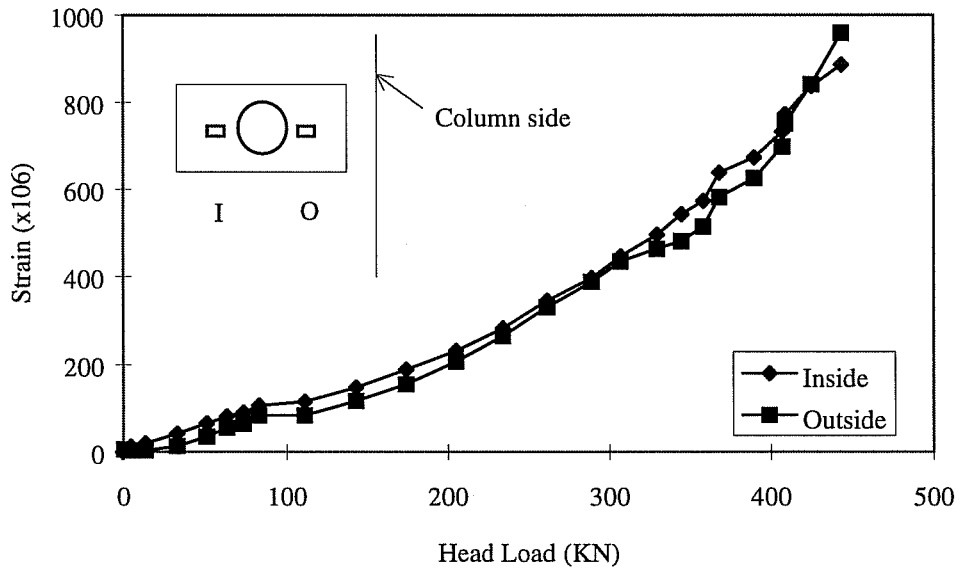


Figure 5.50 Head Strains in the inner and outer sides of the head - Specimen T28

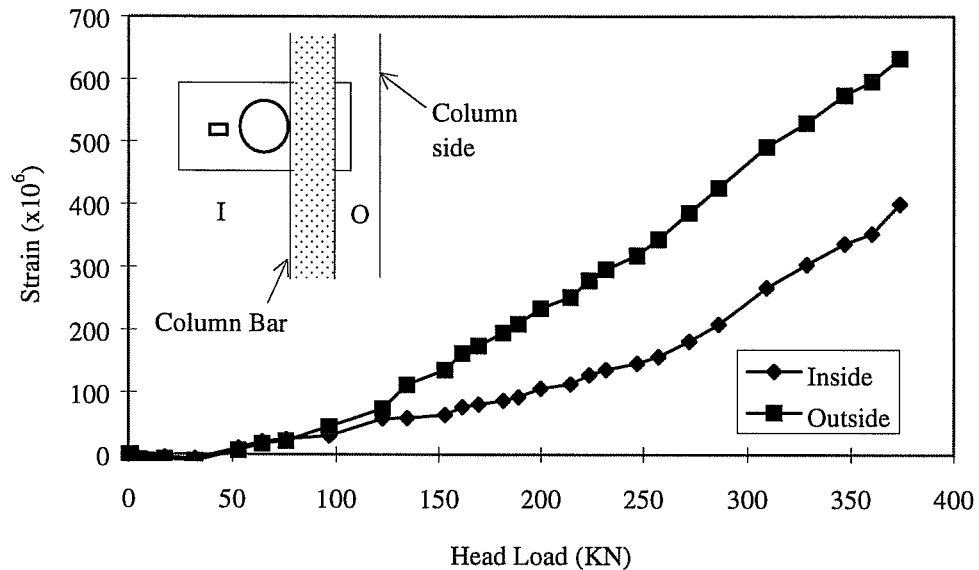


Figure 5.51 Head Strains on the inner and outer sides of the head - Specimen T15

the outer side of the head (anchored behind the column bars) were 60% higher than those on the inner side. The difference between head strains on both sides is larger than that observed in pullout tests in which heads were anchored to longitudinal bars. The larger difference in strains is attributed to the higher stiffness of the column longitudinal bars. While the column longitudinal bars had 51 mm (2 in.) clear concrete cover over them, longitudinal bars in pullout tests had covers between 25 and 13 mm (1 and 0.5 in.). In addition to this, the column bars were longer than the longitudinal bars in pullout tests, and confinement by

ties (outside the joint) made them even more effective in restraining head movement.

5.5 Summary

The experimental results divided the specimens into two major groups depending on the type of failure: side blow-out or shear failure. Emphasis has been placed on reporting experimental results for specimens with side blow-out failure in order to study the effect of the different variables on the anchorage capacity of headed bars.

Based on test results, the concrete cover, lead embedment, and confining reinforcement are the primary factors affecting the anchorage capacities of headed bars. The increase in side cover and lead embedment significantly increased the capacity. Ties through the joint increased the capacity somewhat in addition to maintaining higher residual strengths after failure. An increase in the capacity due to increasing head area was also noted. The effects of aspect ratio, head orientation, and bar diameter were insignificant.

The shear capacity was increased significantly with the increase in column depth. Shear reinforcement in the joint area was effective in increasing the shear capacity. Tie stresses increased steadily after the first diagonal crack was detected, up to failure. The stress distribution in the compressive zone of the

simulated beam was different than that in a beam at a joint, it was difficult to draw any conclusions regarding the shear capacity of joints constructed with headed bars.

Chapter 6

Analysis of Test Results

6.1 Introduction

In Chapter 5 the results of the thirty-two specimens were presented and the effects of different variables were discussed. In this chapter, the behavior of headed bars anchored in exterior joints is compared to that of anchor bolts and headed bars anchored near the edges of concrete cubes. Design methods based on these pullout tests are also compared to results from joint tests. Mathematical and physical models for the anchorage capacity, based on the behavior of exterior joints, are developed .

The behavior of headed bar specimens is also compared to that of hooked bar tests. The embedment length required for hooked bars by the ACI building

embedment length of headed bars as required by models

6.2 Comparison with Deep Embedment Tests

The anchorage capacity of a 25 mm (#8) headed bar embedded in an exterior joint (T12) is compared to that of similar bars embedded near the edges of concrete cubes (obtained from tests conducted by DeVries[2]) in Figure 6.1. All bars had 80×40 mm heads. The clear cover over the bars was 38 mm (1.5 in.) in the exterior joint and 33 mm (1.3 in.) in pullout tests. Anchorages in concrete cubes were 14 to 44% higher. Although there was no development length in the pullout tests, the comparison should not be affected because bond along the embedment length was completely lost before failure for Test T12.

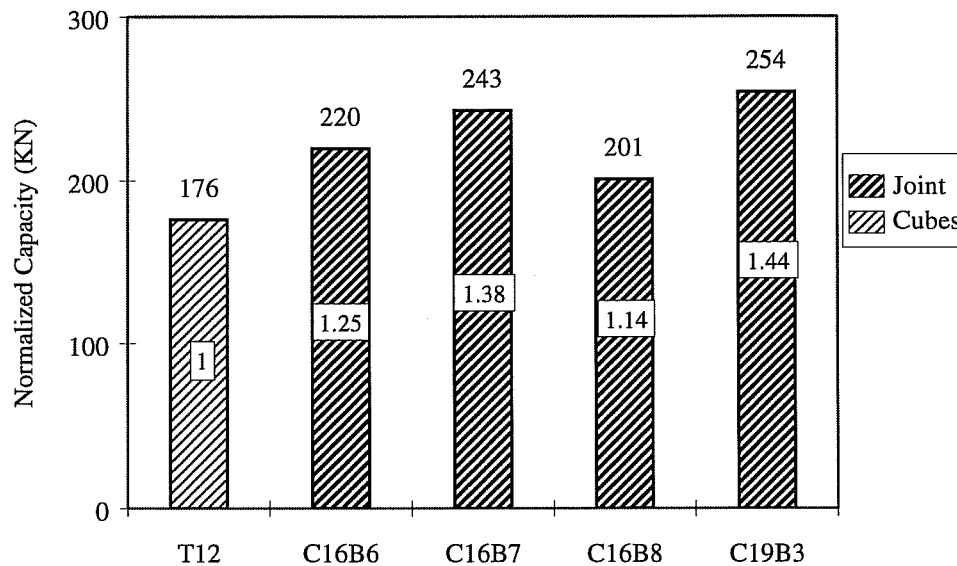


Figure 6.1 Comparison of Anchorage Capacities of Joint and Pull-Out Tests - 25 mm Bars

A similar comparison for 35 mm (#11) bars is presented in Figure 6.2. While the two joint tests presented in this figure had 76 mm (3 in.) clear cover, pullout tests had 84.5 mm (3.3 in.) clear cover over the bars. The first pair of tests (T29 and C7B4) had 100×55 mm heads. The other pair had 90×90 mm heads. Similar difference in the anchorage capacity could be observed (18 and 39% in this case).

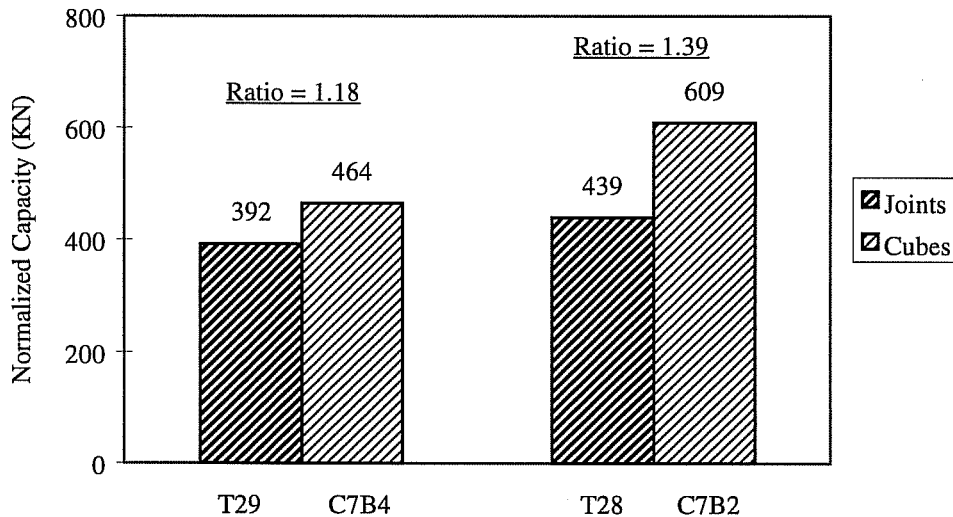


Figure 6.2 Comparison of Anchorage Capacities of Joint and Pull-Out Tests - 35 mm Bars

The load-slip behavior of Test T12 is compared to that of C16B5 and C19B3 in Figure 6.3. The concrete strength in the three tests varied significantly (35.2, 19, and 44 MPa, respectively). The head slips were comparable, indicating

similar behavior for headed bars in joints and cubes. However, it should be noted that in some of the tests with relatively large heads and cover reported by DeVries [2], the head slip at failure was very low (in the order of 0.2 mm).

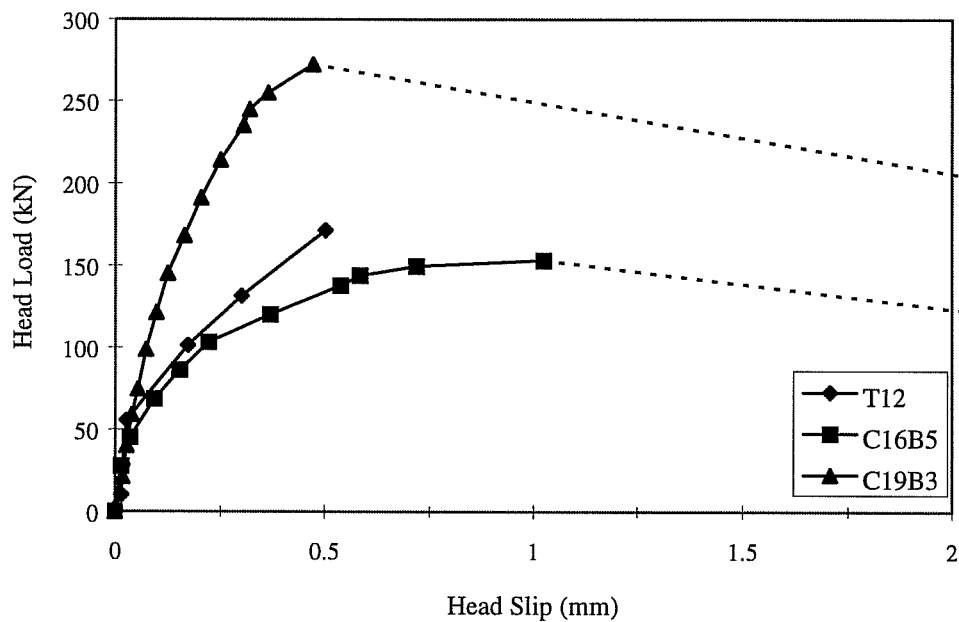


Figure 6.3 Load-Slip Behavior of Joint and Cube Tests

The comparisons presented above indicate that the anchorage capacities of headed bars in exterior joints are significantly lower (by 14 to 44%) than those of bars anchored to concrete cubes. The difference in capacity is attributed to concrete cracking in the joint region (due to shear) before side spalling. The shear cracking pattern had a direct effect on the side-blow out area. Although concrete spalling above the bar was not directly affected by cracks, spalling below the bar

was limited by the diagonal shear crack connecting the head to the top of the compressive zone (Figure 5.3). As a result, the blown out area had a triangular shape (see Section 5.2.1) which is different than that described in previous pull-out studies (compare Figures 3.8 and 5.3).

6.3 Comparison with Existing Design Methods

The force transfer between headed bars and concrete occurs through two mechanisms. The basic mechanism is bearing of the head on concrete. Another force transfer mechanism is the steel-concrete bond along the length of the deformed bar. The discussions presented in the previous chapter demonstrated that the latter mechanism was not effective in increasing the anchorage capacity in most cases, especially when the development length is relatively short and the bond between the steel and concrete along the length of the bar is lost before failure.

The behavior described above is similar to that of anchor bolts embedded in concrete. Previous research on anchor bolts [4] has indicated that for practical values of embedment length and load bearing area, the anchorage capacity is governed by side blow-out failure if the side cover is less than 0.2 to 0.4 times the embedment length. In the first phase of this study, DeVries [2] proposed relationships specially formulated for headed bars to determine the critical

embedment depth at which the failure mode changes from pullout cone to side blow-out, for a given side cover. In this section, the measured anchorage capacity of headed bars in exterior joints, as governed by side blow-out failure, will be compared with equations and design methods previously developed for estimating the side blow-out capacity from pullout tests.

6.3.1 University of Texas Anchor Bolt Studies (Hasselwander)

Although the equations developed by Hasselwander [3] are based on anchor bolts embedded near the edges of piers in which longitudinal and confining reinforcement were placed around the bolts, the anchorage capacities should not be significantly affected. According to Marques [9], the position of longitudinal bars does not affect the anchorage capacity. Although ties improved the anchorage capacity of headed bars, the large tie spacing used by Hasselwander (305 mm or 12 in.) minimized this effect. Hasselwander noted that there was very little difference in load-slip or anchorage capacity with different amounts, types, and locations of pier reinforcement. Based on his test data, Hasselwander developed a best fit equation in this form:

$$T = A_b \sqrt{f'_c} \left[96 + 142 \ln \left(\frac{1}{1 - \frac{C_w}{C'}} \right) \right] \quad 6.1$$

Where T is the anchorage capacity of the anchor bolt in lb, A_b is the net bearing area in in.², C_w is the clear cover over the anchorage device in in., and C' is the clear cover over the bolt in in.. With some algebraic manipulations, and rounding off constants, the above equation was transformed into an acceptable design equation in the form:

$$T = \phi 140 A_b \sqrt{f'_c} \left[0.7 + \ln \left(\frac{2C'}{D_w - D} \right) \right] \quad 6.2$$

in which ϕ is a capacity reduction factor to account for the scatter in test results and other uncertainties, D_w is the washer diameter, and D is the bolt diameter.

The measured capacities of 16 exterior joint tests that resulted in side blow-out failures (the two specimens with confining reinforcement are not included) are compared to the values calculated using both equations proposed by Hasselwander in Table 6.1. Since Hasselwander's best fit equation is based on undeformed anchor bolts with circular washers (or heads), cases similar to that of specimen T23, in which the one of the head dimensions is less than the bar diameter, were not considered. The equation could not be evaluated for this case. This problem did not occur in applying the design equation, in which the ratio between the side covers over the bar and the head was replaced by the difference between the diameters of the circular head and the anchor bolt. In this case, the equation was evaluated for the square and rectangular heads using an equivalent

head diameter, equal to the diameter of a circular head with the same area, using the following equation:

$$D_w = \sqrt{\frac{4 \times A_h}{\pi}} \quad 6.3$$

Where D_w is the equivalent diameter, and A_h is the head area. In addition, the capacity reduction factor was not used since all variables were known in the tests.

Table 6.1 Comparison of Measured and predicted Capacities using Hasselwander's Equations

Test	Head Area (mm ²)	Cover (mm)	Column (mm)	Measured P _{max} (KN)	Equation 6.1		Equation 6.2	
					P _{max} (KN)	meas/comp	P _{max} (KN)	meas/comp
T9	3025	76	381×305	340	377	0.90	336	1.01
T10	2970	38	381×305	271	272	1.00	236	1.15
T12	3200	38	305×305	178	431	0.41	256	0.70
T13	3200	38	381×305	273	450	0.61	267	1.02
T16	3025	76	457×305	426	405	1.05	360	1.18
T20	4225	76	381×305	349	519	0.67	462	0.75
T21	3200	76	305×305	218	562	0.39	385	0.57
T22	1624	76	305×305	183	361	0.51	210	0.87
T23	2970	76	381×305	306	-	-	323	0.95
T24	2970	76	381×305	357	224	1.59	319	1.12
T26	2970	76	533×305	495	350	1.42	314	1.58
T27	3025	76	305×305	198	360	0.55	320	0.62
T28	8100	76	381×305	432	820	0.53	728	0.59
T29	5500	76	381×305	385	824	0.47	556	0.69
T30	3200	76	381×305	279	445	0.63	305	0.92
T32	3800	76	305×305	216	701	0.31	427	0.51
					Average	0.74	0.89	
					σ	0.38	0.29	

The average value of the measured capacity/estimated capacity ratio for the values estimated using the best fit and the design equations is 0.74 and 0.89, respectively. In general, both equations over estimated the anchorage capacity in exterior joints. However the design equation (Equation 6.2) provides a slightly better estimate of the capacity (29% standard deviation compared to 38% for the best fit equation). It should be noted that the estimates of this equation was fairly close to the measured values for most 381×305 mm (15×12 in.) columns (except T20, T28, and T29). As mentioned earlier, this column size provided the minimum embedment required to develop the full capacity of a head with 76 mm (3 in.) cover (see Section 5.2.4-e). As expected, the capacities of T16 and T26 (specimens with longer embedment lengths) were underestimated, because Hasselwander's equations does not include the effect of anchorage along the embedment length on the anchorage capacity. The capacities of T20, T28, and T29 (specimens with larger head areas) were over-estimated because the equations are based on a linear relationship between the head area and the capacities. Test results indicated that the anchorage capacity in exterior joints is less sensitive to the increase in head area (Figure 5.11).

Another significant observation is that the capacity of T12 was over estimated. Although T12 is a 305×305 mm (12×12 in.) column, test results showed that the anchorage capacity was not affected by the small column size

because of the relatively low side cover (38 mm or 1.5 in.). Although the design equation estimated the capacity of T13 accurately, it should be noted that the head contribution to this capacity was only 64% (the rest resulted from anchorage along the development length). In other words, the capacity of T13 was also underestimated. The reason for this is that Hasselwander's design equation is sensitive to the difference between the head dimensions (represented by the equivalent diameter) and the bar diameter, and uses the net bearing area as an indication of the capacity. However, comparison of specimens with different bar diameters and similar total head areas has shown that the anchorage capacity was not affected by the bar diameter (Figure 5.23).

6.3.2 University of Stuttgart Anchor Bolt Studies (Furche and Eligehausen)

The measured capacities of 16 exterior joint tests that resulted in side blow-out failures are compared with values calculated using the equation proposed by Furche and Eligehausen [4] (Equation 2.4) in Table 6.2. The average value of the measured capacity/estimated capacity ratio is 0.76, only 3% higher than that obtained by Hasselwander's best fit equation. However, the standard deviation was significantly lower (24% versus 38%).

The observations noted from Table 6.2 are similar to those discussed above. In general, the equation over estimated the anchorage capacity of headed

Table 6.2 Comparison of Measured and predicted Capacities using Furche and Eligehausen Equation

Test	Head Area (mm ²)	Cover (mm)	Column (mm)	Measured P _{max} (KN)	Furche & Eligehausen		ACI-318	
					P _{max} (KN)	meas/ comp	P _{max} (KN)	meas/ comp
T9	3025	76	381×305	340	416	0.82	329	1.04
T10	2970	38	381×305	271	243	1.11	192	1.41
T12	3200	38	305×305	178	262	0.68	207	0.86
T13	3200	38	381×305	273	273	1.00	216	1.26
T16	3025	76	457×305	426	446	0.96	353	1.21
T20	4225	76	381×305	349	530	0.66	419	0.83
T21	3200	76	305×305	218	459	0.47	363	0.60
T22	1624	76	305×305	183	296	0.62	234	0.78
T23	2970	76	381×305	306	403	0.76	319	0.96
T24	2970	76	381×305	357	397	0.90	314	1.14
T26	2970	76	533×305	495	391	1.27	309	1.60
T27	3025	76	305×305	198	397	0.50	314	0.63
T28	8100	76	381×305	432	765	0.56	605	0.71
T29	5500	76	381×305	385	609	0.63	482	0.80
T30	3200	76	381×305	279	364	0.77	288	0.97
T32	3800	76	305×305	216	494	0.44	391	0.55
					Average	0.76	0.96	
					σ	0.24	0.30	

bars in exterior joints. Although the estimated capacity was more than the measured capacity in most cases of 381×305 mm (15×12 in.) columns, the difference was much higher for 305×305 mm (12×12 in.) columns, indicating the importance of including a factor to reflect the effect of the embedment length. Although the estimated anchorage capacity was a function of the square root of

the head area, the effect of increasing head areas was still over estimated (compare T27 and T28 to T9, and T21 and T32 to T22).

Table 6.2 also includes a comparison between measured capacities and capacities estimated using the design equation for the proposed Chapter 23 governing the anchorage to concrete for the ACI 318 (-98 or -01) Building Code (adapted from equation 2.4 by Furche and Eligehausen). The equation is in customary US units and has the following form:

$$P_u = 160c\sqrt{A_b f'_c} \quad 6.4$$

This equation is a more conservative version of equation 2.4 by Furche and Eligehausen. Although the average value of the measured/estimated capacities ratio is higher, the same trends could be noted.

6.3.3 University of Texas Pullout Tests on Headed Bars (DeVries)

As the empirical equation proposed by DeVries[2] (Equation 2.6) is identical to the one proposed by Furche and Eligehausen, the best fit equation (Equation 6.5) will be used for comparison with the test results, in order to determine the difference between the effects of the variables on headed bars embedded in cubes, and anchored to exterior joints.

$$P_u = 0.0252C_1^{0.609} A_n^{0.577} f'_c{}^{0.671} \quad 6.5$$

Table 6.3 Comparison of Measured and predicted Capacities using DeVries' Equation

Test	Head Area (mm ²)	Cover (mm)	Column (mm)	Measured P _{max} (KN)	Equation	
					P _{max} (KN)	meas/ comp
T9	3025	76	381×305	340	348	0.98
T10	2970	38	381×305	271	249	1.09
T12	3200	38	305×305	178	286	0.62
T13	3200	38	381×305	273	303	0.90
T16	3025	76	457×305	426	382	1.11
T20	4225	76	381×305	349	461	0.76
T21	3200	76	305×305	218	403	0.54
T22	1624	76	305×305	183	243	0.76
T23	2970	76	381×305	306	334	0.91
T24	2970	76	381×305	357	328	1.09
T26	2970	76	533×305	495	322	1.54
T27	3025	76	305×305	198	327	0.61
T28	8100	76	381×305	432	701	0.62
T29	5500	76	381×305	385	539	0.71
T30	3200	76	381×305	279	295	0.95
T32	3800	76	305×305	216	436	0.50
					Average	0.85
					σ	0.27

The average value of ratios of measured/estimated capacity was 0.85, with a standard deviation of 0.27 (Table 6.3). Observations similar to those discussed in the comparison with anchor bolt studies could be noted. Although the estimated capacity for T9 was fairly accurate, the side blow-out capacities of specimens T12 and T13 (specimens with 38 mm side cover) were over-estimated

(note that both of them had the same head load at failure, but anchorage along the lead embedment length increased the capacity of T13). In general, the capacities of all 305×305 mm (12×12 in.) specimens were over-estimated. This observation was expected as the equation used is based on large embedments, in which the blown out area was not affected by the size of the specimens. The equation does not include a term describing the effect on the embedment length (which is equal to the development length in the case of exterior joints) and leads to the underestimation of the capacities of specimens with longer embedment lengths (T16 and T26). As the exponent for head area is more than that used by Furche and Eligehausen, the effect of increasing head areas was still over estimated (compare T27 and T28 to T9, and T21 and T32 to T22).

6.4 Statistical Analysis

Comparison of test results with existing design equations previously developed using pullout test results indicated the need for an equation based on exterior joint tests in which the effect of embedment length and joint cracking are considered. Additionally, limits on the effect of head area on anchorage capacity and a factor for the effects of confining reinforcement are needed.

Some of the variables described in the previous chapter did not have significant effect on the anchorage capacity (aspect ratio, head orientation, and bar

diameter). However, identical specimens, with each variable under study being the only difference, will be compared in order to detect the effects of the four main variables in the best-fit equation accurately. After the weight of each variable is defined, all of the tests will be used to finalize the equation.

a) Concrete Strength

Concrete strength was not one of the variables in this study. However, the governing failure mode (side blow-out) indicates that the tensile strength of concrete (usually described using the square root of the compressive strength) has a direct effect on the anchorage capacity. Most previous studies (in which the concrete strength was one of the variables) involving pullout tests showed that the blow-out capacity is directly proportional to the square root of the concrete strength. In addition, the anchorage capacity of hooked bars, as governed by side spalling, is also a function of the square root of concrete compressive strength. Based on these studies, $\sqrt{f'_c}$ will be used to describe the effect of concrete strength in this report.

b) Embedment Length

Tests T27, T9, T16, and T26 were used to determine the effect of the embedment length, l_d , on the anchorage capacity. The concrete cover over the bar

was 76 mm (3 in.). Anchored bars were 35 mm (#11) with lead embedments varying from 229 mm (9 in.) to 457 mm (18 in.) with increments of 76 mm (3 in.). The normalized capacities of the four tests are plotted against the embedment length in Figure 6.4. Although the four points seem to lay on a straight line indicating a linear relationship, a best fit line does not pass through the origin.

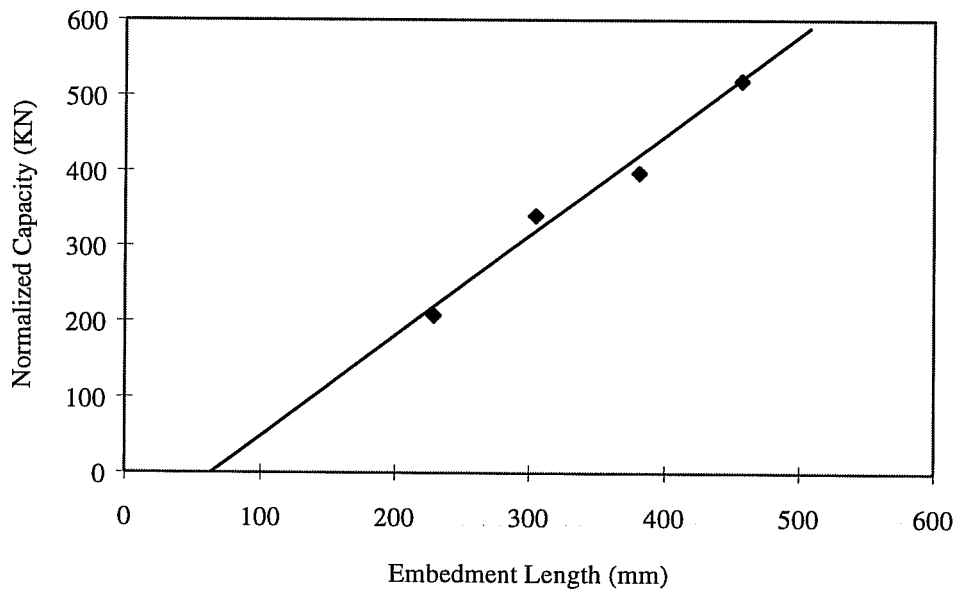


Figure 6.4 Anchorage Capacity versus Embedment Length

A straight line intersecting the X-axis means that there is a minimum embedment length required for the head anchorage to be effective. This could be attributed to the failure pattern described in the previous chapter. A concrete cone

with a depth equal to the concrete cover over the column compression bars was always pulled out (Figure 5.4). Since the cone reduced the effective embedment length to “ l_d-d' ”, where d' is the distance from the extreme compression zone to the centroid of the compression reinforcement, the equation of the straight line in Figure 6.4 is $1.3(l_d-d')$. The X-intercept is 63.5 mm (2.5 in.), or d' . The average value of the measured/estimated capacities ratio is 1.01 with a standard deviation of 0.06.

c) Head Area

Two groups of tests were used to determine the effect of head area on the anchorage capacity. The first group consisted of tests T9, T20, and T28. The second group consisted of tests T21 and T22.

DeVries reported that there was little difference in the results of the regression analysis using the total head area and the net bearing area. Both areas were used in this analysis. In order to avoid complexity of numbers in the final form of the equation, the head area exponents used were limited to 1/3, 1/2, and 1, the values suggested in previous studies. The basic equation used for the analysis had the following form:

$$P_U = K \cdot A^x \quad 6.6$$

Where A is the total or net head area, x is the exponent under study, and K is a factor used to minimize the average of the differences between the measured and computed capacities.

Table 6.4 shows a comparison between the estimated and the measured values. The results from this analysis indicates that the cube root ($x = 1/3$) of the total head area gives the most accurate description of the behavior. The cube root of the net bearing area was slightly less accurate. Increasing the exponent to 1.0 resulted in a large margin of error.

The fact that using the total head area gives a slightly better description of the behavior (compared to the net bearing area) was observed by DeVries. However, the capacity is proportional to the cube root instead of the square root of the area in the case of exterior joints. The lower exponent of the head area agrees with the observations described on comparing the measured capacities to estimations using existing design equations (the increase in head area was less effective in increasing the capacity). This is attributed to severe joint cracking at high loads, which decreases the confinement effect of concrete before failure, and reduces strength gain resulting from increasing the head area.

Table 6.4 Comparison of Functions of Head Area

Test	Bar	Head	Head Area (A) mm ²	Net Area (A _n) mm ²	Pmax (KN)	$P = 22.3\sqrt[3]{A}$	meas/comp	$P = 55\sqrt{A}$	meas/comp	$P = 24.5\sqrt[3]{A_n}$	meas/comp	$P = 6.3\sqrt{A_n}$	meas/comp
T9	35	55x55	3025	2025	340	323	1.06	303	1.13	310	1.10	284	1.20
T20	35	65x65	4225	3225	345	361	0.96	358	0.97	362	0.95	358	0.97
T28	35	90x90	8100	7100	439	448	0.98	495	0.89	471	0.93	531	0.83
						Average	1.00		0.99		1.00		1.00
						$P = 15\sqrt[3]{A}$		$P = 4.2\sqrt{A}$		$P = 16.4\sqrt[3]{A_n}$		$P = 4.8\sqrt{A_n}$	
T21	25	80x40	3200	2700	216	221	0.98	238	0.91	228	0.94	249	0.87
T22	25	58x28	1624	1124	182	176	1.03	169	1.07	171	1.07	161	1.13
						Average	1.00		0.99		1.01		1.00

d) Concrete Cover

The effect of concrete cover on the anchorage capacity could be assessed by comparing the three pairs of tests presented in Figure 5.26. The drop in capacity due to decreasing the cover by half (from 38 mm to 76 mm) ranged between 18 and 26%. All of the existing equations over estimated the drop in load for such decrease in cover. It should also be noted that the significant concrete strength difference might have caused some inaccuracy in comparison for the third pair (the one with 26% difference).

As only two cover sizes were covered in this experimental program, it is difficult to estimate a relationship between the cover and the capacity. However most previous design equations assumed a linear relationship between the side cover and the anchorage capacity [2,4]. Assuming such relationship applies to headed bars in exterior joints, a reduction factor equal to $\frac{C+127}{203}$, C being the clear cover over the bars, could be multiplied by the estimated anchorage capacity in order to substitute for the effect of cover on the anchorage capacity. This factor is based on the ratios presented in Figure 5.26, and calibrated to yield 1 for 76 mm (3 in.) cover. The maximum cover used in this study was 76 mm (3 in.), therefore a limit of 1 for the factor seems prudent.

The effect of cover could also be included by using a specified value for the reduction factor (0.8 in this case), to be multiplied by the ultimate capacity for cases in which the side cover is less than 76 mm (3 in.). Although this method provide simplicity for design purposes, it will not be used in the statistical analysis to improve the accuracy of the mathematical model.

e) Confining Reinforcement

The effect of confining reinforcement on the anchorage capacity could be assessed by comparing the three tests presented in Figure 5.35. Tie spacing of 102 and 51 mm caused an increase in the ultimate capacity by 17 and 29%, respectively. These values were initially used as multipliers for tests T14 and T25 during the statistical analysis, and adjusted or rounded based on the analysis.

6.4.1 Best Fit Equation

The above trends were used to develop mathematical models for the ultimate strength of headed bars anchored in exterior joints. With only 18 specimens, and the majority consisting of 381×305 mm (15×12) columns, it was felt that a regression analysis might not produce the best equation describing the behavior (e.g. the weight of specimens with longer embedments would be very low). Instead the mathematical models were developed by examining their accuracy in describing the ultimate strength of each test, in addition to the overall

standard deviation. Two mathematical models were developed, the first is a function of the total head area, and the second is a function of the net bearing area. The models had the following forms:

$$P_u = 15.6 \cdot \alpha \beta (l_d - d') \sqrt[3]{A} \sqrt{f'_c} \quad 6.7$$

$$P_u = 17.2 \cdot \alpha \beta (l_d - d') \sqrt[3]{A_n} \sqrt{f'_c} \quad 6.8$$

Where

P_u = anchorage capacity, in N

l_d = embedment length, in mm

d' = distance from the face of the column to the centroid of the column longitudinal reinforcement closest to face, in mm

A = total head area, in mm^2

A_n = net bearing area, in mm^2

α = Confining reinforcement factor, taken as 1 for tie spacing more than 100 mm, 1.25 for spacing equal to 100 mm to 51 mm, and 1.4 for tie spacing equal to 50 mm or less

β = cover size factor, taken as $\frac{C+127}{203}$ but not greater than 1

C = clear cover over the anchored bars, in mm

The value of the capacity multiplier for confining reinforcement effects was increased (above than that noticed in the test results) based on comparison between the mathematical model and test data. The values estimated using both models are presented in Table 6.5. The predicted capacities are also compared in

Table 6.5 Comparison of Measured and predicted Capacities using Analytical Models

Test	Head Area (mm ²)	Cover (mm)	Column (mm)	Measured P _{max} (KN)	Equation 6.7		Equation 6.8	
					P _{max} (KN)	meas/ comp	P _{max} (KN)	meas/ comp
T9	3025	76	381×305	340	320	1.06	309	1.10
T10	2970	38	381×305	271	259	1.05	249	1.09
T12	3200	38	305×305	178	183	0.97	191	0.93
T13	3200	38	381×305	273	279	0.98	291	0.94
T14	3025	76	381×305	416	415	1.00	401	1.04
T16	3025	76	457×305	426	451	0.95	435	0.98
T20	4225	76	381×305	349	361	0.97	364	0.96
T21	3200	76	305×305	218	226	0.97	235	0.93
T22	1624	76	305×305	183	180	1.02	176	1.04
T23	2970	76	381×305	306	312	0.98	300	1.02
T24	2970	76	381×305	357	308	1.16	296	1.21
T25	3025	76	381×305	426	434	0.98	418	1.02
T26	2970	76	533×305	495	494	1.00	475	1.04
T27	3025	76	305×305	198	209	0.95	202	0.98
T28	8100	76	381×305	432	437	0.99	461	0.94
T29	5500	76	381×305	385	384	1.00	396	0.97
T30	3200	76	381×305	279	261	1.07	272	1.03
T32	3800	76	305×305	216	232	0.93	245	0.88
					Average	1.00		1.01
					σ	0.06		0.08

Figures 6.5 and 6.6. The average value of the measured/estimated capacities ratio for the values estimated using equation 6.7 was 1.00, with a standard deviation of 0.056. Equation 6.8 provided almost the same average with a slightly higher standard deviation (0.077). The 95% fractile [15] form of both equations is given by

$$P_U = 13.9 \cdot \alpha\beta(1_d - d') \sqrt[3]{A} \sqrt{f'_c} \quad 6.9$$

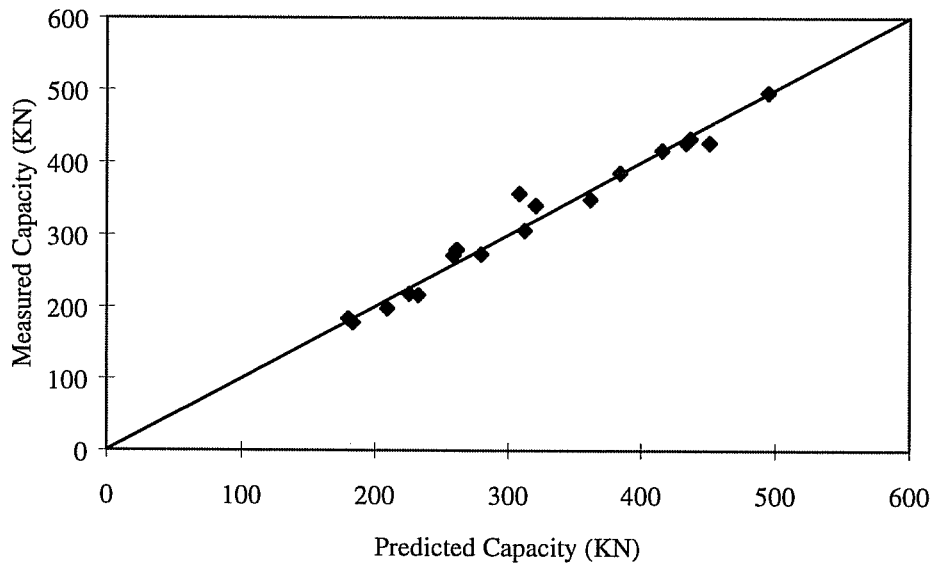
$$P_U = 14.7 \cdot \alpha\beta(1_d - d') \sqrt[3]{A_n} \sqrt{f'_c} \quad 6.10$$

The capacities predicted using these two equations are compared to the measured capacities in Figures 6.5 and 6.6.

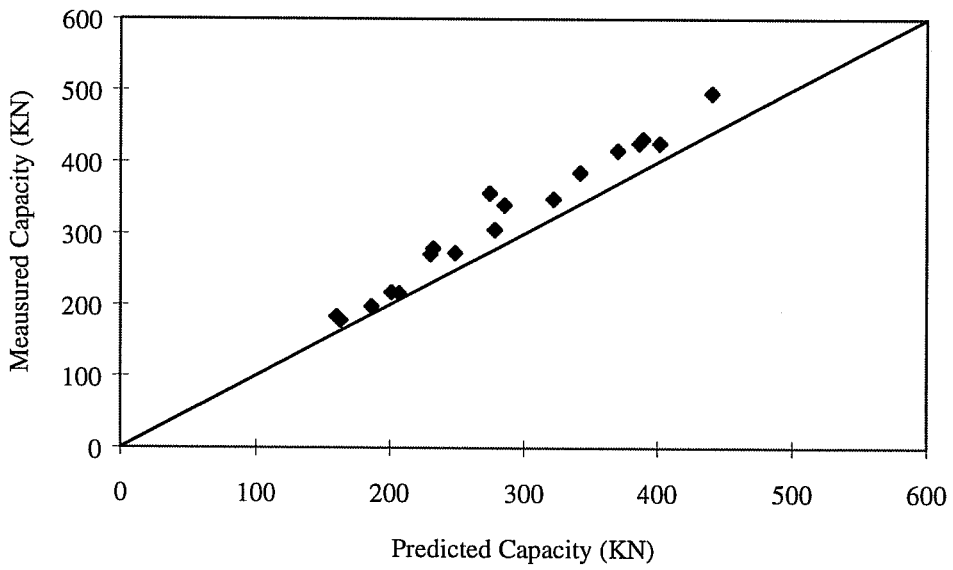
6.5 Physical Model

Both studies conducted by Furche and Eligehausen [4] and by DeVries [2] proposed similar physical models for the side blow-out capacity. The model used in the former study consisted of a 45-degree circular cone resisting lateral bursting. DeVries used a square cone (pyramid) to describe the lateral resistance.

Both models could not be applied directly to predict the anchorage capacity of headed bars in exterior joints, because joint cracking affected the behavior and caused a triangular shaped spalling pattern (Figure 5.3). In this section, the physical model presented in the study by Furche and Eligehausen for

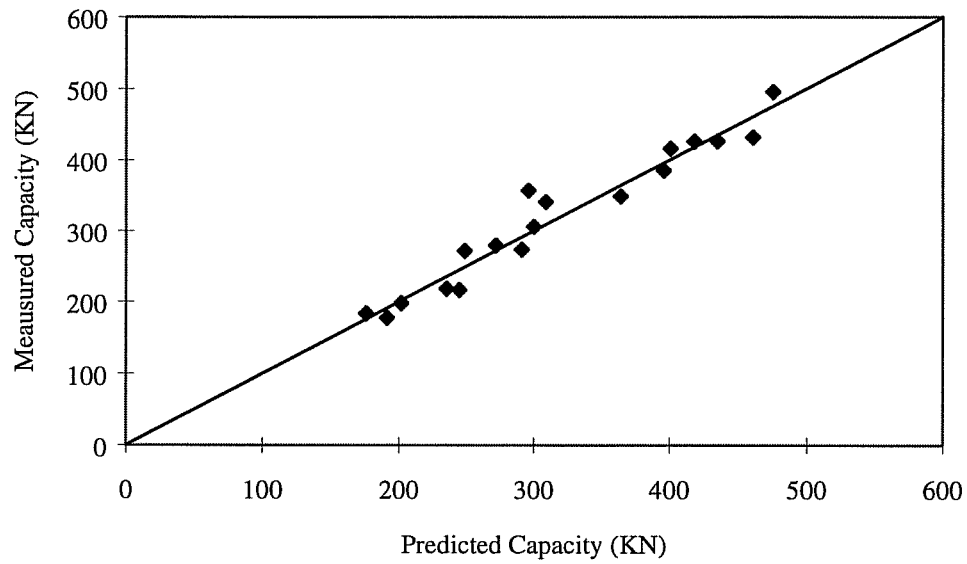


a) Equation 6.7

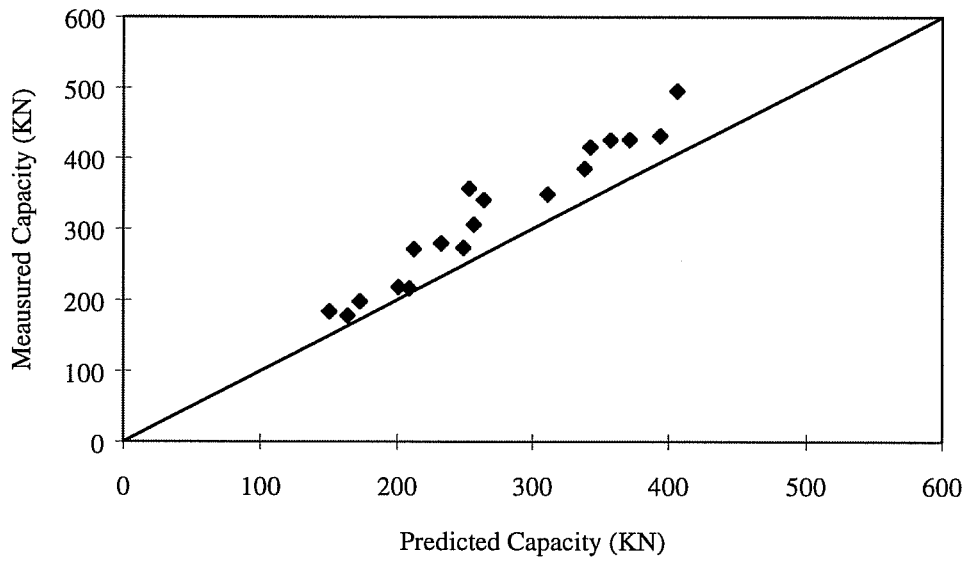


b) Equation 6.9

Figure 6.5 Comparison of Measured and Predicted Capacities using Total Head Area



a) Equation 6.8



b) Equation 6.10

Figure 6.6 Comparison of Measured and Predicted Capacities Using Net Bearing Area

anchor bolts and modified by DeVries for headed bars will be adjusted for exterior joints.

The lateral blow-out resistance is based on a uniform tensile strength acting over the projected area of the spalled concrete. The average tensile strength used by DeVries was $0.5\sqrt{f'_c}$ ($6\sqrt{f'_c}$ in customary units). The spalling pattern (Figure 6.7) consisted of a triangle with a base at the face of the column, and a side along the diagonal shear crack connecting the head of the bar to the top of the compressive zone. Although the other side did not lie over a shear crack, its angle with the horizontal ranged between 60 and 70-degrees (except for specimens T16 and T26 in which the whole side spalled), indicating that it was affected by the shear stresses above the joint. It should be noted that the height of this triangle was reduced by the cone pulled out at failure. The average area of this triangle is given by

$$A_{bo} = l_{\text{deff}} \left[(d_b - d'_b) + l_{\text{deff}} \tan 65^\circ \right] \quad 6.11$$

Where l_{deff} is the effective development length taken as $l_d - d'$, d_b is the depth of the beam, and d'_b is the distance from the extreme compression fibers to the centroid of the compression reinforcement for the beam. Although the joint crack ended at the top of the compression zone in the simulated joints tested in this study, such cracks are expected to connect the center of the heads to the centroid of the

compression zone of the beam (usually very close to the centroid of the compressive force) in a real joint.

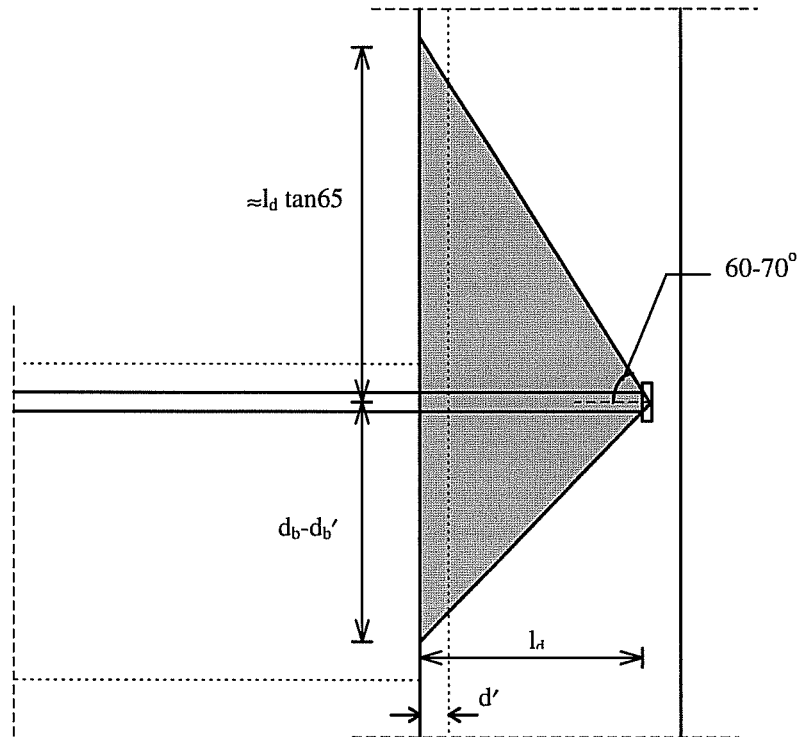


Figure 6.7 Geometry of Blow-Out Failure

The anchorage capacity of a headed bar is a function of the total lateral force resisting side blow-out, Z_U , equal to $0.5\sqrt{f'_c} \cdot A_{bo}$. The relationship is given by

$$P_U = \frac{Z_U}{\alpha} \quad 6.12$$

Based on 57 pullout tests conducted by DeVries, the following function for α will be used

$$\alpha = 0.517 \sqrt{\frac{f_b}{f'_c}}$$

or

$$\alpha = 0.517 \sqrt{\frac{P_u}{A_n f'_c}} \quad 6.13$$

Where f_b is the average bearing stress under the head at ultimate load (based on the net bearing area) in N/mm². Substituting Equation 6.13 in Equation 6.12 results in the following equation

$$P_u = \left(\frac{0.5A_{bo}}{0.517} \right)^{2/3} (A_{net})^{2/3} (f'_c)^{1/3} \quad 6.14$$

The ultimate capacity based on this equation does not consider the effect of side cover or confining reinforcement. The spalled concrete area did not vary with the concrete cover. The lower capacity of specimens with smaller cover is attributed to the early formation of the concrete wedge (see Figure 5.27). In order to account for side cover and confining reinforcement effects the factors α and β from Equation 6.7 were used in Equation 6.14. The predicted capacities are compared to the measured capacities in Table 6.6.

Table 6.6 Comparison of Measured and predicted Capacities using Physical Model

Test	Head Area (mm ²)	Cover (mm)	Column (mm)	Measured P _{max} (KN)	Equation 6.14	
					P _{max} (KN)	meas/ comp
T9	3025	76	381×305	340	281	1.21
T10	2970	38	381×305	271	225	1.20
T12	3200	38	305×305	178	170	1.05
T13	3200	38	381×305	273	269	1.02
T14	3025	76	381×305	416	369	1.13
T16	3025	76	457×305	426	417	1.02
T20	4225	76	381×305	349	332	1.05
T21	3200	76	305×305	218	210	1.04
T22	1624	76	305×305	183	157	1.17
T23	2970	76	381×305	306	271	1.13
T24	2970	76	381×305	357	266	1.34
T25	3025	76	381×305	426	376	1.13
T26	2970	76	533×305	495	452	1.10
T27	3025	76	305×305	198	177	1.12
T28	8100	76	381×305	432	417	1.04
T29	5500	76	381×305	385	358	1.08
T30	3200	76	381×305	279	229	1.22
T32	3800	76	305×305	216	216	1.00
					Average	1.11
					σ	0.09

Although Equation 6.14 resulted in quite accurate predictions (after the inclusion of the factors α and β), even for specimens with relatively large development length (T16 and T26), it should be noted that the modeling for these specimens is not accurate. In these specimens, the increase in anchorage capacity

was a result of bond along the development length rather than an increase in the blow-out capacity, which was not affected by increasing the effective embedment depth (l_d-d') beyond 241 mm (9.5 in.) in the case of specimens with 76 mm (3 in.) cover, or beyond 165 mm (6.5 in.) in the case of specimens with 38 mm cover (T12 and T13, Figure 5.34). This observation is in agreement with conclusions by Furche and DeVries. Both noticed that the blown out area extends approximately 3 times the concrete cover on each side of the head. In the case of exterior joints, the effective embedment length does not influence the capacity if increased beyond three times the cover. However, the effect of concrete bond starts to increase after that point and can be superimposed on the head capacity. In order to model this behavior the value of l_{deff} used in equation 6.11 should be limited to 3 times the concrete cover. As bond along the length of the bar in specimens with effective embedment length equal to or less than $3C$ did not contribute to the capacity, development length in excess of this length only will be used to calculate the increase in bond. The following equation developed by Orangun [16] (in customary units) for the average bond stress along the length of a bar

$$\mu = \left[1.2 + \frac{3C}{d_b} + \frac{50d_b}{l_d} + \frac{A_{tr} f_{yt}}{500s d_b} \right] \sqrt{f'_c} \quad 6.15$$

Where d_b is the bar diameter, l_d is the development length, A_{tr} , f_{yt} , and s are the area, yield strength, and spacing of transverse reinforcement. This equation was modified to predict the anchorage along the development length as follows

$$P_{dev} = [\pi d_b (l_{deff} - d' - 3C)] \left[1.2 + \frac{3C}{d_b} + \frac{50d_b}{(l_{deff} - d' - 3C)} + \frac{A_{tr} f_{yt}}{500s d_b} \right] \sqrt{f'_c} \quad 6.16$$

The predicted capacities are compared to the measured capacities in Table 6.7. Although the new model fits the data well, the standard deviation is higher than that computed in Table 6.6. There might be several reasons for this. The Orangun equation is based on bond along the length of straight bars, without restraint at the end. The blown out area in specimens T16 and T26 were significantly larger than those in the rest of the specimens and they were not triangular shaped. In previous studies of hooked bars, it was concluded that separating the contributions of the hook and the development along the rest of the bar resulted in less accurate models.

6.6 Comparison with Hooked Bar Tests

A comparison between the normalized anchorage capacities of similar headed bar and hooked bar specimens is presented in Table 6.8. The anchorage capacities of 22 mm (#7) and 29 mm (#9) hooked bars were normalized by

Table 6.7 Comparison of Measured and predicted Capacities using the modified Physical Model

Test	Head Area (mm ²)	Cover (mm)	Column (mm)	Measured P _{max} (KN)	Modified Physical Model	
					P _{max} (KN)	meas/ comp
T9	3025	76	381×305	340	281	1.21
T10	2970	38	381×305	271	233	1.16
T12	3200	38	305×305	178	170	1.05
T13	3200	38	381×305	273	207	1.32
T14	3025	76	381×305	416	369	1.13
T16	3025	76	457×305	426	380	1.12
T20	4225	76	381×305	349	332	1.05
T21	3200	76	305×305	218	210	1.04
T22	1624	76	305×305	183	157	1.17
T23	2970	76	381×305	306	271	1.13
T24	2970	76	381×305	357	266	1.34
T25	3025	76	381×305	426	376	1.13
T26	2970	76	533×305	495	359	1.38
T27	3025	76	305×305	198	177	1.12
T28	8100	76	381×305	432	417	1.04
T29	5500	76	381×305	385	358	1.08
T30	3200	76	381×305	279	229	1.22
T32	3800	76	305×305	216	216	1.00
					Average	1.15
					σ	0.11

multiplying by the ratio between the bar diameter and 25 mm (in addition to normalization for differences in concrete strength as described earlier). Bar diameter was used for normalization (instead of bar area) because capacity of standard hooks is governed by compressive stresses on the inside of the hook,

Table 6.8 Comparison between Headed and Hooked bar Specimens

Test	$\frac{\text{Head Area}}{\text{Bar Area}}$	Column Size (mm)	Cover (mm)	P_{\max} Normalized (KN)
T9	3	381×305	76	340
T20	4.2	381×305	76	311
T23	3	381×305	76	369
T24	3	381×305	76	345
T28	8.1	381×305	76	439
T29	5.5	381×305	76	392
J11-90-15-1-H	-	381×305	76	338
J11-180-15-1-H	-	381×305	76	369
J11-90-15-1-L	-	381×305	76	332
11-90-U*	-	381×305	76	323
11-90-U	-	381×305	76	298
11-.15	-	381×305	76	320
T21	6.4	305×305	76	216
T22	3.2	305×305	76	182
T32	7.6	305×305	76	220
J7-90-12-1-H	-	305×305	76	206
J7-180-12-1-H	-	305×305	76	202
7-90-U	-	305×305	76	179
9-.12	-	305×305	76	191
-	-	-	-	-
T27	3	305×305	76	207
J11-90-12-1-H	-	305×305	76	306
-	-	-	-	-
T16	3	457×305	76	397
11-.18	-	457×305	76	387
-	-	-	-	-
T26	3	533×305	76	519
11-.21	-	533×305	76	480

Table 6.8 Comparison between Headed and Hooked bar Specimens
(Continued)

Test	$\frac{\text{Head Area}}{\text{Bar Area}}$	Column Size (mm)	Cover (mm)	P_{\max} Normalized (KN)
T14	3	381×305	76	400
11-90-U-T4	-	381×305	76	403
J-11-90-15-3-L	-	381×305	76	438
11-90-U-T6	-	381×305	76	371
T25	3	381×305	76	440
J11-90-15-3a-L	-	381×305	76	480
T12	6.4	305×305	38	176
7-90-U-SC	-	305×305	44	161
T13	6.4	381×305	38	259
T13-J7-90-15-4-H	-	381×305	38	236

which are directly affected by bar diameter. The design equation for hooked bar anchorage in the ACI 318 Building Code [1] is a direct function of bar diameter.

In general, headed bars had higher anchorage capacities than the average capacities of hooked bars. It should be noted that the heads used in most tests in this study were relatively small, in order to avoid bar yielding before failure. A practical head area would be 8 to 10 times the bar area. Specimen T28 (35 mm bars, with head area 8 times the bar area) had an anchorage capacity 33% higher than the average anchorage capacity of hooked bar tests (Figure 6.8).

Furthermore, the capacity of this specimen was 19% higher than the maximum capacity measured in all hooked bar tests (specimen J11-180-15-1-H). The largest head used with 25 mm bars was 7.6 times the bar area (T32). The anchorage capacity of this specimen was 13% higher than the average hooked bar capacity (Figure 6.9), and 7% higher than the specimen with the maximum capacity (J7-90-12-1-H). The superior behavior of headed bars was also noted in specimens with small cover (38 mm). The capacities of T12 and T13 were about 10% higher than those of 7-90-U-SC (44.5 mm cover) and J7-90-15-H, respectively.

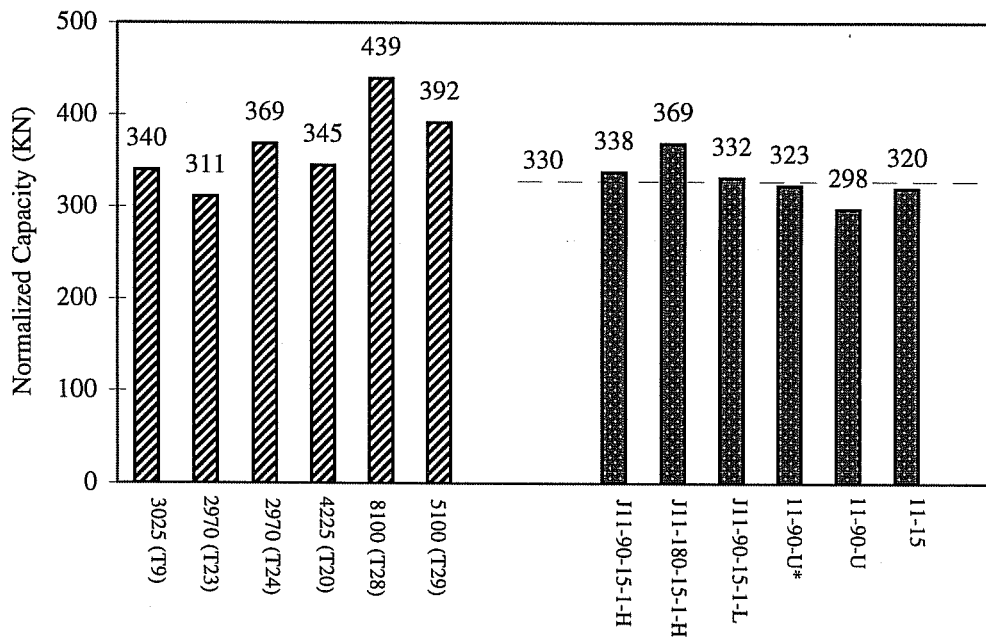


Figure 6.8 Comparison of Capacities of 35 mm Headed Bars with various Head Areas and Hooked Bar Specimens

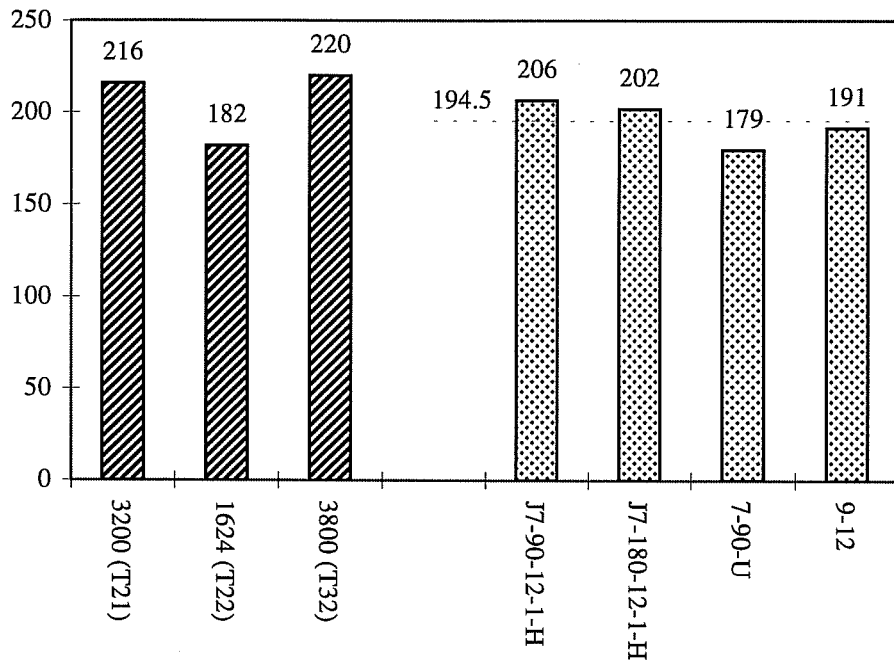


Figure 6.9 Comparison of Capacities of 25 mm Headed Bars with various Head Areas and Hooked Bar Specimens

The load-slip behavior for several headed bar specimens is compared to companion hooked bar specimens in Figures 6.10 to 6.13. In general, headed bars had less slip throughout their load histories. Lower slip leads to finer cracks (at the column face), and allows the beam to develop the moment capacity with lower deformations.

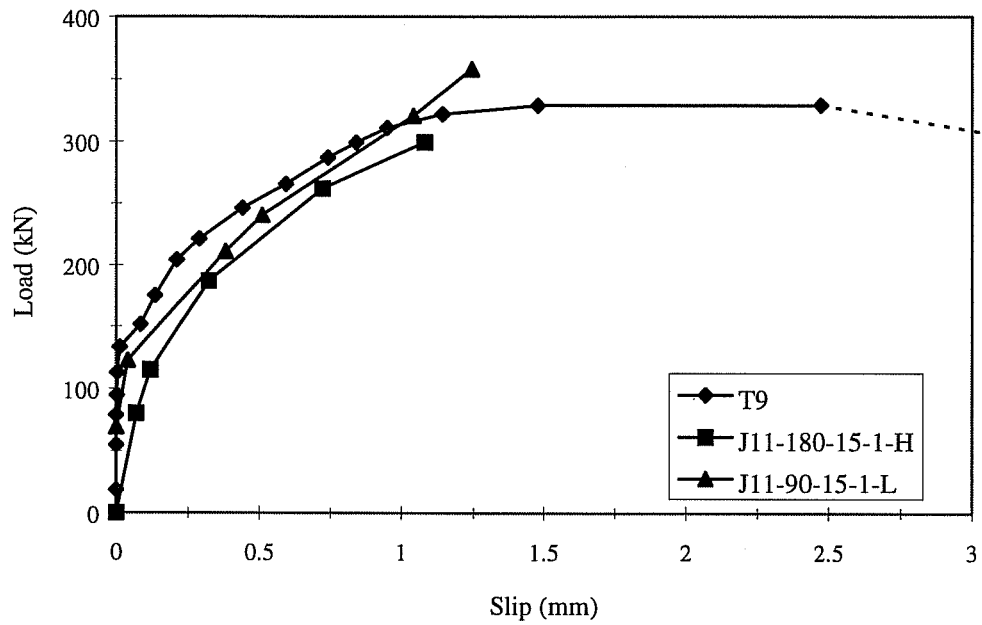


Figure 6.10 Comparison of Load-Slip behavior for Specimen T9 to similar Hooked bar Specimens

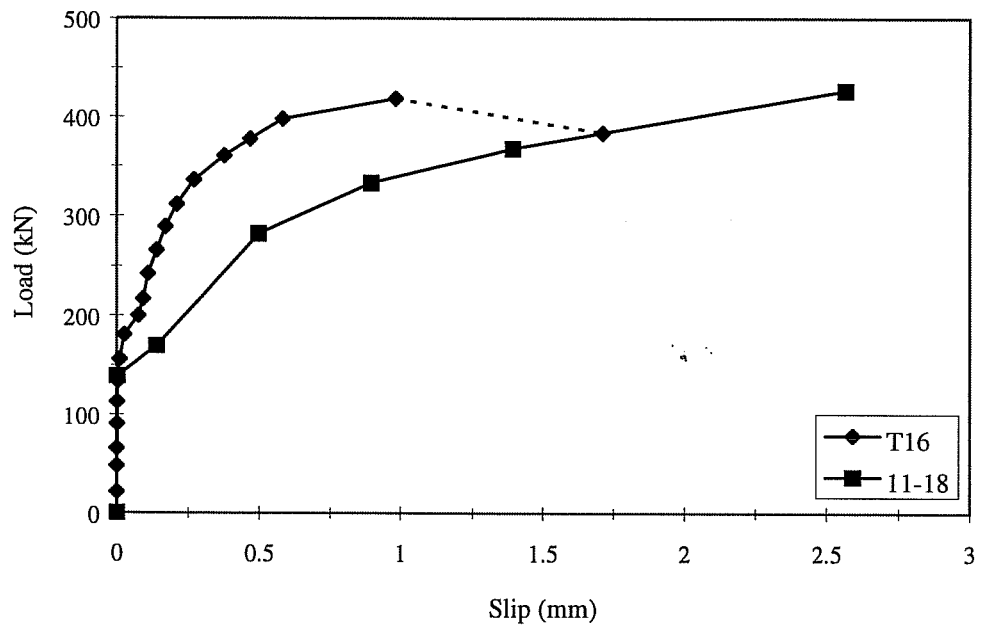


Figure 6.11 Comparison of Load-Slip behavior for Specimen T16 to Specimen 11-18

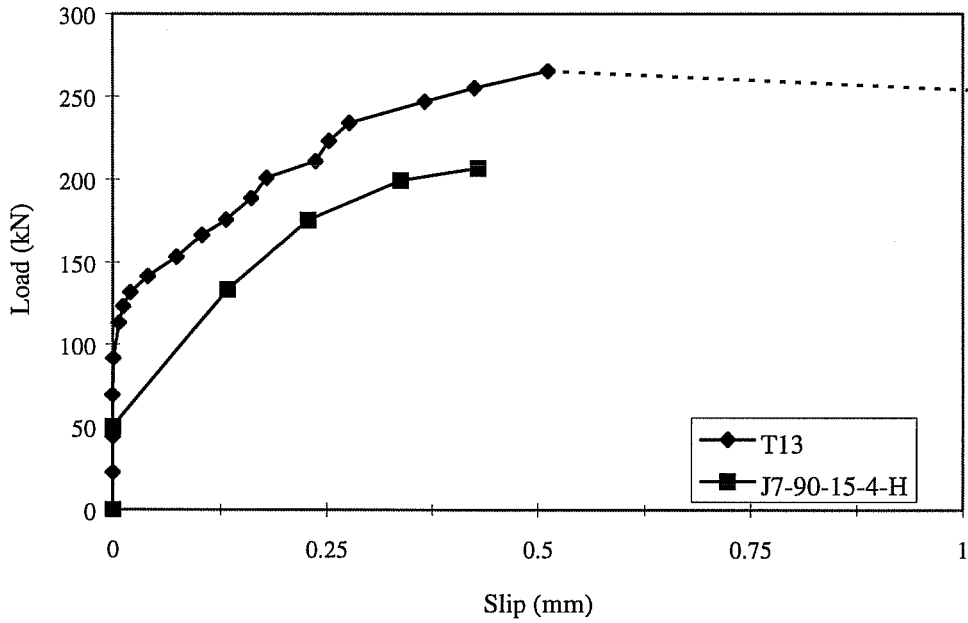


Figure 6.12 Comparison of Load-Slip behavior for Specimen T13 to Specimen J11-90-15-3-H

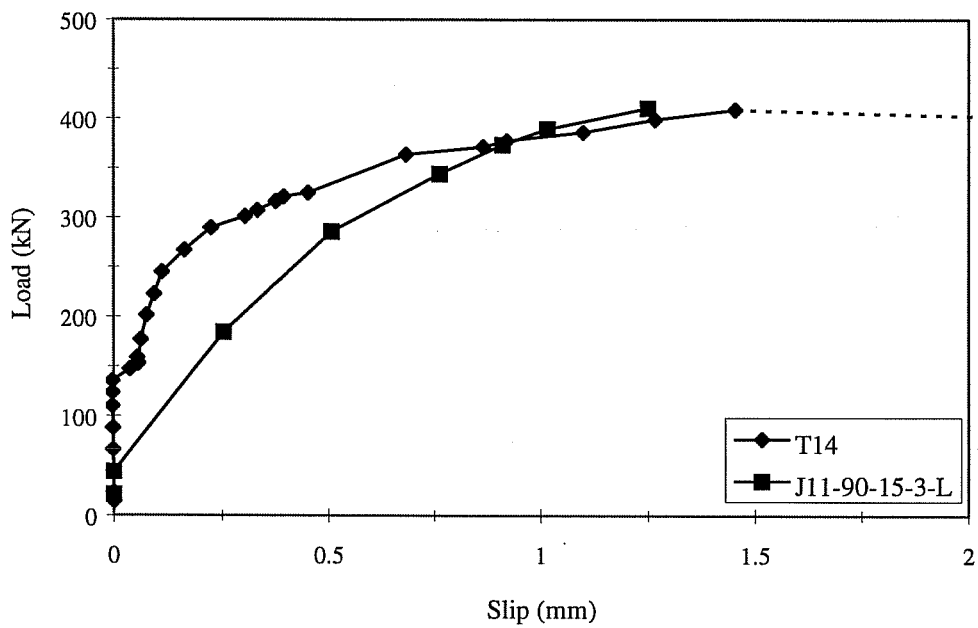


Figure 6.13 Comparison of Load-Slip behavior for Specimen T14 to Specimen J11-90-15-3-L

6.7 Design Implications

The two empirical equations developed for the anchorage capacity of headed bars (Equations 6.9 and 6.10) estimated the measured capacities accurately. Equation 6.9 is a function of the total head area and provides slightly better estimates of the capacity than Equation 6.10. However Equation 6.10 is a function of the net bearing area as recommended in previous studies on anchor bolts and headed reinforcement. A model using the net bearing area will yield zero capacity for a bar without a head. The anchorage capacity will be higher than zero because there is bond along embedment length. When the analytical model predicts a capacity of zero for bars without heads, designers will recognize the need for a different model for the capacity of bars with small or no heads. In that case, anchorages will be provided by bond along the embedment length. For these reasons, Equation 6.10 will be recommended for design of headed bars.

Equation 6.10 does not consider the beneficial effect of anchoring the head behind a crossing bar. This effect could be included by multiplying the estimated capacity by an anchorage condition factor, γ , taken as 1.25 for heads positively anchored behind 25 mm or larger crossing bars. This factor is based on test results presented in Chapter 3. Another modification to produce a simple design equation is using specified values for the reduction factor β (cover size factor). As only two covers were used in the experimental program, the value of

β will be taken as 0.8 for covers less than 76 mm (3 in.) and 1 for all other cases. Above that, the model should not be used to predict capacities of headed bars with clear cover less than 38 mm (1.5 in.).

Designers are more often concerned with the length required to develop the yield stress of the bar rather than the force that the bar can develop. From this point of view, the embedment length can be determined directly by rearranging Equation 6.10 in the following form:

$$l_d = \frac{A_b f_y}{14.7\alpha\beta\gamma\sqrt{A_n}\sqrt{f'_c}} + d' \quad 6.17$$

where

l_d = required embedment length, in mm

A_b = area of the anchored bar, in mm²

f_y = yield stress of the anchored bar, in MPa

d' = distance from the face of the column to the centroid of the column longitudinal reinforcement closest to face, in mm

A_n = net bearing area, in mm²

α = Confining reinforcement factor, taken as 1 for tie spacing more than 100 mm, 1.25 for spacing equal to 100 mm to 51 mm, and 1.4 for tie spacing equal to 50 mm or less

- β = cover size factor, taken as 0.8 for side cover less than 76 mm, and 1 for all other cases
- γ = anchorage condition factor, taken as 1.25 for heads positively anchored behind 25 mm or larger crossing bars, and 1 for all other anchorage conditions.

Equation 6.17 is based on single layered bars in exterior joints. According to DeVries [2] close spacing of bars or corner placement reduced the capacity significantly. In structural elements with multiple layers of bars more than one bar is close to the free concrete side, and a capacity reduction similar to that observed in close spaced bars is expected. Bars anchored in knee joints are expected to experience similar effects to that observed in corner bars. In order to include these effects the reduction factors described in Section 2.7 could be adapted. In this case the interacting blown out areas should be based on triangular shapes (Figure 6.7) rather than square shapes (Figure 2.8). It should be noted that the ACI 318 Building Code provisions for standard hooks are also based on single layered bars in exterior joints and no reduction factors are included. A similar reduction in capacity is expected in multiple layers of hooked bars.

6.7.1 Comparison of Required Embedment for Hooked and Headed Bars

The minimum embedment length for hooked bars required by the ACI 318 Building Code (based on the study by Pinc [11]), is given by (in customary units)

$$l_d = \frac{1200d_b}{\sqrt{f'_c}} \frac{f_y}{60,000} \quad 6.18$$

and l_d could be multiplied by 0.7 for side covers not less than 63.5 mm (2.5 in.) and cover on bar extension beyond the hook 51 mm (2 in.). The reduction factor for confining reinforcement is 0.8, and is applied for stirrup spacing not greater than 3 bar diameters.

For comparison purpose, an exterior joint with 76 mm side cover above the anchored bars, no confining reinforcement, and 25 MPa concrete is assumed. Headed bars are not positively anchored behind longitudinal bars and the cover on the bar extension beyond the hook is 51 mm (2 in.). The anchored bars are required to develop yield stress, taken as 500 MPa (72.5 ksi). The values of α , β , and γ (reduction factors for headed bars) are equal to 1 under these conditions. On the other hand, the required development length for hooked bars is multiplied by a reduction factor equal to 0.7. It should be noted that the values of the steel yield stress and the concrete strength should not affect the comparison as both

types of anchorage are functions of the yield stress of the anchored bars, and the square root of the concrete compressive strength.

In Table 6.9 a comparison between the required embedment length for hooked bars and headed bars with head area equal to 8 and 10 times the bar area, for several bar diameters is presented. The embedment length required for headed bars is about 31 and 36% less than that required for hooked bars. This difference could be even higher if less side cover (e.g. 38 mm or 1.5 in.) or confining reinforcement were used.

Table 6.9 Comparison between Required Embedment for Hooked and Headed Bars

Bar Diameter (mm)	L_{dHook} (mm)	Head Area = 8 Bar Area		Head Area = 10 Bar Area	
		L_d (mm)	L_d/L_{dHook}	L_d (mm)	L_d/L_{dHook}
19	320	217	0.68	205	0.64
22	371	250	0.67	235	0.63
25	421	285	0.68	267	0.63
29	489	333	0.68	311	0.64
32	539	371	0.69	346	0.64
35	590	410	0.69	382	0.65

6.8 Failure Hypothesis for Specimens with Shear Failure

As discussed earlier, most of the bar force is transferred directly from the anchored bars to the concrete through the anchor head at failure. This makes the effect of the anchorage load similar to a horizontally applied load near a support, where the compressive zone resembles this support (Figure 6.14). Considered in this manner, the problem becomes similar to a continuous deep beam.

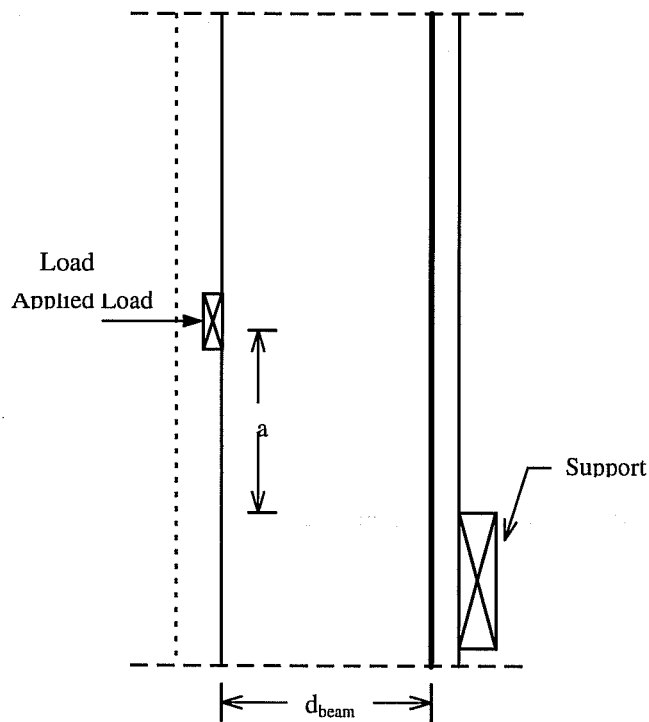


Figure 6.14 Effect of Shear Span on the Shear Strength

In deep beams, arch action can provide an additional method for transmitting the loads to the supports. The effectiveness of the arch action is

dependent on reinforcement details. A marked increase in shear capacity occurs in beams with a/d_b less than about 2.5. Although “a” is usually measured from the face of the support to the edge of the applied load, it is defined in Figure 6.14 as the distance to the center of the head, because the failure plane passed through this point.

The ACI 318 Building Code provisions for deep beams apply to beams with a/d less than 5. The shear strength is limited to $0.66\sqrt{f'_c}$ ($8\sqrt{f'_c}$ in customary units) for a/d less than 2. The shear strength (in customary units) provided by concrete is given by

$$V_c = \left(3.5 - 2.5 \frac{M_u}{V_u d} \right) \left(1.9\sqrt{f'_c} + 2500\rho_w \frac{V_u d}{M_u} \right) bd \quad 6.19$$

except that the term $\left(3.5 - 2.5 \frac{M_u}{V_u d} \right)$ shall not exceed 2.5. As the value of a/d_b for the 381×305 mm (15×12 in.) columns is 1.33 and for 381×305 mm (15×12 in.) columns is 2, the shear capacity predicted is the same as in slender beams ($0.17\sqrt{f'_c}$ or $2\sqrt{f'_c}$ in customary units). Equation 6.19 is known to be very conservative for most practical a/d ratios. Above that, it is based on experimental data from simple beam tests.

Rogowsky and MacGregor [17] conducted an extensive experimental study on the behavior of continuous deep beams. Rogowsky reported that there

was no distinguishable difference in strength between specimens with various types of longitudinal reinforcement. Stirrups up to ρ_v equal to 0.0019 did not affect the behavior either. However, when heavy shear reinforcement was used, with ρ_v equal to 0.006, the strength was significantly improved. In this case, the strength was independent of the a/d_b ratio. Figure 6.15 shows a comparison between the results of Rogowsky's tests (the ones with heavy shear reinforcement were excluded) and specimens T1 through T5. The shear stress for the five specimens was calculated on the basis of a depth equal to the dimension " d_{beam} " (Figure 6.14), to allow comparison with Rogowsky's tests. Although the joint shear capacity is higher than that of continuous deep beams, the data followed the same patterns. The effective column depth resisting shear might be greater than d_{beam} and caused the increase in capacity.

As it was required to avoid shear failures in the test specimens, a design procedure was developed to estimate the shear capacity. The shear capacity of the four 381×305 mm (15×12) specimens (Table 5.4) without shear reinforcement was between 0.49 and $0.63\sqrt{f'_c}$ (5.9 and $7.6\sqrt{f'_c}$ in customary units). On the other hand, the shear capacity of specimen T4, in which the column dimensions were 305×305 mm (12×12 in.) was $0.34\sqrt{f'_c}$ ($4.1\sqrt{f'_c}$ in customary units), indicating significant drop in capacity resulting from depth reduction.

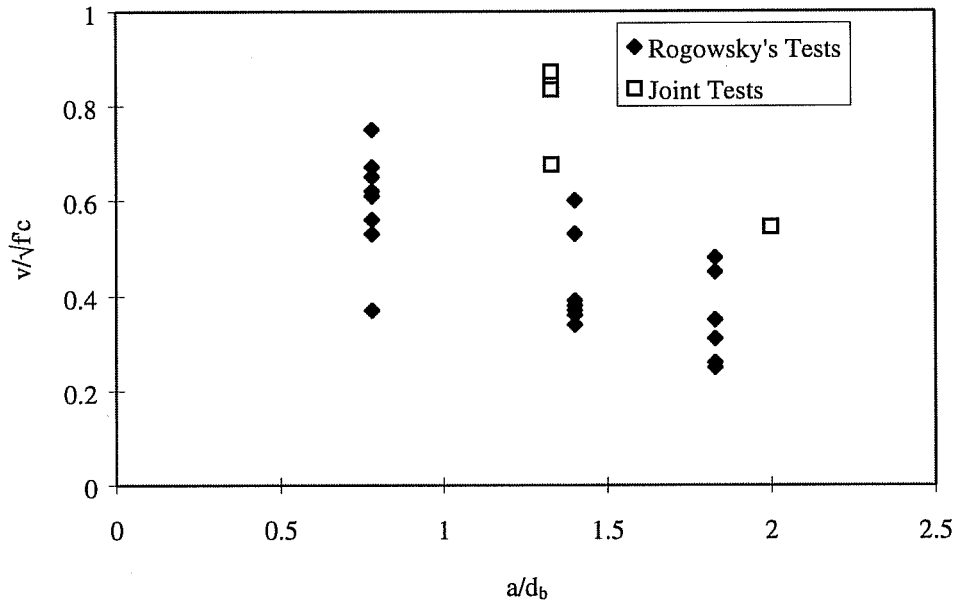


Figure 6.15 Comparison between the Joint Shear Capacity and Continuous Deep Beam Tests

The joint shear resisted by stirrups is plotted against the joint shear for specimen T6 in Figure 6.16. The concrete shear resistance kept increasing after the joint was cracked diagonally (the point where the stirrup forces started increasing), and reached a maximum of $0.56\sqrt{f'_c}$ ($6.73\sqrt{f'_c}$ in customary units) just before failure. The specimen failed as soon as the stirrups yielded, indicating that the concrete shear resistance was dependent on the reinforcement limiting relative movement along the plane of failure. This behavior indicated that the contribution of concrete and reinforcement to the shear resistance could be superimposed.

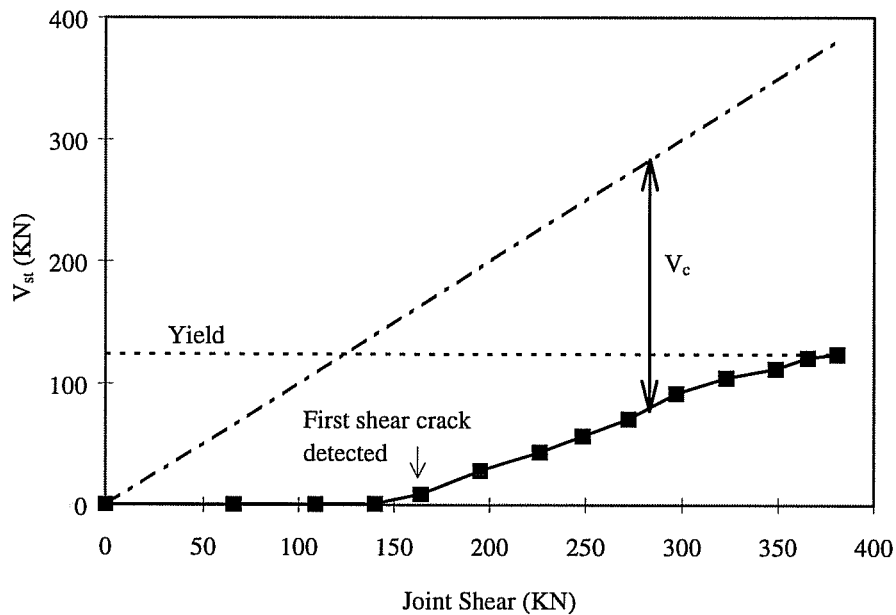


Figure 6.16 Joint Shear resisted by Stirrups - Specimen T6

Based on the above observations, the following equation was developed to provide an estimate for the shear capacity of specimens in which the head was anchored in front of the column longitudinal bars,

$$V = 0.5\sqrt{f'_c}(bd)\frac{d}{a} + A_{st}f_y \quad 6.20$$

Where V is the shear capacity in N, f'_c is the concrete compressive strength in MPa, b and d are the column width and depth in mm, a is the vertical distance from the center of the bar to the top of the compression zone in mm, A_{st} is the cross section area of ties crossing the failure plane in mm^2 , and f_y is the yield stress of the ties in MPa. The actual shear capacities are compared to estimated

capacities (using the above equation) in Table 6.10. The average ratio between the observed and estimated capacities is 1.01, with a standard deviation of 0.13. Specimens with 305×305 mm (12×12 in.) columns (T4, T8, and T17) had capacities lower than that estimated, indicating a more significant influence of the shear span. The effect of this term could not be further studied because the results from two column sizes only were available (for the specimen failing in shear). As the shear behavior of the tested specimens might vary from that of actual beam-column joints, it was decided not to do additional tests to study the effect of the shear span on the shear capacity.

Table 6.10 Comparison of Measured and Predicted Shear Capacities

Specimen	Column Size (mm)	f'_c (MPa)	Effective Reinforcement (mm^2)	Joint shear (KN)	Equation 6.20	$\frac{\text{Measured}}{\text{Computed}}$
T1	381×305	26.7	-	304	259	1.17
T2	381×305	29.4	-	315	272	1.16
T3	381×305	29.4	-	330	272	1.21
T4	305×305	26.7	-	131	150	0.87
T5	381×305	22.5	-	224	238	0.94
T6	381×305	22.5	284	394	363	1.09
T7	381×305	23.2	426	424	429	0.99
T8	305×305	29.6	284	255	282	0.90
T11	381×305	35.0	800	563	636	0.89
T17	305×305	36.1	284	239	270	0.82
					Average	1.00
					σ	0.14

The capacity described above does not apply to the specimens in which headed bars were anchored behind the column longitudinal bars (T15, T18, and T19). These specimens had significantly higher shear capacities, and a different failure pattern (see Section 5.3.1). The increase in shear capacity can be attributed to two mechanisms. First, the column longitudinal bar acts as a relatively stiff bearing surface, preventing failure by sliding along the diagonal crack plane until the loads are large enough to bend it, crushing the concrete in the anchorage area (Figure 5.39). Second, the longitudinal column bars (placed in front of the anchorage head) enhance the arch and tie mechanism by passing through the node.

A comparison between test results from the study by Burguières and the three specimens under consideration is shown in Table 6.11 (γ calculated using Eq. 5.2). The results from Burguières tests had slightly lower shear capacity (except for CJ-6-2.5-U which had 10 mm ties spaced at 64 mm through the joint). It should be noted that both anchorage devices in his tests were bearing on the center column bar rather than the back bar (Figures 4.7 and 4.8), which might have caused a drop in the effective depth resisting shear. The effect of this reduction in depth was not included in Table 6.11.

Table 6.11 Comparison between Specimens with Heads anchored behind Crossing Bars and Burguières Tests

Specimen	γ
T15	1.07
T18	0.96
T19	0.78
CJ-1-0-B	0.76
CJ-4-0-U	0.58
CJ-6-2.5-U	1.04

6.9 Summary

The anchorage capacity of headed bars in exterior joints is lower by 14 to 44% than that of bars embedded near the edges of concrete cubes. Design equations based on pullout tests did not predict the capacity of joint tests accurately. Two analytical models were developed to predict the capacity of headed bars in exterior joints, one based on total head area, and the other on net bearing area. The required embedment length for headed bars as predicted using these models is less than that required by the ACI building code for hooked bars by more than 30%.

Chapter 7

EFFECTS OF CYCLIC LOADING

7.1 Background

In the last three decades a number of studies have provided an understanding of the mechanism of bond transfer in joints, and of the overall behavior under cyclic loading of exterior beam column joints constructed using hooked bars.

Bresler and Bertero [18] reported tests on push-out specimens subjected to low frequency repeated tensile loading producing bar stresses in the service load range. They observed that bond effectiveness was dependent on loading history. Maximum peak stress levels in reinforcement reduced stress transfer effectiveness at lower stresses in subsequent cycles. Since the damage in the boundary layer between steel and concrete increased as the peak level increased, the reduction in stress transfer became more severe. Based on these observations, Bresler and Bertero suggested that special anchorage provisions may be required when the working stress levels is increased for high strength steel bars.

Perry and Jundi [19] subjected eccentric pull-out specimens to repeated static and dynamic loading to determine the effects of repeated loading on the distribution of the bond stresses along reinforcing bars. They concluded that the peak bond stress tend to shift away from the loaded end as the number of cycles of loading and unloading increases. However, there was no evidence from the limited number of tests performed in this study that the failure of a specimen would occur by increasing the number of cycles of loading unless the applied load was at least 80 percent of the ultimate load or greater.

Ismail and Jirsa [20,21] tested 20 specimens to study the effects of monotonic, repeated, or reversed load cycles on the behavior of anchored bars supporting cantilever beams. The bars were intended to simulate the anchorage conditions at exterior beam-column joints in which the beam is subjected to large cyclic overloads well into the yield range of the reinforcement. They found that, for different loading cases, bond deterioration occurred over a significant distance between the beam-column interface and the anchored end of the reinforcing bars. They concluded that the loading history has a substantial influence on the deformation of the anchored bars and the cantilever beam. They also determined that the amount of bond deterioration and yield penetration depended on the magnitude of load more than the number of cycles.

Hassan and Hawkins [22] have reported tests on 13 specimens simulating exterior beam-column connections under various types of loading. They concluded that bond deterioration decreased the stiffness and increased the slip at failure under fully reversed loading. Bars terminating in standard 180-degree hooks had resistances dependent on the lead embedment only. Large movements of the hook occurred once the yielding penetrated to the end of the lead embedment.

Several studies addressed the overall behavior of exterior beam column joints under cyclic loading. Hanson and Connor [23] tested seven full scale exterior beam-column joints, and demonstrated the importance of properly detailed joints in achieving ductile frame behavior. Test results indicated that adequate energy dissipation can be achieved near the joint if proper attention is given to anchorage of beam bars. Hanson [24] tested five additional specimens with grade 60 steel and concluded that these bars can be used with satisfactory results in structures which are designed to develop ductile behavior.

An extensive investigation towards understanding the behavior of exterior beam-column joints was conducted in the University of Canterbury [25,26,27]. The results of 13 full scale specimens indicated that the continued effects of joint deterioration and anchorage failures caused relatively poor performance under cyclic loading. Considerably improved behavior was reported

for specimens which contained a stub beam at the opposite face of the column through which the beam bars were extended and anchored with 90-degree hooks.

Lee et al [28] tested eight exterior beam column joints and concluded that the beam longitudinal steel anchored in the joint yielded at a location just before the hook during the first cycle of severe earthquake loading, and that the increase in transverse reinforcement in the joint resulted in a drop in shear resisted by concrete.

The observations noted in these studies were confirmed by recent Japanese studies. According to Otani [29], the tension in beam reinforcement often causes cone-type failures at the beam-column interface, resulting in a reduction in the anchorage length. He suggested that beam longitudinal reinforcement should be anchored with 90-degree hooks, with the development length measured from the critical section at the column face. Kaku and Asakusa [30] found that beams can develop higher moments beyond yield when the lead development length is more than ten times the bar diameter. According to Hokkaido University tests [30], slip was observed when tension was applied to hooked bars, but when the load was reversed push-in slip did not occur. Furthermore, column axial load caused a reduction in slip.

The following conclusions could be drawn from previous studies on bond deterioration in exterior joints:

- 1) The two major modes of failure for exterior joints exposed to cyclic loading are deterioration of bond between concrete and reinforcing bars, and shear deterioration of the joint itself.
- 2) Reversed cyclic loading cause bond deterioration along the lead embedment length (before the hook). The magnitude of load has more influence on bond deterioration than the number of cycles.
- 3) Under severe earthquake loading, yield occurs at a location just before the hook which becomes responsible for transferring the bar force to the concrete. Slip of 180-degree hooks is significantly higher than 90-degree hooks under seismic loads.

7.2 Experimental Program

One exterior beam to column subassembly was constructed and tested to examine the effect of headed bars on the behavior under cyclic loading. The goal of this phase of the research program was to provide an insight to potential benefits of using headed bars in connections exposed to seismic loads. Although one specimen might not be enough for complete understanding of the effect of different variables on the overall behavior of exterior joints, it was enough to meet the objectives of this phase of the study. In order to determine the effects of using headed bars on the behavior and to compare that behavior with hooked bars, the

specimen tested was similar to one reported in the literature that was constructed with standard 90-degree hooked bars. The choice of the hooked bar specimen was based on three criteria. The specimen should be a full scale model of an exterior joint to eliminate scale effects. The shear capacity of the joint should be relatively high, in order to minimize effects of shear deterioration on the behavior of the specimen. The overall behavior of the specimen should be unsatisfactory, especially in anchorage, in order to examine potential benefits of using headed bar anchorages.

Based on these criteria, Unit 4, tested by Smith [26] in the second phase of the study conducted at the University of Canterbury was chosen as a proof test prototype, for the headed bar specimen. Unit 4 was a model of a joint in a 2-story reinforced concrete building consisting of single bay frames spanning 6 meters (20 ft.) with interstory heights of 3 meters (10 ft.). The specimen represented the first floor exterior beam-column connection with points of contraflexure occurring 1.2 meters (4 ft.) above and below the center line of the first story.

Concrete dimensions and reinforcement details for Unit 4 are shown in Figure 7.1. The measured material strength are presented in Table 7.1. The beam reinforcement consisted of two 29 mm (#9) bars in the top and the bottom giving $\rho = \rho' = 0.013$. The column reinforcement consisted of four 22 mm (#7) bars placed at the corners of the column. The ratio of the total ultimate design capacity

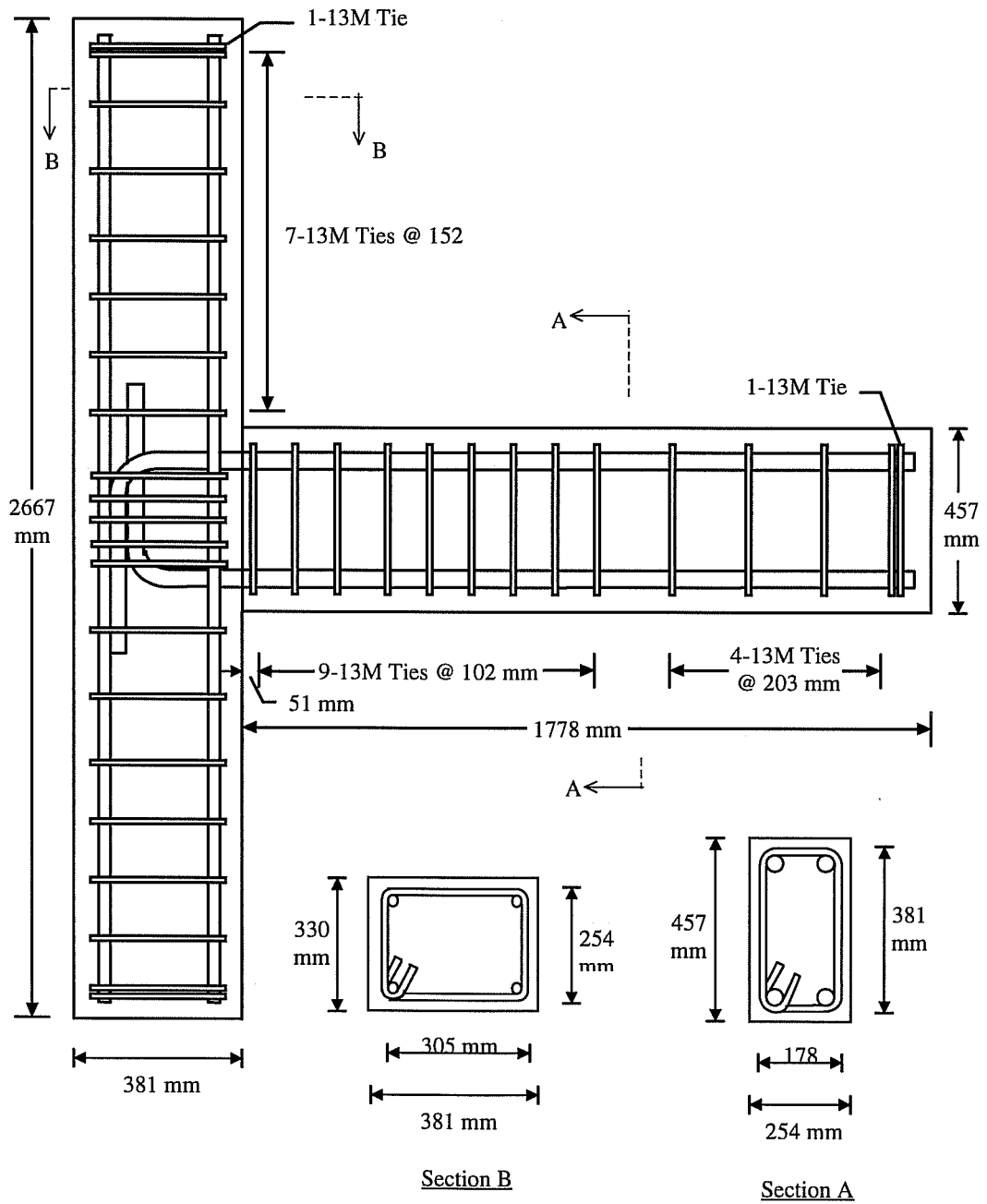


Figure 7.1 Concrete Dimensions and Reinforcement Details of Unit 4 [26]

Table 7.1 Properties of Materials used by Smith [26]

Reinforcing Bars	Yield (MPa)	Ultimate (MPa)
Beam Bars	296	479
Column Bars	274	441
Ties	311	459
Concrete Compressive Strength		20.5

of the column to that of the beam is 1.33. The lead embedment length for the hooked bars were longer than that required by the ACI 318-95 Building Code [1] Section 12.5 (252 mm or 9.9 in.). However, the embedment lengths did not meet the requirements of Section 21.5.4 (Chapter 21, Special Provisions for Seismic Design). Five 13 mm (#4) hoops were provided in the joint region to take all the joint shear.

7.2.1 Specimen Design

Concrete dimensions and reinforcement details for the headed bar specimen are shown in Figure 7.2. The specimen geometry is almost identical to Unit 4, except that standard hooks were replaced by heads. However, it was not possible to obtain Grade 40 reinforcement. Instead, Grade 60 reinforcement was used, and 25 mm (#8) beam bars were used instead of 29 mm (#9) in order to

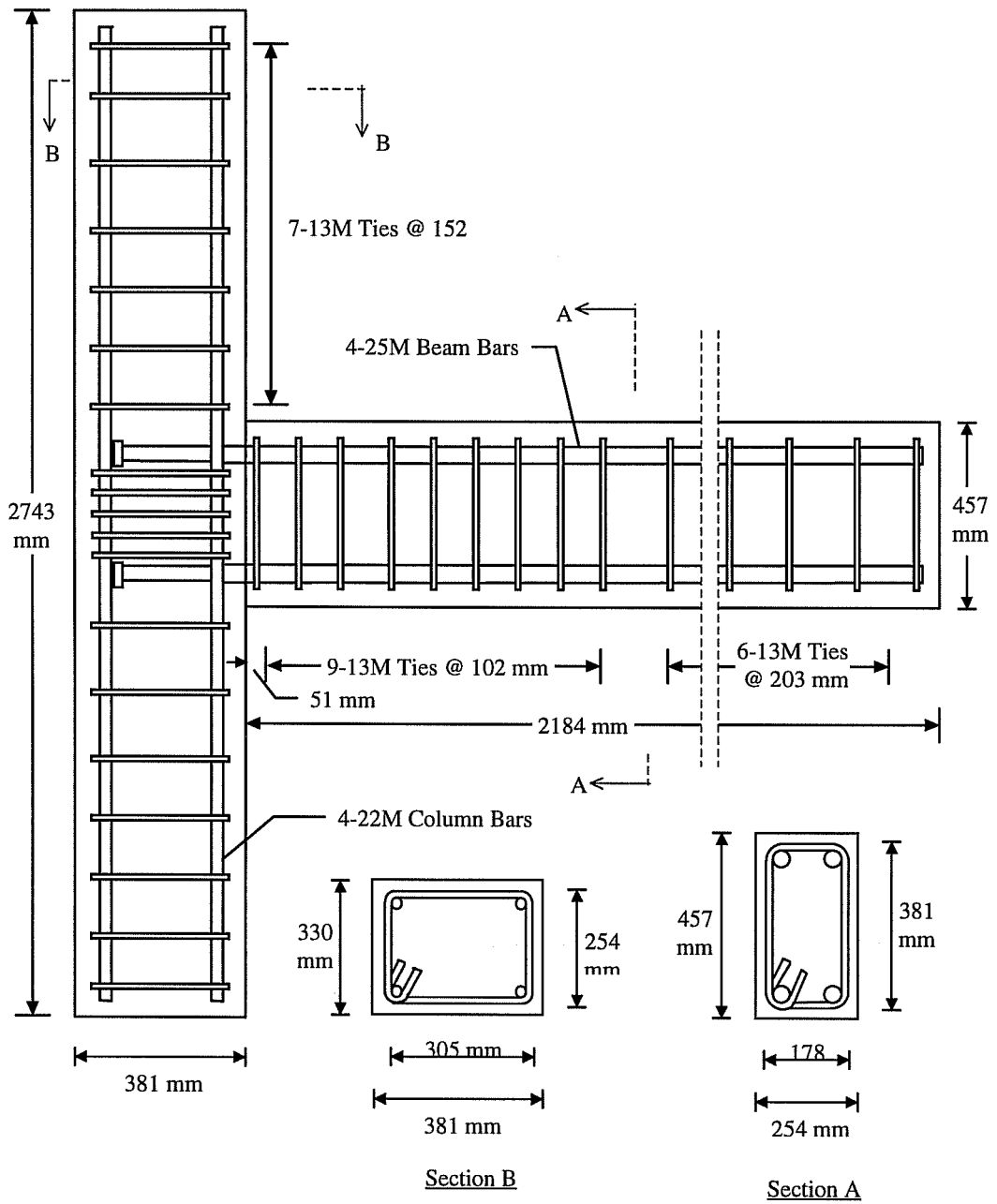
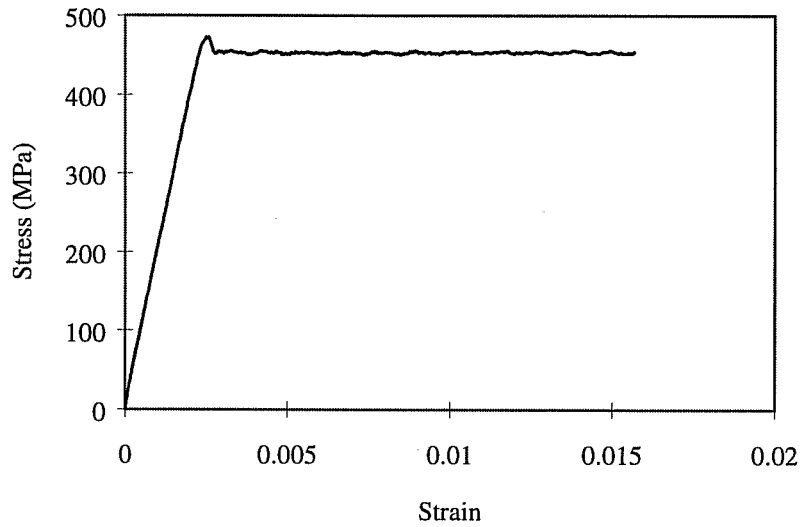
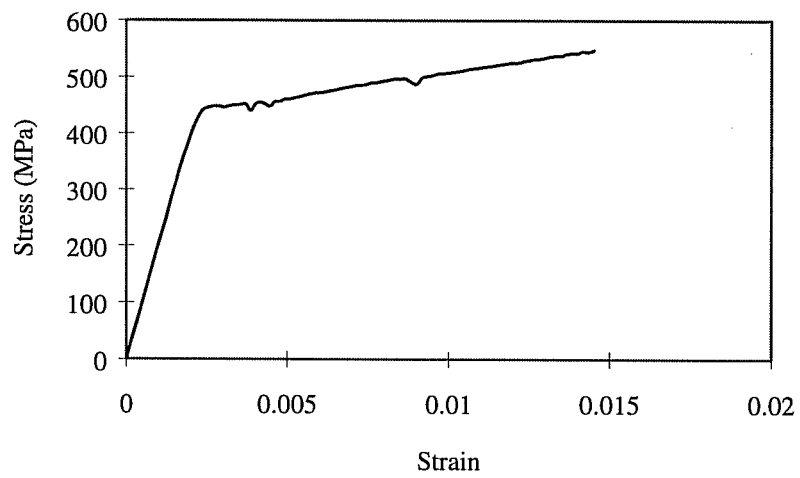


Figure 7.2 Concrete Dimensions and Reinforcement Details of the Headed Bar Specimen

keep the moment capacity and joint shear as close as possible to that of Unit 4. Square heads 10 times the bar area ($70 \times 70 \times 16$ mm) were used for beam bar anchorages. The head area was not based on previous experimental data from this study or the literature due to the lack of information on the behavior under seismic loads. The head area was chosen based on the proposed ASTM specification for T headed bars. It should be noted that the requirements of this specifications are conservative and are expected to change as more research becomes available. The measured material properties are summarized in Table 7.2 and Figures 7.3 and 7.4. The yield and ultimate moments for the beam (based on measured material properties and 0.4% maximum concrete strain) are 155 KN-m (1375 kip-in.) and 175 KN-m (1550 kip-in.) , respectively. The yield and ultimate moments for the column are 97 KN-m (860 kip-in.) and 122 KN-m (1080 kip-in.). The beam moment capacity is significantly higher than that of the hooked bar specimen (131 KN-m yield and 134 KN-m ultimate). Although the difference in material properties and moment capacity is expected to cause some difference between the behavior of the two specimens, the comparison would still give an indication of the influence of headed bars on the overall behavior.



a) Beam Headed Bars



b) Column Bars

Figure 7.3 Stress-Strain curves for Specimen Reinforcement

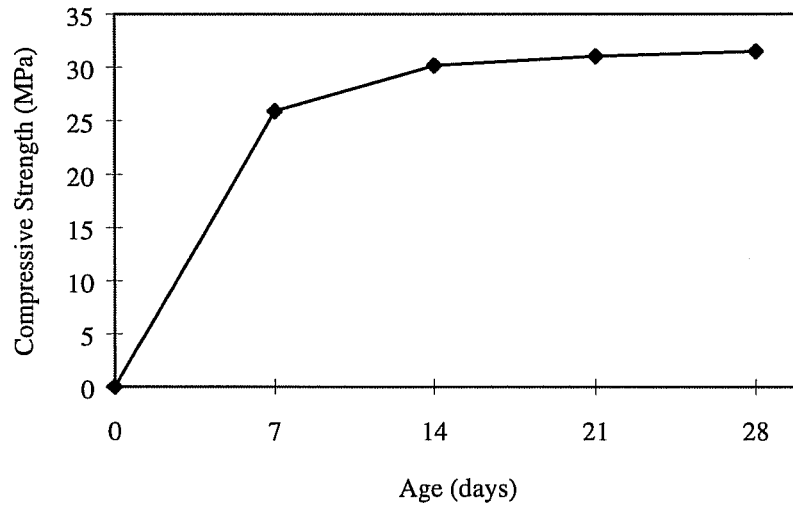


Figure 7.4 Concrete Strength Gain

Table 7.2 Properties of Materials used for the test specimen

Reinforcing Bars	Yield (MPa)	Ultimate (MPa)
Beam Bars	447	616
Column Bars	696	439
Ties	311	459
Concrete Compressive Strength		29.6

7.2.2 Specimen fabrication

Stirrups were cut and bent to the required dimensions by the vendor. Tie wires were used to assemble the cages after instrumentation of all bars and ties

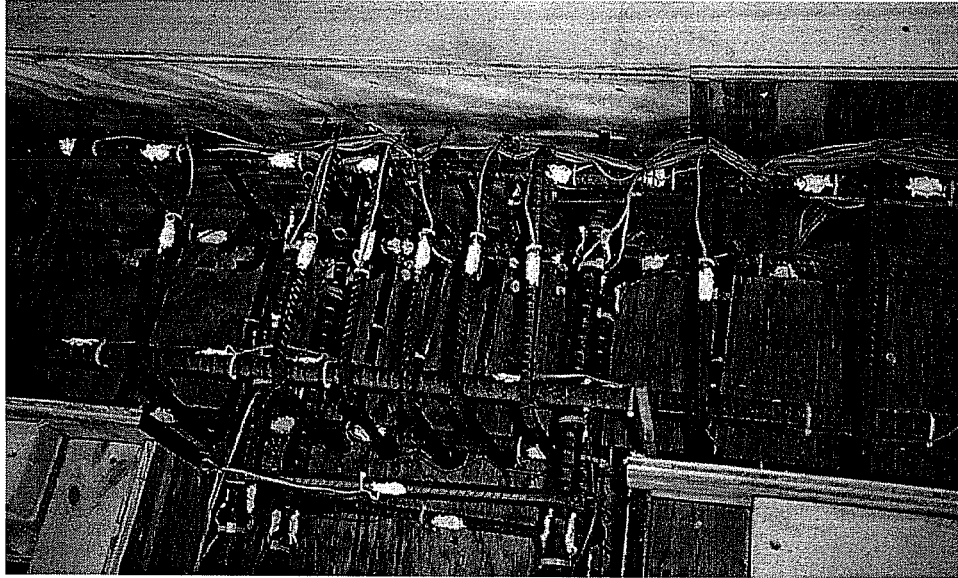
was complete. The form used for casting the test specimen was built using 19 mm (3/4 in.) plywood stiffened with 51×108 (2×4 in.) lumber. The form was prepared so that the specimen could be cast in a horizontal position, with one of the sides towards the top (Figure 7.5). After the form was aligned and oiled, the reinforcement cage was dropped inside. Steel chairs and wooden spacers were used to maintain the required side cover.

Concrete was placed in the forms directly from the ready-mix truck. Spud vibrators were used to consolidate the fresh concrete. Eighteen standard 152×305 mm (6×12 in.) concrete cylinders were cast with the specimen. After the exposed concrete surface (the side of the specimen) was screeded and trowelled to form a smooth surface it was covered with polyethylene plastic sheets for curing.

7.2.3 Instrumentation

The specimen was heavily instrumented to determine the loads, beam deflections and rotations, joint distortions and rotations, and reinforcement strains.

The applied load was determined using a 220 KN (50 kip) capacity load cell. Beam deflection was measured using a linear potentiometer at a distance equal to 1067 mm (42 in.) from the face of the column. Beam rotation was measured at a point 203 mm (8 in.) from the inside face of the column by means



a) Joint Reinforcement



b) Specimen ready for Casting

Figure 7.5 Reinforcement Cage and Form before casting

of two linear potentiometers spaced 330 mm (13 in.) from the center of the beam (Figure 7.6). The total rotation of the joint was measured using two potentiometer at the same spacing (attached to the lab floor in this case). Rotations were calculated from total deflections and distances between deflection measurements. Joint shear deformations were approximated by measuring length changes across two opposite corners of the joint and using the law of cosines to obtain angular deformations. Slip of the headed bars was measured using a threaded rod attached to the head and a linear potentiometer using the same procedure described in Section 3.2.5. Over 70 electrical resistance strain gages were attached to beam, column, and joint reinforcement. All instruments were connected to a data acquisition system and readings were taken at each load increment. An electronic voltmeter with was also connected to the load cell to monitor the load application.

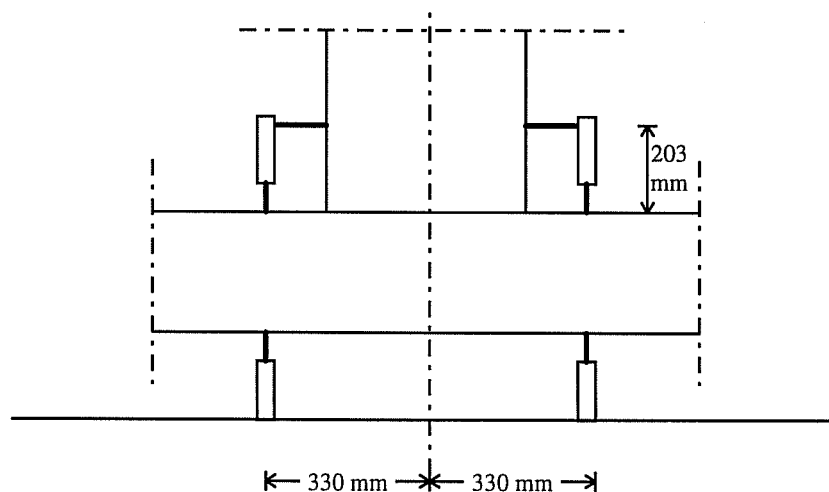


Figure 7.6 Instrumentation for measuring rotations

7.2.4 Test Setup

The test setup used is shown in Figures 7.7 and 7.8. The column was placed horizontally over two hinges bolted to a steel beam, while the beam was in a vertical position. The distance between the centerlines of the hinges was 2.4 meters (8 ft.). A double action hydraulic ram bolted to a reaction wall was used to apply the beam shear force 1450 mm (57 in.) away from the face of the column. The ram had a capacity of 330 KN (75 kip) and a 610 mm (24 in.) stroke. No axial load was applied to the column. The horizontal reactions were provided by friction between the hinges and the steel beam, and between the steel beam and the laboratory floor. In order to utilize this friction, the beam was post-tensioned to the lab floor with eight 32 mm (1 1/4 in.) bolts and each hinge was tied to the beam with four similar bolts.

7.2.5 Test Procedure

The loading history used by Smith is shown in Figure 7.9. This cyclic loading represented two earthquakes, separated by two excursions into the elastic range. The loading program used in this test was designed to follow similar rotations as those applied by Smith in the first few cycles, to allow comparison of behavior. As the main objective of this test is to study the effect of cyclic loading on the anchorage of headed bars, the rotations in the last five cycles were less than

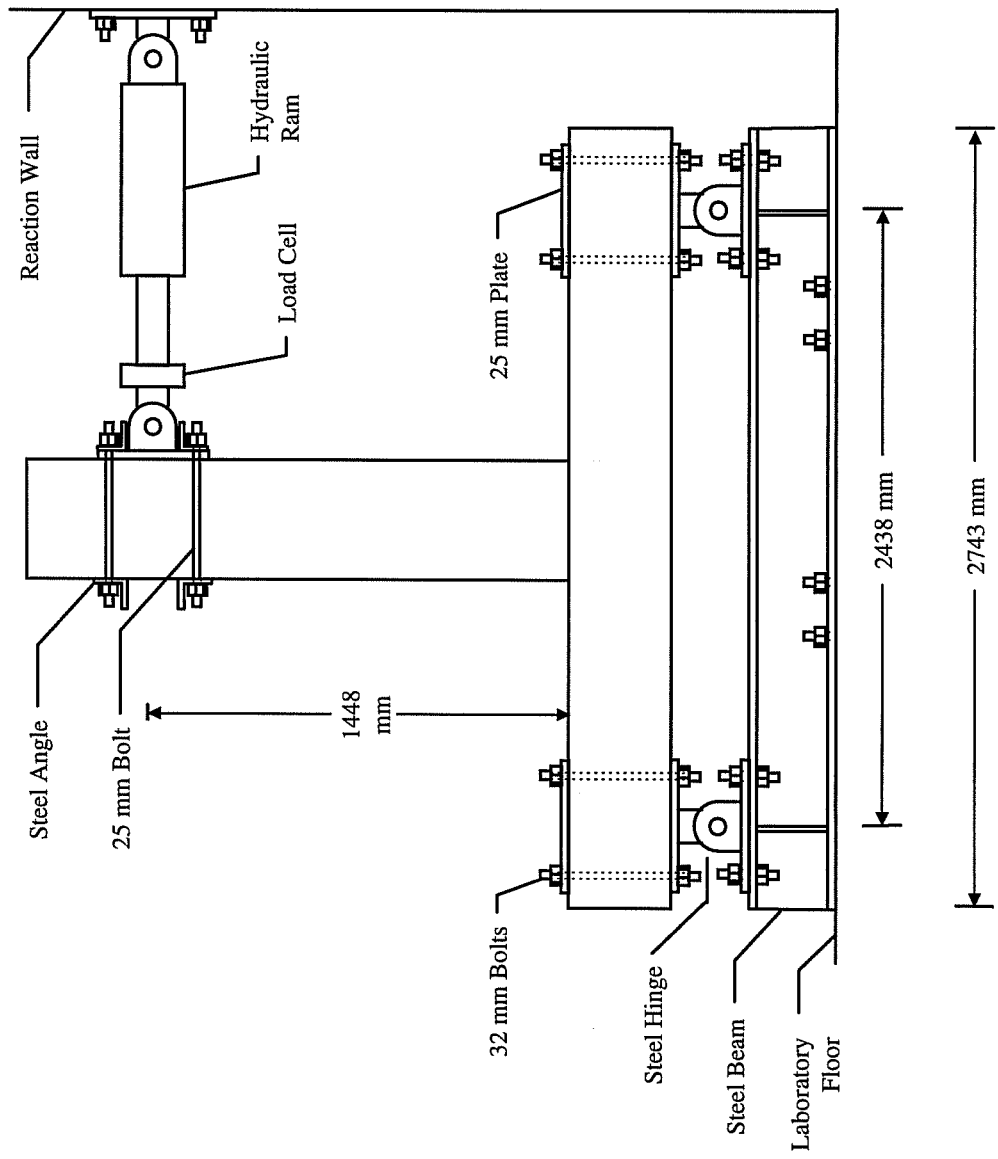


Figure 7.7 Schematic of the Test Setup

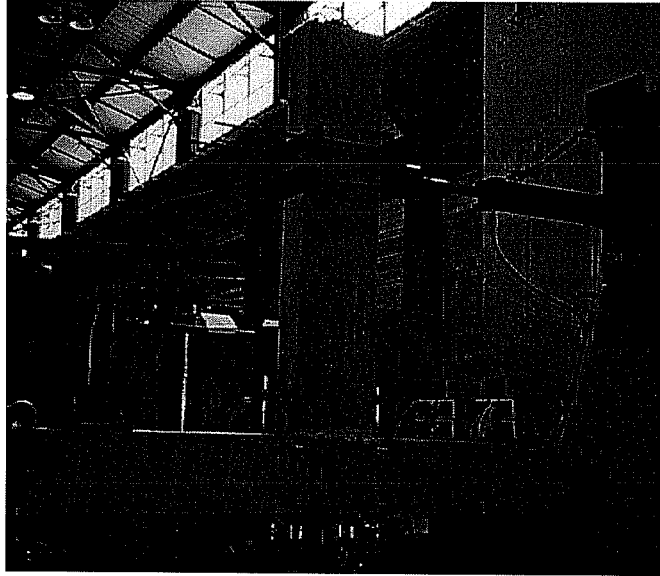


Figure 7.8 Test setup

those used by Smith to avoid destruction of the specimen and to allow examining bond deterioration under a large number of cycles with bar stresses beyond yield. In these five cycles decisions about forces or displacements to be induced at the subsequent load cycle were made on the basis of the behavioral history and the appearance of the specimen. This procedure should not have affected bond deterioration which is a function of the maximum bar force rather than rotations. The loading history used for this test is shown in Figure 7.10. The first five rotations induced varied slightly from those used by Smith due to errors during testing.

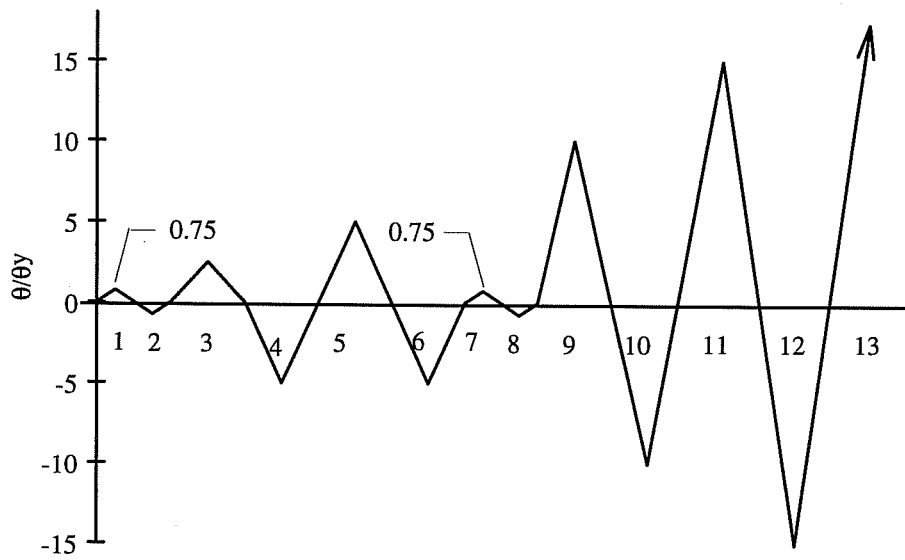


Figure 7.9 Load History used by Smith [26]

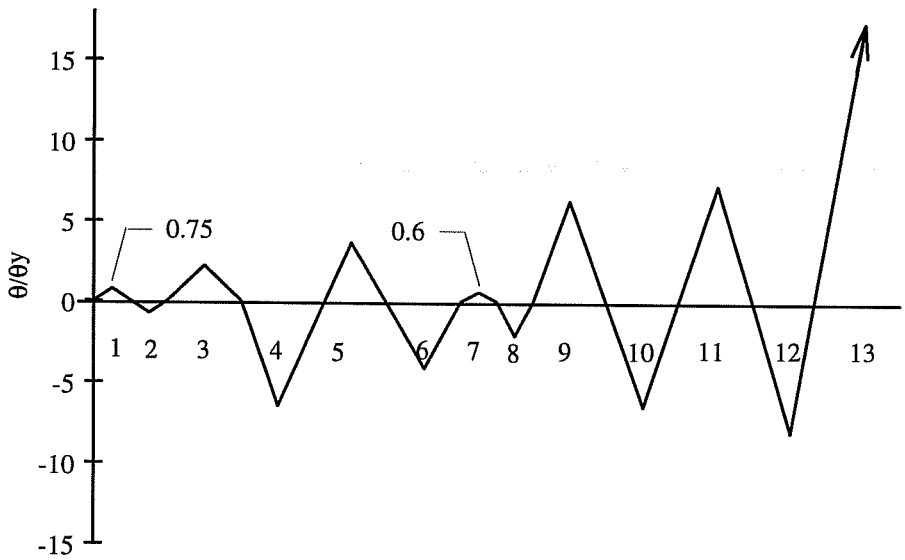


Figure 7.10 Load History applied

7.3 Test Results

In the following sections, the behavior of the beam column joint is presented and discussed. Cracking patterns, relationships between applied load and the measured deformations, and strain data from gages on the reinforcement will be used to describe the behavior. These results will also be compared the behavior of the joint with that of Unit 4 (tested by Smith), in order to assess the influence of using headed bars instead of hooked bars in exterior joints under seismic loading.

7.4 Cracking Pattern

Figures 7.11 to 7.18 show the formation of cracks with increasing number of cycles and deformation levels. After the first 2 cycles, with moments up to 75% of yield in each direction, cracks extending more than half the depth of the sections were noted in both the beam and the column. In addition, two diagonal cracks connecting opposite corners of the joint were noted. After cycle 4, the beam crack at the face of the column became wider indicating that the reinforcement yielded over a considerable length. Several diagonal cracks were evenly distributed on the side of the joint. Although the number of cracks increased significantly after cycle 6, their width did not increase, indicating that compression in the joint was being developed over a wider region or strut area.

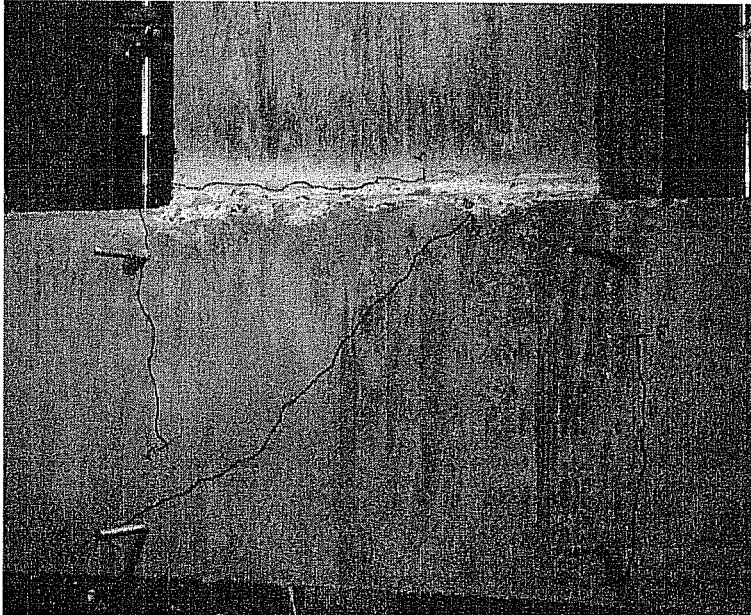


Figure 7.11 Cracking Pattern after Cycle 1

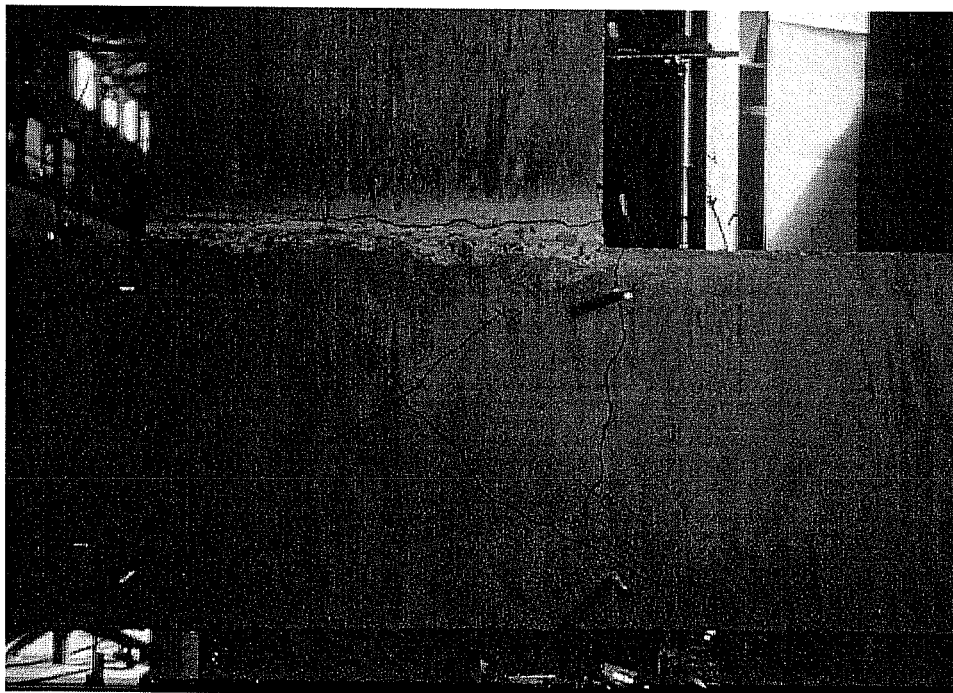


Figure 7.12 Cracking Pattern after Cycle 2



Figure 7.13 Cracking Pattern after Cycle 4

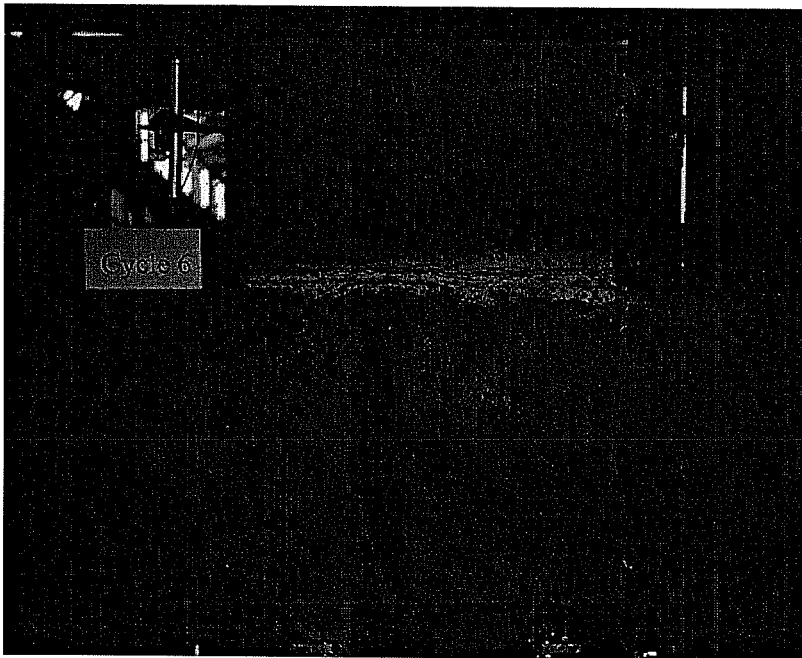
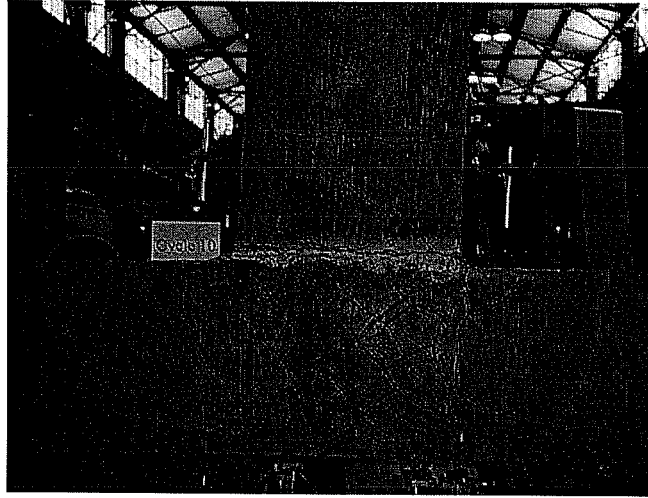


Figure 7.14 Cracking Pattern after Cycle 6



a) Overall View



b) Beam-Column Interface

Figure 7.15 Crcking Pattern after Cycle 10



a) Overall View

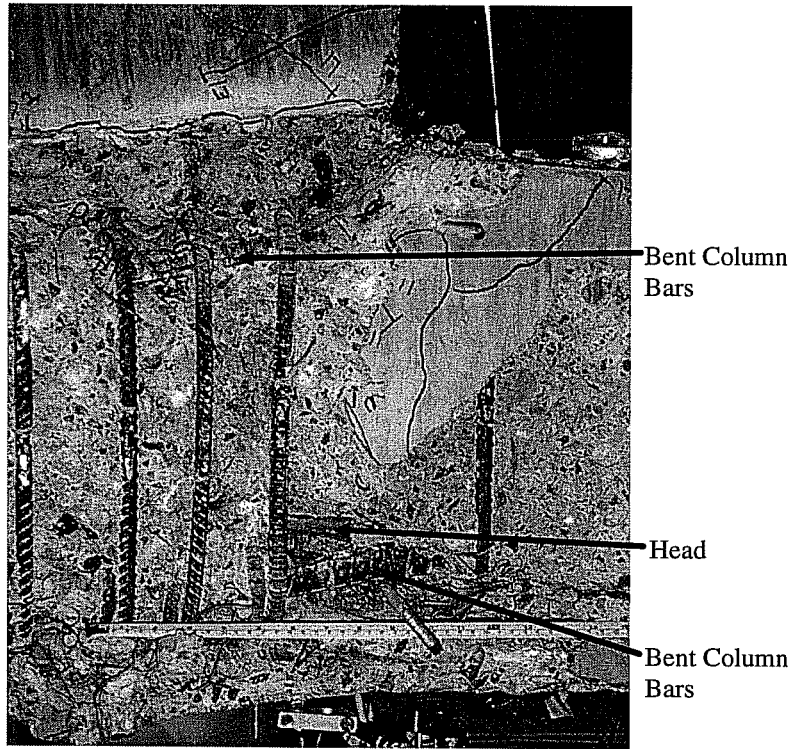


b) Beam-Column Interface

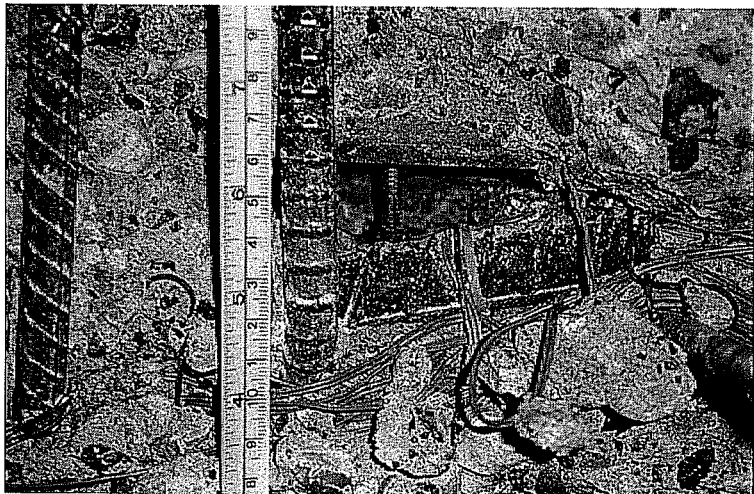
Figure 7.16 Cracking Pattern after Cycle 12



Figure 7.17 Cracking Pattern after Cycle 13



a) Joint



b) Anchorage Zone

Figure 7.18 Appearance after removing the cover

Splitting cracks along the column longitudinal bars were noted, indicating large slips of these bars. There was little difference in the cracking pattern after cycle 8. Cycles 9 and 10 induced severe cracking in the joint. The beam flexural crack at the face of the joint was more than 3 mm (0.12 in.) wide. This crack became even wider after cycles 11 and 12. At this point, the diagonal shear cracks in the joint were 5 mm (0.2 in.) wide. At the end of cycle 13 it was obvious that the side concrete cover over the joint spalled. The cover was removed, and the joint core was examined. The joint shear cracks were relatively fine, indicating that severe deterioration occurred in the cover only. Although the outer edge of one of the heads could be seen, there were no signs of anchorage deterioration. In the last load cycle, the anchored head caused severe damage to the column section and bent the longitudinal bars (Figure 7.18).

The crack pattern of the test specimen was similar to that of Unit 4 up to cycle 8. However two main differences could be noted at the end of the test. First, the bond failure characterized by high slip noted in Unit 4 was not developed in the headed bar specimen. Second, there were no signs of damage of the column section in the hooked bar specimen. It should be noted that this damage occurred in the headed bar specimen only at the end of cycle 13 (with a beam rotation equal to 17 times the yield rotation). In the case of hooked bar

anchorage, concrete crushing inside the hook allowed large slips and loss of capacity before such damage occurred.

7.5 Load Deformation Relationships

7.5.1 Beam Load - Beam Drift

The load-drift diagram is shown in Figure 7.19 . The curve represents typical flexural behavior. The first two cycles were not linear due to cracking of the concrete section. Yield strain was first measured at a point 89 mm (3.5 in.) inside the joint, at a load 5% less than the theoretical yield load. This phenomena was also noted in Unit 4. The specimen maintained most of its stiffness through cycle 3 and a part of cycle 4. In this cycle, the beam was pushed up to 6.1% drift (7.8 times the drift at yield) causing the permanent deformation noted in the following cycles.

Smith [26] used the applied load - beam rotation curve to describe the behavior of Unit 4 (Figure 7.20). This curve is plotted for the headed bar specimen in Figure 7.21. Although the applied rotations for this specimen were lower than that of Unit 4, it is obvious that the headed bar specimen had superior behavior in terms of maintaining stiffness and capacity.

Table 7.3 shows the measured degradation of beam moments carried by both test specimens with increasing number of cycles. Rotation ratios are based

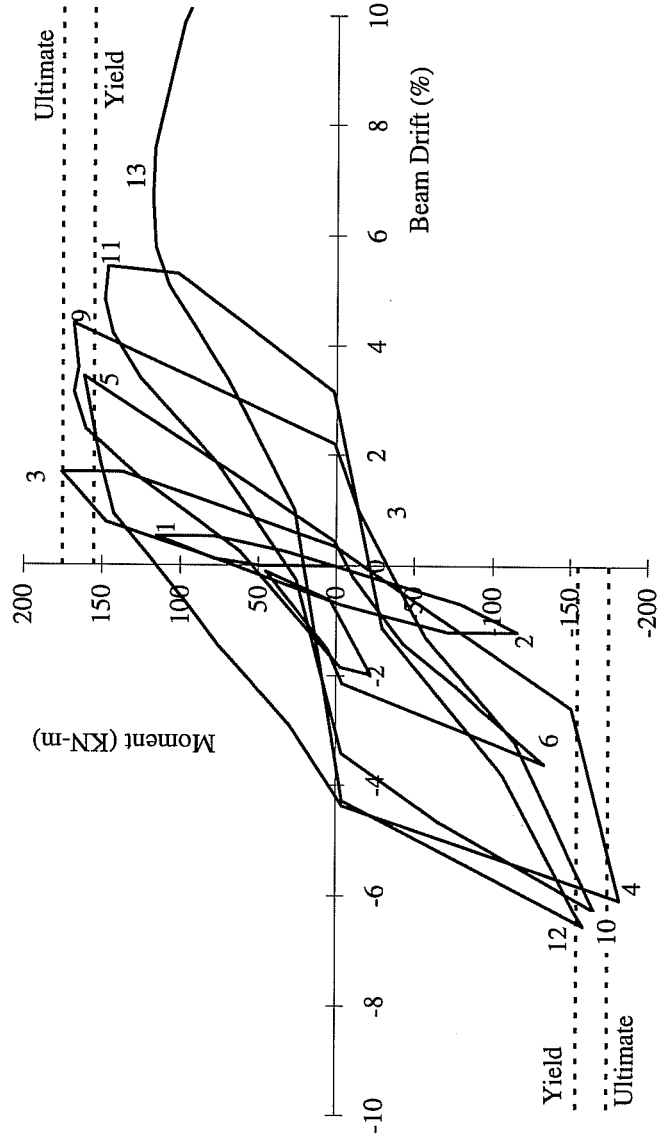


Figure 7.19 Applied Load versus Beam Drift for the Headed bar Specimen

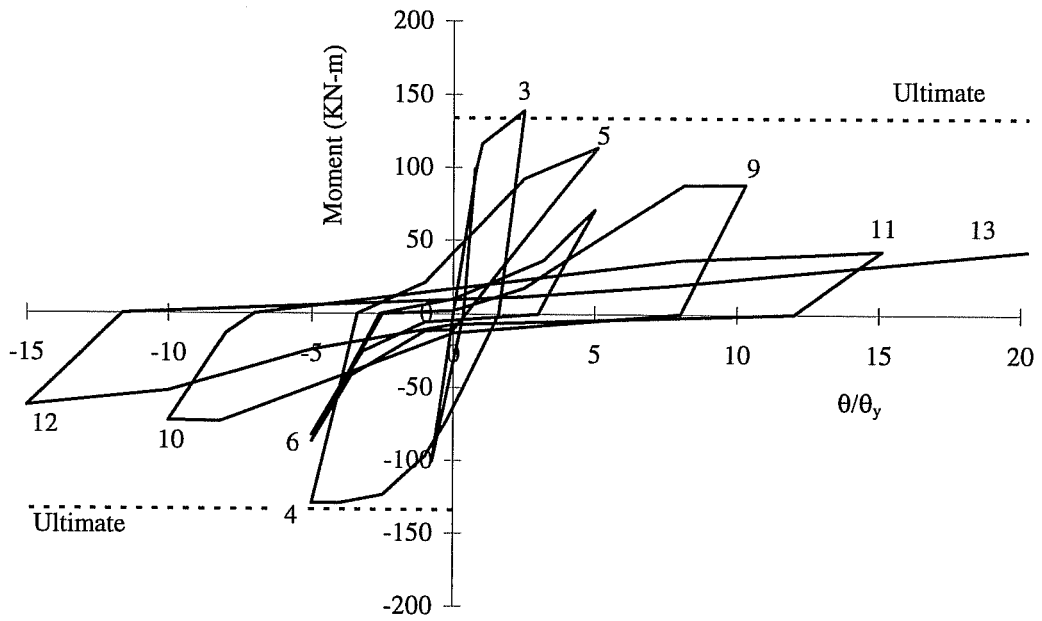


Figure 7.20 Applied Load versus Beam Ductility for Unit 4 (Tested by Smith [26])

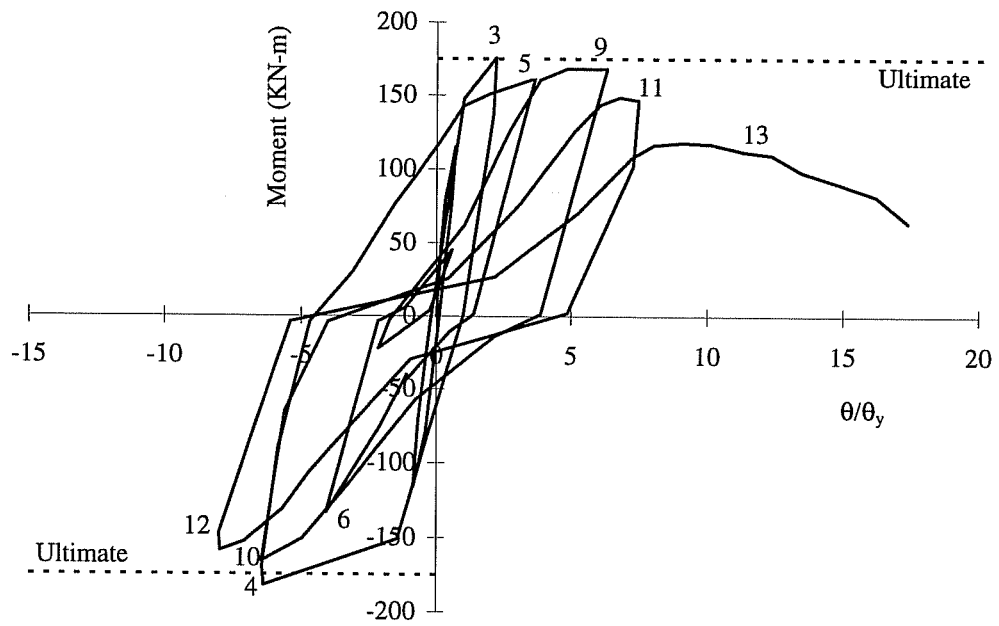


Figure 7.21 Applied Load versus Beam Ductility for the Headed Bar Specimen

Table 7.3 Comparison of Moment Degradation

Cycle	3	4	5	6	9	10	11	12	13
Headed Bar Specimen									
θ/θ_y	2.2	-6.44	3.66	-4.1	6.29	-6.45	7.44	-8	10
M/M_u	1	1.04	0.92	0.76	0.96	0.95	0.85	0.91	0.66
Hooked Bar Specimen									
θ/θ_y	2.5	-5	5	-5	10	-10	15	-15	20
M/M_u	1.04	0.97	0.85	0.65	0.66	0.55	0.32	0.47	0.31

on the comparison of the maximum measured rotation in each cycle and the measured rotation when yield was first noted. The moment ratios were calculated from the measured moments at the peak of each inelastic cycle and the theoretical ultimate moment. Although the beam rotation for the headed bar specimen at cycle 10 (after 5 inelastic cycles) was slightly higher than that of Unit 4 at cycle 6 (after 3 inelastic cycles), moment degradation was significantly lower. It should be noted that the drop in moment for the headed bar specimen in cycle 6 was not due to bond deterioration. The preceding cycle in that direction (cycle 4) imposed a rotation equal to 6.4 times the yield rotation, which caused significant inelastic elongation in the reinforcing bars. As the rotation in cycle 6 was lower than that of cycle 4 it was not allowed to develop its potential capacity. This observation

could also be noted from Figure 7.21. The stiffness of the curve in this cycle was relatively high, indicating the potential for increase in capacity with additional drift. The headed bar specimen was capable of developing 91% of the beam theoretical ultimate moment (or 105% of the yield moment) in cycle 12, after 8 inelastic load cycles, and at a rotation equal to 8 times the rotation at yield. It is believed that up to this cycle there was no significant anchorage deterioration at the head. The slight drop in capacity (9%) is mostly attributed to the spalling of the concrete in the beam compressive zone, which lead to the reduction of the beam moment arm.

7.5.2 Joint Deformation

The total joint rotation is plotted against the applied load in Figure 7.22. Joint rotation was calculated from data obtained from the linear potentiometers spaced 330 mm (13 in.) on each side of the beam centerline and measuring the deflection of the bottom of the column relative to the laboratory floor. The curve indicates very stiff behavior up to the last three cycles. However, it should be noted that the rotation was measured at points 102 mm (4 in.) outside the joint (Figure 7.6). The rotation at the center of the joint was probably higher. The linear potentiometers were not placed closer to the joint centerline in order to prevent spalling of the back of the joint from affecting the data. The large rotations in the last few cycles

in Figure 7.22 are attributed to the damage of the column section at the face of the joint which caused rigid body motion of the column segment.

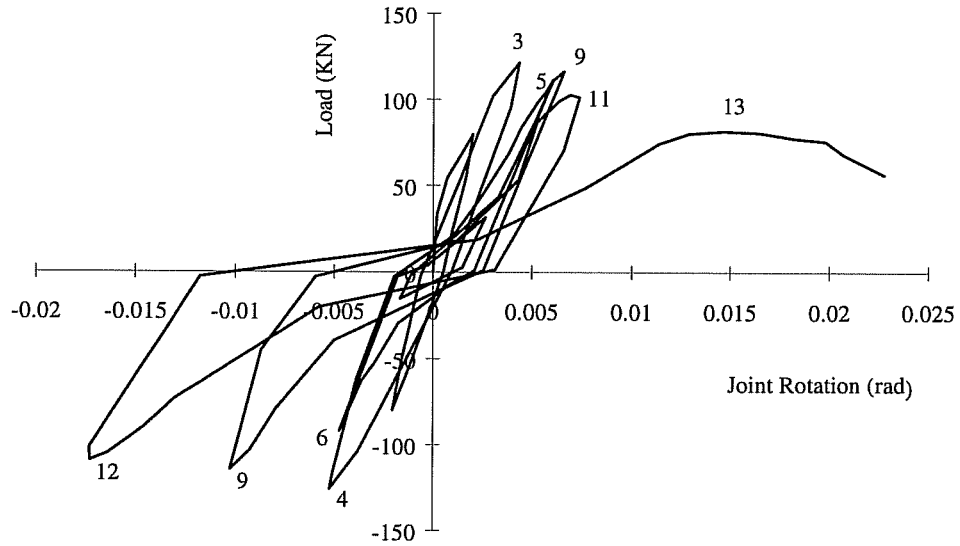


Figure 7.22 Applied load versus joint Rotation for the Headed Bar Specimen

Shear is the main parameter controlling the design of joints. The angular distortion of the joint, or the shear strain, is plotted against the applied load in Figure 7.23. Shear strains were calculated using linear potentiometers connecting opposite corners of the joint. Considering the deformed configuration of a joint shown in Figure 7.24, joint shear deformation can be calculated as:

$$\gamma_1 = \frac{\sqrt{(d + \delta_1)^2 - b^2} - b}{b} \quad 7.1$$

The second component of the joint shear deformation, γ_2 , is calculated using the same equation. The average of γ_1 and γ_2 is used for plotting Figure 7.23. The shear distortion curve did not show significant degradation up to the last 4 cycles. The behavior was similar to that of the applied load - joint rotation curve. Although Smith did not measure shear deformation in his test, comparison with other studies indicated that the joint shear distortion of the tested specimen is in the same order as that observed in different joint specimens reported in the literature.

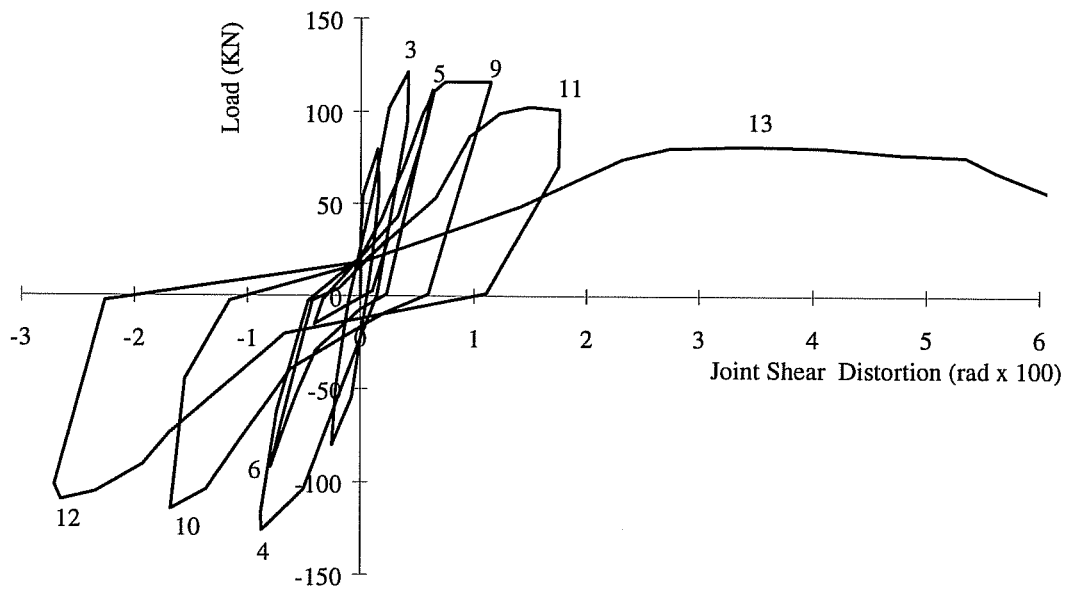


Figure 7.23 Applied Load versus Joint Shear Distortion

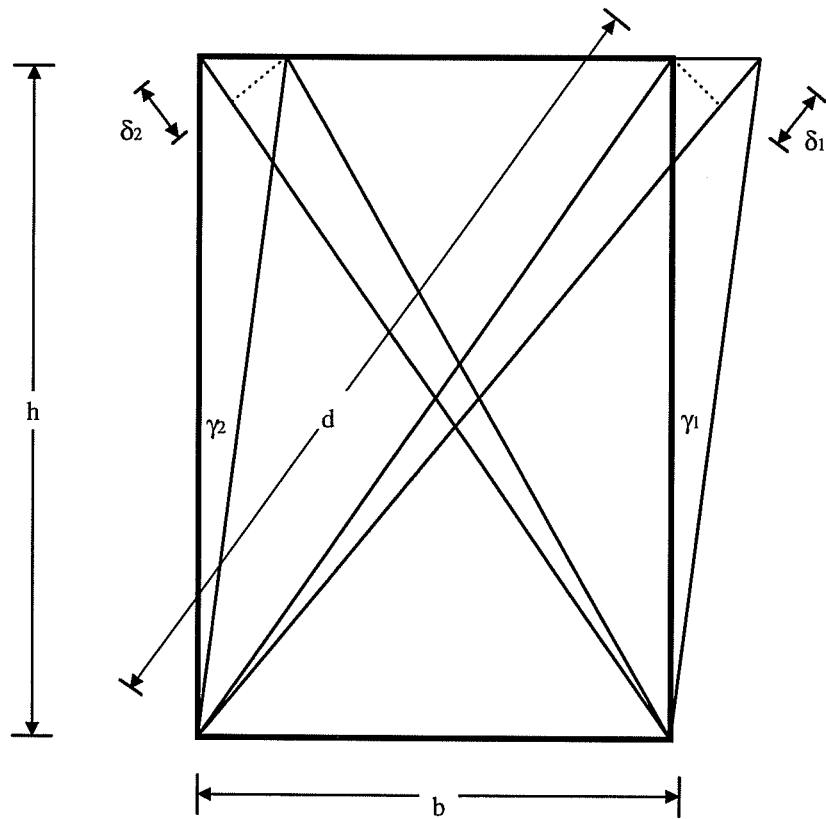


Figure 7.24 Schematic diagram to measure Joint Distortion

7.5.3 Head Slip

The head slip of a positive and a negative beam bar are plotted against the applied load (for the first 8 cycles) in Figure 7.25 and 7.26. The last four cycles are not included in these figures because the spalling of the concrete at the back of the column (used as the reference for slip) affected the data. The bar presented in Figure 7.26 was exposed to tensile stresses in the first cycle, while the other bar was under compression in the same cycle. The head slip for the first bar was 0.3

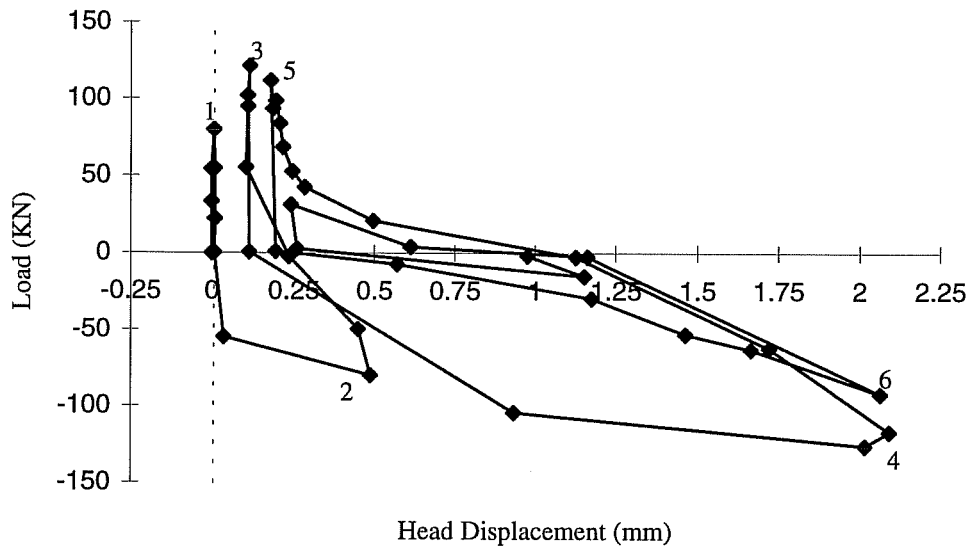


Figure 7.25 Applied load versus Head Slip - Beam Bar under compression in Cycle1

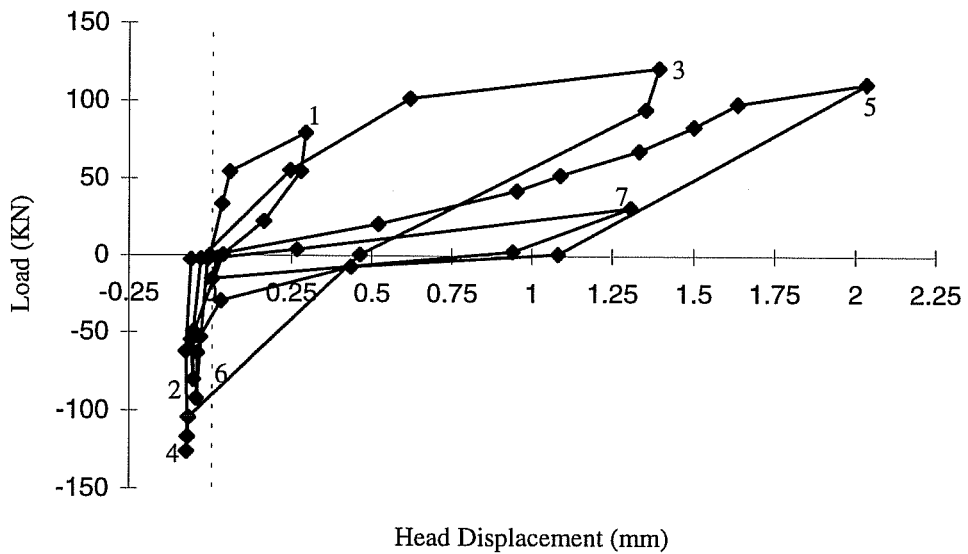


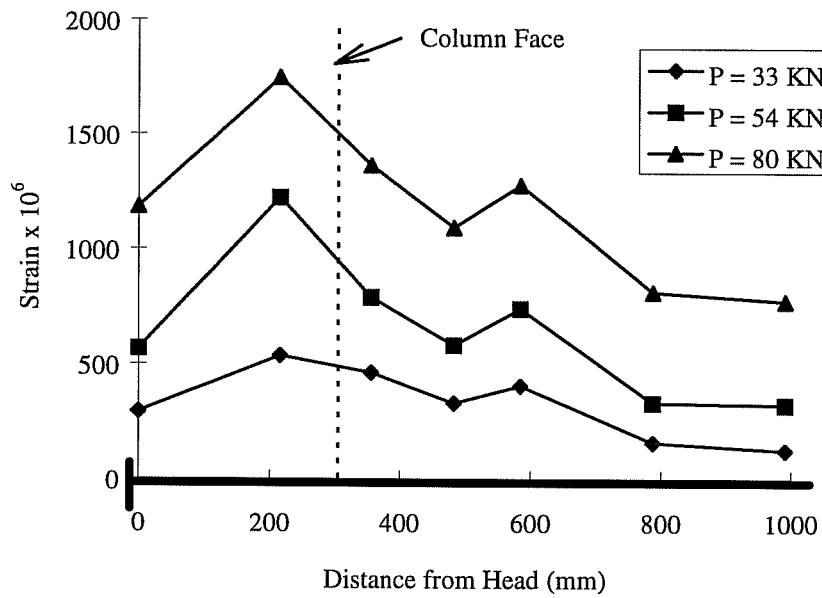
Figure 7.26 Applied load versus Head Slip - Beam Bar under tension in Cycle1

mm (0.012 in.) at 75 % of the yield load (first cycle). On the other hand, the no slip was measured for the other bar, indicating that most of the compressive forces were resisted by concrete and the bar compression was transferred to concrete along the lead embedment. In the second cycle the head slip was 0.06 mm (2.4×10^{-3} in.) for the first bar, and 0.5 mm (0.02 in.) for the second bar (in the opposite directions). Head slip due to bar compression was noted in this cycle because the first cycle in tension caused some bond deterioration along the length of the bar, thus increasing force transfer through the head. The beam compressive zone was cracked in the first cycle which led to an increase in steel compression. In the following cycles the behavior of both bars was very similar and head slips due to tension reached 2 mm (0.08 in.). In spite of that, push-in slip was minimal because effect of the column bars passing behind the heads and increasing the effective bearing area. The effect of the column bars was magnified because of the large number of ties which stiffened the column bars.

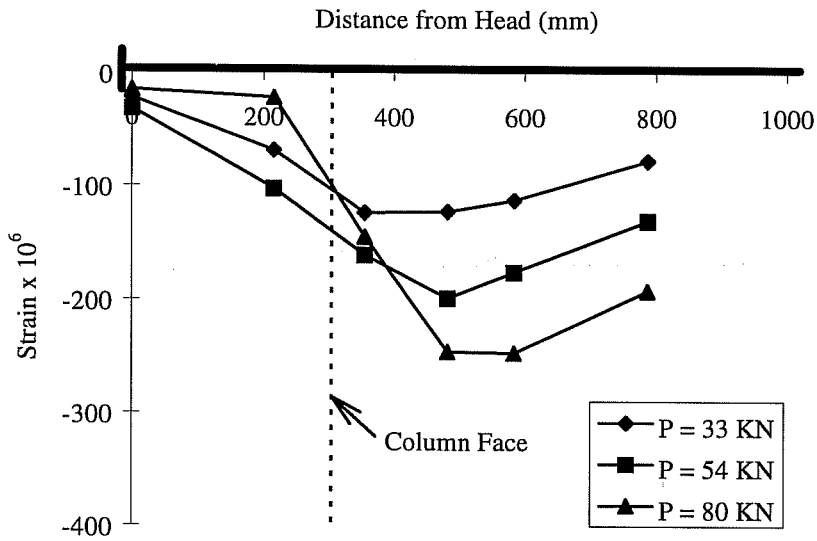
7.6 Measured Strains in Reinforcement

7.6.1 Beam Bar Stresses

The strain profiles along a positive and a negative longitudinal beam bar for the first loading cycle are shown in Figure 7.27. For the first bar, under tension in this cycle, the strains close to the head were relatively high at the



a) Positive Beam Bar (under tension)



b) Negative Beam Bar (under compression)

Figure 7.27 Strains along Beam Bars during the first 3 increments of Cycle 1

maximum load, indicating that the head was responsible for transferring a significant amount of the bar tensile force to concrete. The second bar was under compression in this cycle. Compressive strains were much lower, especially through the joint. The strains close to the head were negligible, indicating that most of the compressive forces were transferred to the concrete along the embedment length.

Figures 7.28 and 7.29 show the strains at two positions on the first bar, plotted against the beam tip load. The bar strains just before the head reached yield in the third cycle, indicating that the head was responsible for transferring all of the bar load to the concrete. The compressive strains before the head were also relatively high (27% of yield) in the fourth cycle indicating that the head was responsible for transferring larger compressive forces to the concrete after the loss of bond along the lead embedment length. Bond deterioration along the lead embedment length was also observed by Smith in the hooked bar specimen. In his case, strains just before the hook exceeded yield in the third cycle, and the hook became responsible for transferring the bar forces to the concrete for the rest of the cycles.

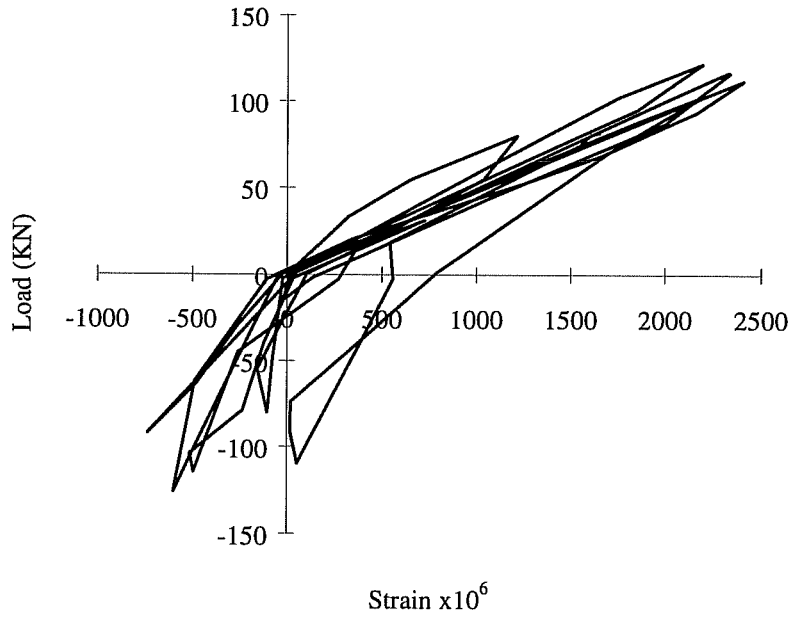


Figure 7.28 Applied Load versus Bar Strain at the Head

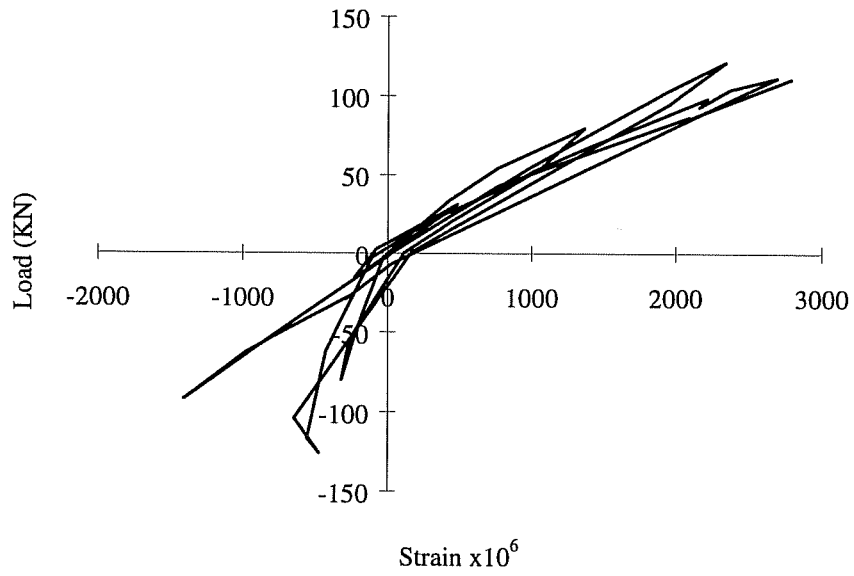


Figure 7.29 Applied Load versus Strain 356 mm from head (Beam Bar)

7.6.2 Column Bars

The strain profiles along a longitudinal column bar for the first loading cycle are shown in Figure 7.30. At the maximum load in this cycle, the bar tensile stress penetrated the joint to the compressive side of the column. This phenomena is common when the depth of the joint does not provide adequate development length. The four column bars had similar strain profiles. The strains measured at a point 127 mm (5 in.) outside the joint are plotted with the applied force in Figure 7.31. In the last increment of the second cycle, bar strains changed from compression to tension, indicating that the joint did not provide adequate development length at 75% of the yield load. Tensile strains were measured in all subsequent cycles (in both directions).

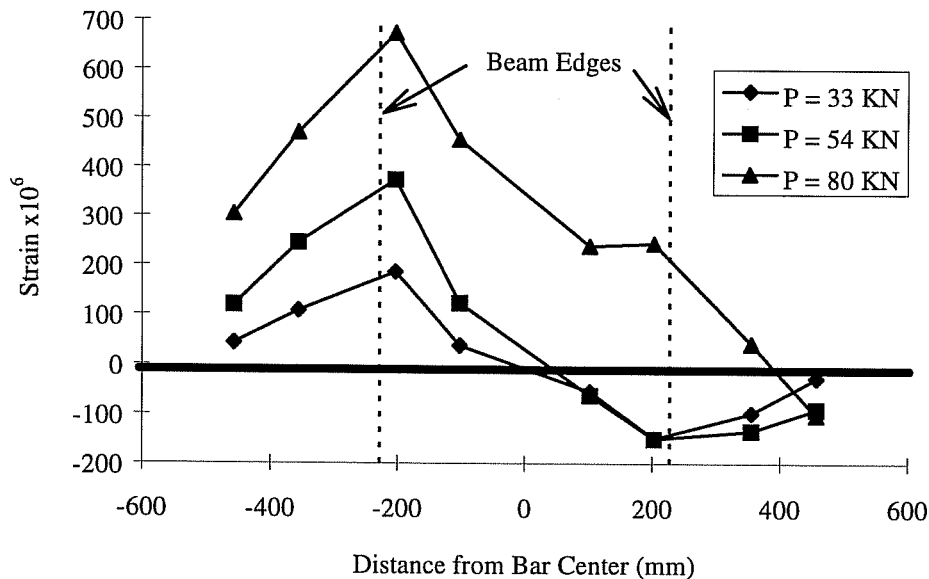


Figure 7.30 Strains along a column Bar during the first 3 increments of Cycle 1

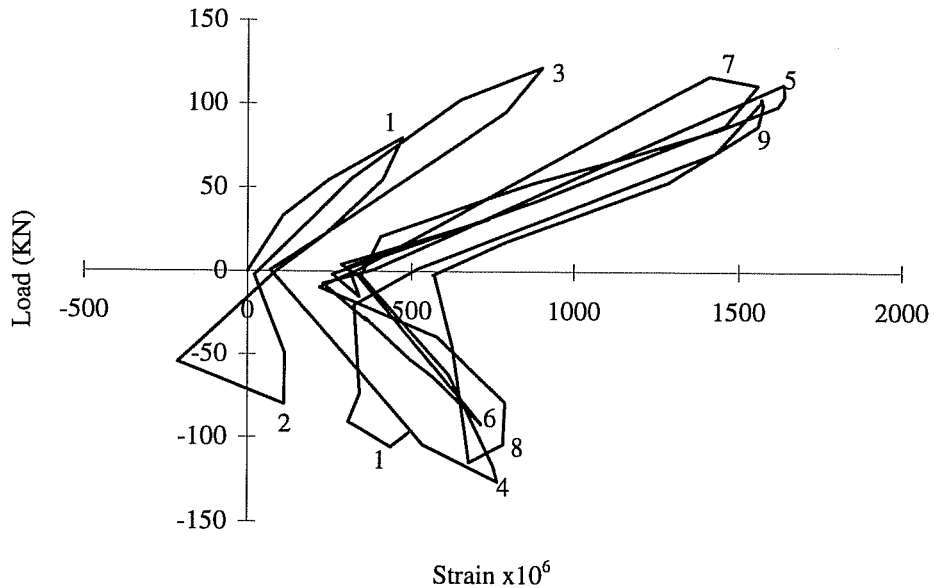


Figure 7.31 Applied Load versus Column Bar Strain - 127 mm outside Joint

7.7.3 Joint Ties

Strains in the tie at the center of the joint are plotted against the applied load (for the first 10 cycles) in Figure 7.32. No strains were measured in the first three load increments of the first load cycle. The strain increased suddenly in the last load increment in this cycle due to the diagonal shear crack. The measured strains decreased with reversing the load as the crack was closed. However, in the last increment of the second cycle, strain increased again to the maximum value measured in the first cycle. This increase is attributed to the orthogonal shear

crack which developed at the end of this cycle. The tie yielded in the second inelastic cycle. Strains increased significantly in subsequent cycles as a result of joint deterioration.

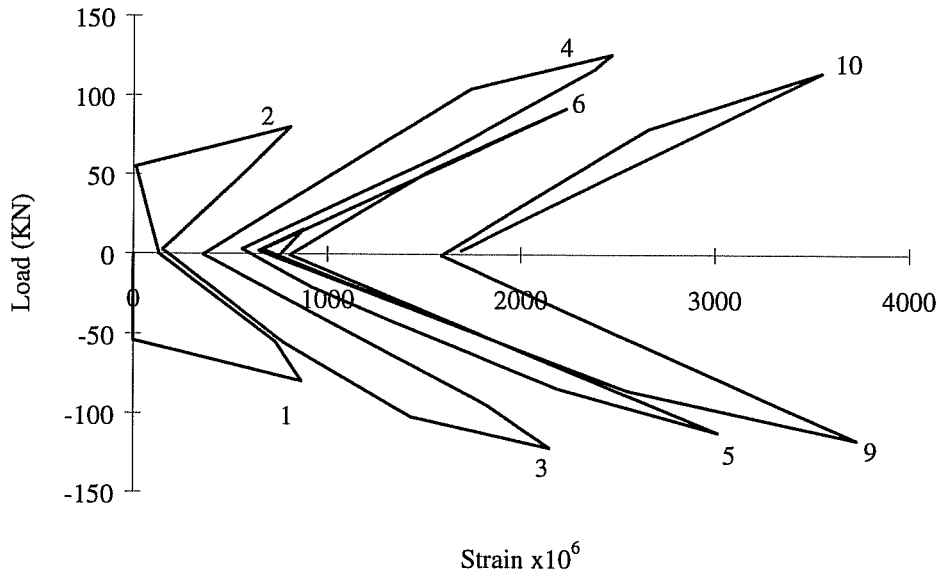


Figure 7.32 Applied Load versus Tie Strains - Tie at center of Joint

The strains in the tie at the top of the joint are plotted in Figure 7.33. The strain behavior in the first cycle is similar to that described above. However, strains did not increase in the second cycle, indicating that the second shear crack did not cross this tie. Although the tie strains increased with loads in both directions in the following cycles, strains were always higher in positive cycles,

indicating that this tie was more effective in resisting shear forces when the adjacent beam bars were under tension.

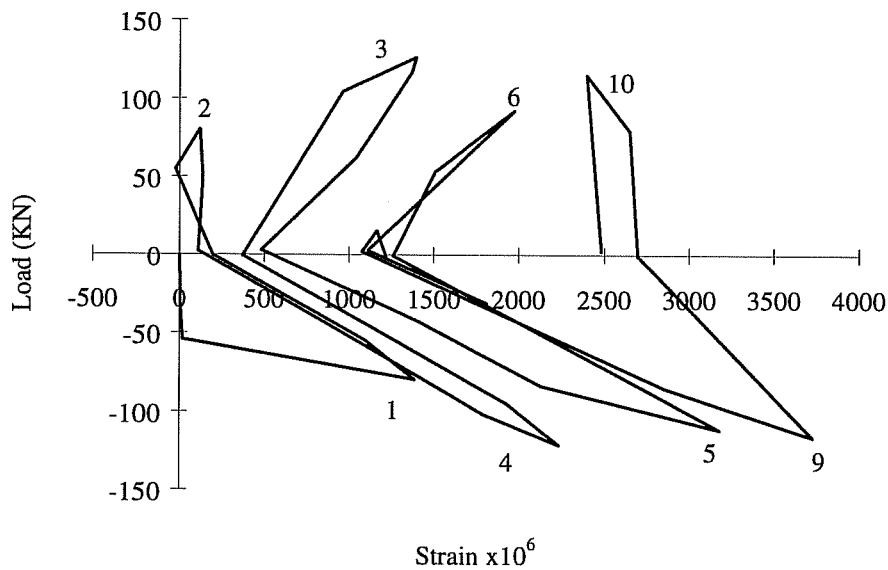


Figure 7.33 Applied Load versus Tie Strains - Tie at the top of the Joint

Although strength differences prevented direct comparison with tie stresses measured by Smith, some similarities were noted. In both cases, the tie at the center of the joint yielded in the second inelastic cycle. The maximum strains throughout the load history were measured in this tie. The main difference between the two tests is that the headed bar anchorage did not start deteriorating after the confining reinforcement yielded.

The total shear force and the shear resisted by concrete in the joint are plotted against the beam drift for the first, second, and third load cycles in Figures 7.34 to 7.36. The following expression was used to calculate the joint shear force;

$$V_{jt} = A_s f_s - V_{col}$$

Where V_{jt} is the total shear force in the joint, A_s and f_s are the area and the stress of beam reinforcement under tension, and V_{col} is the shear force in the column (obtained by static equilibrium using the measured applied load). The amount of shear resisted by ties was computed using measured strains. The difference between the tie forces and the total joint shear is the shear resisted by concrete.

In the first loading cycle, the shear resisted by concrete reached 165 KN (37 kip) or $0.29\sqrt{f'_c}$ in the second load increment, but dropped to 104 KN (23.5 kip) at the end of the cycle due to the opening of the diagonal crack and the increase in stresses in the ties. Similar behavior was noted in the second cycle, although the drop in shear resisted by concrete was slightly less in this case. The shear resisted by concrete dropped significantly in the third cycle due to joint deterioration. The level of shear resisted by concrete was relatively low in the tested specimen due to two reasons. First, the large number of stirrups decreased the portion of shear resisted by concrete once cracking occurred. Second, shear deterioration of the joint is known to occur more rapidly in situations where there is low or no axial loads.

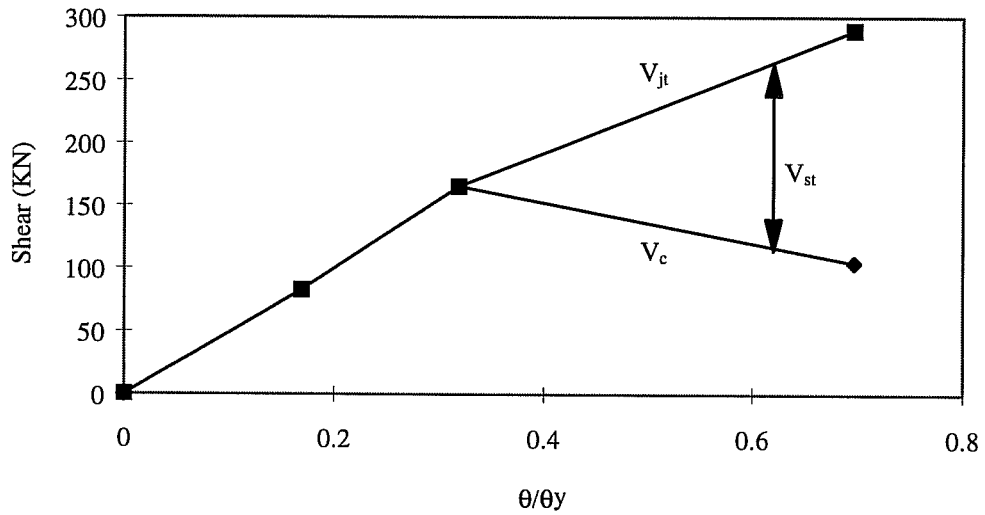


Figure 7.34 Plot of Joint Shear resisted by Concrete and Transverse Reinforcement - Cycle 1

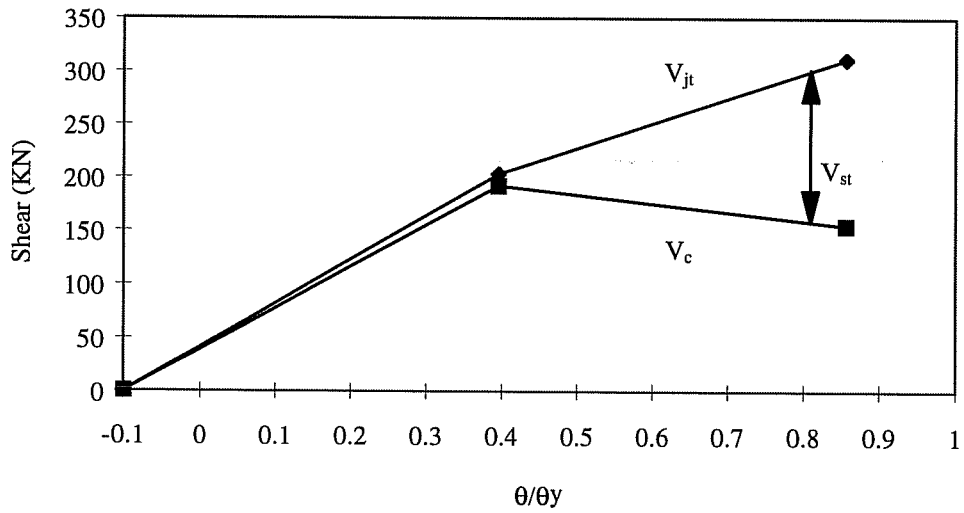


Figure 7.35 Plot of Joint Shear resisted by Concrete and Transverse Reinforcement - Cycle 2

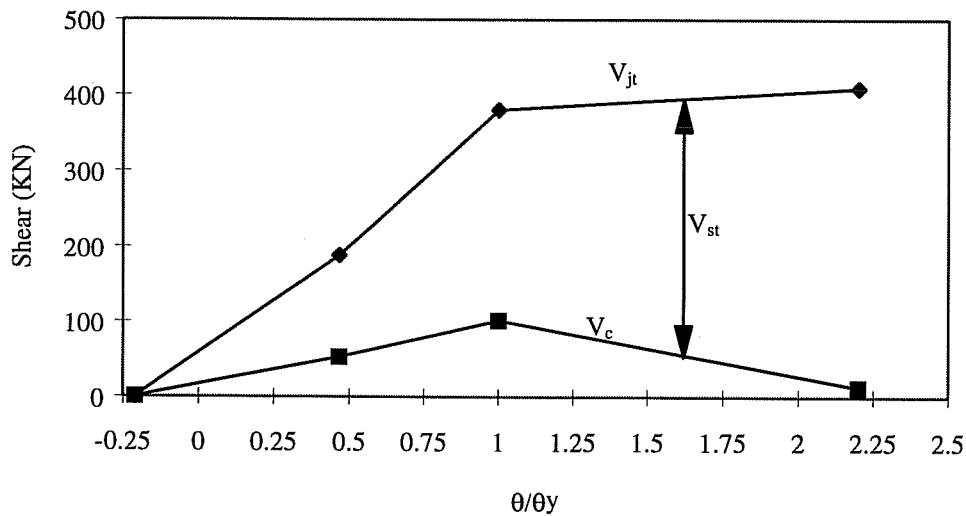


Figure 7.36 Plot of Joint Shear resisted by Concrete and Transverse Reinforcement - Cycle 3

7.8 Summary

The overall behavior of the exterior joint constructed using headed bars was superior to that of Unit 4. No signs of bond deterioration were observed throughout the load history in spite of using beam bars with higher strength (compared to that of Unit 4). The fact that headed bar anchorages are dependent on the head made the bar stresses irrelevant.

Head slips under cyclic loading were increased with the number of cycles. However, part of the measured increase is due to spalling of the back of the column (used as a reference point for measuring slip).

Chapter 8

SUMMARY AND CONCLUSIONS

8.1 Introduction

The introduction of high strength steel and concrete in reinforced concrete structures requires an efficient form of mechanical anchorage. Headed bars provide a practical alternative to hooked bars. Headed bars eliminate congestion problems caused by standard hooks also. Other attributes are minimal slip, ease of placement, and more accurate dimensions of reinforcing cages.

Previous research on the behavior of joints constructed with headed bars is very limited and covers only knee joints. There has been no systematic study of the effect of the different variables on the anchorage capacity of headed bars in joints was addressed.

The objective of this study was to determine the anchorage behavior of headed bars in joints. The study was divided into three phases: Basic studies on headed bars, anchorage in exterior joints, and effects of seismic (cyclic) loading.

8.2 Basic Studies of Headed Bar Anchorage

Fourteen pull-out tests on bars embedded in concrete cubes were conducted to investigate the effects of cyclic loading and anchoring the head behind a crossing bar on the anchorage behavior and capacity of headed bars. The variables included number of load cycles, size of crossing bars, and head dimensions. The following conclusions were made concerning the variables investigated:

- 1) Cycling the load between 5 and 80% of the ultimate capacity, up to 15 cycles, did not significantly influence the anchorage capacity of headed bars.
- 2) The increase in slip due to load cycling was dependent on the maximum load of each cycle. If this load was beyond the elastic range of a headed bar (where the stiffness under monotonic loading would have dropped significantly), permanent deformations accumulated with each cycle. If the maximum load was within the elastic range, the increase in slip was minimal.
- 3) Placing a crossing bar in the anchorage zone of the head improved the anchorage capacity through two mechanisms. First, the crossing bar provided a lateral restraint against side blow-out by mobilizing more concrete to resist spalling failure. Second, the crossing bar increased the effective bearing area of the head which led to lower bearing stresses.

- 4) Although the increase in anchorage capacity rose with an increase in diameter of the crossing bar, it was conservative to limit this increase for design purposes to 25% for heads positively anchored behind 25 mm or larger crossing bars. A positive anchorage means that the clear head dimension is at least equal to half the crossing bar diameter.

In this phase 11 exploratory tests investigating the possibility of using headed bars as transverse reinforcement were also conducted. The performance of headed bars in orientations simulating closed hoops was studied by constructing simple specimens in which headed bars overlapping at a corner at right angles to each other were subjected to static loads.. All of the anchorage situations were capable of developing the yield force of the bars, even with slight construction errors. The results obtained from this limited number of tests indicated that there is a great potential for the use of these bars as transverse reinforcement.

8.3 Anchorage in Exterior Joints

Thirty-two large scale specimens simulating exterior joints in a structure were tested to assess the effects of different variables on the behavior of joints under monotonic loading. The variables included size of anchored bars, head dimensions and orientation, embedment length, concrete cover, and confining

reinforcement. The following observations and conclusions were made concerning the behavior of headed bars in exterior joints:

- 1) The bar load was transferred to concrete through two mechanisms; anchorage along the lead embedment length, and bearing of the head on concrete. In most cases the first mechanism was not effective in increasing the ultimate load because large slip at failure caused bond deterioration along the lead embedment.
- 2) Although anchorage along the lead embedment increased the ultimate load in few cases, the contribution of the two mechanisms should be considered as a unit because both are affected by the lead embedment length.
- 3) Head aspect ratio and orientation do not have significant effect on the anchorage capacity of headed bars.
- 4) Bar diameter does not have significant effect on the anchorage capacity of the load-slip behavior of headed bars.
- 5) The anchorage capacity increased with the increase of side concrete cover. Increased side cover provides a larger mass of concrete to resist side blow-out.
- 6) Confining reinforcement improved concrete bearing capacity under the head and increased the ultimate load. Both slip and load drop at failure were significantly lower in specimen with confining reinforcement.

- 7) The anchorage capacity of headed bars as obtained from pullout tests is significantly higher than that obtained from exterior joint tests. The difference in capacity is attributed to joint shear cracking before anchorage failure.

The proposed design equation for the development length required to develop yield stress in a headed bar terminating in an exterior joint is

$$l_d = \frac{A_b f_y}{14.7\alpha\beta\gamma\sqrt{A_n}\sqrt{f'_c}} + d'$$

Where

l_d = required embedment length, in mm

A_b = area of the anchored bar, in mm²

f_y = yield stress of the anchored bar

d' = distance from the face of the column to the centroid of the column longitudinal reinforcement closest to face, in mm

A_n = net bearing area, in mm²

α = Confining reinforcement factor, taken as 1 for tie spacing more than 100 mm, 1.25 for spacing equal to 100 mm to 51 mm, and 1.4 for tie spacing equal to 50 mm or less

β = cover size factor, taken as 0.8 for side cover less than 76 mm, and 1 for all other cases

γ = anchorage condition factor, taken as 1.25 for heads positively anchored behind 25 mm or larger crossing bars, and 1 for all other anchorage conditions.

The embedment length required by this equation for a bar with a head area equal to 8 times the bar area is at least 30% less than that required by the ACI Building Code for a bar terminating in a standard hook.

8.4 Effects of Seismic Loading

One exterior beam-column subassembly was tested under cyclic loading to provide an insight to potential benefits of replacing hooked bars by headed bars in seismic areas. The behavior of the specimen was compared with a similar specimen constructed using hooked bars, which was reported in the literature.

The overall behavior of the headed bar specimen was superior to that of the hooked bar specimen. Capacity degradation was minimal, and no signs of bond deterioration were observed. The test ended after the column section was damaged and its longitudinal bars were bent.

Measured joint shear distortion and joint rotation were comparable to that of exterior joints as reported in the literature. Measured strains along headed bars,

column longitudinal bars, and joint ties were similar to those of the companion hooked bar specimen.

It should be noted that head thickness was not one of the variables in this study. The head thicknesses used were sufficient to avoid yielding of the head. Therefore conclusions (including the proposed design equation) are based on the results in which head yielding was precluded.

8.5 Recommendations for Further Research

Although this study provided a better understanding of behavior of headed bars in joints, additional research is needed to fully understand the behavior of headed bars in concrete members. Future research should cover the following areas:

- 1) The effects of light weight aggregate concrete on the anchorage behavior of headed bars.
- 2) The effects of epoxy coating on the anchorage behavior of headed bars.
- 3) Although previous research proposed simple models for the stresses in the heads, a more comprehensive study is required to cover the effects of crossing bars in the anchorage zone, head shape, and concrete strength on head stresses.

- 4) Only one joint specimen was tested under cyclic loading in this study. Although the headed bar specimen behavior was better than the companion hooked bar specimen, much work remains to be done in this area. Future research is needed to investigate the effects of axial loading and the amount of transverse reinforcement on the behavior of joints constructed using headed bars.

References

1. ACI Committee 318, "Building Code Requirements for Reinforced Concrete," ACI 318-95, American Concrete Institute, Detroit, 1995
2. DeVries, R.A., "Anchorage of Headed Reinforcement in Concrete," PhD. Dissertation, The University of Texas at Austin, Austin, Texas, December 1996.
3. Hasselwander, G.; Jirsa, J.O.; and Breen, J.E., "Strength and Behavior of Single Cast-in-Place Anchor Bolts Subject to Tension," Anchorage to Concrete, SP-103, American Concrete Institute, Detroit, 1987.
4. Furche, J., and Eligehausen, R., "Lateral Blowout Failure of Headed Studs near a Free Edge," Anchors in Concrete - Design and Behavior, SP-130, American Concrete Institute, Detroit, 1991, pp. 235-252.
5. Dr. Techn. Olav Olsen a.s., "Important Aspects for Further Development Concerning the use of T-Headed Bars in Concrete Design and Construction - Final Report" Norway, 1993.
6. Collins, Michael P., and Gupta, P.R., "Shear Behavior of Reinforced Concrete Members Subjected to High Axial Compression," A study conducted for Metalock Industrier A/S, Norway.
7. McConnell, Scott W., and Wallace, John W., "Behavior of Reinforced Concrete Beam-Column Knee-Joints Subjected to Cyclic Loading," Report No. CU/CEE-95/07, Structural Engineering Research Laboratory, Department of Civil Engineering, Clarkson University, Postdam, NY, June 1995.
8. SEQAD Structural Engineers, Solana Beach, Ca, "Seismic Response of a Bridge Column/Cap-Beam Knee Joint Designed With Headed Reinforcement," Report No. 95/12, Job No. 94/17, Prepared for Headed Reinforcement Corporation, Canada, 1995.

9. Jirsa, J.O., and Marques J.L., "Study of Hooked Bar Anchorages in Beam-Column Joints," ACI Journal, Proceedings, V. 72, No. 5, May 1975, pp. 198-209.
10. ACI Committee 318, "Building Code Requirements for Reinforced Concrete," ACI 318-71, American Concrete Institute, Detroit, 1971.
11. Pinc, R.L.; Watkins, M.D.; and Jirsa, J.O., "Strength of Hooked Bar Anchorages in Beam-Column Joints," CESRL Report No. 77-3, University of Texas at Austin, Nov. 1977.
12. Hamad, B.S.; Jirsa, J.O.; and D'Abreu de Paulo, "Anchorage Strength of Epoxy-Coated Bars," ACI Journal, Proceedings, V. 90, No. 2, Marh-April 1993, pp. 210-217.
13. Burguieres, S.T., "A Study of Mechanical Anchorages in Beam-Column Joints," Final Report to Erico Products, Civil Engineering Structures Research Laboratory, The University of Texas at Austin, 1973.
14. Untrauer, R.E., and Henry, R.L.. "Influence of Normal Pressure on Bond Strength," ACI Journal, Proceedings, V. 62, May 1965, pp. 577-585.
15. Natrella, Mary G., Experimental Statistics, National Bureau of Standards Handbook 91, Washington, D.C., 1963, Reprinted 1966.
16. Orangun, C.O.; Jirsa, J.O.; and Breen, J.E., "A Reevaluation of Test Data of Development Length and Splices," ACI Journal, Proceedings, V>74, March 1977, pp. 114-122.
17. Rogowsky, D.M.; MacGregor, J.G.; and Ong, See Y., "Tests of Reinforced Concrete Deep Beams," ACI Journal, Proceedings, V. 83, No. 4, July-Aug. 1986, pp. 614-623.
18. Bresler, B., and Bertero, V., "Behavior of Reinforced Concrete under Repeated Loading," Journal of the Structural Division, ASCE, Vol. 94, No. ST6., June 1968, pp. 1567-1590.

19. Perry, E.S., and Nabil, Jundi, "Pullout Bond Stress Distribution under Static and Dynamic Repeated Loading," *ACI Journal, Proceedings*, V. 66, May 1969, pp. 377-380.
20. Ismail, M.A.F., and Jirsa, J.O., "Bond Deterioration in Reinforced Concrete Under Low Cycle Loads," *ACI Journal, Proceedings*, Vol. 69, June 1972, pp. 334-343.
21. Ismail, M.A.F., and Jirsa, J.O., "Behavior of Anchored Bars Under Low Cycle Overloads Producing Inelastic Strains," *ACI Journal, Proceedings*, Vol. 69, July 1972, pp. 433-438.
22. Hassan, F.M., and Hawkins, N.M., "Anchorage of Reinforcing Bars for Seismic Forces," *Reinforced Concrete in Earthquake Zones, SP-53*, American Concrete Institute, Detroit, 1977.
23. Hanson, N.W., and Conner, H.W., "Seismic Resistance of Reinforced Concrete Beam-Column Joints," *Journal of the Structural Division, ASCE*, Vol. 93, ST5, October 1967, pp. 533-560.
24. Hanson, N.W., "Seismic Resistance of Frames with Grade 60 Reinforcement," *Journal of the Structural Division, ASCE*, Vol. 97, ST6, June 1971, pp. 1685-1700.
25. Megget, L.M., "Anchorage of Beam Reinforcement in Seismic Resistant Reinforced Concrete Frames," Report to the University of Canterbury, Christchurch, New Zealand, in partial fulfillment of the requirements for the degree of Master of Engineering, 1971.
26. Smith, B.J., "Exterior Reinforced Concrete Joints with Low Axial Load under seismic Loading," Report to the University of Canterbury, Christchurch, New Zealand, in partial fulfillment of the requirements for the degree of Master of Engineering, 1972.
27. Renton, G.W., "The Behavior of Reinforced Concrete Beam-Column under Cyclic Loading," Report to the University of Canterbury, Christchurch, New Zealand, in partial fulfillment of the requirements for the degree of Master of Engineering, 1972.

28. Lee, D.L.N., "Original and Repaired Behavior of R.C. Beam-Column Subassemblages Subjected to Earthquake Type Loadings," Technical Report 76R4, Department of Civil Engineering, University of Michigan, Ann Arbor, 1976.
29. Otani, S., "The Architectural Institute of Japan Proposal for Ultimate Strength Design Requirements for RC Buildings with Emphasis on Beam-Column Joints," Design of Beam-Column Joints for Seismic Resistance, SP-123, American Concrete Institute, Detroit, 1991.
30. Kaku, T., and Asakusa, H., "Ductility Estimation of Exterior Beam-Column Subassemblages in Reinforced Concrete Frames," Design of Beam-Column Joints for Seismic Resistance, SP-123, American Concrete Institute, Detroit, 1991.

Vita

Tarek Refaat Bashandy was born in Cairo, Egypt, on June 29, 1970, the son of Refaat Bashandy and Susan Ali. After graduating Port-Said High School, Cairo, Egypt, in 1987, he entered the Faculty of Engineering, Cairo University, Cairo, Egypt. He graduated in July, 1992, receiving the degree of Bachelor of Science in Engineering. In September, 1992, he joined the army, and in May 1993, he accepted a position as a structural Engineer with Bechtel-Egypt. In January, 1994, he entered The Graduate School of The University of Texas at Austin. He graduated in May, 1995, receiving the degree of Master of Science in Engineering. He has worked at the University of Texas at Austin as a Teaching Assistant and as a Graduate Research Assistant at the Phil M. Ferguson Structural Engineering Laboratory.

Permanent address: 13 Mekka Street,
El - Mohandeseen, Giza,
Egypt.

This dissertation was typed by the author.